The extension of drug delivery potential using Tiara[*n*]uril

Rajni Sharma

A thesis submitted in fulfilment of the requirements for the degree of

Doctor of Philosophy

School of Science

University of New South Wales, Canberra

April 2020

Thesis/Dissertation sheet

Surname/Family Name	:	Sharma
Given Name/s	:	Rajni
Abbreviation for degree as given in the University calendar	:	PhD
Faculty	:	Chemistry
School	:	School of Science
Thesis Title	:	**The extension of drug delivery potential using Tiara[*n*]uril**

Tiara[*n*]uril is a new class of glycoluril-based macrocyclic hosts, characterized by the presence of a positively charged cavity comprising of glycoluril moieties linked to two pyrazolium groups. Being a recently discovered macrocycle, only a few Tu[*n*] derivatives have been synthesized and reported. However, these Tu[*n*]'s are restricted to homologues no larger than Tu[3], which indicates synthetic opportunities towards the attainment of higher homologues through variation of substitutions on the glycoluril moieties.

Presented in this thesis is the synthesis of new members of Tu[*n*] family - tetrahydrothiophenetiara[*n*]uril (THT_nTu[*n*]). A reaction sequence was designed to achieve homologues of Tu[*n*] (n>3) through equatorial introduction of THT functionality. This synthetic route provided access to two THT functionalized Tu[*n*]'s - $THT_3Tu[3]^{2+}$ and $THT_4Tu[4]^{2+}$, where the later represents the first example of higher homologue in Tu[*n*] family. The structural properties of purified $THT_3Tu[3]^{2+}$ and $THT_4Tu[4]^{2+}$ were fully elucidated using different techniques. Furthermore, attempts to bias the product distribution towards $THT_4Tu[4]^{2+}$ was illustrated through the use of different acids, which indicated the influence of an anionic template in attaining improved higher homologue (*n*=4) proportion.

The second objective of the work was to develop an understanding of the binding capabilities of methyl and THT substituted Tu[*n*]'s to establish their potential for functional applications. The binding association of $Me_{10}Tu[3]^{2+}$, $THT_3Tu[3]^{2+}$ and $THT_4Tu[4]^{2+}$ were explored with a selection of guests suitable for the testing of a preliminary understanding. The association towards an inorganic (HCl), and organic guest (L-glutamine) was demonstrated through an increase in pK_a for HCl and changes in CD and fluorescence outcome for the amino acid. In addition, the cavity encapsulating feature of $THT_4Tu[4]^{2+}$ was established with the guests - dioxane and d_8-dioxane. The binding constants were determined using comparative binding and d_8-dioxane was found to bind more strongly than dioxane. Furthermore, $Me_{10}Tu[3]^{2+}$ was investigated for it's possible effectiveness as a solubilizing excipient for the poorly soluble oral drugs. The preliminary results indicated formation of association complexes as reflected by changes in their solubilities at two pH conditions - 3.5 and 7.4. These solubility results suggests that $Me_{10}Tu[3]^{2+}$ or related Tu[*n*]'s may have potential in future drug delivery applications.

FOR OFFICE USE ONLY	Date of completion of requirements for Award:

ORIGINALITY STATEMENT

‘I hereby declare that this submission is my own work and to the best of my knowledge it contains no materials previously published or written by another person, or substantial proportions of material which have been accepted for the award of any other degree or diploma at UNSW or any other educational institution, except where due acknowledgement is made in this thesis. Any contribution made to the research by others, with whom I have worked at UNSW or elsewhere, is explicitly acknowledged in the thesis. I also declare that the intellectual content of this thesis is the product of my own work, except to the extent that assistance from others in the project’s design and conception or in style, presentation and linguistic expression is acknowledged.’

Signed …….....

Date……

INCLUSION OF PUBLICATIONS STATEMENT

UNSW is supportive of candidates publishing their research results during their candidature as detailed in the UNSW Thesis Examination Procedure.

Publications can be used in their thesis in lieu of a Chapter if:

- The student contributed greater than 50% of the content in the publication and is the "primary author", ie. the student was responsible primarily for the planning, execution and preparation of the work for publication
- The student has approval to include the publication in their thesis in lieu of a Chapter from their supervisor and Postgraduate Coordinator.
- The publication is not subject to any obligations or contractual agreements with a third party that would constrain its inclusion in the thesis

Please indicate whether this thesis contains published material or not.

☐ ***This thesis contains no publications, either published or submitted for publication***

☒ ***Some of the work described in this thesis has been published and it has been documented in the relevant Chapters with acknowledgement***

☐ ***This thesis has publications (either published or submitted for publication) incorporated into it in lieu of a chapter and the details are presented below***

CANDIDATE'S DECLARATION

I declare that:

- I have complied with the Thesis Examination Procedure
- where I have used a publication in lieu of a Chapter, the listed publication(s) below meet(s) the requirements to be included in the thesis.

Name	Signature	Date (dd/mm/yy)
Rajni Sharma		

COPYRIGHT STATEMENT

Signed ……

Date ……..

AUTHENTICITY STATEMENT

‘I certify that the Library deposit digital copy is a direct equivalent of the final officially approved version of my thesis.’

Signed ……

Date ……..……..

ACKNOWLEDGEMENT

"Treat people as if they were what they ought to be and you will help them become what they are capable of becoming"

- Goethe

Through thick and thin the support and guidance bestowed upon me by my supervisor Dr. Day has been nothing short of his relentless pursuit into making me a person I am capable of becoming. Dr. Anthony Day truly guided me to hone my skills through his impeccable interpersonal skills and his excellence in the genre. His expertise in the field of chemistry has enhanced my knowledge and technical prowess. His humility and humble demeanour have always inspired me, and I admire his patience, persistence and engagement in guiding me to complete my work presented herein this thesis. Thank you for being my guiding light and bringing me this far. I specially would like to acknowledge the compassion Dr. Day had extended during my tough times. You are an excellent supervisor and it has been my true pleasure working under your supervision.

My deepest gratitude for my co-supervisor Dr. Cliff Woodward for extending his support in calculating the binding constants for my experiment, his exceptional computational techniques has helped me garner vital information. Thank you for giving perspective to my learning experience.

My sincere thanks to Dr. Grant Collins and Dr. Lynn Wallace for their encouragement and support. Their constructive feedbacks during group meetings have enhanced my learnings. Thank you both for being a source of inspiration.

My special thanks to Dr. Barry Gray for his prompt help extended during my PhD candidature, especially with NMR. Thanks to Dr. Damian Buck for his assistance during

lab demonstrations. My sincere thanks to Dr. Jonathon Beves for his help with the crystallography and Dr. Terry Frankcombe for performing ESP modelling for my compound.

I would also like to thank my dear friends for their unconditional and unwavering support and understanding through tough times. Thank you all for your sharing and memories, I will always cherish these unforgettable moments.

I am keeping the best for the last to not to say thanks but to express my indubitable love and gratitude to my pillars of strength my parents, words are not enough to acknowledge your feats and hard work you have invested in my upbringing. You have been the foundation to my growth. Special praise for my in-laws and to my life - my husband, their constant encouragement and support has bolstered my ambitions and I am really grateful to them. To my brother and sister, your perseverance has been inspiring. The work presented herein is a homage to my family and their hard work.

TABLE OF CONTENTS

CHAPTER 4

ABBREVIATIONS

The following abbreviations are used in this work

Q[*n*]	Cucurbit[*n*]uril
Me_{10}Q[5]	DecamethylQ[5]
Me_{12}Q[6]	DodecamethylQ[6]
CyH	Cyclohexano
CyP	Cyclopentano
CyB	Cyclobutano
$(HO)_{12}$Q[6]	PerhydroxyQ[6]
Ph_2Q[6]	DiphenylQ[6]
Ph_4Q[6]	TetraphenylQ[6]
Me_6Q[6]	HexamethylQ[6]
TCyPQ[6]	TetracyclopentanoQ[6]
m-TriCyPQ[6]	meta-tricyclopentanoQ[6]
TMeQ[6]	TetramethylQ[6]
o-TMeQ[6]	ortho-tetramethylQ[6]
TcyHQ[6]	TetracyclohexanoQ[6]
m-HmeQ[6]	meta-hexamethylQ[6]
p$(CyH)_2$Q[6]	para-dicyclohexaneQ[6]
Me_2Q[7]	DimethylQ[7]
CyHQ[7]	mono-CyclohexanoQ[7]

MePhQ[7]	Methyl-phenylQ[7]
ClBuQ[7]	Cl-Butyl-Q[7]
Me_4Q[8]	TetramethylQ[8]
Cy_2Q[8]	DicyclohexanoQ[8]
Me_4Q[6]	TetramethylQ[6]
CyP_5Q[5]	PentacyclopentanoQ[5]
CyP_6Q[6]	HexacyclopentanoQ[6]
CyP_7Q[7]	HeptacyclopentanoQ[7]
THF	Tetrahydrofuran
HmQ[6]	Hemicucurbit[6]uril
HmQ[12]	Hemicucurbit[12]uril
CyH_6HmQ[6]	HexacyclohexanoHemiQ[6]
BU[6]	Bambus[6]uril
Bn_{12}BU[6]	DodecabenzylBU[6]
Bn_8BU[4]	OctabenzylBU[4]
Me_{10}PrQ[5]	DecamethylpressoQ[5]
ns-Q[6]	Nor-seco-Q[6]
bis-ns-Q[6]	Bis-nor-seco-Q[6]
bis-ns-Q[10]	Bis-nor-seco-Q[10]
Tu[*n*]	Tiara[*n*]uril
Me_6Tu[3]	HexamethylTu[3]

Me_{10}Tu[3]	DecamethylTu[3]
CyP_3Tu[3]	TricyclopentanoTu[3]
m-$XyMe_8$Tu[2]	meta-xylene-dipyrazoliumTu[2]
p-$XyMe_8$Tu[2]	para-xylene-dipyrazoliumTu[2]
NaOAc	Sodium acetate
THT	Tetrahydrothiophene
TFA	Trifloroacetic acid
hr	Hour
RT	Room temperature
MeOH	Methanol
DMSO-d6	Deuterated dimethylsulfoxide
DMF	Dimethylformamide
min	Minute
DCM	Dichloromethane
Mp	Melting point
IR	Infrared spectroscopy
equiv.	Equivalent
°C	Degree Celsius
ESMS	Electrospray Mass Spectrometry
NMR	Nuclear Magnetic Resonance
DCOSY	Dipolar Correlation Spectroscopy

NOESY	Nuclear Overhauser Effect Spectroscopy
ppm	Parts per million
d	Doublet
Å	Angstrom
δ	Chemical shift
J	Coupling constant
$THT_3Tu[3]$	TetrahydrothiopheneTu[3]
$THT_4Tu[4]$	TetrahydrothiopheneTu[4]
μM	Micromolar
mM	Millimolar
$K^+C_8H_5O_4^-$	Potassium hydrogen phthalate
[θ]	Molar ellipticity
2,6-ANS	2-Anilinonaphthalene-6-sulphonic acid
N_2	Nitrogen
TGA	Thermogravimetric analysis

STRUCTURES COMPILATION

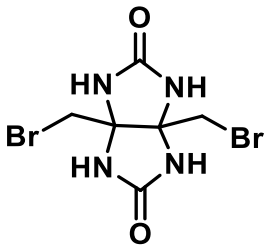

1

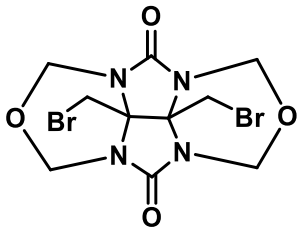

2

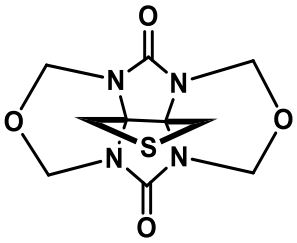

3

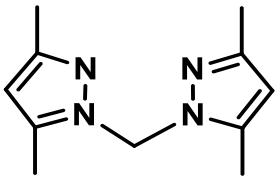

4

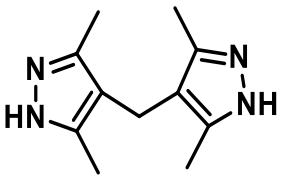

5

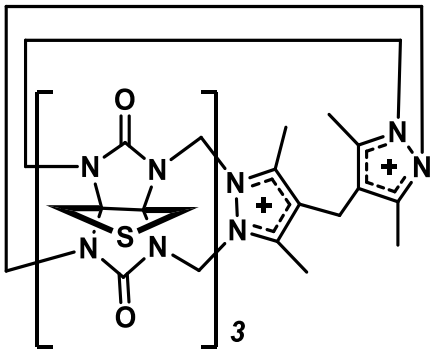

6

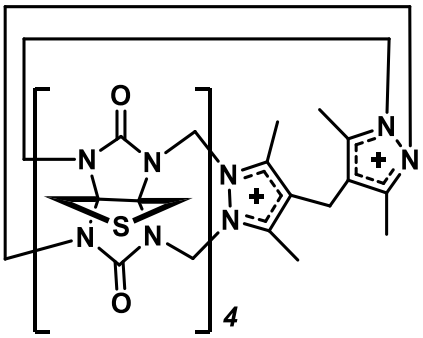

7

ABSTRACT

Tiara[*n*]uril (Tu[*n*]) is a new class of glycoluril-based macrocyclic hosts, structurally characterized by the presence of a positively charged cavity comprising of glycoluril moieties linked to two pyrazolium groups. Being a recently discovered macrocyclic host, only a few derivatives of Tu[*n*] have been synthesized and reported. However, these reported Tu[*n*] examples are restricted to homologues no larger than Tu[3], which conceivably indicates associated synthetic opportunities towards the attainment of higher homologues through variation of substitutions on the glycoluril moieties.

Presented in this thesis is the synthesis of new members of the Tu[*n*] family - tetrahydrothiophenetiara[*n*]uril (THT_nTu[*n*]) using tetrahydrothiophene glycoluril diether. A reaction sequence was designed and implemented to achieve higher homologues of Tu[*n*] (n > 3) through introduction of THT functional group equatorially. This synthetic route provided access to two homologues of THT functionalized Tu[*n*]'s - $THT_3Tu[3]^{2+}$ and $THT_4Tu[4]^{2+}$, where the later represents the first example of a higher homologue in Tu[*n*] family (*n* = 3 and 4). The structural properties of purified $THT_3Tu[3]^{2+}$ and $THT_4Tu[4]^{2+}$ were fully elucidated using NMR, ESMS, single crystal X-ray diffraction, TGA and elemental analysis. Furthermore, attempts to bias the product distribution towards $THT_4Tu[4]^{2+}$ was illustrated through the use of different acids, which indicated the influence of an anionic template in attaining improved proportion of the higher homologue, *n* = 4.

The second objective of the work presented in this thesis was to develop an understanding of the binding capabilities of methyl and THT substituted Tu[*n*]'s in order to establish their potential for future functional applications. The binding association of $Me_{10}Tu[3]^{2+}$, $THT_3Tu[3]^{2+}$ and $THT_4Tu[4]^{2+}$ were explored with a selection of guest molecules suitable

for the testing of a preliminary understanding. The association towards an inorganic guest (HCl), and an organic guest (L-glutamine) was demonstrated through an increase in pK_a value for HCl and changes in the CD spectra and a fluorescence outcome that involved a competitive dye displacement method for the amino acid. In addition, the cavity encapsulating feature of $THT_4Tu[4]^{2+}$ was established with the guests - dioxane and d_8-dioxane. The binding constants were determined for the two guests using comparative binding studies and d_8-dioxane was found to bind more strongly than dioxane. Furthermore, $Me_{10}Tu[3]^{2+}$ was investigated to determine its possible effectiveness as an excipient for the improvement of aqueous solubility of poorly soluble oral drugs. The preliminary results indicated the formation of association complexes as reflected by changes in their solubilities at two different pH conditions - pH 3.5 and 7.4. These solubility results suggests that $Me_{10}Tu[3]^{2+}$ or related Tu[*n*]'s may have potential in future drug delivery applications.

CITATIONS

Material from this thesis is in preparation for publication or has been presented in the following forms.

1. **Tiara[*n*]uril: a glycoluril-based macrocyclic host with cationic walls**., Chandrakumar, P. K; Dhiman, R; Woodward, C. E; Iranmanesh, H; Beves, J. E; Day, A. I. (DOI: 10.1021/acs.joc.8b02913.).

2. **Tetrahydrothiophenetiara[*n*]uril: Glycoluril based macrocyclic host with cationic walls**., Dhiman, R., Day, A. I; RACI Organic Chemistry Conference "Organic 18", Perth, Australia, 2018.

3. **Glycoluril derived cucurbituril analogues and the Emergence of most recent example of Tiara[*n*]uril**., Dhiman. R., Day, A. I - Manuscript under preparation.

CHAPTER 1
INTRODUCTION

1.1 General introduction

In nature, various well-crafted examples of macromolecules and their assemblies exist that primarily rely on reversible non-covalent interactions for their catalytic and molecular recognition properties.[1] Similarly, these reversible intermolecular forces form the basis of supramolecular chemistry for creating self-assemblies.[2] In 1987, the Nobel prize for Chemistry awarded to Donald J. Cram, Jean-Marie Lehn and Charles J. Pederson marked the establishment of supramolecular chemistry with equitable synthetic capability as traditional chemistry.[3-5] Since then, this field has gained considerable interest among various interdisciplinary research areas. Among them, a significant research area of supramolecular chemistry is the design and synthesis of macrocyclic compounds that act as molecular containers with specific recognition properties.[6] These macrocycles serve as structural and functional building blocks that can encapsulate guest molecules within their cavities thereby altering their properties. Besides, these cavities can be chemically manipulated to fine-tune their properties. The most popular classes of macrocyclic compounds that have been best investigated include cyclodextrins, calixarenes, crown ethers, and cucurbiturils. Despite relatively poor recognition properties, cyclodextrin remains as the receptor of choice for industrial applications owing to economically viable biosynthetic procedure, commercial availability and biocompatibility.[7-8] This indicates that there is much scope for advancement in the synthesis of macrocyclic hosts with distinct recognition properties and practical applications. In general, this chapter focuses on various glycoluril-based supramolecular hosts and related compounds.

1.2 Cucurbit[*n*]uril

The cucurbit[*n*]uril (abbreviated as Q[*n*] hereafter, *n* = the number of repetitive glycoluril units) are the family of robust macrocyclic hosts of which the first member was reported by Behrend et al. in 1905.[9] Q[6], the first member of Q[*n*] homologue series to be discovered, was formed as a self-assembled product of glycoluril and formaldehyde under acidic conditions. It was not until 1981 when Mock and co-workers reinvestigated and uncovered the structural constitution of Q[6]. Q[6] was described as a macrocycle consisting of six repetitive glycoluril units connected by twelve methylene bridges. It was named as "cucurbituril" due to its structural resemblance to a pumpkin, a member of the botanical family *cucurbitaceae.*[10] With emerging interest in Q[*n*] chemistry, Kim and Day groups used modified reaction conditions and successfully isolated Q[5], Q[7], Q[8] - three new members of the Q[*n*] family (Figure 1.1).[11-12]

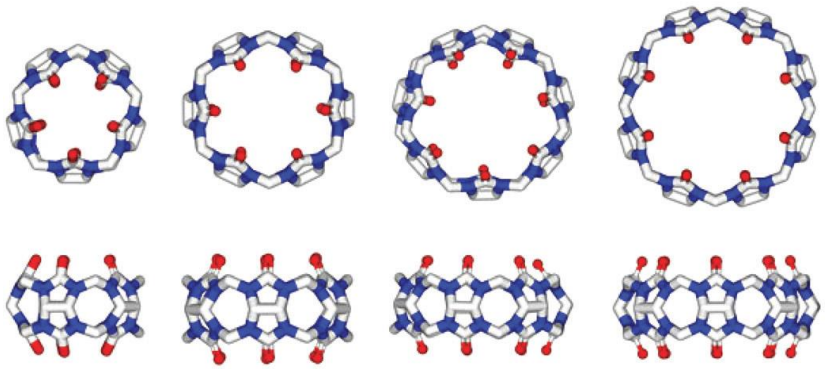

Figure 1.1 The X-ray crystal structures of Q[5-8] left to right respectively. Reprinted from ref 13 with copyright permission from Royal Society of Chemistry.

Day and co-workers reported Q[10] as an inclusion complex, (Q[5]@Q[10]) and purified it using 1,12-diaminododecane to displace Q[5] (Figure 1.2).[14-15] Later, Isaacs's group employed an alternative method using melaminediamine to displace Q[5] followed by a reaction with acetic anhydride to obtain pure Q[10].[16] More recently, Tao and co-workers

reported twisted Q[*n*] (tQ[*n*]) consisting of 13-15 glycoluril units. The distinct twisted structural feature imparts chirality to the macrocycle depending on the direction of twist (Figure 1.2).[17-18]

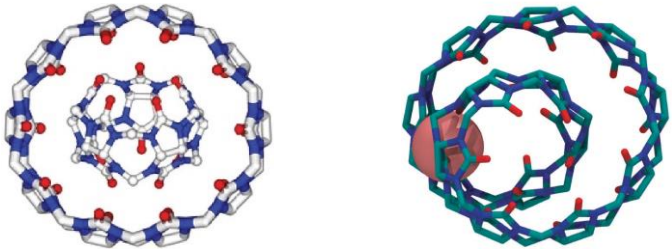

Figure 1.2 The X-ray crystal structure of Q[5]@Q[10] (left) [Reprinted from ref 13 with copyright permission from Royal Society of Chemistry] and a top view of Eu^{3+}- tQ[14] complex (right).[19]

1.2.1 Synthesis and mechanism of Q[*n*] formation

The synthesis of Q[*n*] involves the condensation reaction between unsubstituted glycoluril (R_1 and R_2 = H) and formaldehyde (H_2CO) under acidic conditions (Scheme 1.1)

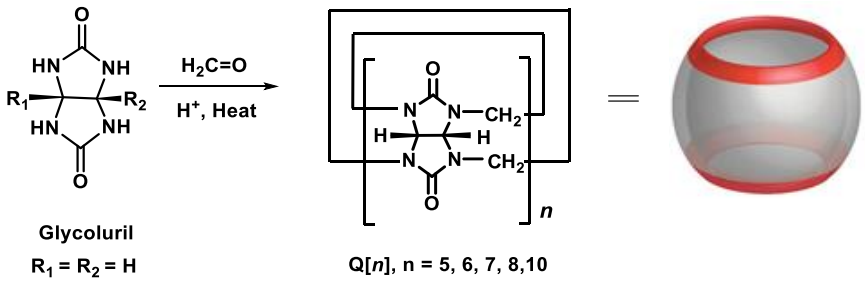

Scheme 1.1 Synthetic scheme for Q[n] formation

The current state-of-the-art in the understanding of Q[*n*] formation has progressed extensively and is mainly drawn from the work of the Day and Isaacs groups.[12, 20-21] The

first step involves the formation of dimer by linking two glycoluril units through methylene linkers. This results in the formation of the diastereomeric mixture of thermodynamically stable C-shaped and kinetically favoured S-shaped glycoluril dimers. Further, the oligomers longer than dimer are formed by the combination of chain-growth (successive addition of glycoluril monomer to growing oligomeric chain) and step-growth (condensation of two oligomers forming longer oligomers) polymerization processes. As only the C-shaped diastereomer undergo cyclization to form Q[*n*], the kinetically favoured S-shaped oligomers undergo intramolecular transformation to thermodynamically stable C-shaped oligomers.

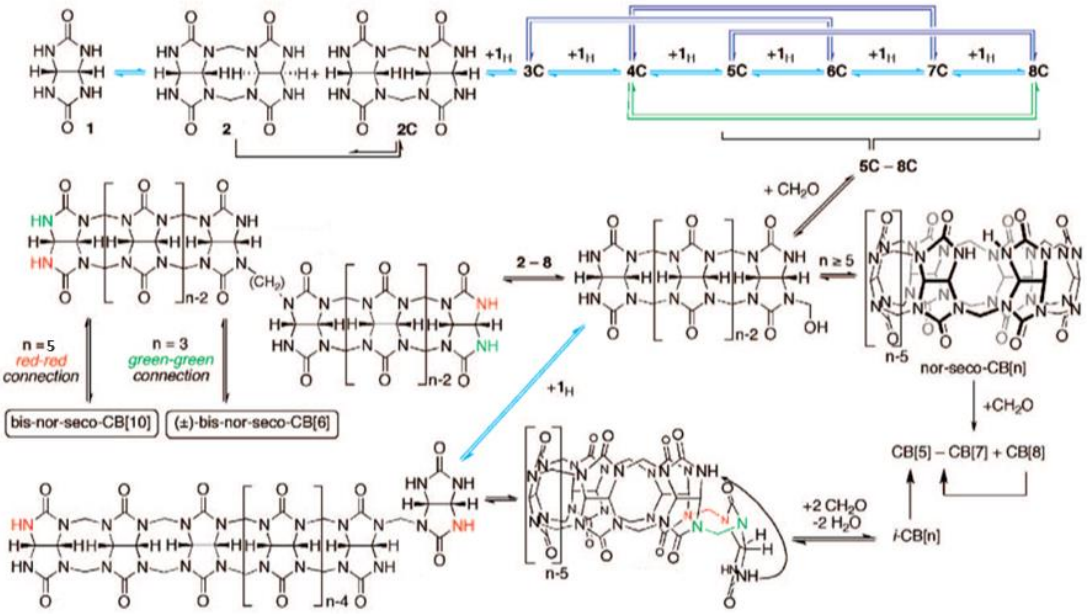

Figure 1.3 Representation of essential elements of mechanism of Q[n] formation. Chain-growth polymerization (aqua arrows) and step-growth polymerization (purple arrows). Reprinted with permission from ref 21. Copyright @ 2011 WILEY-VCH Verlag GmbH & Co. KGaA, Weinheim.

Moreover, when the C-shaped oligomers reaches the appropriate length of pentamer or longer the oligomers undergo macrocyclization forming various cyclic intermediates suchas nor-seco-Q[6] in chain-growth, bis-nor-seco-Q[10] and (±)-bis-nor-seco-Q[6] in

step-growth polymerization processes that ultimately forms respective Q[*n*] (Figure 1.3).[21]

1.2.2 Fundamental properties of Q[*n*]

1.2.2.1 Dimensions

Q[*n*] are symmetrical cyclic oligomers formed from *n* repetitive glycoluril units. The number of repeating glycoluril units constituting Q[*n*] determines the cavity size of each member, which in turn governs the nature, and size of the guest to be encapsulated. The depth of the Q[*n*] homologues remains constant while the portal and cavity diameter and the cavity volume increase systematically from Q[5] to Q[10] (Table 1.1).[22]

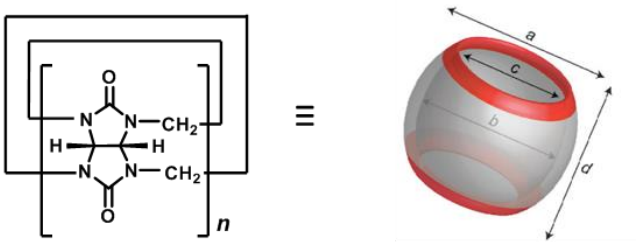

Q[*n*]: n = 5, 6, 7, 8, 10

***Table 1.1 Dimensions of Q[n]*[22]**

	Q[5]	**Q[6]**	**Q[7]**	**Q[8]**	**Q[10]**
Outer diameter (Å) - a	13.1	14.4	16.0	17.5	17.5
Cavity diameter (Å) - b	4.4	5.8	7.3	8.8	10.7-12.6
Portal diameter (Å) - c	2.4	3.9	5.4	6.9	9.0-11.0
Depth (Å) - d	9.1	9.1	9.1	9.1	9.1
Cavity volume (Å^3)	82	164	279	479	870

1.2.2.2 Stability

Q[*n*] homologues are characterized by high chemical and thermal stability. Day et al. reported the relative thermal stability of Q[*n*] in concentrated HCl at 100 °C with no detectable decomposition for Q[5] to Q[7] for at least 24 hr. Contrary, Q[8] decomposed to smaller homologues under identical conditions.[12] In addition, thermal gravimetric analysis demonstrated no decomposition up to 420 °C for Q[*n*] (*n* = 5, 6, 8), while Q[7] decomposed at the lower temperature of 370 °C.[23] Furthermore, Q[*n*] constructs are endowed with higher chemical stability that poses a limitation on approaches to direct methods for functionalization of Q[*n*].[22]

1.2.2.3 Solubility

Solubility in aqueous solution is crucial to various biological applications. The relatively low solubility of Q[*n*] in water and organic solvents is the potential limitation towards expanding their applications. Q[5] and Q[7] (20-30 mM) possess moderate aqueous solubility, whereas Q[6] and Q[8] (0.018 mM and < 0.01 mM) exhibits low solubility in water. Considerable enhancement in solubility is achieved in the presence of ammonium ions, alkali and alkaline earth metals.[7, 24] Q[10] has low solubility in water (< 50 μM) whereas twisted Q[*n*]'s have good water solubility which is in contrast to the conventional Q[*n*]'s.[16, 18]

1.2.2.4 Acidity

Q[*n*] are weak bases due to the presence of electronegative carbonyl portals that functions as proton acceptor. The pK_a value of the conjugate acid of Q[6] and Q[7] has been measured to be 3.02 and 2.2, respectively.[25-26] Although the pK_a values of other Q[*n*]

(n = 5, 8, 10) have not been reported, the systematic variation in the number of carbonyl groups may impart slight change in the acidity with respect to Q[6] and Q[7].

1.2.3 Functionalization or substitution of Q[*n*]

Although extensive research has been established for the unsubstituted Q[*n*], however, they are restricted in their practical applications due to their poor solubility in common solvents. Functionalization is one possible way to modify the solubility profile to a wide range of solvent systems. In addition, manipulation of the electronic properties of the cavity and portal through substitution can possibly influence the host-guest recognition behaviour and could provide a route to the formation of new supramolecular structures with diverse applications.[27] In principle, the substitution on Q[*n*] can be achieved following two approaches. The first method involves the use of substituted glycoluril or its diether derivative and the second method involves direct functionalization of unsubstituted Q[*n*]. Both methodologies afford fully and partially substituted Q[*n*].

1.2.3.1 Fully substituted Q[*n*] from substituted glycoluril

The first approach employs glycoluril or its cyclic diether bearing substitution at the equatorial position for the synthesis of fully substituted Q[*n*] (Scheme 1.2).

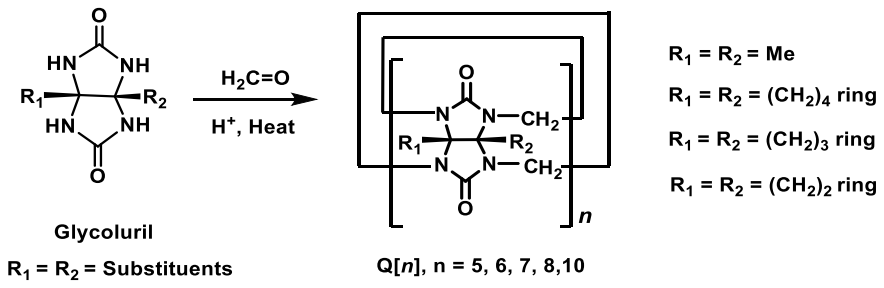

Scheme 1.2 Synthetic scheme for substituted Q[n]

The first example of fully substituted Q[*n*], Me_{10}Q[5] (Scheme 1.2, $R_1 = R_2 = Me$) was reported by Stoddart et al. in 1992. Me_{10}Q[5] was formed as the primary product with poor solubility in common solvents. In a later study (2004), Me_{12}Q[6] was also isolated but with only 2% yield.[28-29] Following the first example of fully substituted Q[*n*], Kim et al. successfully synthesized the cyclohexanoQ[*n*], (CyH_5Q[5] and CyH_6Q[6]) (Scheme 1.2, $R_1 = R_2 = (CH_2)_4$ ring). CyH_5Q[5] dominated the product distribution with about 10% yield for CyH_6Q[6]. Compared to methyl substitution, these homologues were reported to have increased solubility in water and organic solvents.[30] Later in 2012, Day et al. reported the first example of fully substituted Q[*n*] family that provided access to homologues higher than Q[6]. Use of cyclopentanoglycoluril (Scheme 1.2, $R_1 = R_2 = (CH_2)_3$ ring) along with templating Li^+ ion biased the product distribution towards higher homologues and afforded CyP_5Q[5], CyP_6Q[6] and CyP_7Q[7] in 45%, 38% and 16% yields, respectively.[27] The formation of substituted Q[8] has been the most recent success in the pursuit of higher homologues of fully substituted Q[*n*]. Successfully demonstrated by Day et al., the cyclobutanoglycoluril diether (Scheme 1.2, $R_1 = R_2 = (CH_2)_2$ ring) afforded CyB_5Q[5], CyB_6Q[6], CyB_7Q[7] and CyB_8Q[8] with relative yields of 35-40%, 44-50%, 10-12% and 3-5% by weight, respectively.[31]

The successful outcomes mentioned in the above section of substituted Q[*n*] demonstrates the effect the substitution can have on the distribution of higher homologues of Q[*n*]. This aspect of substitution is discussed in detail in Chapter 2 of the thesis.

1.2.3.2 Fully substituted Q[*n*] through direct functionalization

The second approach involves the direct functionalization of the unsubstituted Q[*n*]. Due to the high chemical stability of Q[*n*], this approach appeared unrealistic; however, attempts made by Kim et al. resulted in a positive outcome. It was reported that the use

of the oxidant $K_2S_2O_8$ in water resulted in direct functionalization of Q[5-8] forming perhydroxylated Q[*n*] (Scheme 1.3).

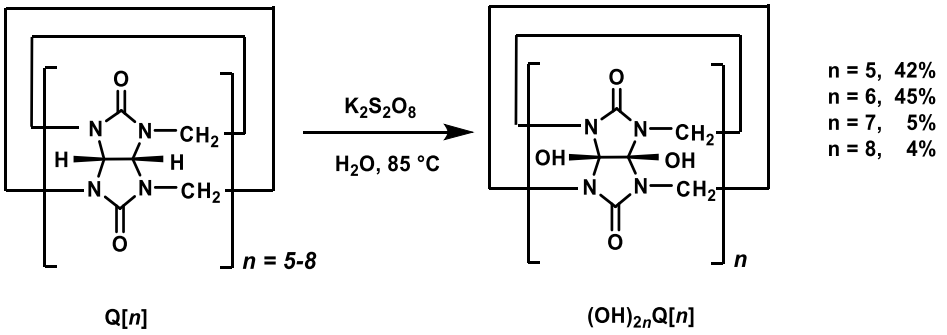

Scheme 1.3 Direct functionalization of Q[n]

However, the yields of the product for higher homologues Q[7] and Q[8] were much lower compared to the smaller homologues Q[5] and Q[6] which accounted for 42% and 45% yields, respectively. The perhydroxylated Q[*n*] paved the way for further functionalization and was demonstrated by synthesizing a thiol-ether derivative of Q[6] from $(HO)_{12}$Q[6]. The synthetic scheme involved a reaction between $(HO)_{12}$Q[6] and allyl bromide in the presence of NaH, followed by photochemical reaction with pentanethiol, affording thio-ether substituted Q[6].[32] This represented the first example of direct covalent derivatization at Q[*n*].

1.2.3.3 Synthesis of partially substituted Q[*n*] using substituted glycoluril

The partially substituted Q[*n*] has been explored with an objective to obtaining larger Q[*n*] homologues equipped with different functionalities or to alter the Q[*n*] cavity shape through positional substitution.[22] Scheme 1.4 illustrates three different methods for the synthesis of partially substituted Q[*n*] involving the use of substituted and unsubstituted glycoluril units. These methods form a complex mixture of partially substituted Q[*n*]

along with unsubstituted Q[*n*], each method requiring the isolation of product using a variety of different purification techniques.

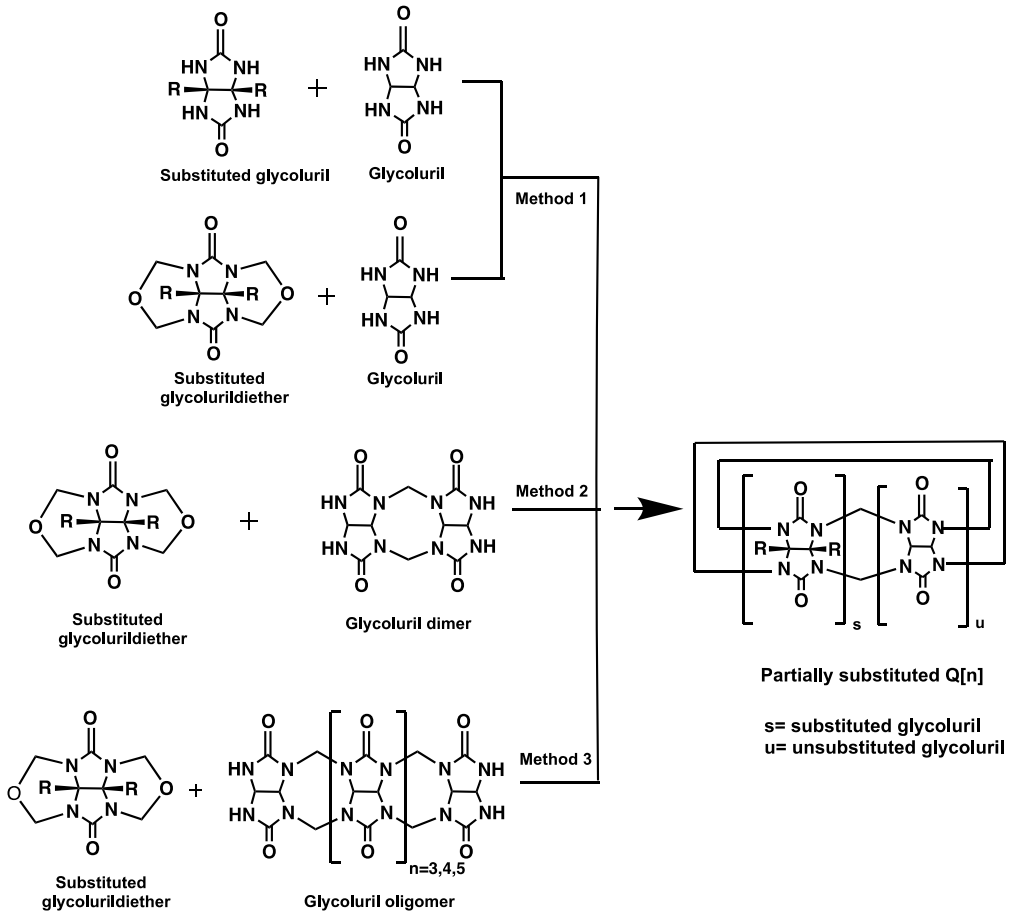

Scheme 1.4 Synthetic scheme for partially substituted Q[n]

The **method 1** utilizes the combination of substituted glycoluril or its diether and unsubstituted glycoluril. In 2002, Nakamura and co-workers synthesized unsymmetrical partially substituted Q[*n*] wherein the co-oligomerisation reaction between diphenylglycoluril and unsubstituted glycoluril in the ratio 1:5 formed $Ph_2Q[6]$ and Q[6] along with minimal amount of $Ph_4Q[6]$ (Scheme 1.5).[33]

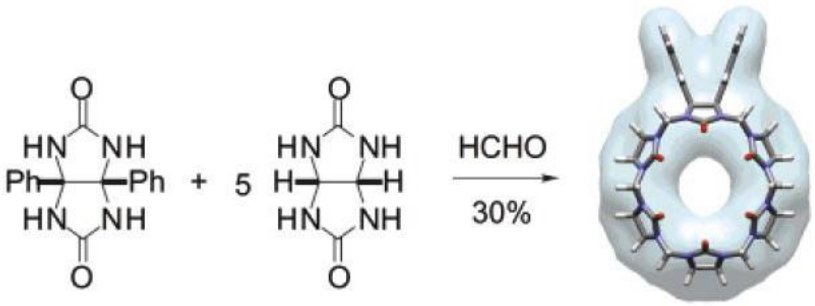

Scheme 1.5 Synthetic scheme for Ph_2Q[6]. Reprinted with permission from ref 33. Copyright @ 2002, American Chemical Society.

Following this example of partially substituted Q[*n*], Day et al. demonstrated a method for introducing higher orders of substitution in partially substituted Q[*n*]. The synthetic procedure involved the condensation of dimethylglycoluril diether and unsubstituted glycoluril forming symmetrical hexamethylQ[6] (Me_6Q[6]) as major product along with a range of other substitution patterns for the homologues 5-7. In this reaction it was reported that the substitution pattern for Me_6Q[6] had each alternate glycoluril moiety carrying substitution.[34] Similar to this, Tao and co-workers reported two symmetrical tetracyclopentanoQ[6] (TCyPQ[6]) and meta-tricyclopentanoQ[6] (m-TriCyPQ[6]) hosts. These were synthesized from 2:1 and 1:1 ratio of cyclopentanoglycoluril diether and unsubstituted glycoluril, respectively.[35] Further, Dognon et al. reported the synthesis of four new partially substituted cyclohexylQ[6] with increased water solubility compared to conventional Q[6]. The enhanced solubility was attributed to the number of cyclohexyl units present in each partially substituted Q[*n*]. Each unit increased the water solubility by a factor of 170 by limiting the formation of intermolecular C-H···O hydrogen bonds.[36]

The **method 2** involves the reaction between substituted glycoluril diether and glycoluril dimer. A symmetrical tetramethylQ[6] (TMeQ[6]) synthesized from the acid catalyzed reaction between dimethylglycoluril diether and glycoluril dimer (1:1 ratio) was reported

by Day et al. in 2004. In contrast to the regular spheroidal cavity shape, TMeQ[6] was reported to be ellipsoidal. The altered cavity shape was predicted to be a subtle angle influence at the point of substitution. TMeQ[6] displayed good water solubility which enabled investigating the host-guest chemistry.[37] Another example of partially substituted Q[6] using the same methodology was reported by Yu et al. Four partially substituted Q[6] - ortho-tetramethylQ[6] (o-TMeQ[6]), tetracyclohexanoQ[6] (TcyHQ[6]), meta hexamethylQ[6] (m-HmeQ[6]) and para-dicyclohexaneQ[6] (p$(CyH)_2$Q[6]) were synthesized and characterized using x-ray diffraction of their guest inclusion complexes. The reported distortion of Q[6]'s cavity shape due to guest binding corresponds to the presence of substitution.[38]

The reaction between substituted glycolurils or their diethers and glycoluril oligomers constitutes the **method 3**. In 2012, Isaacs et al. presented a building block approach for the synthesis of partially substituted Q[7]. This approach involved the condensation between glycoluril diether and glycoluril hexamer resulting in a range of monofunctionalized Q[7] (Me_2Q[7], CyHQ[7], MePhQ[7] and ClBuQ[7]). Of all these monofunctionalized Q[7], Me_2Q[7] and CyHQ[7] exhibited similar guest recognition properties and enhanced water solubility compared to Q[7].[39] In another study, following the same synthetic approach, Isaacs's group synthesized the first disubstituted Q[8] (Me_4Q[8] and Cy_2Q[8]) using 2.5 mol equivalent of substituted glycoluril diether and glycoluril hexamer under acidic conditions (Scheme 1.6). Both of the derivatives displayed improved water solubility with molecular recognition properties comparable to normal Q[8].[40] The high water solubility of the resulting partially substituted Q[7], and Q[8] renders them suitable as solubilizing agents for poorly soluble drugs.[39-40]

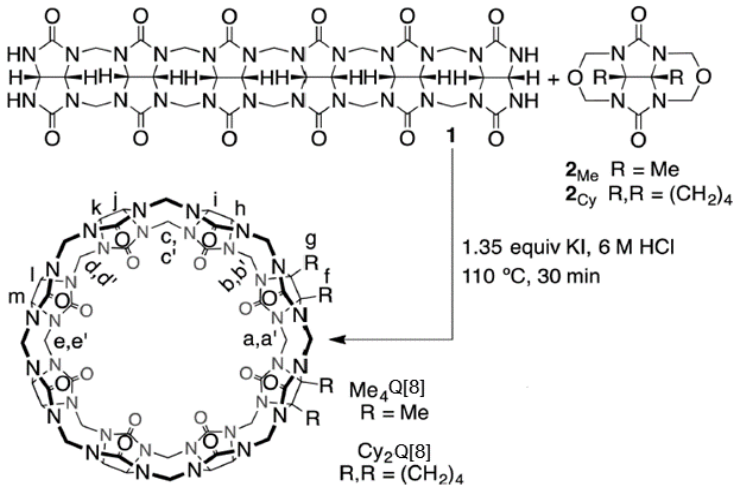

Scheme 1.6 Synthetic scheme for partially substituted Q[8]. Reprinted with permission from ref 40. Copyright @ 2015, American Chemical Society.

.

1.2.3.4 Partially substituted Q[*n*] through direct functionalization

Inspired by the work of Kim et al.[32], Scherman et al. in 2012 reported the first preparation of monohydroxyQ[6] through controlled oxidation of Q[6] in the presence of $(NH_4)_2S_2O_8$ (APS) oxidant and bisimidazolium guest (Scheme 1.7).

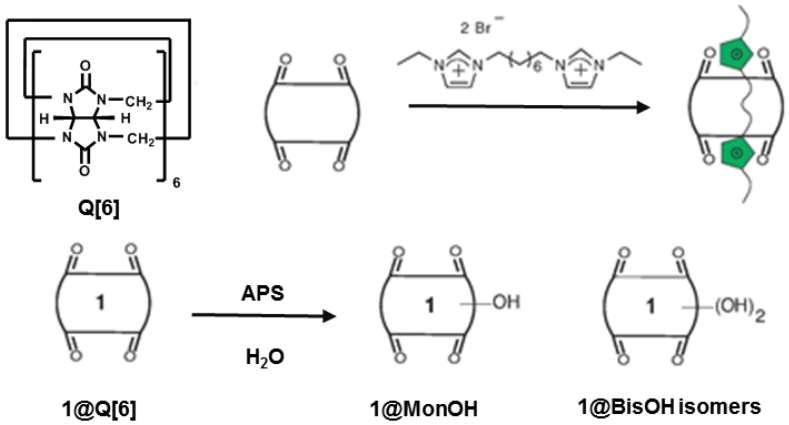

Scheme 1.7 Synthetic scheme for monofunctionalization of Q[6][41].

The guest greatly enhanced the solubility of Q[6] before oxidation and provided control over the oxidation stoichiometry and final product ratio. The mono-OH Q[6] was

subjected to further chemical modifications that afforded a pathway for new functionalized derivatives.[41]

Recently, Quari et al. demonstrated another example of monohydroxy Q[*n*]. In this case, direct functionalization of Q[5-8] was achieved through a photolysis reaction using hydrogen peroxide at 254 nm (Scheme 1.8). The resulting mono-OH Q[5-8] were formed in high yields as compared to the persulfate method employed by Scherman et al.[42]

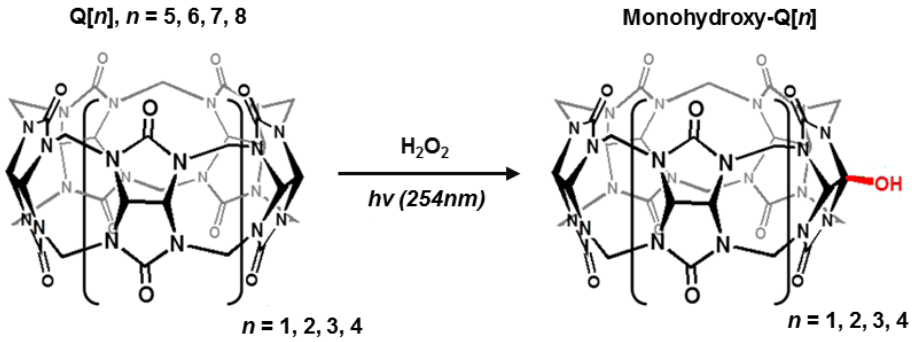

Scheme 1.8 Synthetic scheme for monohydroxy-Q[n]. Reprinted with permission from ref 42. Copyright @ 2015, American Chemical Society.

1.2.4 Host-guest recognition properties of Q[*n*]

Q[*n*] has outstanding host-guest complexation properties, attributed to its remarkable structural features. Q[*n*] are symmetrical macrocycles endowed with identical carbonyl fringed portals and hydrophobic cavity (Figure 1.1). The dipolar nature of the carbonyl portals permits interactions with cationic guests through ion-dipole, dipole-dipole and hydrogen bonding whereas the driving force for the encapsulation of guest within the hydrophobic cavity is the non-covalent hydrophobic interactions. Also, the availability of different portal and cavity sizes in Q[*n*] series broadens their binding potential to a wide range of guests.

Q[5]

Q[5] is the smallest macrocycle of the Q[*n*] family, and due to its small portal diameter (2.4 Å) and cavity volume (82 $Å^3$), the encapsulation potential of Q[5] is limited to fewer small guest molecules. Q[5] and its derivatives binds H^+, alkali, alkaline earth metals and ammonium ions through portal interactions and encapsulate a few gaseous molecules (noble gases, NO, N_2O, O_2, CO, CO_2, CH_4), solvent molecules (CH_3OH and CH_3CN) and haloalkanes (CH_3F, CH_2F_2 and CH_3Cl) within its hydrophobic cavity.[7, 43-44] Contrary to the normal affinity towards neutral and cationic guests, Q[5] and its methyl derivatives display high affinity towards anions such as NO_3^- and Cl^-, assisted by molecular capsules formed with metal ions (lanthanides, praseodymium, strontium, zinc).[45-47]

Q[6]

Q[6] is the predecessor cucurbituril, formed mainly as the major product during Q[*n*] synthesis. With dimensions slightly larger than Q[5], Q[6] potentially interacts with larger guests. Since the pioneering work by Mock et al., the host-guest properties of Q[6] have been extensively studied. Q[6] form stable complexes with alkyl and aryl substituted ammonium salts and diammonium ions especially α, ω-alkyl diammonium ions of varied chain length.[48-49] The ammonium ion interacts with the portal through ion-dipole interactions or hydrogen bonding, while the alkyl and aryl part is bound within the hydrophobic cavity of Q[6]. The binding of Q[6] with neutral guests such as THF, xenon, CF_3COOH, imidazolium-based guest molecules, amino acids, dipeptides, aromatic compounds have also been reported.[50-56] The affinity of Q[6] towards protonated aliphatic amines has been utilized in the construction of rotaxanes and pseudorotaxanes wherein Q[6] and alkyl amine act as wheel and axle respectively.[57-59] Q[6] also binds catecholamines such as adrenaline and isoprenaline which forms kinetically driven

needle-like crystals that transform to the thermodynamically stable prismatic form over a length of time.[60-61] Similar to Q[5], Q[6] also exhibits portal interactions with H^+, alkali, alkaline earth metals and have been reported to bind transition metals and lanthanides cations.[26, 62-64]

Q[7]

Q[7], the third member of the Q[*n*] family has a portal diameter (5.4 Å) and cavity diameter (7.3 Å) larger than Q[6], hence a wide range of guests can be recognized by Q[7]. The larger portal and cavity diameter affords Q[7] with an inner cavity volume of 279 $Å^3$, which is large enough to form inclusion complexes with bulkier molecules like naphthalene, ferrocene, bicyclooctanes, stilbene, viologen, o-carborane, cobaltocene and adamantylamine derivatives.[7, 65] The higher binding affinities driven by the expulsion of high energy water molecules, larger cavity volume, good water solubility (30 mM) and excellent recognition properties makes Q[7] a widely exploited Q[*n*] for aqueous specific applications. For example, the inclusion complexes of platinum-based drugs suggest the potential application of Q[7] to reduce toxicity in cancer treatment, and the water solubility of the insoluble drugs such as albendazole increases with Q[7] encapsulation.[66-67] Also, interaction of Q[7] with peptides, proteins, dyes, and biomolecules illustrates its potential in biosensing applications.[68-70] Furthermore, Q[7] has been utilized in different fields such as stimuli responsive underwater adhesives, catalysis, supramolecular energy-transfer motifs, separation techniques.[19, 71-72]

Q[8]

Q[8], due to its voluminous cavity possesses the ability to bind two aromatic guests within its cavity simultaneously. This demonstrates the cooperativity between the binding of first

and second aromatic ring forming 1:2 complexes. Kim et al. reported the formation of a hetero-termolecular complex between 2,6-dihydroxynapthalene, a pyridinium derivative and Q[8].[73] Further, numerous studies were conducted that demonstrated the double encapsulation ability of Q[8] with various guest molecules such as naphthyl derivatives, coumarin, N-phenylpiperazine, 9-aminoacridinium, anthracene derivatives, berberine, neutral red, phenylpyridinium derivatives and peptides containing tryptophan and phenylalanine residues.[65] Q[8] have also been reported to form a complex with two fullerene molecules, each bound externally at the portal.[74] Recently Day et al. investigated the effect of Q[8] encapsulation on the anticancer activity of mitoxantrone used in the treatment of breast cancer. The 2:1 complex of mitoxantrone and Q[8] displayed better anticancer activity and decreased cardiotoxic side effect of free drug in healthy mice.[75]

Q[10]

Similar to Q[8], Q[10] also forms ternary complexes with guest molecules due to its larger volume (870 $Å^3$). Isaacs et al. demonstrated this potential through two separate works that resulted in the formation of 2:1 complex with melaminediamine and metalated porphyrin respectively.[16, 76] The encapsulation of metal complexes in Q[10] have been studied in detail by Day group.[77-79] As an example, the inclusion of iridium(III)polypyridyl complex in Q[10] reported a 40-fold enhancement in luminescence intensity with prolonged emission lifetime compared to free metal complex.[77]

The above section detailed the synthetic aspects related to Q[*n*] family and the recognition properties of each Q[*n*] homologue, which vary mainly with their different cavity and portal sizes. Due to their remarkable recognition properties and high affinity binding towards the guests, Q[*n*] finds applications in diverse fields such as drug delivery, catalysis, sensing, molecular container etc.[19, 80-82]

1.2.5 Drug delivery applications of Q[*n*] and its derivatives

Q[*n*] are valuable molecular containers with excellent host-guest complexation properties that have been shown to facilitate the drug efficiency and efficacy by various means such as improved drug solubility, increased stability, increased therapeutic activity, and targeted drug delivery.[80] In literature, various examples of drugs that have been studied with Q[*n*] are reported.[81]

Of these, a few are highlighted in this section:

Albendazole is a broad-spectrum antiparasitic drug used in the treatment of parasitic diseases. In addition, it exhibits significant anti-proliferative activity against a range of tumors. However, its anti-cancer activity is limited by its low aqueous solubility. Studies performed by Day et al. investigated the effects of albendazole encapsulation in Q[6-8]. Solubility enhancement by 2000-fold was observed for Q[6] and Q[7] inclusion complexes.[67] Incorporation of partial substitution in Q[6] (Me_4Q[6]) further enhanced the solubility of encapsulated albendazole by 400 fold with respect to Q[6] encapsulated drug.[83] In another study, Day et al. examined the solubility and cytotoxicity aspects of Q[*n*] encapsulated albendazole derivative, (2-methoxyethyl) 5-propylthio-1H-benzimidazole-2-yl carbamate) (MEABZ). This derivative displayed slightly higher solubility and an enhanced cytotoxic effect in a range of cancer cell lines compared to albendazole. In addition, its inclusion complex with Q[7] and Q[8] exhibited increased solubility compared to albendazole with negligible change in MEABZ cytotoxic activity.[84] Scherman et al. demonstrated the Q[7] encapsulation effect on the stability and anticancer efficacy of tomozolomide, a primary chemotherapy drug against glioblastoma multiforme (GBM). The encapsulation resulted in decreased rate of the drug degradation

under physiological conditions along with dramatic increase in drug activity towards primary GBM cell lines (Figure 1.4).[85]

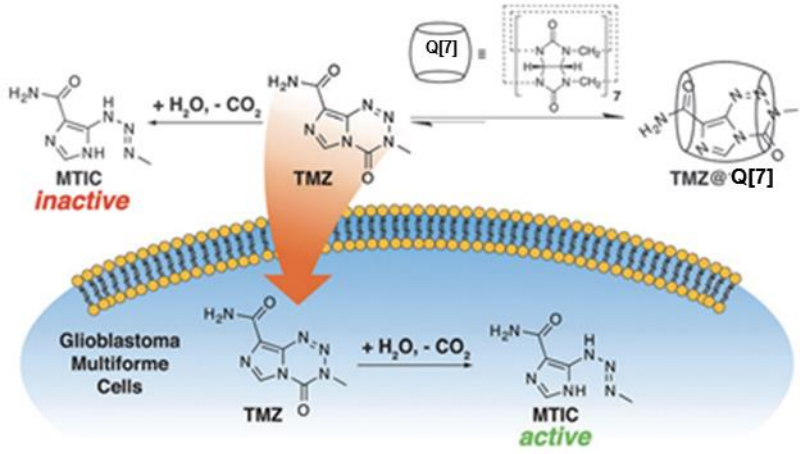

Figure 1.4 Representation of the degradation of temozolomide (TMZ) to 5-(3-methyl-triazen-1-yl)imidazole-4-carboxamide (MTIC) outside of the cell and the mechanism of stabilisation of TMZ through complexation with the nanocontainer Q[7]. Reprinted from ref 85 with copyright permission from Royal Society of Chemistry.

Another example of Q[*n*] drug delivery potential is the targeted delivery of the anticancer drug oxaliplatin. Oxaliplatin is used for the treatment of advanced colorectal carcinoma. But it is associated with peripheral neuropathy, and moderate myelotoxicity in oxaliplatin treated patients. Isaacs and co-workers synthesized a monofunctionalized Q[7] (Q[7]$(CH_2)_4Cl$), which was covalently linked to targeting ligand biotin to form Q[7]-biotin conjugate. The encapsulated oxaliplatin in the cavity of Q[7]-biotin conjugate exhibited higher in-vitro bioactivity than free oxaliplatin towards cancer cells. This effect, if translated to an in-vivo system could potentially reduce the dose-dependent side effects of the drug.[86] Apart from encapsulation of the drug within Q[*n*] cavity as specified in the above examples, other alternative approach for targeted drug delivery involved loading the drug into the core of a vesicle. One such example has been illustrated through the

work of Kim et al. A vesicle formed from an amphiphilic Q[6] derivative with a disulphide bond was modified to hold folate-spermidine conjugate (polyamine tags). It was observed that the cytotoxic effect of loaded drug doxorubicin increased due to selective cellular uptake and reduction-triggered release into the HeLa cells' cytoplasm (Figure 1.5).[87]

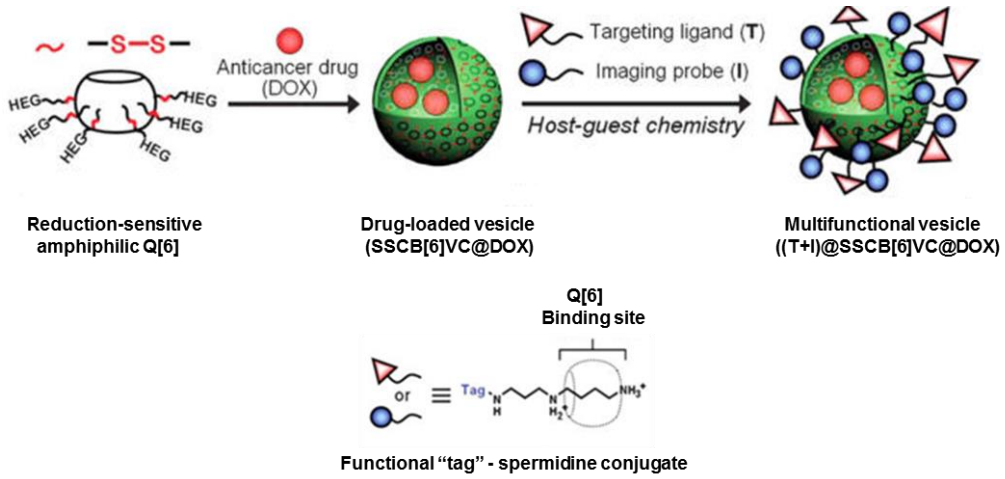

Figure 1.5 Representation of the reduction-sensitive Q[6] based vesicle (SSCB[6]VC) with noncovalently modifiable surface. Reprinted with permission from ref 87. Copyright @ 2010 Wiley-VCH Verlag.

The above section reviewed Q[*n*] applications in the context of drug delivery systems and highlighted the potential exhibited by Q[*n*] homologues as drug delivery vehicles. With the development of more new derivatives and supramolecular forms, this prospective of Q[*n*] could be expanded further to numerous other therapeutic applications.

1.2.6 Other applications of Q[*n*] and their derivatives

In addition to drug delivery aspects mentioned above, Q[*n*] and their derivatives have a broad range of applications. A variety of reported applications include new scaffolds for antibiotics[88], absorption materials for gases and volatile substances[89-90], metal

nanoparticle systems[91], catalysis[19], self-assembling systems[92], as ion channels[93], 2D-polymers[94], waste water treatment [95-97], and supramolecular bracelets.[98]

1.3 Related Q[*n*] compounds and analogues

1.3.1 Hemicucurbit[*n*]uril (HmQ[*n*])

Ethyleneurea, viewed as glycoluril cut in half along the equator has been reported in the literature to undergo a Mannich reaction with formaldehyde, forming linear oligomers.[99] In 2004, Miyahara et al. developed optimized conditions and synthesized new macrocyclic hosts using ethyleneurea as the building block, named Hemicucurbit[*n*]uril (HmQ[*n*]). The synthetic procedure involved condensing formaldehyde and ethyleneurea using 4M and 1M HCl to form HmQ[6] and HmQ[12], respectively. These homologues characteristically form an alternate arrangement of the ethyleneurea units, creating a hydrophobic cavity due to the hydrogen atoms pointing to inside of the cavity (Scheme 1.9). Consequently, these homologues accommodate anionic guests (SCN^-, I^-, Cl^- and NCO^-) through C-H···anion interactions rather than common metal ions which is in contrast to Q[*n*] host-guest chemistry.[100-101]

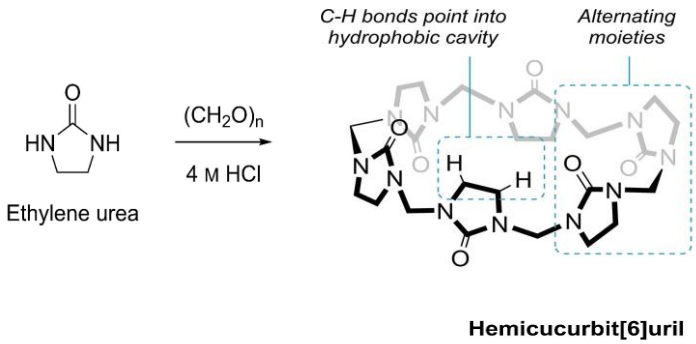

Scheme 1.9 Synthesis of HmQ[6] and its structural features. Reprinted with permission from ref 102. Copyright @ 2018 Wiley-VCH Verlag GmbH & Co. KgaA, Weinheim.

However, interaction with selected transition metals like Co^{2+}, UO^{2+}, and Ni^{2+} have been reported.[103] HmQ[6] demonstrates its application as a supramolecular catalyst in esterification and aerobic oxidation of heterocyclic compounds whereas HmQ[12] does not possess any catalytic effect.[104-105] Recently, Riina and co-workers presented the synthesis of chiral CyH_6HmQ[6] in 85% yield. The new chiral HmQ[6] formed complexes with carboxylic acids, halides, and amines, and were also found to interact with methoxyphenylacetic acid in organic medium forming diastereomeric complex.[106]

1.3.2 Bambusuril (BU[*n*])

Sindelar et al. reported a new synthetic macrocyclic host Bambus[*n*]uril (BU[6]), obtained from the condensation reaction between 2,4-dimethylglycoluril and formaldehyde using 5.4 M HCl in 30% yield. The X-ray crystal structure illustrates six repetitive glycoluril units linked by a flexible single row of methylene bridges. The glycoluril units are arranged in an alternate configuration, with a convex face where the methine protons point to the inside, creating an electropositive cavity deeper than Q[*n*] (Figure 1.6).

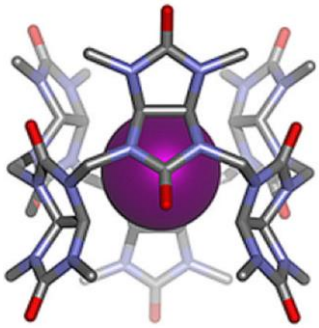

Figure 1.6 The X-ray crystal structure of BU[6] with encapsulated iodide ion. Reprinted with permission from ref 102. Copyright @ 2018 Wiley-VCH Verlag GmbH & Co. KgaA, Weinheim.

Even though the structural features of BU[6] are comparable to Q[6] (carbonyl portals) and to HmQ[6] (alternate arrangement), they however, possess distinct physical and supramolecular properties. BU[6] exhibits high affinity towards halide ions in the preference $I^- > Br^- > Cl^- > F^-$ in aqueous and organic media, indicating selective binding ability. The inclusion of anions has been attributed to the significantly positively charged cavity that stabilizes anions through 12 C-H···A^- hydrogen bonds. While the cavity encapsulation of the halide ion decreased the water solubility of BU[6] (0.02 gL^{-1}), solubility enhancement was observed in a mixture of methanol and chloroform.[107]

Of importance is the possibility of substitution at the 2,4-positions of the glycoluril which allows the formation of different BU[*n*] derivatives with tuned solubilities. For instance, replacement of the methyl group with a benzyl substituent resulted in macrocycles Bn_{12}BU[6] and Bn_8BU[4], the former being soluble in chloroform.[108] Conversely, the analogous compound with 4-carboxybenzyl substitution in Bn_{12}BU[6] (Figure 1.7) has solubility in neutral and basic aqueous solution and is the first water soluble BU[*n*].[109]

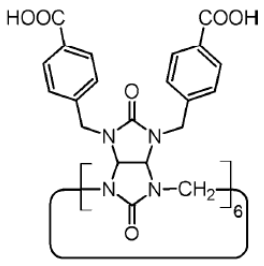

Figure 1.7 The structure of water-soluble bambus[6]uril. Reprinted with permission from ref 109. Copyright @ 2015 Wiley-VCH Verlag GmbH & Co. KgaA, Weinheim.

Recently, other successful attempts to prepare bambusuril derivatives have been reported. Heck et al. described the preparation of allylbambus[*n*]uril derivatives and their further modification by cross-metathesis, enabling selective monofunctionalization (Figure 1.8).[110] Similar to this work, Reany and co-workers synthesized semithiobambusurils,

with half of the carbonyl groups replaced with thiocarbonyl moieties. In addition to anion binding ability, the resulting modified bambusurils were able to interact with thiophilic metal cations due to the presence of sulphur moeities.[111-112]

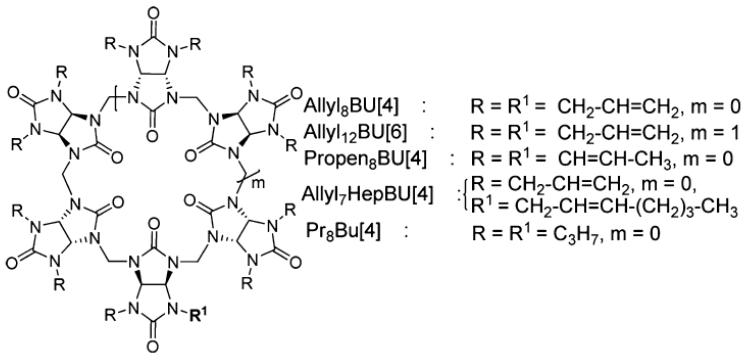

Figure 1.8 Representation of different substituted BU[n]. Reprinted with permission from ref 110. Copyright @ 2013, American Chemical Society.

These reports of HmQ[*n*] and BU[*n*] are examples that manifest the ability to tailor properties such as their recognition behaviour towards different guests, through functionalization similar to Q[*n*].

1.3.3 Cucurbit[*n*]uril analogues

The detailed study of the mechanistic pathway for Q[*n*] formation by Isaacs and co-workers provided access to different reaction intermediates such as dimers and oligomers of glycoluril and their diether derivatives.[21] This facilitated tailor-made synthesis of Q[5-7] analogues with control over shape, size, solubility and functionalization pattern. The synthetic approach involved a condensation reaction between a nucleophilic glycoluril surrogate, such as bis(phthalhydrazide) and substituted glycoluril diether (monomer, dimer or trimer) substituted with ester, carboxylic acid or imide functional groups (Scheme 1.10). These analogues exhibits enhanced solubilities in water and organic solvents that related to the presence of different functional groups. Contrary to

conventional Q[*n*]'s, these analogues are kinetically formed products, hence chemically unstable and possess elongated, oval shaped cavities that differs in cavity length and volume with respect to Q[*n*] analogues.[113-114] The incorporation of bis(phthalhydrazide) walls in these Q[*n*] analogues render them with inherent fluorescent properties, allowing investigation of host-guest complexation using UV/Vis and fluorescence spectroscopy. By observation using the fluorescence technique, Q[6] analogues displayed superior recognition properties towards alkanediamines of longer chain length, nitro aromatics, amino acids and nucleobases with association constants up to $K_a \approx 10^6\ M^{-1}$.[115] In addition, Q[6] analogues exhibits higher binding affinity towards benzene ($K_a \approx 10^4\ M^{-1}$) and Nile Red ($K_a \approx 10^6\ M^{-1}$).

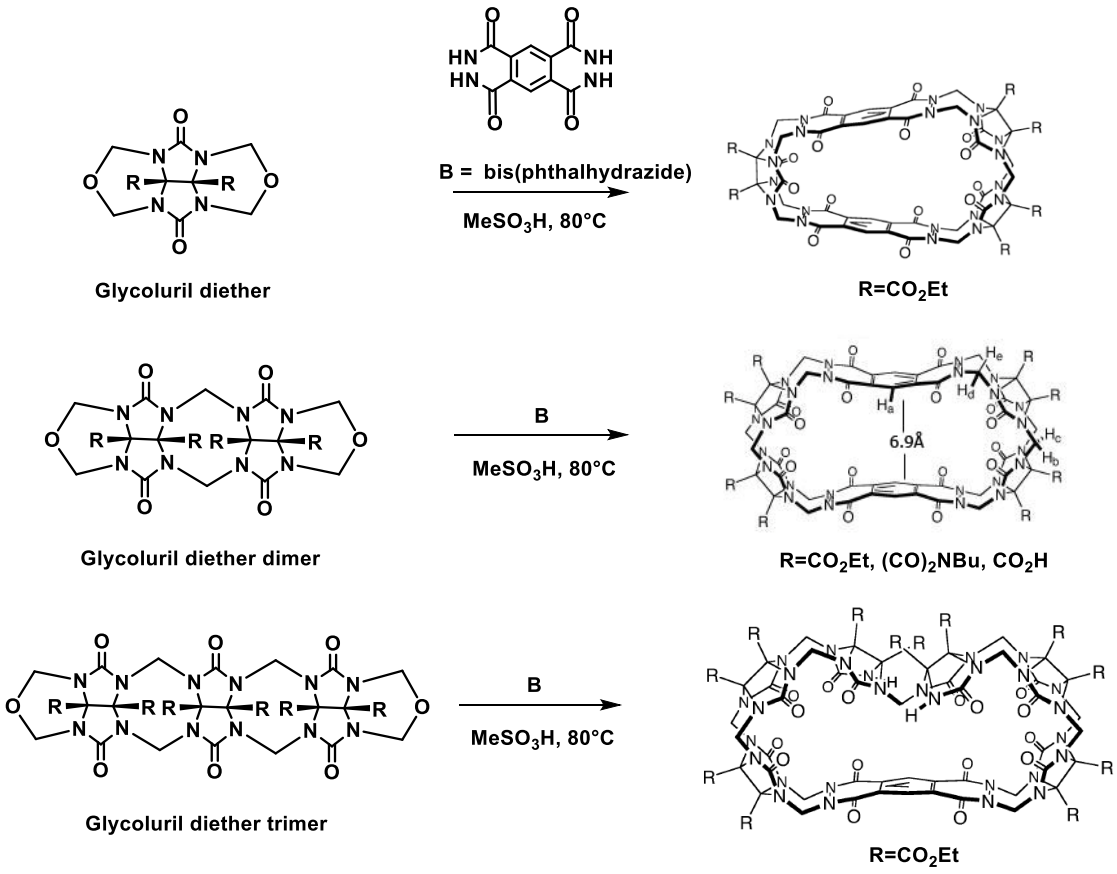

Scheme 1.10 Synthetic scheme for Q[5-7] analogues. Adapted with permission from ref 113. Copyright @ 2003, American Chemical Society.

The stronger binding affinities towards guests, particularly aromatics, corresponded to the partial aromatic nature of the analogue walls, allowing π-π interactions.[116] Due to the distinct structural features, these analogues could potentially be used as fluorescent molecular sensors.

In addition to the above stated Q[*n*] analogues, some recent Q[*n*] analogues have been reported. Inspired by Nolte et al. work on propanediurea derived molecular clips[117], Sindelar and co-workers attempted to synthesize a macrocycle employing propanediurea as a building block. The optimized synthetic procedure involved reaction between propanediurea and paraformaldehyde in the ratio 1:3.1 under acidic conditions (Scheme 1.11). The resulting product was a five membered macrocycle termed as decamethylpressoQ[5] (Me_{10}PrQ[5]). Me_{10}prQ[5] differs slightly in dimensions to normal Q but has comparable water solubility and thermal stability with respect to Q[5] and Me_{10}Q[5]. The recognition property of Me_{10}prQ[5] was investigated towards methane and was compared to Q[5] and Me_{10}Q[5]. Interestingly, the CH_4@Me_{10}prQ[5] complex demonstrated 3 and 1.5 times more stability than CH_4@Q[5] and CH_4@Me_{10}Q[5] complexes, respectively.[118] The synthesis of the same molecule was also reported by Wang and co-workers.[119]

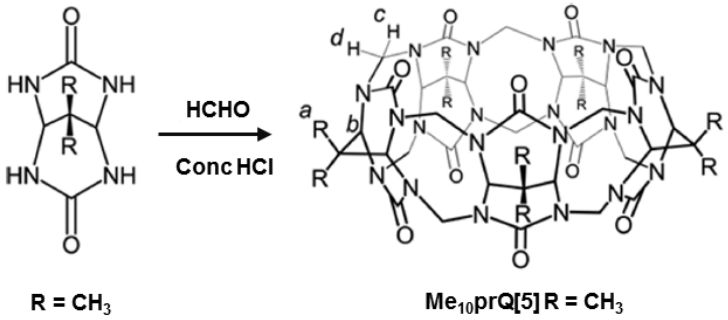

Scheme 1.11 Synthetic scheme for Me_{10}prQ[5]. Reprinted with permission from ref 118. Copyright @ 2015, American Chemical Society.

Following this, the Wang group reported the synthesis of two helianthus-like Q[*n*] analogues, $CyP_4TD[4]$ and $CyP_5TD[5]$, from the acid catalyzed reaction between cyclopentanopropanediurea (CyP-TD) and formaldehyde. Of the two analogues, $CyP_5TD[5]$ displayed better solubility in water and organic solvents compared to $CyP_4TD[4]$.[120] Further, Tian et al. presented another study involving the synthesis of propanediurea based Q[*n*] analogue, which is the first example of the smallest Q[*n*] analogue. They synthesized $Me_8TD[4]$ (Figure 1.9) through template directed condensation of dimethylpropanediurea and formaldehyde under acid catalysed conditions. $CaCl_2$ was used as a template and the pure product isolated in 2% yield. The cavity dimensions of $Me_8TD[4]$ are considerably reduced compared to Q[5] and it possesses an excellent binding affinity towards Ag^+ ion (10^6 M^{-1}).[121] Similar to this work, Wang and co-workers reported another example of Q[*n*] analogue, TD[4] and TD[5] formed from propanediurea and formaldehyde condensation using $CaCl_2$ and $BaCl_2$ templates, respectively.[122] Yet in an another work, Wang's group synthesized two new Q[*n*] analogues, NH-ns-TD[4] and bis-ns-TD[8] (Figure 1.9), formed as a result of series of optimisation studies. The maximum yield was achieved by using HCl (>3M) and Ca^{2+} (0.14 equivalents relative to propanediurea).

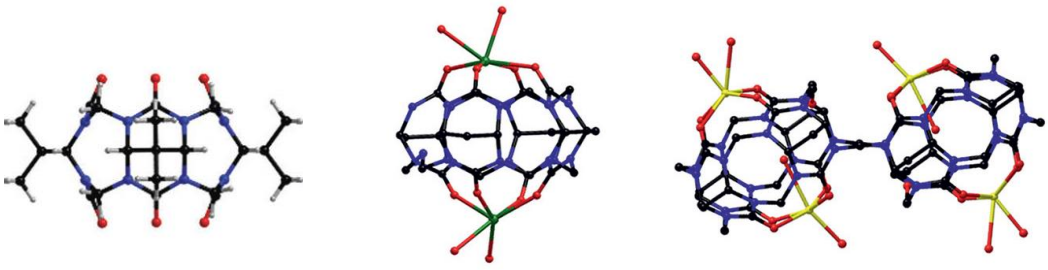

Figure 1.9 Crystal structures of $Me_8TD[4]$, NH-ns-TD[4].2$CaCl_2$ and bis-ns-TD[8].4NaCl left to right respectively. [121, 123]

The structural features are comprised of reactive secondary NH and functional ureidyl groups for NH-ns-TD[4] and two equivalent cavities for bis-ns-TD[8], thereby, making them suitable for further modifications to form functionalized derivatives or supramolecular constructs.[123]

1.4 Cucurbit[*n*]uril congeners

The Q[*n*] synthesis involves a stoichiometric balance (1:2 molar ratio) between glycoluril and formaldehyde. The in-depth exploration of the underlying mechanism of Q[*n*] formation by Isaacs and co-workers provided insight into the existence of various Q[*n*] congeners. These congeners were discovered and isolated from formaldehyde starved reaction processes.[21]

1.4.1 Macrocyclic Q[*n*] congeners

1.4.1.1 Nor-seco-Q[6] (ns-Q[6])

According to IUPAC nomenclature, "nor-sec" implies the deletion of CH_2 group from the parent compound. ns-Q[6] serves as one of the final intermediates in the synthetic pathway to Q[6] formation and structurally differs by having one missing CH_2 linker from Q[6] (Figure 1.10). However, ns-Q[6] retains similar recognition properties as Q[6].[21] In general, aldehydes (except formaldehyde) are not reactive enough to undergo Q[*n*] formation.[124] However, this receptor interestingly functions as the first aldehyde reactive Q[*n*] synthon. Under acidic conditions, ns-Q[6] reacts with o-phthalaldehyde forming ns-Q[6] derivative with different upper and lower portal sizes that markedly influence its binding properties (Figure 1.10). Similar to ns-Q[6], this derivative forms diastereoselective complexes with unsymmetrical guests and additionally exhibits the

unique ability to assist back-folding of long-chain alkanediammonium ions in water due to non-identical portals.[125]

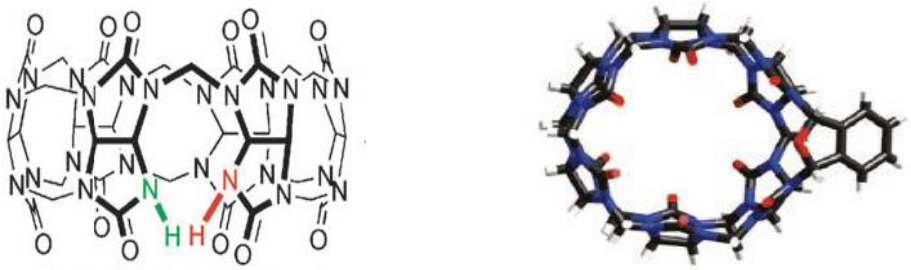

Figure 1.10 Nor-seco-Q[6] (left)[21], o-pthalaldehyde derivative of nor-seco-Q[6] (right) [Reprinted with permission from ref 125. Copyright @ 2008, American Chemical Society].

1.4.1.2 (±)-Bis-nor-seco-Q[6] (bis-ns-Q[6])

Contrary to conventional and substituted Q[*n*], (±)-bis-ns-Q[6] presents the first chiral congener of the Q[*n*] family. It is formed based on a step-growth process involving condensation of two glycoluril trimers followed by macrocyclization (Figure 1.11). The macrocyclic molecule is characterized by having deformed portals with reduced electrostatic potential due to two intramolecular NH···O=C hydrogen bonds. This leads to diminished affinity of (±)-bis-nor-seco-Q[6] towards cationic guests, while its cavity size was determined to be in between Q[6] and Q[7].[21, 126] Also, these constructs exhibit diastereoselectivity towards chiral amines, amino acids, amino alcohols and meso-diamines, thereby, enhancing their application by enabling the formation of enantioselective molecular devices.[127]

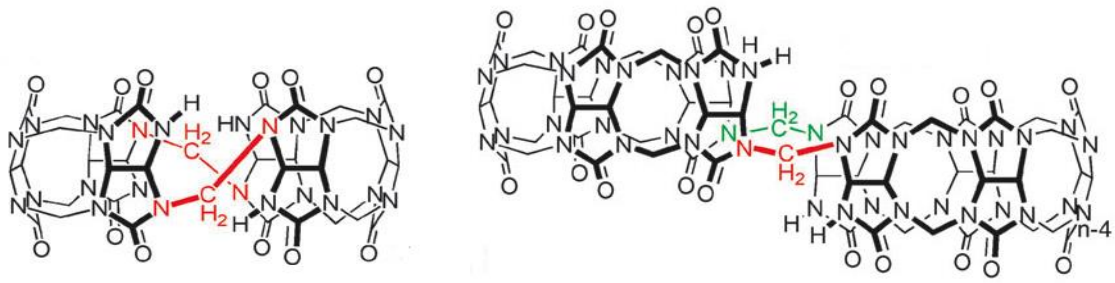

Figure 1.11 Representation of (±)-bis-nor-seco-Q[6] (left) and bis-nor-seco-Q[10] (right).[126]

1.4.1.3 Bis-nor-seco-Q[10] (bis-ns-Q[10])

bis-ns-Q[10] is formed in a similar way to (±)-bis-ns-Q[6] except that two C-shaped glycoluril pentamers are involved.[21] The structural features constitute two symmetry equivalent cavities that are not in register vertically with off-set carbonyl portals (Figure 1.11). The two cavities allow the formation of ternary (1:2) complexes with common guests of Q[*n*] such as ammonium and diammonium compounds. Perhaps more importantly, this macrocycle displays homotropic allosteric phenomenon during interaction with guest molecules whereby binding of the first equivalent of guest would pre-organize the second binding site for an identical guest. The pre-organization is indicated by change in the nonbonded $CH_2 \cdots CH_2$ distance between the two single methylene bridges linking both cavities, which in turn depends on the guest size. (Figure 1.12). This behaviour was demonstrated by formation of only homomeric complexes when a mixture of two guests quite different in size interacts with bis-ns-Q[10]. Conversely, with a mixture of similarly sized guests both homomeric and heteromeric ternary complexes were observed.[128]

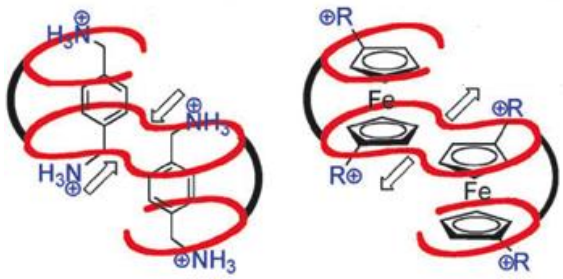

Figure 1.12 Homotropic allosterism observed in the host-guest interactions of bis-nor-seco-Q[10]. The nonbonded $CH_2\cdots CH_2$ distance indicated by the arrows decreases for the smaller guest p-xylenediammonium and increases for the larger ferrocene guest.[126]

1.4.1.4 Inverted Q[*n*] (n = 6, 7)

The inverted Q[6] and Q[7] (iQ[6], iQ[7]) are structurally distinguished by the presence of a single glycoluril unit with its convex face pointing into the cavity (Figure 1.13). These were isolated from normal Q[*n*] reaction mixture in low yields of 2.0 and 0.4% respectively. iQ[*n*]'s were suggested to be formed from bis-ns-Q[6] intermediate with addition of two equivalents of formaldehyde under acidic conditions. Owing to their unique structure, they possess smaller cavities and larger portals, which leads to reduced binding affinities towards various guests relative to their Q[*n*] counterparts. However, distinct preference was observed for flatter guests.[129]

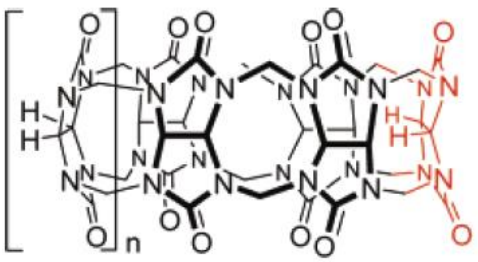

Figure 1.13 Representation of iQ[6] (n = 1) and iQ[7] (n = 2). Reprinted with permission from ref 129. Copyright @ 2005, American Chemical Society.

Besides different recognition properties, iQ[*n*] holds significance in unveiling the mechanism of Q[*n*] formation. The product submission experiment performed by the Isaacs group demonstrated ring contraction of iQ[6] and iQ[7] to normal Q[5] and Q[6] respectively, under aqueous acidic conditions. In contrast, anhydrous acidic conditions lead to quantitative transformation of iQ[6] to Q[6] due to intramolecular isomerization. The direct conversion of iQ[*n*] to Q[*n*] suggests that they are the remaining portions of some kinetic intermediates of the Q[*n*] synthesis.[21, 129]

1.4.2 Acyclic Q[*n*] congeners

Nolte and co-workers designed and investigated molecular clips that could be contemplated as simple acyclic Q[*n*] congeners. These molecular clips were comprised of one glycoluril unit (diphenylglycoluril or propanediurea) sealed on both sides with aromatic side-walls. It was observed that the propanediurea based clips exhibited higher binding affinity towards aromatic guests compared to diphenyl substituted glycoluril.[117, 130] Following these examples, the Isaacs group synthesized and investigated a range of acyclic Q[*n*] congeners with more than one glycoluril unit and variability in the substitution (R) of the glycoluril units (e.g. R = CO_2Et substitution).[131-135] The synthesis of methylene bridged glycoluril dimers with o-xylylene side-walls served as the model that reduced the complexity of Q[*n*] formation. It was demonstrated that the formation of methylene bridged glycoluril dimers in acidic 1,2-dichloroethane delivered S- and C-shaped diastereomers as kinetic products. However, the thermodynamic stability of the C-shaped dimer over S-shaped dimer was confirmed by product resubmission experiments (Figure 1.14). Furthermore, a series of labelling experiments established the intramolecular conversion of S- to C-shaped diastereomers. These results are aligned with

the previous finding of iQ[*n*] conversion to Q[*n*] that also involved the intramolecular isomerization of the S-shaped structural motif of iQ[*n*] (Figure 1.13).[136]

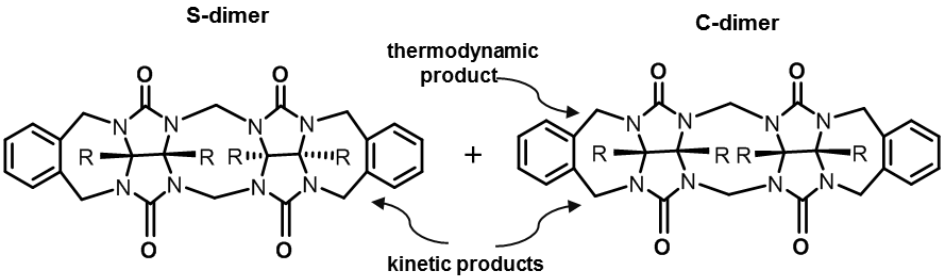

Figure 1.14 Representation of the S-shaped (left) and C-shaped (right) glycoluril dimer.[131]

Contrary to the above findings, the change in reaction conditions to aqueous acidic conditions afforded S-shaped diastereomer as the sole kinetic product and the isomerization to C-shaped dimer was mediated through enthalpy-driven intermolecular process.[137] This signifies an influence from the solvent system in the synthesis of Q[*n*]. In addition to insights into the mechanistic aspects of the formation of Q[*n*], these congeners were also explored as molecular hosts due to their ease of derivatization and non-constrictive binding of guest molecules. The host-guest chemistry of glycoluril dimers was studied in a few cases[138], however, elaborative investigations were conducted on the glycoluril tetramer guarded at both ends by o-xylylene moieties (R = CH_2COOH, Figure 1.15). These acyclic Q[*n*] congeners retained the recognition ability with almost the same affinity but lower selectivity towards various common guests with respect to Q[*n*]. The lower selectivity was attributed to the structural flexibility which was evident in x-ray crystal structures of p-xylylenediamine and spermine complexes.[139]

Intrigued by the comparable Q[*n*] recognition chemistry, investigations were conducted to explore the potential of these acyclic Q[*n*] congeners for practical applications. Various

structural modifications such as changing the solubilizing group (-COOH, -SO_3Na, -OH, and -$NH_3^+Cl^-$), the aromatic side-wall (substituted benzene or substituted naphthalene), the number of glycoluril units, and the linker length on the aromatic side-walls were employed for scrutinizing their drug solubilizing prospects.[6, 140-143] In the case of different solubilizing groups, congeners with anionic sulphonate groups (SO_3^-) exhibited stronger binding affinity towards experimental drugs, hence displayed more efficient drug solubilizing properties. In addition, the congeners equipped with naphthalene side-walls along with SO_3^- were better solubilizing agents compared to their benzene counterparts.[6, 140].

Similar results were observed for the cationic host (R = $NH_3^+Cl^-$) with naphthalene side-walls toward nucleotides (Figure 1.15).[143] The stronger binding affinities of these naphthalene guarded congeners were ascribed to the larger hydrophobic π-surface of naphthalene side-walls, facilitating better binding of hydrophobic guests, especially aromatic guest molecules.[140, 143]

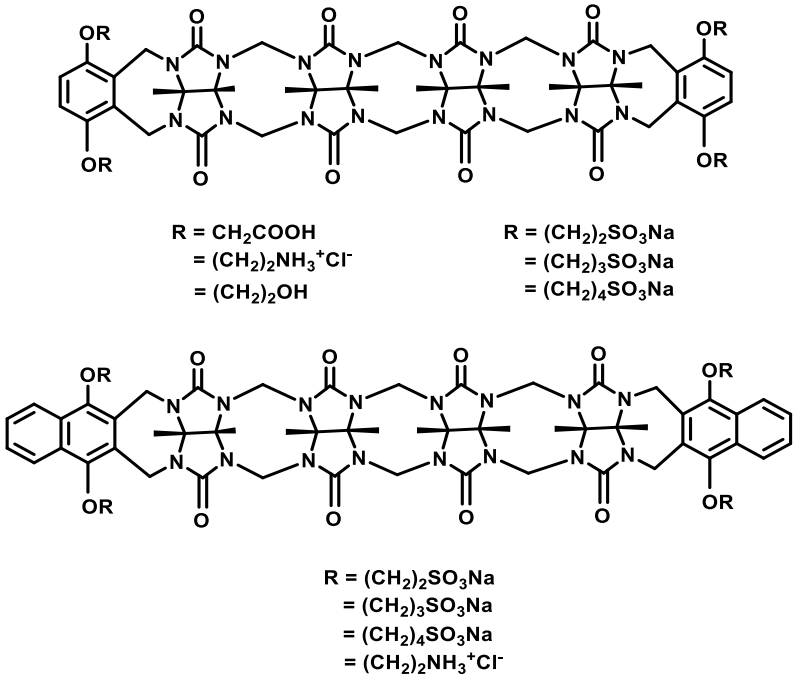

Figure 1.15 Representation of acyclic Q[n] congeners with benzene (top) and naphthalene (bottom) side-walls. [6, 139-143]

Another factor as a determinant of the host-guest chemistry is the number of glycoluril units (*n*) constituting the acyclic Q[*n*] congeners. Studies were conducted with *n* ranging from 1- 4 in these acyclic Q[*n*] congeners (Figure 1.15). For *n* = 3 or 4, the aromatic side-walls were in close proximity to each other, thereby creating a hydrophobic cavity together with glycoluril units. However, the affinity of the congener with *n* = 4 towards various drugs was stronger than for *n* = 3. Also, the solubilizing ability of compounds with *n* = 1 - 2 were dependent on the substitutions on the aromatic side-walls and the drug. The dimer-based compounds organize their aromatic side-walls roughly parallel to one another, facilitating interactions with aromatic guests through π-π bonding. All of these results demonstrate the effectiveness of the acyclic Q[*n*] congener based on glycoluril tetramer with naphthalene side-walls and the SO_3Na solubilizing group to be the best fit for use as a solubilizing excipient for insoluble pharmaceuticals.[141] The most limiting factor for using it as a solubilizing excipient, however, was its lowest solubility

in this series of acyclic Q[*n*] congeners. The solubility enhancement by several times was achieved by altering the alkyl chain length $(CH_2)_y$ between the naphthalene side-walls and the SO_3Na groups (y = 2 or 4 carbons, compared to 3 in original compound, Figure 1.15). In spite of enhanced solubility of compounds with chain length of 2 or 4, these were observed to be less potent solubilizing agents compared to the original compound. But at the same time the compound with the 2-carbon chain length achieved higher drug concentration due to higher inherent solubility.[142] These outcomes demonstrates that the acyclic Q[*n*] congeners have potential as solubilizing excipients in drug formulations.

Recently, in our group a new class of acyclic Q[*n*] congeners named as "pincers" were synthesized and investigated for their host-guest binding potential. These compounds possess similarity to the above mentioned acyclic Q[*n*] congeners in having central glycoluril units (*n*) but differ by having two cationic pyrazolium moieties in place of the substituted naphthalene or benzene side walls. Three pincer derivatives with glycoluril units ranging from n = 1-3 (monopincer, dipincer, and tripincer) were isolated (Figure 1.16).

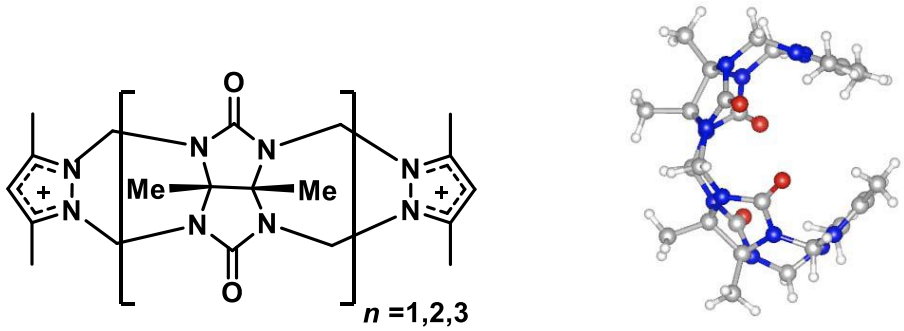

Figure 1.16 Representation of pincer compounds and the X-ray crystal structure of dipincer on the right.[144]

Further, due to their cationic nature, preliminary investigations to explore the binding properties towards anionic guests were demonstrated. Binding constants for three anionic guests with dipincer compound were derived employing competitive binding fluorescence technique. It was observed that π-π interactions and the negative charge of anions could be important factors in the process of binding. These preliminary results suggest investigation of a wide range of potential guests to evaluate the optimal binding features of the pincer molecules for further derivatization.[144]

1.5 Tiara[*n*]uril

The above-mentioned supramolecular hosts are characterized by specific structural features and host-guest complexation chemistry; however, none of these constructs have a positively charged cavity. Also, the solubility profile of these macrocyclic hosts is mostly confined to the mixture of organic or aqueous solvents. Very recently, Day et al. reported a new water-soluble macrocyclic host derived from glycoluril with the exceptional structural feature of having cations built into its walls, named as tiara[*n*]uril and abbreviated as Tu[*n*], where n is the number of repetitive glycoluril units.[145]

1.5.1 The Evolution of Tiara[*n*]uril

The discovery of Tu[*n*] stemmed from the use of pyrazole as a formaldehyde scavenger during the synthesis of fully substituted methyl and tetrahydrothiophene substituted Q[*n*] in our group. The investigation was carried out as an approach to removing methylene groups from glycoluril diethers to address the reason for the predominant formation of smaller homologues and to achieve the goal of homologues higher than a hexamer. However, instead of the expected reaction between formaldehyde and pyrazole, a facile condensation between dimethylglycoluril diether and pyrazole under acidic reaction

conditions was observed. The resultant products obtained were two cationic pyrazolium adducts (n = 1, 2) in the ratio 1.8:1 respectively (Scheme 1.12).[145]

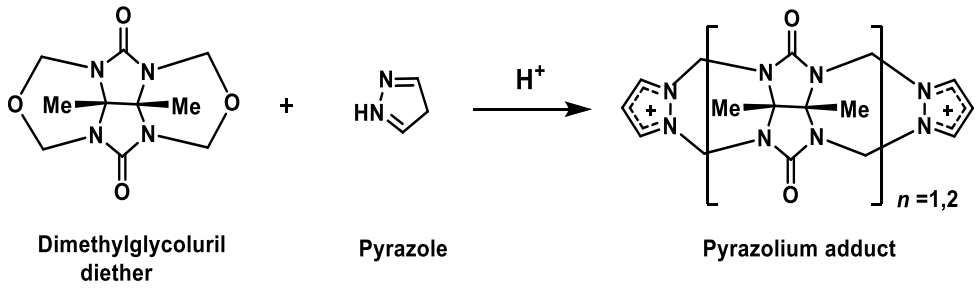

Scheme 1.12 Synthetic scheme for methyl substituted pyrazolium adduct[145]

Following the formation of these new derivatives, investigations were conducted with an objective to explore the potential to synthesize a macrocycle where the two pyrazole rings were connected. The acid catalyzed condensation of dimethylglycoluril with dipyrazole methane wherein two pyrazole rings were linked by methylene linkers furnished a new macrocycle, hexamethylTu[3] (Me_6 Tu[3]$^{2+}$) in 60% yield (Scheme 1.13).

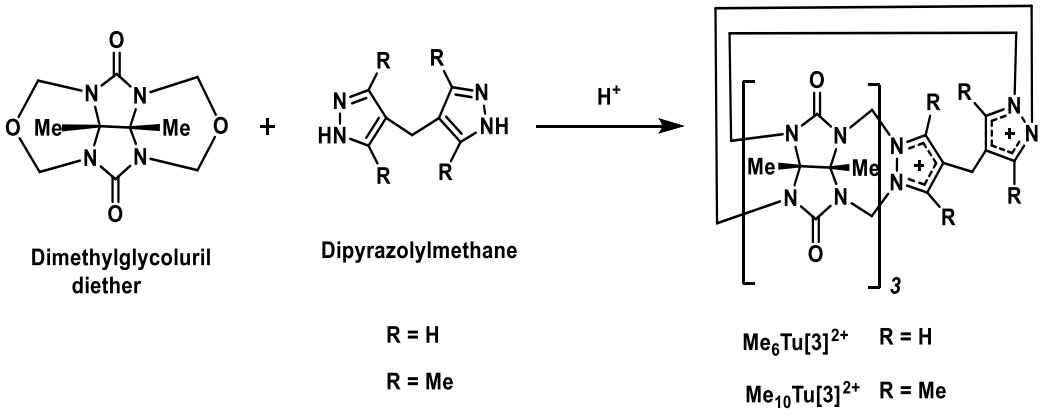

Scheme 1.13 Synthetic scheme for Me_6 Tu[3]$^{2+}$ and Me_{10}Tu[3]$^{2+}$ 145

The resulting macrocycle is novel and one of its kind but was found to be unstable under basic conditions including weakly basic aqueous NaOAc. To circumvent the instability issue, methyl substituted dipyrazole methane was employed that successfully afforded another novel macrocyclic host, decamethylTu[3] ($Me_{10}Tu[3]^{2+}$) with 65% yield (Scheme 1.13). Contrary to $Me_6Tu[3]^{2+}$, $Me_{10}Tu[3]^{2+}$ was found to be stable under basic conditions.

1.5.2 Structural features and properties

Both the novel macrocycles share the same structural peculiarities except for four additional methyl groups in $Me_{10}Tu[3]^{2+}$. Tu[3] was described as a symmetrical dicationic macrocycle with a cavity. One side of the cavity is a concave wall composed of three glycoluril moieties with their carbonyl groups forming two identical arcs above and below the cavity, and the remaining cavity completed by the two adjacent planar facets composed of pyrazolium ions (Figure 1.17).

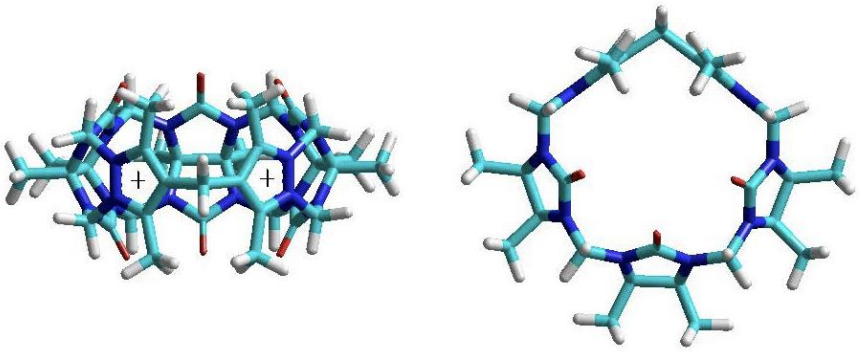

Figure 1.17 Molecular model of Me_{10} Tu[3]$^{2+}$ side view (left) and top view (right) illustrating resemblance to tiara[146]

The molecular shape bears a resemblance to a tiara with the carbonyl oxygen of glycoluril units jewelling the front and dipyrazolium wall forming the band at the back, hence named

as tiara[*n*]uril. $Me_{10}Tu[3]Cl_2$ exhibits good water solubility of 73g/L that allows the investigation of its binding properties in pure water. $Me_{10}Tu[3]Cl_2$ with positively charged pyrazolium walls of the cavity could facilitate the encapsulation of anionic guests screened from the solvent, and the carbonyl portals could serve as H-bond acceptor. To test this hypothesis, preliminary studies were carried out to determine the association with simple inorganic guests such as HCl, HSO_4^- and organic molecules like amino acids. It was demonstrated that binding of HCl and HSO_4^- with $Me_{10}Tu[3]^{2+}$ resulted in pK_a value change compared to free HCl and H_2SO_4 respectively. Also, association with amino acids were observed through changes in circular dichroism (CD) spectrum of the guest molecule on addition of host Tu[3]. These positive outcomes signify the binding potential of $Me_{10}Tu[3]Cl_2$ and is discussed in detail in Chapter 3 of the thesis.

1.5.3 Approaches to higher homologues

Intrigued by the non-formation of homologues higher than Tu[3] with methyl substituted glycoluril, Day and co-workers explored two approaches to the formation of homologues with an objective to achieving $n > 3$. The first approach involved increasing the distance between the pyrazole moieties through the incorporation of different spacer groups that included m-xylene, p-xylene, and bisphenylene. It was observed that both m-xylylpyrazole and p-xylylpyrazole formed new cationic macrocycles, *m*-$XyMe_8Tu[2]$ and *p*-$XyMe_8Tu[2]$, respectively (Scheme 1.14). Although here the resultant host molecules incorporated only two glycoluril units in the macrocycle, however, the cavity size remained unchanged compared to $Me_{10}Tu[3]Cl_2$ with a slight variation in the cavity shape. Moreover, to further increase the distance between dipyrazole groups, the bisphenyl spacer was used with an anticipation that the significantly greater distance

would facilitate higher homologues. In contrast, the dipyrazolylbiphenyl provided only polymeric material instead of Tu[*n*], evident as broad resonances by ^{1}H NMR.

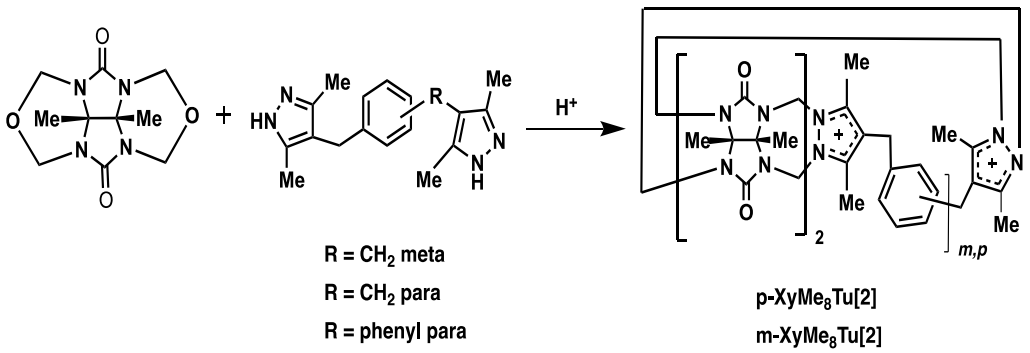

Scheme 1.14 Synthetic scheme for m-XyMe$_8$Tu[2] and p-XyMe$_8$Tu[2] [145]

The second approach involved the use of alternatively substituted glycoluril, which is known to have the propensity to form higher homologues in the synthesis of Q[*n*]. Cyclopentanoglycoluril diether was employed as a starting substitute to dimethylglycoluril diether. Contrary to the expectations, only $Me_4CyP_3Tu[3]$ was obtained as an isolated product (Scheme 1.15). Although higher homologues were not observed with mentioned substitution change, this provided another example of differently functionalized Tu[3] with the same cavity size.

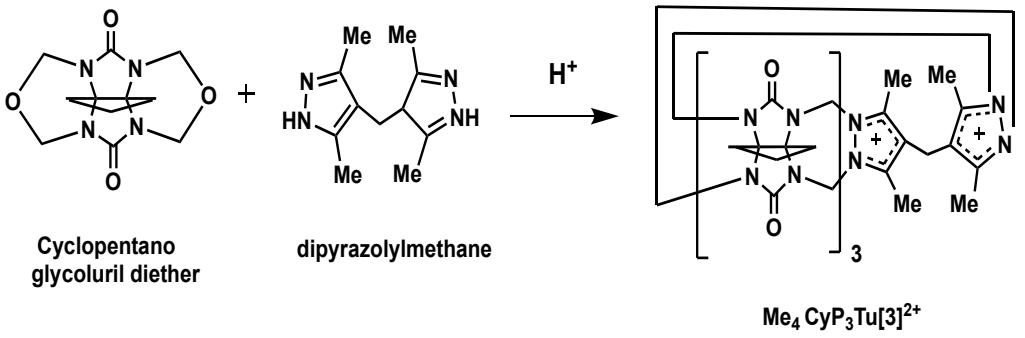

Scheme 1.15 Synthetic scheme for Me$_4$CyP$_3$Tu[3] [145]

1.6 Aims of the Research

With the advancement in supramolecular chemistry, the quest for synthetic host molecules has progressively increased in order to expand the potential applications to diverse fields. Although decent growth has been observed in the synthesis of macrocyclic hosts with the potential to recognize cationic guests, however, development of anionophoric macrocyclic hosts effective in protic solvents remains a challenge. The recent synthesis of a new class of glycoluril-based macrocyclic host, tiara[*n*]uril, thus serves as a promising host molecule towards anions with H-bond donors in pure water in contrast to the afore-mentioned supramolecular hosts. As mentioned in section 1.5, very few examples have been reported of tiara[*n*]uril with different substitutions. Also, the product distribution is specifically confined to smaller homologues with two-three glycoluril units. This provides an extensive opportunity to further explore this novel class of host molecule with respect to the attainment of higher homologues with different functionality.

The work presented in this thesis discusses: -

1. The synthesis of substituted glycoluril incorporating the tetrahydrothiophene (THT) moiety as functional group.
2. The synthesis of new tiara[*n*]urils employing THT substituted glycoluril with an objective to obtaining homologues with n > 3 and to determine the difference in homologues distribution between the existing functionalized tiara[*n*]uril.
3. To explore the host-guest complexation properties of the methyl and THT substituted Tu[*n*] with the purpose to understand the binding potential in relation to the Tu[*n*]'s structural features, and to establish a possible drug delivery system

utilizing Tu[*n*] as solubilizing agent for therapeutic agents, especially anionic drugs.

1.7 References

1. Stryer, L., *Biochemistry*. W. H. Freeman Company: New York, 1995; Vol. 4.
2. Anslyn, E. V., Supramolecular Analytical Chemistry. *The Journal of Organic Chemistry* **2007,** *72* (3), 687-699.
3. Cram, D. J., The Design of Molecular Hosts, Guests, and Their Complexes (Nobel Lecture). *Angewandte Chemie International Edition in English* **1988,** *27* (8), 1009-1020.
4. Lehn, J. M., Supramolecular Chemistry - Scope and Perspectives Molecules, Supermolecules, and Molecular Devices (Nobel Lecture). *Angewandte Chemie International Edition in English* **1988,** *27* (1), 89-112.
5. Pedersen, C. J., The Discovery of Crown Ethers (Noble Lecture). *Angewandte Chemie International Edition in English* **1988,** *27* (8), 1021-1027.
6. Zhang, B.; Zavalij, P. Y.; Isaacs, L., Acyclic CB[*n*]-type Molecular Containers: Effect of Solubilizing Group on Their Function as Solubilizing Excipients. *Organic & Biomolecular Chemistry* **2014,** *12* (15), 2413-2422.
7. Lagona, J.; Mukhopadhyay, P.; Chakrabarti, S.; Isaacs, L., The Cucurbit[*n*]uril Family. *Angewandte Chemie International Edition* **2005,** *44* (31), 4844-4870.
8. Tiwari, G.; Tiwari, R.; Rai, A. K., Cyclodextrins in Delivery Systems: Applications. *Journal of Pharmacy and Bioallied Sciences* **2010,** *2* (2), 72.
9. Behrend, R.; Meyer, E.; Rusche, F., Condensation Products from Glycoluril and Formaldehyde. *Liebigs Annalen Chem* **1905,** *339*, 1-37.
10. Freeman, W. A.; Mock, W. L.; Shih, N. Y., Cucurbituril. *Journal of the American Chemical Society* **1981,** *103* (24), 7367-7368.
11. Kim, J.; Jung, I.-S.; Kim, S.-Y.; Lee, E.; Kang, J.-K.; Sakamoto, S.; Yamaguchi, K.; Kim, K., New Cucurbituril Homologues: Synthesis, Isolation, Characterization,

and X-ray Crystal Structures of Cucurbit[*n*]uril (*n* = 5, 7, and 8). *Journal of the American Chemical Society* **2000,** *122* (3), 540-541.

12. Day, A.; Arnold, A. P.; Blanch, R. J.; Snushall, B., Controlling Factors in the Synthesis of Cucurbituril and Its Homologues. *The Journal of Organic Chemistry* **2001,** *66* (24), 8094-8100.
13. Cong, H.; Ni, X. L.; Xiao, X.; Huang, Y.; Zhu, Q.-J.; Xue, S.-F.; Tao, Z.; Lindoy, L. F.; Wei, G., Synthesis and Separation of Cucurbit[*n*]urils and Their Derivatives. *Organic & Biomolecular Chemistry* **2016,** *14* (19), 4335-4364.
14. Day, A. I.; Blanch, R. J.; Arnold, A. P.; Lorenzo, S.; Lewis, G. R.; Dance, I., A., Cucurbituril-Based Gyroscane: A New Supramolecular Form. *Angewandte Chemie International Edition* **2002,** *41* (2), 275-277.
15. Pisani, M. J.; Zhao, Y.; Wallace, L.; Woodward, C. E.; Keene, F. R.; Day, A. I.; Collins, J. G., Cucurbit[10]uril Binding of Dinuclear Platinum(II) and Ruthenium(II) Complexes: Association/dissociation Rates from Seconds to Hours. *Dalton Transactions* **2010,** *39* (8), 2078-2086.
16. Liu, S.; Zavalij, P. Y.; Isaacs, L., Cucurbit[10]uril. *Journal of the American Chemical Society* **2005,** *127* (48), 16798-16799.
17. Cheng, X.-J.; Liang, L.-L.; Chen, K.; Ji, N.-N.; Xiao, X.; Zhang, J.-X.; Zhang, Y.-Q.; Xue, S.-F.; Zhu, Q.-J.; Ni, X.-L.; Tao, Z., Twisted Cucurbit[14]uril. *Angewandte Chemie International Edition* **2013,** *52* (28), 7252-7255.
18. Li, Q.; Qiu, S.-C.; Zhang, J.; Chen, K.; Huang, Y.; Xiao, X.; Zhang, Y.; Li, F.; Zhang, Y.-Q.; Xue, S.-F.; Zhu, Q.-J.; Tao, Z.; Lindoy, L. F.; Wei, G., Twisted Cucurbit[*n*]urils. *Organic Letters* **2016,** *18* (16), 4020-4023.
19. Assaf, K. I.; Nau, W. M., Cucurbiturils: From Synthesis to High-affinity Binding and Catalysis. *Chemical Society Reviews* **2015,** *44* (2), 394-418.

20. Huang, W.-H.; Zavalij, P. Y.; Isaacs, L., Cucurbit[*n*]uril Formation Proceeds by Step-Growth Cyclo-oligomerization. *Journal of the American Chemical Society* **2008,** *130* (26), 8446-8454.

21. Isaacs, L., The Mechanism of Cucurbituril Formation. *Israel Journal of Chemistry* **2011,** *51* (5-6), 578-591.

22. Kim, K.; Selvapalam, N.; Ko, Y. H.; Park, K. M.; Kim, D.; Kim, J., Functionalized Cucurbiturils and Their Applications. *Chemical Society Reviews* **2007,** *36*, 267-79.

23. Lee, J. W.; Samal, S.; Selvapalam, N.; Kim, H.-J.; Kim, K., Cucurbituril Homologues and Derivatives: New Opportunities in Supramolecular Chemistry. *Accounts of Chemical Research* **2003,** *36* (8), 621-630.

24. Buschmann, H.-J.; Jansen, K.; Meschke, C.; Schollmeyer, E., Thermodynamic Data for Complex Formation Between Cucurbituril and Alkali and Alkaline Earth Cations in Aqueous Formic Acid Solution. *Journal of Solution Chemistry* **1998,** *27* (2), 135-140.

25. Hwang, I.; Jeon, W. S.; Kim, H.-J.; Kim, D.; Kim, H.; Selvapalam, N.; Fujita, N.; Shinkai, S.; Kim, K., Cucurbit[7]uril: A Simple Macrocyclic, pH-Triggered Hydrogelator Exhibiting Guest-Induced Stimuli-Responsive Behavior. *Angewandte Chemie International Edition* **2007,** *46* (1-2), 210-213.

26. Buschmann, H. J.; Cleve, E.; Schollmeyer, E., Cucurbituril As a Ligand for the Complexation of Cations in Aqueous Solutions. *Inorganica Chimica Acta* **1992,** *193* (1), 93-97.

27. Wu, F.; Wu, L.-H.; Xiao, X.; Zhang, Y.-Q.; Xue, S.-F.; Tao, Z.; Day, A. I., Locating the Cyclopentano Cousins of the Cucurbit[*n*]uril Family. *The Journal of Organic Chemistry* **2011,** *77* (1), 606-611.

28. Flinn, A.; Hough, G. C.; Stoddart, J. F.; Williams, D. J., Decamethylcucurbit[5]uril. *Angewandte Chemie International Edition in English* **1992,** *31* (11), 1475-1477.

29. Sasmal, S.; Sinha, M. K.; Keinan, E., Facile Purification of Rare Cucurbiturils by Affinity Chromatography. *Organic Letters* **2004,** *6* (8), 1225-1228.

30. Zhao, J.; Kim, H.-J.; Oh, J.; Kim, S.-Y.; Lee, J. W.; Sakamoto, S.; Yamaguchi, K.; Kim, K., Cucurbit[*n*]uril Derivatives Soluble in Water and Organic Solvents. *Angewandte Chemie International Edition* **2001,** *40* (22), 4233-4235.

31. Zhao, Y.; Mandadapu, V.; Iranmanesh, H.; Beves, J. E.; Day, A. I., The Inheritance Angle: A Determinant for the Number of Members in the Substituted Cucurbit[*n*]uril Family. *Organic Letters* **2017,** *19* (15), 4034-4037.

32. Jon, S. Y.; Selvapalam, N.; Oh, D. H.; Kang, J.-K.; Kim, S.-Y.; Jeon, Y. J.; Lee, J. W.; Kim, K., Facile Synthesis of Cucurbit[*n*]uril Derivatives via Direct Functionalization: Expanding Utilization of Cucurbit[*n*]uril. *Journal of the American Chemical Society* **2003,** *125* (34), 10186-10187.

33. Isobe, H.; Sato, S.; Nakamura, E., Synthesis of Disubstituted Cucurbit[6]uril and Its Rotaxane Derivative. *Organic Letters* **2002,** *4* (8), 1287-1289.

34. Day, A. I.; Arnold, A. P.; Blanch, R. J., A Method for Synthesizing Partially Substituted Cucurbit[*n*]uril. *Molecules* **2003,** *8* (1), 74-84.

35. Wu, L.-H.; Ni, X.-L.; Wu, F.; Zhang, Y.-Q.; Zhu, Q.-J.; Xue, S.-F.; Tao, Z., Crystal Structures of Three Partially Cyclopentano-substituted Cucurbit[6]urils. *Journal of Molecular Structure* **2009,** *920* (1), 183-188.

36. Lewin, V.; Rivollier, J.; Coudert, S.; Buisson, D.-A.; Baumann, D.; Rousseau, B.; Legrand, F.-X.; Kouřilová, H.; Berthault, P.; Dognon, J.-P.; Heck, M.-P.; Huber, G., Synthesis of Cucurbit[6]uril Derivatives and Insights into Their Solubility in Water. *European Journal of Organic Chemistry* **2013,** *2013* (18), 3857-3865.

37. Zhao, Y.; Xue, S.; Zhu, Q.; Tao, Z.; Zhang, J.; Wei, Z.; Long, L.; Hu, M.; Xiao, H.; Day, A., Synthesis of a Symmetrical Tetrasubstituted Cucurbit[6]uril and Its Host-

guest Inclusion Complex with 2,2 ′-bipyridine. *Chinese Science Bulletin* **2004,** *49* (11), 1111.

38. Yu, D.-H.; Ni, X.-L.; Tian, Z.-C.; Zhang, Y.-Q.; Xue, S.-F.; Tao, Z.; Zhu, Q.-J., Host-guest Inclusion Complexes of Four Partial Alkyl-substituted Cucurbit[6]urils with Some Probe Guests. *Journal of Molecular Structure* **2008,** *891* (1), 247-253.
39. Vinciguerra, B.; Cao, L.; Cannon, J. R.; Zavalij, P. Y.; Fenselau, C.; Isaacs, L., Synthesis and Self-Assembly Processes of Monofunctionalized Cucurbit[7]uril. *Journal of the American Chemical Society* **2012,** *134* (31), 13133-13140.
40. Vinciguerra, B.; Zavalij, P. Y.; Isaacs, L., Synthesis and Recognition Properties of Cucurbit[8]uril Derivatives. *Organic Letters* **2015,** *17* (20), 5068-5071.
41. Zhao, N.; Lloyd, G. O.; Scherman, O. A., Monofunctionalised Cucurbit[6]uril Synthesis using Imidazolium Host-guest Complexation. *Chemical Communications* **2012,** *48* (25), 3070-3072.
42. Ayhan, M.; Karoui, H.; Hardy, M.; Rockenbauer, A.; Charles, L.; Rosas, R.; Udachin, K.; Tordo, P.; Bardelang, D.; Ouari, O., Erratum: Comprehensive Synthesis of Monohydroxy-Cucurbit[*n*]urils (n = 5, 6, 7, 8): High Purity and High Conversions (Journal of the American Chemical Society (2015) 137 (10238-10245) DOI: 10.1021/jacs.5b04553). *Journal of the American Chemical Society* **2016,** *138*.
43. Kumar, C. P.; Wu, F.; Woodward, C. E.; Day, A. I., The Influence of Equatorial Substitution and K^+ Ion Concentration: An Encapsulation Study of CH_4, CH_3F, CH_3Cl, CH_2F_2 and CF_4, in Q[5], $CyP_5Q[5]$ and a $CyP_5Q[5]$-carboxylate Derivative. *Supramolecular Chemistry* **2014,** *26* (9), 670-676.
44. Buschmann, H.-J.; Cleve, E.; Jansen, K.; Wego, A.; Schollmeyer, E., Complex Formation between Cucurbit[*n*]urils and Alkali, Alkaline Earth and Ammonium Ions in Aqueous Solution. *Journal of Inclusion Phenomena and Macrocyclic Chemistry* **2001,** *40* (1), 117-120.

45. Liu, J.-X.; Long, L.-S.; Huang, R.-B.; Zheng, L.-S., Molecular Capsules Based on Cucurbit[5]uril Encapsulating "Naked" Anion Chlorine. *Crystal Growth & Design* **2006,** *6* (11), 2611-2614.

46. Zhang, Y.-Q.; Zhu, Q.-J.; Xue, S.-F.; Tao, Z., Chlorine Anion Encapsulation by Molecular Capsules Based on Cucurbit[5]uril and Decamethylcucurbit[5]uril. *Molecules* **2007,** *12* (7), 1325-1333.

47. Liu, J.-X.; Long, L.-S.; Huang, R.-B.; Zheng, L.-S., Interesting Anion-Inclusion Behavior of Cucurbit[5]uril and Its Lanthanide-Capped Molecular Capsule. *Inorganic Chemistry* **2007,** *46* (24), 10168-10173.

48. Mock, W. L.; Shih, N. Y., Host-guest Binding Capacity of Cucurbituril. *The Journal of Organic Chemistry* **1983,** *48* (20), 3618-3619.

49. Liu, L.; Zhao, N.; Scherman, O. A., Ionic Liquids as Novel Guests for Cucurbit[6]uril in Neutral Water. *Chemical Communications* **2008,** (9), 1070-1072.

50. El Haouaj, M.; Luhmer, M.; Ko, Y. H.; Kim, K.; Bartik, K., NMR Study of the Reversible Complexation of Xenon by Cucurbituril. *Journal of the Chemical Society, Perkin Transactions 2* **2001,** (5), 804-807.

51. Haouaj, M. E.; Ho Ko, Y.; Luhmer, M.; Kim, K.; Bartik, K., NMR Investigation of the Complexation of Neutral Guests by Cucurbituril. *Journal of the Chemical Society, Perkin Transactions 2* **2001,** (11), 2104-2107.

52. Zhao, N.; Liu, L.; Biedermann, F.; Scherman, O. A., Binding Studies on CB[6] with a Series of 1-Alkyl-3-methylimidazolium Ionic Liquids in an Aqueous System. *Chemistry – An Asian Journal* **2010,** *5* (3), 530-537.

53. Kolman, V.; Marek, R.; Strelcova, Z.; Kulhanek, P.; Necas, M.; Svec, J.; Sindelar, V., Electron Density Shift in Imidazolium Derivatives upon Complexation with Cucurbit[6]uril. *Chemistry – A European Journal* **2009,** *15* (28), 6926-6931.

54. Buschmann, H. J.; Schollmeyer, E.; Mutihac, L., The Formation of Amino Acid and Dipeptide Complexes with α-Cyclodextrin and Cucurbit[6]uril in Aqueous Solutions Studied by Titration Calorimetry. *Thermochimica Acta* **2003,** *399* (1), 203-208.

55. Jansen, K.; Wego, A.; Buschmann, H.-J.; Schollmeyer, E., Influence of Salts and Humic Acids on the Complexation of Aromatic Molecules with the Macrocyclic Ligand Cucurbituril. *Vom Wasser* **2000,** *94*, 177-190.

56. Jansen, K.; Wego, A.; Buschmann, H.-J.; Schollmeyer, E., ^{1}H-NMR Spectroscopic Studies of the Complex Formation between Aromatic Amines and Cucurbituril in Aqueous Solutions. *Vom Wasser* **2000,** *95*, 229-236.

57. Im Jun, S.; Wook Lee, J.; Sakamoto, S.; Yamaguchi, K.; Kim, K., Rotaxane-based Molecular Switch with Fluorescence Signaling. *Tetrahedron Letters* **2000,** *41* (4), 471-475.

58. Efremova, O. A.; Mironov, Y. V.; Kuratieva, N. V.; Fedorov, V. E., Novel Supramolecular Compounds based on Cucurbit[6]uril, 1,8-diaminooctane and Octahedral Thiohydroxo Anions with Cluster Core [Re6S8]. *Inorganica Chimica Acta* **2010,** *363* (15), 4411-4415.

59. Wu, W.-J.; Wu, F.; Day, A. I., Molecular Snuggle and Stretch of a Tetraammonium Chain in the Construction of a Hetero-[4] pseudorotaxane with CyclopentanoQ[6] and Classical Q[7]. *The Journal of Organic Chemistry* **2017,** *82* (11), 5507-5515.

60. Danylyuk, O.; Fedin, V. P.; Sashuk, V., Host-guest Complexes of Cucurbit[6]uril with Isoprenaline: The Effect of the Metal ion on the Crystallization Pathway and Supramolecular Architecture. *CrystEngComm* **2013,** *15* (37), 7414-7418.

61. Danylyuk, O.; Fedin, V. P.; Sashuk, V., Kinetic Trapping of the Host-guest Association Intermediate and Its Transformation into a Thermodynamic Inclusion Complex. *Chemical Communications* **2013,** *49* (18), 1859-1861.

62. Buschmann, H.-J.; Cleve, E.; Mutihac, L.; Schollmeyer, E., The Formation of Alkali and Alkaline Earth Cation Complexes with Cucurbit[6]uril in Aqueous Solution: A Critical Survey of Old and New Results. *Journal of Inclusion Phenomena and Macrocyclic Chemistry* **2009,** *65*, 293-297.

63. Buschmann, H. J.; Cleve, E.; Jansen, K.; Schollmeyer, E., Determination of Complex Stabilities with Nearly Insoluble Host Molecules: Cucurbit[5]uril, Decamethylcucurbit[5]uril and Cucurbit[6]uril as Ligands for the Complexation of Some Multicharged Cations in Aqueous Solution. *Analytica Chimica Acta* **2001,** *437* (1), 157-163.

64. Buschmann, H.-J.; Jansen, K.; Schollmeyer, E., Cucurbit[6]uril as Ligand for the Complexation of Lanthanide Cations in Aqueous Solution. *Inorganic Chemistry Communications* **2003,** *6* (5), 531-534.

65. Barrow, S. J.; Kasera, S.; Rowland, M. J.; del Barrio, J.; Scherman, O. A., Cucurbituril-Based Molecular Recognition. *Chemical Reviews* **2015,** *115* (22), 12320-12406.

66. Wheate, N. J.; Buck, D. P.; Day, A. I.; Collins, J. G., Cucurbit[*n*]uril Binding of Platinum Anticancer Complexes. *Dalton Transactions* **2006,** (3), 451-458.

67. Zhao, Y.; Buck, D. P.; Morris, D. L.; Pourgholami, M. H.; Day, A. I.; Collins, J. G., Solubilisation and Cytotoxicity of Albendazole Encapsulated in Cucurbit[*n*]uril. *Organic & Biomolecular Chemistry* **2008,** *6* (24), 4509-4515.

68. Chinai, J. M.; Taylor, A. B.; Ryno, L. M.; Hargreaves, N. D.; Morris, C. A.; Hart, P. J.; Urbach, A. R., Molecular Recognition of Insulin by a Synthetic Receptor. *Journal of the American Chemical Society* **2011,** *133* (23), 8810-8813.

69. Kasera, S.; Herrmann, L. O.; Del Barrio, J.; Baumberg, J. J.; Scherman, O. A., Quantitative Multiplexing with Nano-self-assemblies in SERS. *Scientific Reports* **2014,** *4*, 6785.

70. Assaf, K. I.; Nau, W. M., Cucurbiturils as Fluorophilic Receptors. *Supramolecular Chemistry* **2014,** *26* (9), 657-669.

71. Ryan, S. N. T.; Del Barrio, J. S.; Ghosh, I.; Biedermann, F.; Lazar, A. I.; Lan, Y.; Coulston, R. J.; Nau, W. M.; Scherman, O. A., Efficient Host-guest Energy Transfer in Polycationic Cyclophane-Perylene Diimide Complexes in Water. *Journal of the American Chemical Society* **2014,** *136* (25), 9053-9060.

72. Ahn, Y.; Jang, Y.; Selvapalam, N.; Yun, G.; Kim, K., Supramolecular Velcro for Reversible Underwater Adhesion. *Angewandte Chemie International Edition* **2013,** *52* (11), 3140-3144.

73. Kim, H. J.; Heo, J.; Jeon, W. S.; Lee, E.; Kim, J.; Sakamoto, S.; Yamaguchi, K.; Kim, K., Selective Inclusion of a Hetero-guest Pair in a Molecular Host: Formation of Stable Charge-transfer Complexes in Cucurbit[8]uril. *Angewandte Chemie International Edition* **2001,** *40* (8), 1526-1529.

74. Jiang, G.; Li, G., Preparation and Biological Activity of Novel Cucurbit[8]uril–fullerene Complex. *Journal of Photochemistry and Photobiology B: Biology* **2006,** *85* (3), 223-227.

75. Konda, S. K.; Maliki, R.; McGrath, S.; Parker, B. S.; Robinson, T.; Spurling, A.; Cheong, A.; Lock, P.; Pigram, P. J.; Phillips, D. R., Encapsulation of Mitoxantrone within Cucurbit[8]uril Decreases Toxicity and Enhances Survival in a Mouse Model of Cancer. *ACS Medicinal Chemistry Letters* **2017,** *8* (5), 538-542.

76. Liu, S.; Shukla, A. D.; Gadde, S.; Wagner, B. D.; Kaifer, A. E.; Isaacs, L., Ternary Complexes Comprising Cucurbit[10]uril, Porphyrins, and Guests. *Angewandte Chemie International Edition* **2008,** *47* (14), 2657-2660.

77. Alrawashdeh, L. R.; Day, A. I.; Wallace, L., Strong Enhancement of Luminescence from an Iridium Polypyridyl Complex via Encapsulation in Cucurbituril. *Dalton Transactions* **2013,** *42* (47), 16478-16481.

78. Pisani, M. J.; Zhao, Y.; Wallace, L.; Woodward, C. E.; Keene, F. R.; Day, A. I.; Collins, J. G., Cucurbit[10]uril Binding of Dinuclear Platinum (II) and Ruthenium (II) Complexes: Association/dissociation Rates from Seconds to Hours. *Dalton Transactions* **2010,** *39* (8), 2078-2086.

79. Li, F.; Feterl, M.; Warner, J. M.; Day, A. I.; Keene, F. R.; Collins, J. G., Protein Binding by Dinuclear Polypyridyl Ruthenium (II) Complexes and the Effect of Cucurbit[10]uril Encapsulation. *Dalton Transactions* **2013,** *42* (24), 8868-8877.

80. Day, A.; Grant Collins, J., Cucurbituril Receptors and Drug Delivery. *Supramolecular Chemistry from Molecules to Nanomaterials* **2012,** *3*, 983-1000.

81. Ma, X.; Zhao, Y., Biomedical Applications of Supramolecular Systems Based on Host-guest Interactions. *Chemical Reviews* **2014,** *115* (15), 7794-7839.

82. Sinn, S.; Biedermann, F., Chemical Sensors Based on Cucurbit[*n*]uril Macrocycles. *Israel Journal of Chemistry* **2018,** *58* (3-4), 357-412.

83. Zhao, Y., Cucurbit[*n*]uril - A Delivery Host for Anti-cancer Drugs. PhD Thesis, University of New South Wales, Canberra, 2009.

84. Zhao, Y.; Pourgholami, M. H.; Morris, D. L.; Collins, J. G.; Day, A. I., Enhanced Cytotoxicity of Benzimidazole Carbamate Derivatives and Solubilisation by Encapsulation in Cucurbit[*n*]uril. *Organic & Biomolecular Chemistry* **2010,** *8* (14), 3328-3337.

85. Appel, E. A.; Rowland, M. J.; Loh, X. J.; Heywood, R. M.; Watts, C.; Scherman, O. A., Enhanced Stability and Activity of Temozolomide in Primary Glioblastoma Multiforme Cells with Cucurbit[*n*]uril. *Chemical Communications* **2012,** *48* (79), 9843-9845.

86. Cao, L.; Hettiarachchi, G.; Briken, V.; Isaacs, L., Cucurbit[7]uril Containers for Targeted Delivery of Oxaliplatin to Cancer Cells. *Angewandte Chemie International Edition* **2013,** *52* (46), 12033-12037.

87. Park, K. M.; Lee, D. W.; Sarkar, B.; Jung, H.; Kim, J.; Ko, Y. H.; Lee, K. E.; Jeon, H.; Kim, K., Reduction-sensitive, Robust Vesicles with a Non-covalently Modifiable Surface as a Multifunctional Drug-delivery Platform. *Small* **2010,** *6* (13), 1430-1441.

88. Choi, J.; Kim, J.; Kim, K.; Yang, S.-T.; Kim, J.-I.; Jon, S., A Rationally Designed Macrocyclic Cavitand that Kills Bacteria with High Efficacy and Good Selectivity. *Chemical Communications* **2007,** (11), 1151-1153.

89. Dantz, D. A.; Meschke, C.; Buschmann, H.-J.; Schollmeyer, E., Complexation of Volatile Organic Molecules from the Gas Phase with Cucurbituril and β-Cyclodextrin. *Supramolecular Chemistry* **1998,** *9* (2), 79-83.

90. Miyahara, Y.; Abe, K.; Inazu, T., "Molecular" Molecular Sieves: Lid-free Decamethylcucurbit[5]uril Absorbs and Desorbs Gases Selectively. *Angewandte Chemie International Edition* **2002,** *41* (16), 3020-3023.

91. Li, H.; Yang, Y.-W., Gold Nanoparticles Functionalized with Supramolecular Macrocycles. *Chinese Chemical Letters* **2013,** *24* (7), 545-552.

92. Vinciguerra, B.; Cao, L.; Cannon, J. R.; Zavalij, P. Y.; Fenselau, C.; Isaacs, L., Synthesis and Self-assembly Processes of Monofunctionalized Cucurbit[7]uril. *Journal of the American Chemical Society* **2012,** *134* (31), 13133-13140.

93. Jeon, Y. J.; Kim, H.; Jon, S.; Selvapalam, N.; Oh, D. H.; Seo, I.; Park, C.-S.; Jung, S. R.; Koh, D.-S.; Kim, K., Artificial Ion Channel Formed by Cucurbit[*n*]uril Derivatives with a Carbonyl Group Fringed Portal Reminiscent of the Selectivity Filter of K^+ Channels. *Journal of the American Chemical Society* **2004,** *126* (49), 15944-15945.

94. Yang, H.; Ma, Z.; Wang, Z.; Zhang, X., Fabricating Covalently Attached Hyperbranched Polymers by Combining Photochemistry with Supramolecular Polymerization. *Polymer Chemistry* **2014,** *5* (4), 1471-1476.

95. Karcher, S.; Kornmüller, A.; Jekel, M., Cucurbituril for Water Treatment. Part I: Solubility of Cucurbituril and Sorption of Reactive Dyes. *Water Research* **2001,** *35* (14), 3309-3316.

96. Kornmüller, A.; Karcher, S.; Jekel, M., Cucurbituril for Water Treatment. Part II: Ozonation and Oxidative Regeneration of Cucurbituril. *Water Research* **2001,** *35* (14), 3317-3324.

97. Karcher, S.; Kornmüller, A.; Jekel, M., Removal of Reactive Dyes by Sorption/complexation with Cucurbituril. *Water Science and Technology* **1999,** *40* (4), 425-433.

98. Li, Z.-F.; Wu, F.; Zhou, F.-G.; Ni, X.-L.; Feng, X.; Xiao, X.; Zhang, Y.-Q.; Xue, S.-F.; Zhu, Q.-J.; Lindoy, L. F.; Clegg, J. K.; Tao, Z.; Wei, G., Approach to 10-Unit "Bracelet" Frameworks Based on Coordination of Alkyl-Substituted Cucurbit[5]urils and Potassium Ions. *Crystal Growth & Design* **2010,** *10* (12), 5113-5116.

99. Staudinger, V. H.; Niessen, G., Über Die Kondensation Von Formaldehyd Mit Disubstituierten Thioharnstoffen. 419. Mitteilung über Makromolekulare Verbindungen. *Die Makromolekulare Chemie: Macromolecular Chemistry and Physics* **1955,** *15* (1), 75-90.

100. Miyahara, Y.; Goto, K.; Oka, M.; Inazu, T., Remarkably Facile Ring-size Control in Macrocyclization: Synthesis of Hemicucurbit[6]uril and Hemicucurbit[12]uril. *Angewandte Chemie International Edition* **2004,** *43* (38), 5019-5022.

101. Buschmann, H.-J.; Cleve, E.; Schollmeyer, E., Hemicucurbit[6]uril, a Selective Ligand for the Complexation of Anions in Aqueous Solution. *Inorganic Chemistry Communications* **2005,** *8* (1), 125-127.

102. Andersen, N. N.; Lisbjerg, M.; Eriksen, K.; Pittelkow, M., Hemicucurbit[*n*]urils and Their Derivatives-Synthesis and Applications. *Israel Journal of Chemistry* **2018,** *58* (3-4), 435-448.

103. Buschmann, H.-J.; Zielesny, A.; Schollmeyer, E., Hemicucurbit[6]uril a Macrocyclic Ligand with Unusual Complexing Properties. *Journal of Inclusion Phenomena and Macrocyclic Chemistry* **2006,** *54* (3-4), 181-185.

104. Cong, H.; Yamato, T.; Feng, X.; Tao, Z., Supramolecular Catalysis of Esterification by Hemicucurbiturils under Mild Conditions. *Journal of Molecular Catalysis A: Chemical* **2012,** *365*, 181-185.

105. Cong, H.; Yamato, T.; Tao, Z., Hemicucurbit[6]uril-induced Aerobic Oxidation of Heterocyclic Compounds. *Journal of Molecular Catalysis A: Chemical* **2013,** *379*, 287-293.

106. Aav, R.; Shmatova, E.; Reile, I.; Borissova, M.; Topic, F.; Rissanen, K., New Chiral Cyclohexylhemicucurbit[6]uril. *Organic Letters* **2013,** *15* (14), 3786-3789.

107. Svec, J.; Necas, M.; Sindelar, V., Bambus[6]uril. *Angewandte Chemie International Edition* **2010,** *49* (13), 2378-2381.

108. Havel, V.; Svec, J.; Wimmerova, M.; Dusek, M.; Pojarova, M.; Sindelar, V., Bambus[*n*]urils: a New Family of Macrocyclic Anion Receptors. *Organic Letters* **2011,** *13* (15), 4000-4003.

109. Yawer, M. A.; Havel, V.; Sindelar, V., A Bambusuril Macrocycle that Binds Anions in Water with High Affinity and Selectivity. *Angewandte Chemie International Edition* **2015,** *54* (1), 276-279.

110. Rivollier, J.; Thuery, P.; Heck, M.-P., Extension of the Bambus[*n*] uril family: Microwave Synthesis and Reactivity of Allylbambus[*n*]urils. *Organic Letters* **2013,** *15* (3), 480-483.

111. Swager, T. M.; Koo, B., Semithiobambusurils Binding with Anions and Metal Ions. *Synfacts* **2015,** *11* (03), 0258-0258.

112. Singh, M.; Solel, E.; Keinan, E.; Reany, O., Dual-Functional Semithiobambusurils. *Chemistry-A European Journal* **2015,** *21* (2), 536-540.

113. Lagona, J.; Fettinger, J. C.; Isaacs, L., Cucurbit[*n*]uril Analogues. *Organic Letters* **2003,** *5* (20), 3745-3747.

114. Lagona, J.; Fettinger, J. C.; Isaacs, L., Cucurbit[*n*]uril Analogues: Synthetic and Mechanistic Studies. *The Journal of Organic Chemistry* **2005,** *70* (25), 10381-10392.

115. Lagona, J.; Wagner, B. D.; Isaacs, L., Molecular-recognition Properties of a Water-soluble Cucurbit[6]uril Analogue. *The Journal of Organic Chemistry* **2006,** *71* (3), 1181-1190.

116. Wagner, B. D.; Boland, P. G.; Lagona, J.; Isaacs, L., A Cucurbit[6]uril Analogue: Host Properties Monitored by Fluorescence Spectroscopy. *The Journal of Physical Chemistry B* **2005,** *109* (16), 7686-7691.

117. Jansen, R. J.; de Gelder, R.; Rowan, A. E.; Scheeren, H. W.; Nolte, R. J., Molecular Clips Based on Propanediurea. Exceptionally High Binding Affinities for Resorcinol Guests. *The Journal of Organic Chemistry* **2001,** *66* (8), 2643-2653.

118. Ustrnul, L.; Kulhanek, P.; Lizal, T.; Sindelar, V., Pressocucurbit[5]uril. *Organic Letters* **2015,** *17* (4), 1022-1025.

119. Jiang, X.; Yao, X.; Huang, X.; Wang, Q.; Tian, H., A Cucurbit[5]uril Analogue from Dimethylpropanediurea-formaldehyde Condensation. *Chemical Communications* **2015,** *51* (14), 2890-2892.

120. Wu, Y.; Xu, L.; Shen, Y.; Wang, Y.; Wang, Q., Helianthus-like Cucurbit[4]uril and Cucurbit[5]uril Analogues. *New Journal of Chemistry* **2017,** *41* (15), 6991-6994.

121. Wu, Y.; Xu, L.; Shen, Y.; Wang, Y.; Zou, L.; Wang, Q.; Jiang, X.; Liu, J.; Tian, H., The Smallest Cucurbituril Analogue with High Affinity for Ag^{+}. *Chemical Communications* **2017,** *53* (29), 4070-4072.

122. Shen, Y.; Zou, L.; Wang, Q., Template-directed Synthesis of Cucurbituril Analogues using Propanediurea as a Building Block. *New Journal of Chemistry* **2017,** *41* (16), 7857-7860.

123. Dai, C.; Shen, Y.; Wang, Q., Two Propanediurea-based Cucurbituril Analogues: Bis-ns-TD[8] and NH-ns-TD[4]. *Synlett* **2018,** *29* (18), 2381-2384.

124. Ma, D.; Gargulakova, Z.; Zavalij, P. Y.; Sindelar, V.; Isaacs, L., Reasons Why Aldehydes Do Not Generally Participate in Cucurbit[*n*]uril Forming Reactions. *The Journal of Organic Chemistry* **2010,** *75* (9), 2934-2941.

125. Huang, W.-H.; Zavalij, P. Y.; Isaacs, L., Folding of Long-chain Alkanediammonium Ions Promoted by a Cucurbituril Derivative. *Organic Letters* **2008,** *10* (12), 2577-2580.

126. Isaacs, L., Cucurbit[*n*]urils: From Mechanism to Structure and Function. *Chemical Communications* **2009,** (6), 619-629.

127. Huang, W. H.; Zavalij, P. Y.; Isaacs, L., Chiral Recognition Inside a Chiral Cucurbituril. *Angewandte Chemie International Edition* **2007,** *46* (39), 7425-7427.

128. Huang, W.-H.; Zavalij, P. Y.; Isaacs, L., Nor-seco-cucurbit[*n*]uril Molecular Containers. *Polymer Preprints (American Chemical Society, Division of Polymer Chemistry)* **2010,** *51* (2), 154-155.

129. Isaacs, L.; Park, S.-K.; Liu, S.; Ko, Y. H.; Selvapalam, N.; Kim, Y.; Kim, H.; Zavalij, P. Y.; Kim, G.-H.; Lee, H.-S., The Inverted Cucurbit[*n*]uril Family. *Journal of the American Chemical Society* **2005,** *127* (51), 18000-18001.

130. Reek, J. N.; Engelkamp, H.; Rowan, A. E.; Elemans, J. A.; Nolte, R. J., Conformational Behavior and Binding Properties of Naphthalene-walled Clips. *Chemistry-A European Journal* **1998,** *4* (4), 716-722.

131. Witt, D.; Lagona, J.; Damkaci, F.; Fettinger, J. C.; Isaacs, L., Diastereoselective Formation of Methylene-bridged Glycoluril Dimers. *Organic Letters* **2000,** *2* (6), 755-758.

132. Wu, A.; Chakraborty, A.; Fettinger, J. C.; Flowers Ii, R. A.; Isaacs, L., Molecular Clips that Undergo Heterochiral Aggregation and Self-Sorting. *Angewandte Chemie International Edition* **2002,** *41* (21), 4028-4031.

133. Wu, A.; Chakraborty, A.; Witt, D.; Lagona, J.; Damkaci, F.; Ofori, M. A.; Chiles, J. K.; Fettinger, J. C.; Isaacs, L., Methylene-bridged Glycoluril Dimers: Synthetic Methods. *The Journal of Organic Chemistry* **2002,** *67* (16), 5817-5830.

134. Wang, J.; Wang, M.; Xiang, J.; Cao, L.; Wu, A.; Isaacs, L., Dimeric Packing of Molecular Clips Induced by Interactions Between π-Systems. *CrystEngComm* **2015,** *17* (12), 2486-2495.

135. Wu, A.; Mukhopadhyay, P.; Chakraborty, A.; Fettinger, J. C.; Isaacs, L., Molecular Clips Form Isostructural Dimeric Aggregates from Benzene to Water. *Journal of the American Chemical Society* **2004,** *126* (32), 10035-10043.

136. Chakraborty, A.; Wu, A.; Witt, D.; Lagona, J.; Fettinger, J. C.; Isaacs, L., Diastereoselective Formation of Glycoluril Dimers: Isomerization Mechanism and Implications for Cucurbit[*n*]uril Synthesis. *Journal of the American Chemical Society* **2002,** *124* (28), 8297-8306.

137. Stancl, M.; Gargulakova, Z.; Sindelar, V., Glycoluril Dimer Isomerization under Aqueous Acidic Conditions Related to Cucurbituril Formation. *The Journal of Organic Chemistry* **2012,** *77* (23), 10945-10948.

138. Burnett, C. A.; Witt, D.; Fettinger, J. C.; Isaacs, L., Acyclic Congener of Cucurbituril: Synthesis and Recognition Properties. *The Journal of Organic Chemistry* **2003,** *68* (16), 6184-6191.

139. Ma, D.; Zavalij, P. Y.; Isaacs, L., Acyclic Cucurbit[*n*]uril Congeners are High Affinity Hosts. *The Journal of Organic Chemistry* **2010,** *75* (14), 4786-4795.

140. Zhang, B.; Isaacs, L., Acyclic Cucurbit[*n*]uril-type Molecular Containers: Influence of Aromatic Walls on Their Function as Solubilizing Excipients for Insoluble Drugs. *Journal of Medicinal Chemistry* **2014,** *57* (22), 9554-9563.

141. Gilberg, L.; Zhang, B.; Zavalij, P. Y.; Sindelar, V.; Isaacs, L., Acyclic Cucurbit[*n*]uril-type Molecular Containers: Influence of Glycoluril Oligomer Length on Their Function as Solubilizing Agents. *Organic & Biomolecular Chemistry* **2015,** *13* (13), 4041-4050.

142. Sigwalt, D.; Moncelet, D.; Falcinelli, S.; Mandadapu, V.; Zavalij, P. Y.; Day, A.; Briken, V.; Isaacs, L., Acyclic Cucurbit[*n*]uril-Type Molecular Containers: Influence of Linker Length on Their Function as Solubilizing Agents. *ChemMedChem* **2016,** *11* (9), 980-989.

143. Sigwalt, D.; Zavalij, P. Y.; Isaacs, L., Cationic Acyclic Cucurbit[*n*]uril-type Containers: Synthesis and Molecular Recognition Toward Nucleotides. *Supramolecular Chemistry* **2016,** *28* (9-10), 825-834.

144. Lu, W. Exploration of Cucurbit[*n*]uril (Q[*n*]) and Their Derivatives as Potential Linkers in Hydrogels and Metal-organic Frameworks (MOF). PhD Thesis, University of New South Wales, Canberra, 2018.

145. Chandrakumar, P. K.; Dhiman, R.; Woodward, C. E.; Iranmanesh, H.; Beves, J. E.; Day, A. I., Tiara[*n*]uril: A Glycoluril-Based Macrocyclic Host with Cationic Walls. *The Journal of Organic Chemistry* **2019,** *84* (7), 3826-3831.

146. Chandrakumar, P. K. Exploration of New Cucurbit[*n*]uril and a Novel Glycoluril Based Macrocycle-tiara[*n*]uril. PhD Thesis, University of New South Wales, Canberra, 2016.

CHAPTER 2

TETRAHYDROTHIOPHENETIARA[*n*]URIL

2.1 Introduction

A glycoluril is a bicyclic derivative of urea that was first prepared from allantoin by Rheineck in 1865.[1] A decade later, Schiff introduced a general synthetic approach to glycouril formation involving the acid catalyzed condensation of urea with α-dicarbonyl compounds.[2] The choice of the α-dicarbonyl compound employed could potentially result in glycoluril derivatives with different substitutions (R_1 = R_2 = H or a variety of substituents) at the cis-fused junction (C3a and C6a, Figure 2.1). Besides acid catalyzed preparation of glycolurils, there are a small number of alternative methods involving the use of potassium hydroxide, heteropolyoxometalates, and phosphoric anhydride, which have also been reported.[3-5] The characteristics of glycoluril that make them interesting as structural and chemical motif are their mildly nucleophilic uriedo nitrogen groups, concave faces that are inherent in the cis-fused structure of two imidazolidin-2-one rings and the combination of hydrogen bond acceptor (C=O) and donor (NH) functional groups. Due to these unique properties, glycolurils and their derivatives serve as the synthetic building blocks for supramolecular hosts such as cucurbiturils[6-7] and acyclic congeners[8], supramolecular self-assembled constructs[9-10], biomimetic templates[11], pharmaceuticals[12], fertilizers[5], and explosives.[13]

Of all the glycoluril based molecular constructs, particular attention has been turned to Q[*n*] in terms of synthesizing a variety of derivatives by utilizing suitably substituted glycolurils. Along with the substituted glycolurils, their diethers (Figure 2.1) have become particularly important as synthetic monomers for partially and fully substituted Q[*n*].

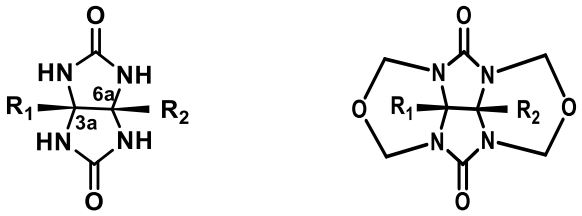

Figure 2.1 Representation of glycoluril (left) and glycoluril diether (right) R_1 and R_2 are H or the substituents.

The objective of using differently substituted glycolurils has been to introduce the functionality, to study the effect of these functionalities on the intrinsic properties of the formed Q[*n*] and to obtain substituted higher Q[*n*] homologues (where $n > 6$). For instance, different binding affinities were observed for various guests towards Q[6], Me_4Q[6] and CyP_6Q[6] as a consequence of different substitutions at the equatorial position, demonstrating the functionality effect on the electronic properties of formed Q[*n*] (Figure 2.2).[14] In addition to Q[*n*], the usefulness of these glycolurils as a building block has been shown in the synthesis of a variety of alternative supramolecular hosts as already discussed in Chapter 1. Among them, the recent synthesis of Tu[*n*]'s, a glycoluril based, water-soluble macrocycle with positively charged cavities is interesting and is the area of research for this project.[15] The emergence of Tu[*n*] as a new class of macrocyclic hosts render possibilities for synthetic modifications leading to interesting new Tu[*n*] derivatives including formation of homologues higher than are currently available and functionalization at the portals and equatorial position of the glycoluril units. The work presented in this chapter discusses the synthesis of higher homologues of Tu[*n*] using alternative functionalized glycoluril diether and dipyrazolyl methane as the starting precursors.

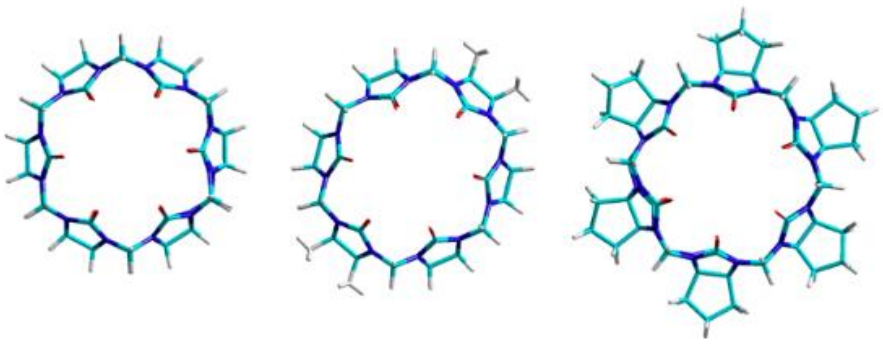

Figure 2.2 The structures of Q[6], Me_4Q[6] and CyP_6Q[6] left to right, respectively.[14]

2.1.1 The effect of the dihedral angle (β) on higher homologue distribution

In the Q[*n*] family, the importance of the effect of substitution on the proportional distribution of homologues has been demonstrated through the synthesis of fully substituted Q[*n*]'s incorporating different substitutions at the equatorial positions (Chapter 1, Section 1.2.3.1). The recent synthesis of the family of cyclopentano (CyP) and cyclobutano (CyB) substituted Q[*n*] by Day and co-workers are two examples that have provided access to higher homologues, Q[7] and Q[8] respectively.[16-17] The proposed reason for the difference in the homologue distribution and their corresponding yields was attributed to the dihedral angle (β) of the glycoluril diether employed as the initial reactant (Figure 2.3). It was reported that the dihedral angle at the concave face of the two fused imidazolidinone rings is an influential factor in controlling higher homologue distribution. The type of substitution present at the fused junction, in turn, governs the dihedral angle.[16]

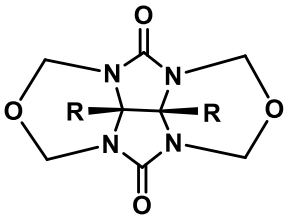

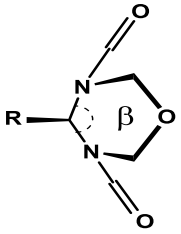

1 R = R =Me
2 R = R = $(CH_2)_4$ ring
3 R = R = $(CH_2)_3$ ring
4 R = R = $(CH_2)_2$ S ring
5 R = R = $(CH_2)_2$ ring

Side view

Figure 2.3 Representation of the substituted glycoluril diethers and side view showing the dihedral angle (β).

Table 2.1 shows the dihedral angles of glycoluril diethers with different substitutions determined from single-crystal X-ray diffraction data. It is apparent that the yields of higher homologues increase with the increase in the β angle. In case of methyl substitution, the observed yield of Q[6] was strikingly low with only 2%.[18] Change of substitution to cyclohexane (CyH) considerably increased the Q[6] percentage yield to 10%, which directly correlates with the wider dihedral angle.[19] With the cyclopentano substitution[16], the angle was increased by 1.2° compared to methyl, affording a significant increase in the yield of Q[6] from 2% to 38% and a decent yield of 16% for $CyP_7Q[7]$ (Figure 2.4).

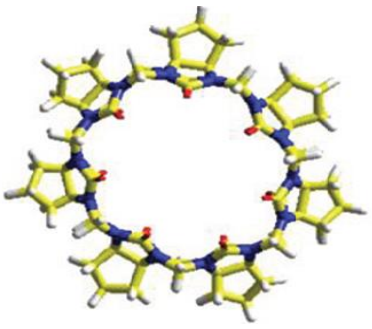

Figure 2.4 Representation of the structure of $CyP_7Q[7]$.[16]

However, when the glycoluril is substituted with the tetrahydrothiophene (THT) group[20-21], the β angle increases by 0.33° and 1.53° relative to cyclopentano and methyl substitution, providing yields of 60 and 25% of $THT_5Q[5]$ and $THT_6Q[6]$, respectively. Although the cyclopentano ring without substitution successfully demonstrated homologues distribution as high as Q[7], the cyclopentano ring with a sulphur functionality i.e., THT afforded homologues no higher than Q[6] for fully substituted Q[*n*]'s. However, in the case of partially substituted $THT_mQ[n]$, the use of THT functionality lead to the formation of higher homologues - $THT_{(1,2)}Q[7]$ and THTQ[8].[21] These findings imply that the dihedral angle while important, it is not the only determinant to higher homologues, especially when functionality is included. Further increase in the dihedral angle by 1.69° for cyclobutano substitution[17] with respect to cyclopentano substitution resulted in the modest 3-5% yield of $CyB_8Q[8]$.

Table 2.1 Dihedral angles for glycoluril diethers with different substitutions[16-17, 21]

Glycoluril substitution R =					
	Methyl	Cyclohexano	Cyclopentano	Tetrahydro thiophene	Cyclobutano
Mean plane angle β (°)	108.88°	109.31°	110.08°	110.41°	111.77°
Homologue distribution	$Me_{10}Q[5]$ - 98% $Me_{12}Q[6]$ - 2%	$CyH_5Q[5]$ - 80% $CyH_6Q[6]$ - 10%	$CyP_5Q[5]$ - 45% $CyP_6Q[6]$ - 38% $CyP_7Q[7]$ - 16%	$THT_5Q[5]$ - 60% $THT_6Q[6]$ - 25%	$CyB_5Q[5]$ - 35-40% $CyB_6Q[6]$ - 44-50% $CyB_7Q[7]$ - 10-12% $CyB_8Q[8]$ - 3-5%

All these examples suggest that the larger dihedral angle of the concave face of glycoluril diether plays a pivotal role in the formation of higher homologues by influencing the

curvature of the glycoluril oligomers formed during the reaction process before the final macrocyclization step takes place.

2.1.2 Tiara[*n*]uril and higher homologue formation

As a new class of supramolecular hosts, Tu[*n*] may exhibit considerable potential for a variety of future applications for guest molecules that are anionic or electronegative. In relation to the known Tu[*n*] family, one of the key areas that needs exploration are methods to the formation of higher homologues that are equipped with larger sized cavities. Higher homologues would provide cavities with an increased volume enabling the accommodation of larger guests. In addition, the use of different substituents at glycoluril units could have substantial effect on the electronic properties of the cavity and portals of newly formed Tu[*n*]'s. As illustrated in Chapter 1, one of the approaches followed by Day and co-workers towards the synthesis of higher homologues of Tu[*n*] involved the use of differently substituted glycoluril diethers. The idea was based on the anticipation that the increase in the dihedral angle would provide a positive outcome towards the distribution ratio of homologues similar to Q[*n*]'s. It was reported that the glycoluril diether substituted with methyl or the cyclopentano ring when condensed with dipyrazolylmethane formed Tu[3] (Chapter 1, Scheme 1.13 and 1.15) as the only homologue.[15] In both cases, the formed Me_{10}Tu[3] and CyP_3Tu[3] has cavity size similar to Q[5].[15, 22] With methyl substitution, this is in agreement with the homologue distribution based on the β angle (Table 2.1). However, the formation of only CyP_3Tu[3] with cyclopentano substitution, which is known to have a propensity to form higher Q[*n*] homologues was intriguing in that the reaction was indifferent to the substitution. Therefore, new Tu[*n*]'s were explored employing THT glycoluril diether. The wider dihedral angle of THT glycoluril diether compared to the cyclopentano substitution provides a possibility for the formation of homologues with more than 3 glycoluril units

incorporated within a macrocycle. In addition, THT moiety maintains the five-membered ring of cyclopentane with the inclusion of a sulphur atom as part of the ring. The use of this substitution was expected to provide insight into the influence of functionality on higher homologue distribution and possible changes to the electronic properties of the formed Tu[*n*]'s.

2.2 Aims of the study

The aims of this chapter are as follows,

1. To synthesize functionalized Tu[*n*] using THT substituted glycoluril diether and to investigate the possible influence of functionalization on homologues of Tu[*n*] formed.
2. To explore the possible effect of acid strength and type to optimise the synthesis of Tu[*n*].
3. In addition, to investigate possible anionic template effects on the homologue distribution ratio toward new Tu[*n*]'s.

2.3 Experimental

2.3.1 Materials

The starting materials and Dowex ion exchange resin were purchased from commercial sources and used without further purification. Dowex 50WX2 cation exchange resin was used for column chromatographic purification of cationic macrocycles.

2.3.2 Instrumental methods

All one dimensional and two dimensional ^{1}H NMR spectra were obtained using Varian 400 MHz, 100 MHz for ^{13}C NMR and chemical shifts are reported in ppm. All the NMR experiments were performed at 25 °C unless and otherwise specified. Decomposition temperature was determined employing thermogravimetric analysis technique on STA 449. Mass spectral analysis were carried out at the Australian National University. Elemental analysis was performed by Campbell Microanalytical laboratory at the University of Otago, New Zealand. The X-ray diffraction measurements were carried out at 100 K on a Bruker D8 Quest Single Crystal diffractometer using Incoatec IμS 3.0 Microfocus Source with Mo-Kα radiation (λ = 0.710723 Å). Symmetry related absorption corrections using the program SADABS[34] were applied and the data were corrected for Lorentz and polarisation effects using Bruker APEX3 software.[35] The structure was solved with SHELXT[36] (intrinsic phasing) and the full-matrix least-square refinements were carried out using SHELXL-2016[36] through Olex2[37] suite of software. The non-hydrogen atoms were refined anisotropically. Hyperchem modelling was carried out on HyperChem professional 8.0.7 for Windows Molecular Modelling System.

2.3.3 General Procedures and Methodology

2.3.3.1 Chromatography

Column chromatography was performed using Dowex 50WX2 cation-exchange resin, (200-400 mesh), eluting with 0.5M HCl/45% HCO_2H solvent system.

2.3.3.2 Thermogravimetric analysis (TGA)

Thermogravimetric analysis was carried out by heating the samples over the temperature range of 50 to 1000 °C under a nitrogen purge of 20 mL/min. The heating rate was maintained at 20 K/min and 5 K/min for THT_3Tu[3] and THT_4Tu[4], respectively. The percentage mass loss and decomposition temperature for respective sample was obtained from the resulting thermogram.

2.3.3.3 Hyperchem modelling

Molecular modelling was performed using Hyperchem software. The 2D molecular structure of the host and the guest were drawn separately, and the overall charge allotted using semi empirical (PM3) method followed by optimization for the minimum energy state. The guest was then translated into the cavity of the host and geometry optimization calculations were performed employing MM+ force field.

2.3.3.4 Electron surface potential map (ESP)

Surface potential map was performed on the geometry relaxed structure modelled with ωB97XD/6-31G(d.p), gas phase.

2.3.3.5 Experimental procedures

Synthesis of dibromodimethyl glycoluril

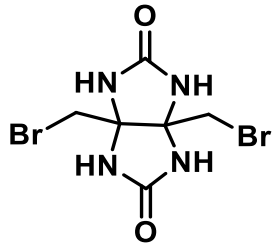

1

1,4-dibromobutane-2,3-dione (10.0 g, 41.0 mmol) and ethanol (48 mL) were stirred under a nitrogen atmosphere until all the solids have dissolved forming a clear yellow solution. Urea (4.92 g, 82.0 mmol) and 4.8 mL of TFA was then added and the solution stirred for approximately an hour until all the solid have dissolved. The reaction mixture was further stirred for 48 hr at RT. The crude product was filtered and washed at least thrice with MeOH and air-dried. The obtained product was used for the subsequent steps without purification. The physical data of **1** was consistent with that previously reported.[23]

^{1}H NMR (DMSO-d_6): δ 7.58 (4H, s), 3.87 (2H, s), 3.38 (2H, s).

Synthesis of dibromodimethyl glycoluril diether

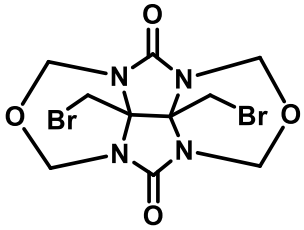

2

Dibromodimethyl glycoluril **1** (7.00 g, 21.0 mmol), paraformaldehyde (2.86 g, 94.5

mmol) and 32% HCl (25 mL) were combined together in a round bottom flask and stirred for 20 hr at RT under a nitrogen atmosphere. 200 mL of water was then added to the reaction mixture and stirred for a further 10 min. The dark green crude product thus obtained after stirring was filtered and washed with MeOH and air-dried. The physical data of **2** was consistent with that previously reported.[17]

^{1}H NMR (DMSO-d_6): δ 5.25 (4H, d, *J* = 12.5 Hz), 5.06 (4H, d, J = 12.5 Hz), 4.62 (4H, s).

Synthesis of tetrahydrothiophene glycoluril diether

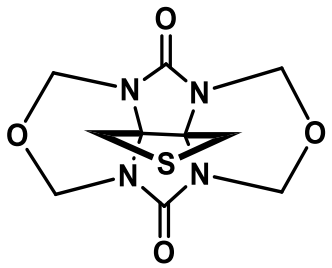

3

Diether **2** (1 g, 2.43 mmol), sodium sulphide $Na_2S.9H_2O$ (874 mg, 3.64 mmol), anhydrous sodium carbonate (495 mg, 4.77 mmol) were combined together and then under nitrogen atmosphere, 5 mL of dry DMF was subsequently added. The reaction mixture was stirred rapidly in a preheated oil bath at 80 °C. After 20 min the sealed flask was removed and sonicated to help break up the lumps of $Na_2S.9H_2O$. The reaction was then completed between 80°- 85 °C over a total of 4 hr. The reaction was cooled to RT and decanted into water. The resulting dark brown solution was filtered under vacuum and washed with excess of MeOH in order to remove any excess DMF. The product was air-dried to afford a cream coloured solid material (60% overall yield). This was a slightly modified procedure and the physical data of **3** was consistent with that previously reported.[20]

^{1}H NMR (DMSO-d_6): δ 3.45 (4H, s), 4.96 (4H, d, *J* = 12.0 Hz), 5.25 (4H, d, *J* = 12.0 Hz).

Synthesis of bis(3,5-dimethyl-1H-pyrazol-1-yl)methane

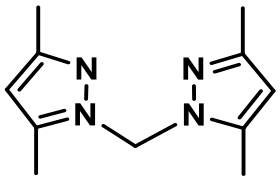

4

3,5-Dimethylpyrazole (7.4 g, 77.1 mmol), 40% tetrabutylammonium chloride (4 mL), 50% NaOH (65 mL) and DCM (130 mL) were combined. The mixture was refluxed for 8 hr with vigorous stirring. The stirred mixture was cooled to RT and the organic phase extracted using DCM and dried over anhydrous K_2CO_3. The solvent was then removed using rotary evaporation to give compound **4** as a viscous liquid (9.85 g) which was used without purification. The physical properties were identical to those previously reported.[24-25]

^{1}H NMR ($CDCl_3$): δ 2.17 (6H, s), 2.40 (6H, s), 5.77 (2H, s), 6.04 (2H, s).

Synthesis of bis(3,5-dimethyl-1H-pyrazol-1-yl)methane HBr salt

Compound **4** (9.85 g) was dissolved in 48% HBr solution (50 mL). The solvent was reduced to near dryness using the rotary evaporator to obtain a crystalline residue (sometimes the HBr salt remained as a viscous yellow liquid). Addition of 50 mL of acetone to the oil and allowing the solution to stand overnight at RT afforded off-white crystals. The crystals of the HBr salt of compound **4**, were then collected by decanting the acetone.[20]

^{1}H NMR ($CDCl_3$): δ 2.55 (6H, s), 2.76 (6H, s), 6.28 (2H, s), 7.42 (2H, s).

Synthesis of bis(3,5-dimethyl-1H-pyrazol-4-yl)methane

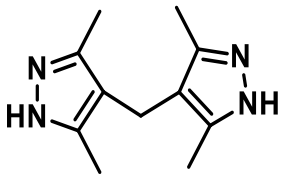

5

The HBr salt of compound **4** was placed in an appropriate reaction flask and then heated gradually in a Kugel Rohr apparatus oven up to 200 °C (the flask was open and vented into a fume cupboard). After reaching 200 °C, the desired temperature was maintained for atleast 1 hr. After an hour, the crystalline white solid melted and then turned into off-white solid. The resulting solid after cooling to RT was dissolved in water and solid NaOH added until pH 10 was obtained. The solid suspension formed was collected by filtration and dried under vacuum, to give dipyrazole **5** as an off-white solid (82% overall yield). The physical data was consistent with that previously reported.[26]

^{1}H NMR (DMSO-d_6): δ 1.99 (12H, s), 3.34 (2H, s), 11.87 (2H, s).

Synthesis of bis(3,5-dimethyl-1H-pyrazol-4-yl)methane HCl salt

Compound **5** was converted to HCl salt by dissolving the product in 10 mL of 37% HCl. Excess acid was then removed to near dryness using the rotary evaporator to obtain product **5a** as an off-white solid.

^{1}H NMR (D_2O): δ 2.2 (12H, s), 3.67 (2H, s).

Synthesis of bis(3,5-dimethyl-1H-pyrazol-4-yl)methane HSO_4^- salt

Compound **5** was converted to the hydrogen sulphate (HSO_4^-) salt by dissolving it in a minimum volume of conc. H_2SO_4. The HSO_4^- salt was then precipitated by the addition of dry diethyl ether followed by ethanol. The product **5b** was obtained as a fine white powder after filtration.

^{1}H NMR (D_2O): δ 2.22 (12H, s), 3.68 (2H, s).

Synthesis of bis(3,5-dimethyl-1H-pyrazol-4-yl)methane $CH_3SO_3^-$ salt

Compound **5** was converted to the methane sulphonate ($CH_3SO_3^-$) salt by dissolving the product in a minimum volume of CH_3SO_3H. The $CH_3SO_3^-$ salt was precipitated by adding methanol followed by diethyl ether. The product **5c** was then filtered to obtain a white precipitate.

^{1}H NMR (D_2O): δ 2.22 (12H, s), 2.77 (6H, s), 3.68 (2H, s).

General procedure for the synthesis of tetrahydrothiophenetiara[*n*]uril (THT$_n$Tu[*n*])

A mixture of dipyrazole methane **5** or its salt **5a**, **5b** or **5c** (1.0 mmol) and THT glycoluril diether **3** (2.0 mmol) were combined together and ground to form a fine powder using mortar and pestle. To the ground mixture, 2 mL of 12 M acid was then added and the mixture stirred for 30 min at RT. The temperature was increased to 50 °C and maintained at that temperature for 90 min. The temperature of the reaction mixture was then increased to 90 °C and stirred further for 3 hr. After 3 hr, an additional portion of glycoluril diether (1.0 mmol) was added and the mixture left to stir overnight at 90 °C. The mixture was cooled to RT and the HCl was evaporated to obtain the brown coloured crude solid

material. The crude mixture was examined by ^{1}H NMR to investigate the formation of products. ^{1}H NMR analysis revealed the peaks corresponding to the desired products along with number of other products that included THT$_n$Q[n] and different polymeric material.

Synthesis of $THT_3Tu[3]Cl_2$ and $THT_4Tu[4]Cl_2$

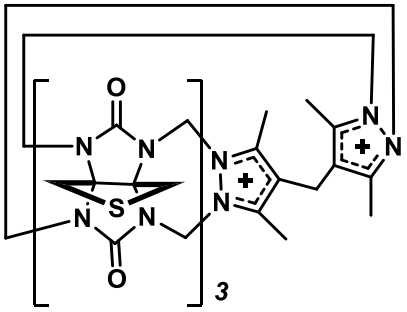

6

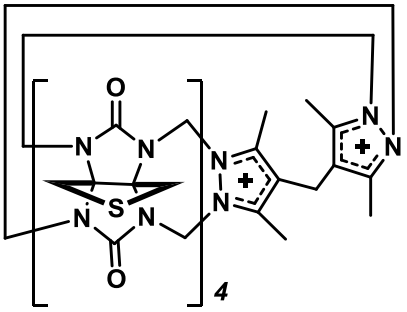

7

$THT_3Tu[3]Cl_2$ **6** and $THT_4Tu[4]Cl_2$ **7** were prepared as described in the general procedure from THT glycoluril diether **3** (3.93 mmol) and bis(3,5-dimethyl-1H-pyrazol-4-yl)methane HCl salt **5a** (1.31 mmol) using 2 mL of 37% HCl to give after purification white needle like crystals for $THT_3Tu[3]Cl_2$ (36% overall yield) and spherical crystals for $THT_4Tu[4]Cl_2$ (18% overall yield).

$THT_3Tu[3]Cl_2$

Mp > 390 °C, IR (KBr, cm^{-1}): 3600-3050 s-br, 2983m, 2926m, 1741s, 1617m, 1463s, 1443s, 1375m, 1330s, 1306s, 1153m, 1105m, 992m, 921s, 832m, 764s, 615m. ^{1}H NMR (D_2O): δ 2.71 (12H, s), 3.48 (4H, s), 3.53 (4H, s), 3.59 (4H, s), 3.78 (2H, s), 4.50 (4H, d, J = 16.0 Hz), 5.65 (4H, d, J = 16.0 Hz), 5.89 (4H, d, J = 16.0 Hz), 6.38 (4H, d, J = 16.0

Hz). ^{13}C NMR (D_2O): δ 10.9, 15.8, 38.2, 39.8, 41.4, 45.7, 52.1, 85.9, 86.3, 87.6, 117.2, 146.7, 154.8, 155.7. MS (ES): *m/z* 451.3 ($M^{2+}/2$). Anal calc. for $C_{37}H_{42}N_{16}O_6S_3.7H_2O.2Cl^-$ (1100.058) Require: C, 40.39; H, 5.13; N, 20.37; S, 8.74. Found: C, 40.25; H, 4.78; N, 20.42; S, 8.53.

$THT_4Tu[4]Cl_2$

Mp > 410°C, IR (KBr, cm^{-1}): 3600-3100 s-br, 3018w, 2924m, 2852w, 1740s, 1458s, 1334w, 1458s, 1334w, 1299s, 1150m, 1107w, 994m, 928s, 837m, 763s, 615m. ^1H NMR (D_2O): δ 2.64 (12H, s), 3.54 - 3.56 (12H, m), 3.65 (4H, s), 3.68 (2H, s), 4.40 - 4.49 (6H, 2 d's, *J* = 16.0 Hz), 5.69 (4H, d, *J* = 16.0 Hz), 5.73 (4H, d, *J* = 16.0 Hz), 5.74 (2H, d, *J* = 16.0 Hz), 6.35 (4H, d, *J* = 16.0 Hz). ^{13}C NMR (D_2O): δ 10.5, 16.0, 37.3, 38.3, 38.6, 40.7, 45.9, 46.0, 52.5, 85.9, 86.9, 87.0, 87.1, 115.4, 146.9, 155.4, 155.7. MS (ES): *m/z* 563.4 ($M^{2+}/2$). Anal calc. for $C_{45}H_{50}N_{20}O_8S_4.9H_2O.1HCOOH.\ 2Cl^-$ (1406.357) Require: C, 39.28; H, 5.01; N, 19.91; S, 9.12. Found: C, 38.90; H, 4.87; N, 19.93; S, 8.71.

Synthesis of $THT_3Tu[3](HSO_4)_2$ and $THT_4Tu[4](HSO_4)_2$

$THT_3Tu[3](HSO_4)_2$ and $THT_4Tu[4](HSO_4)_2$ were prepared as described in the general procedure from THT glycoluril diether **3** (3.93 mmol) and bis(3,5-dimethyl-1H-pyrazol-4-yl)methane HSO_4^- salt **5b** (1.31 mmol) using 2 mL of 12 M H_2SO_4 in place of HCl. Upon completion of the reaction, the mixture was cooled to RT and MeOH was added to aid precipitation and remove excess H_2SO_4.

Synthesis of $THT_3Tu[3](CH_3SO_3)_2$ and $THT_4Tu[4](CH_3SO_3)_2$

$THT_3Tu[3](CH_3SO_3)_2$ and $THT_4Tu[4](CH_3SO_3)_2$ were prepared as described in the procedure from THT glycoluril diether **3** (3.93 mmol) and bis(3,5-dimethyl-1H-pyrazol-

4-yl)methane $CH_3SO_3^-$ salt **5c** (1.31 mmol) using 2 mL of 12 M CH_3SO_3H as replacement to HCl. After overnight stirring, MeOH was added to the cooled crude reaction mixture to form precipitate and to remove excess acid.

2.3.3.6 Purification of tetrahydrothiophenetiara[*n*]uril (THT$_n$Tu[*n*])

The purification of the crude reaction mixture was achieved through a combination of Dowex cation exchange column chromatography and a crystallization process. The crude product was dissolved in a minimum volume of 50% HCO_2H, loaded onto dowex 50WX2 cation exchange resin and eluted using 45% HCO_2H/0.5 M HCl solvent system. The column fractions were collected and monitored continuously by ^{1}H NMR to detect the presence of resonances corresponding to the desired THT$_n$Tu[*n*]. The ^{1}H NMR spectrum of the fractions eluting later from the column revealed the presence of a mixture of THT$_3$Tu[3] and THT$_4$Tu[4]. For separation of the two homologues, these fractions were mixed and evaporated to dryness to obtain solid residues. Further, these residues were dissolved in water, heat concentrated and allowed to cool to obtain crystalline product through the process of crystallization.

2.4 Results and Discussion

2.4.1 Synthesis of tetrahydrothiophenetiara[*n*]uril (THT$_n$Tu[*n*])

Although the successful formation of Me$_{10}$Tu[3] and CyP$_3$Tu[3] present examples of Tu[3] that carry different substitutions, the formation of homologues larger than Tu[3] have not been reported. This absence provided the motivation to design a reaction sequence that could potentially lead to new functionalized Tu[*n*]'s which also had the objective to achieving higher homologues (where n > 3). The dihedral angle effect on

higher Q[*n*] proportionality as illustrated in section 2.1.1, suggests an opportunity that could be extrapolated to favour the formation of higher Tu[*n*] homologues. Since the reaction of Tu[*n*] is assumed to take place through step-growth polymerization followed by macrocyclization[27], the wider dihedral angle would in this case, result in the formation of glycoluril oligomers with a smaller arc and the potential for a greater number of glycoluril units prior to - cyclization and condensation with the dipyrazolium moiety, forming macrocycles with larger cavities (Scheme 2.1). Given that the THT glycoluril diether β angle is larger than the CyP glycoluril diether (Table 2.1), it was anticipated that THT glycoluril diether could serve as a workable building block for achieving higher homologues of Tu[*n*]. In addition, the presence of the sulphur atom imparts to the ring potential chemical opportunities for further modifications to achieve new functionalized Tu[*n*]'s. Moreover, in the event that new THT$_n$Tu[*n*]'s were formed, these could also be manipulated to establish drug delivery systems including through the formation of gold nanoparticle conjugates.[28]

The synthesis of THT$_n$Tu[*n*] was designed with an intention to favour homologues larger than Tu[3]. The previously reported procedure for Tu[*n*] synthesis with methyl and cyclopentano substituents was performed with 32% HCl using tetramethyldipyrazolyl methane as a free base **5**, affording Tu[3] as the only homologue. To determine the effect of THT towards the formation of Tu[*n*] homologues, our initial attempt involved performing the reaction using previously employed synthetic conditions (Scheme 2.1). To our surprise, the ^{1}H NMR of crude mixture revealed the formation of more than one homologue for THT$_n$Tu[*n*] and various other byproducts that included THT$_n$Q[*n*] and polymeric material. This outcome indicated a positive influence of the THT functionality towards Tu[*n*] homologues.

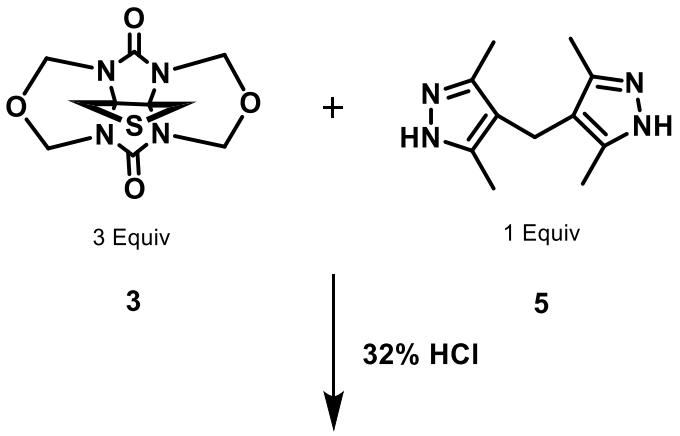

Scheme 2.1 Synthetic scheme for THT$_n$Tu[n]$^{2+}$

However, the proportion of higher homologue formed was less and the byproducts including THT$_n$Q[n] and polymeric material were more prominent in the ^{1}H NMR spectrum. Further, in order to maximize the probability for the formation of higher homologues, the procedure was optimized by modifying some of the reaction conditions (using acid with high strength and the salt form of tetramethyldipyrazolyl methane **5**). The synthesis involved the condensation of THT glycoluril diether **3** and tetramethyldipyrazolyl methane HCl salt **5a** in the ratio 3:1 using 37% HCl. The use of the higher strength HCl, i.e. 37% HCl along with the salt form of tetramethyldipyrazolyl methane afforded improved homologue distribution for the resulting THT$_n$Tu[n] when compared to the reaction carried out using 32% HCl and tetramethyldipyrazolyl methane as a free base. In addition, ^{1}H NMR of the crude reaction mixture was relatively clearer with lower quantities of byproducts.

In both the cases, the methodology involved conducting the reaction over a period of 30 min at RT, 90 min at 50°C, followed by extended overnight stirring at 90°C. In this reaction sequence, the addition of THT glycoluril diether was carried out in a step-wise

manner with the introduction of two portions at the start of the reaction and the third portion being added after maintaining the temperature to 90°C for 3 hr. The intent of this order of addition was to starve the reaction of the availability of THT glycoluril diether, in order to reduce the formation of $THT_nQ[n]$. Upon completion of the reaction after overnight heating, HCl was removed to obtain solid brown residue that was then analyzed by ^1H NMR. The ^1H NMR spectrum of crude material appeared to be rather complicated compared to $Me_{10}Tu[3]Cl_2$[20], indicating the formation of a number of products.

Spectral analysis of the crude revealed characteristic methylene doublets in the range of 4.4 - 5.7 ppm region that were similar to the methylene linkers of the glycoluril in $THT_nQ[n]$.[20] However, typical methylene doublets were also observed over 5.8 - 6.5 ppm chemical shift range as downfield resonances consistent with the previously observed methylene proton resonances linked to the pyrazolium groups.[20] Additionally, the peaks corresponding to THT ring protons and the methyl protons on the pyrazolium moiety further indicated that the THT substituted Tu[*n*] might have formed (Figure 2.5).

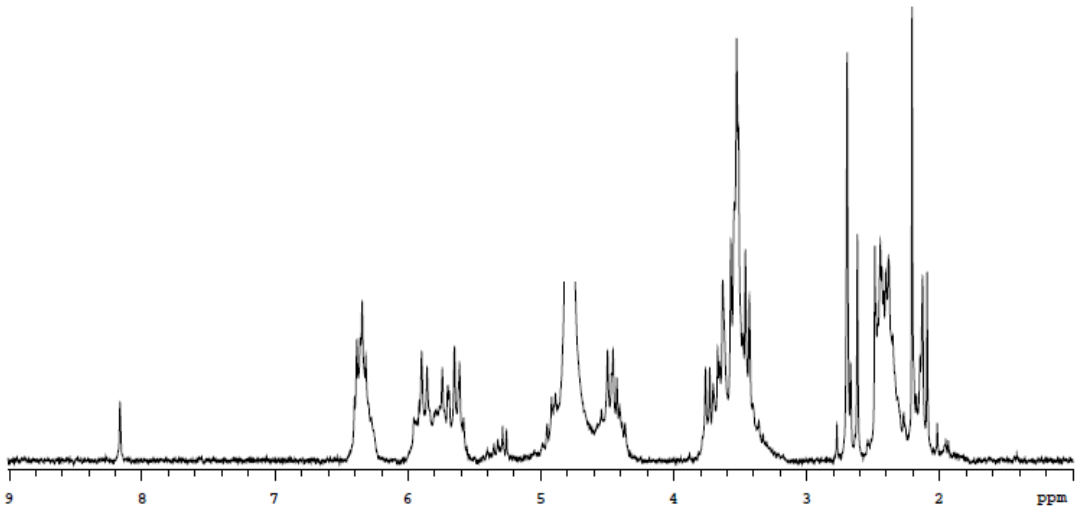

Figure 2.5 The ^1H NMR spectrum of the crude reaction mixture between 3 and 5a after 20hr at 90 °C in D_2O.

However, due to the complexity of the NMR spectrum, arriving at a conclusion of different $THT_nTu[n]$ homologues being formed was not possible until complete purification was achieved.

Having demonstrated the increased higher homologue proportion with 37% HCl, further synthesis employing different acids was conducted to ascertain the influence of acid type on the distribution ratios of $THT_nTu[n]$ homologues. The description related to the reactions employing different acids is presented later in this chapter in section 2.5.

2.4.2 Purification and Structural elucidation of $THT_nTu[n]$

To evaluate and fully characterize the formed $THT_nTu[n]$ homologues, the crude reaction mixture was purified and the products isolated. The purification process involved the combination of cation exchange chromatography and crystallization. The order of elution for the crude reaction mixture was found to be $THT_5Q[5]$ in the initial fractions followed by some unknown impurities, with $THT_nTu[n]$ eluting almost at the end. The ^1H NMR of the later fractions was more complex than known Tu[3]'s with multiple proton resonances overlapping in the region of 4.3 - 4.7 ppm and 5.5 - 5.9 ppm. In addition, the presence of resonances corresponding to THT ring protons and two singlets for the pyrazolium CH_3 protons in the region 2.6 - 2.75 ppm indicated the formation of more than one homologue. Next, the major experimental difficulty faced was the separation of the formed homologues. Due to their similar properties both tend to elute together through the column and the fractions contained a mixture of $THT_3Tu[3]$ and $THT_4Tu[4]$. As a result, these fractions were combined together and subjected to chromatography multiple times in an attempt to achieve separation. However, these attempts proved unsuccessful. Therefore, further purification was achieved through a process involving crystallization. Various combinations of different solvent systems were also explored; however,

crystallization using the pure water facilitated separation of both homologues most efficiently. The process of recrystallization was repeated several times to obtain pure $THT_3Tu[3]$ and $THT_4Tu[4]$ in the chloride form. The pure products were then thoroughly analyzed spectroscopically with 1D NMR and ESMS. Also, for a better understanding of the structural features of the new homologues, 2D NMR techniques (DCOSY and NOESY) were used to obtain elaborative information regarding the coupling and spatial arrangements of the protons.

$THT_3Tu[3]Cl_2$ - Structural elucidation

^{1}H NMR **-** $THT_3Tu[3]$ crystallizes as the chloride from water forming white needle-like crystals. The addition of a small volume of 90% formic acid to the copious $THT_3Tu[3]$ fractions was found to enhance the crystallization process effectively. The ^{1}H NMR spectrum displayed four sets of doublets at 4.50, 5.65, 5.89, and 6.38 ppm each integrated for 4 protons (Figure 2.6). These peaks represent magnetically non-equivalent methylene bridged protons at the center of the glycoluril oligomer moiety (labelled at $\mathbf{g_A}$ and $\mathbf{g_B}$) and those between the pyrazole group and at the end of the glycoluril oligomer moiety (labelled at $\mathbf{f_A}$ and $\mathbf{f_B}$). A pair of upfield doublets at 4.50 and 5.65 ppm show similar chemical shift to the methylene proton resonances of $THT_nQ[n]$[20] which is consistent with two adjacent glycoluril units. The remaining protons of $THT_3Tu[3]$ occur as singlets, three singlet resonances in the range 3.4 - 3.6 ppm corresponds to the THT ring protons, a singlet at 2.71 ppm and 3.78 ppm each represents the chemically identical CH_3 group on pyrazolium unit and CH_2 group (labelled at **b)**, respectively. The methylene protons in the macrocycle are non-equivalent due to magnetically different environments. Consequently, these protons experience different shielding that causes their resonances to appear at different chemical shift values. This was confirmed using DCOSY technique

that revealed the correlation between the methylene peaks appearing between 5.89 - 6.38 ppm and 4.50 - 5.65 ppm, respectively, indicating geminal protons to be in two different stereochemical orientations (Appendices A1). The above interpretation was additionally upheld by employing NOESY that provided extra information in regard to through space correlations with structurally near protons. From the spectrum, it could be construed that the pyrazolium methyl groups are correlated with the methylene protons appearing at 6.38 ppm, suggesting the protons marked at $\mathbf{f_B}$ to be in plane with CH_3 groups and hence appearing downfield.

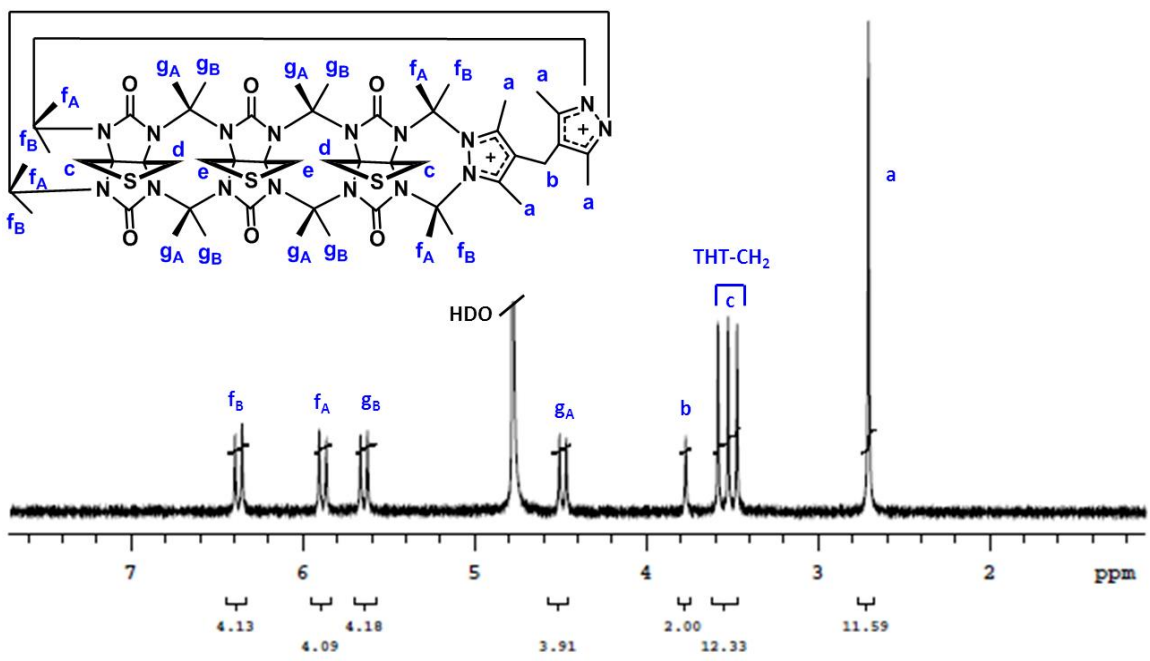

Figure 2.6 The ^{1}H NMR spectrum of $THT_3Tu[3]Cl_2$ in D_2O with assignment of significant resonance.

Another interesting aspect revealed by NOESY is the correlation of the THT methylene protons. The THT methylene protons labelled at **c** show long-range coupling with the $\mathbf{f_A}$ protons and are aligned with the middle resonance of the set of 3 singlets for THT ring protons indicating that the correlation with **c** is consistent with these protons occurring at the middle singlet (3.53 ppm). Similar to $\mathbf{f_A}$ protons, the $\mathbf{g_A}$ protons cross correlate with

the remaining THT proton singlets (3.48 and 3.59 ppm). However, due to insignificant chemical shift separation, it was difficult to clearly differentiate between the resonances for **d** and **e** protons. In addition, a correlation is also observed across peaks labelled at **a** (CH_3) and **b** (the CH_2 between the two pyrazolium rings) (Appendices A2).

^{13}C NMR **-** The structure of $THT_3Tu[3]$ deduced from the ^{1}H NMR spectrum was supported by ^{13}C NMR spectrum, which accounted for the presence of fourteen different carbons. The characteristic peaks at 155.7 and 154.8 ppm are assigned to the two different carbonyls endorsing the presence of two chemically different glycoluril units (in a ratio of 2:1). The quaternary carbons of the dipyrazolium unit appears at 146.7 and 117.2 ppm (CH_3-**C** and CH_2-**C** in a ratio 2:1) while carbons corresponding to CH_2 and chemically identical CH_3 groups are observed at 15.8 and 10.9 ppm, respectively. Typical peaks for THT carbons appear at 38.2, 39.8 and 41.4 ppm values. The remaining carbons representing the methylene linkers and glycoluril quaternary carbons are assigned to the peaks at 45.7, 52.1 (CH_2)-, 85.9, 86.3 and 87.6 (C)- ppm respectively (Appendices A3).

ESMS **-** The m/z peak at 451.3 is consistent with the dicationic structure $(THT_3Tu[3]^{2+})/2$ suggesting the presence of three methylene linked glycoluril units also linked to the dipyrazolium methane moiety as a macrocycle, further supporting the formation of $THT_3Tu[3]$.

$THT_4Tu[4]Cl_2$ - Structural elucidation

^{1}H NMR **-** Besides a difficult purification process, the structural elucidation of $THT_4Tu[4]$ proved to be rather tricky. Due to the presence of a plane of symmetry in the macrocycle, the coupling between the magnetically non-equivalent protons resulted in near coincidental chemical shifts of the resonances leading to a complex ^{1}H NMR

spectrum (Figure 2.7). The analysis of the spectrum revealed resonances explicit to the pyrazolium CH_2 group, 16 THT ring protons and CH_3 groups at 3.68, 3.65 - 3.54 and 2.64 ppm, respectively. Moreover, the chemical shift range from 4.4 to 6.4 ppm shows multiple coinciding resonances that pertain to the methylene linkers between the adjacent glycoluril units and between the glycoluril and pyrazolium moieties. The overlapping peaks from 5.67 - 5.76 ppm integrated to 10 protons, indicative of 3 overlapped doublets with an integral ratio of 2:4:4, whereas, the resonances corresponding to values between 4.40 - 4.49 ppm integrated to 6 protons addressing the presence of two doublets with an integral ratio of 4:2.

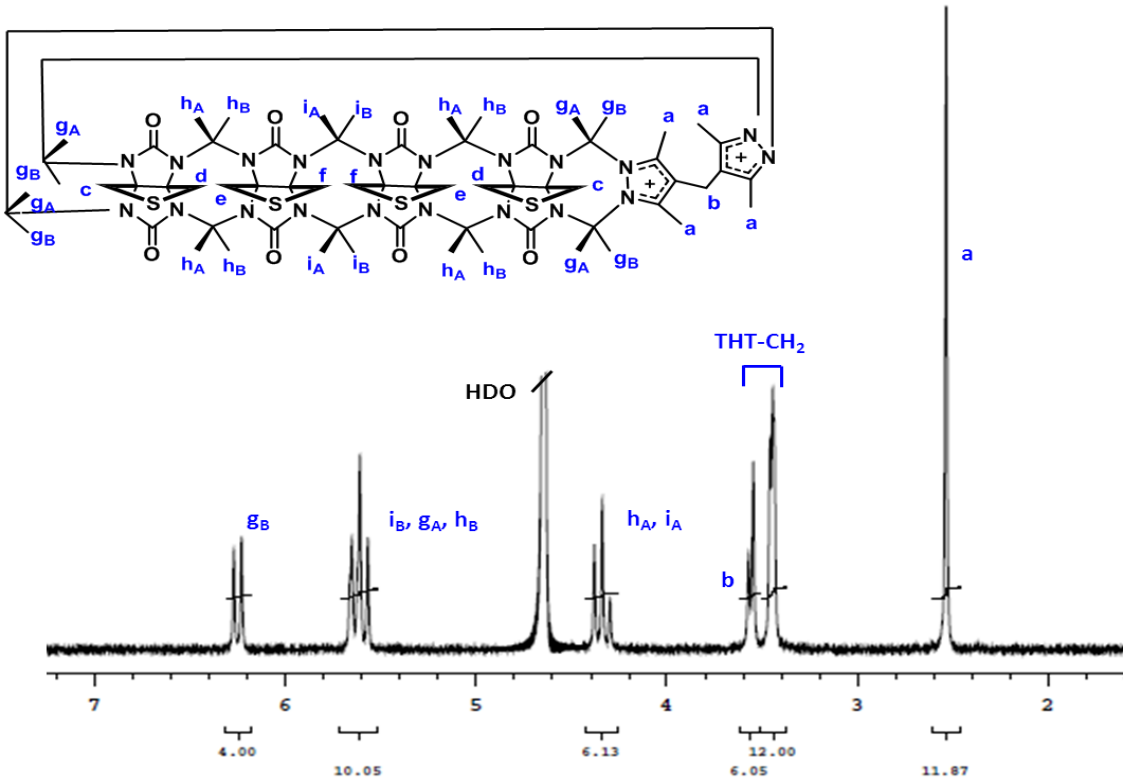

Figure 2.7 The ^{1}H NMR spectrum of $THT_4Tu[4]Cl_2$ in D_2O with assignment of significant resonances.

Further to this, the relationship between these doublets and their corresponding peak values was unveiled through DCOSY analysis (Appendices A4). The occurrence of cross peaks between the resonances at 6.4 and 5.77 ppm, 5.72 and 4.5 ppm, and 5.77 and 4.45 ppm demonstrates correlation and peaks are assigned to protons labelled at $\mathbf{g_A}$, $\mathbf{g_B}$, $\mathbf{h_A}$, $\mathbf{h_B}$, $\mathbf{i_A}$ and $\mathbf{i_B}$, respectively (Figure 2.7). Analogous to $THT_3Tu[3]$, the NOESY result was similar, with correlations between the protons of THT methylene groups and $\mathbf{g_A}$, $\mathbf{h_A}$ and $\mathbf{i_A}$, protons being indistinguishable due to the overlapped peaks (Appendices A5).

^{13}C NMR **-** The ^{13}C NMR spectrum of $THT_4Tu[4]$ was similar to $THT_3Tu[3]$, and hence, interpretation was straightforward. The only difference observed apart from the slight change in the chemical shift values was the extra signals pertaining to the additional glycoluril unit present within the macrocycle. The presence of 16 different resonances in ^{13}C NMR were consistent with 16 different carbons present in the macrocycle, additionally confirming the formation $THT_4Tu[4]$ (Appendices A6).

ESMS **-** The peak for dication ($THT_4Tu[4]^{2+}/2$) at 563.4 also confirmed the compound to be $THT_4Tu[4]$.

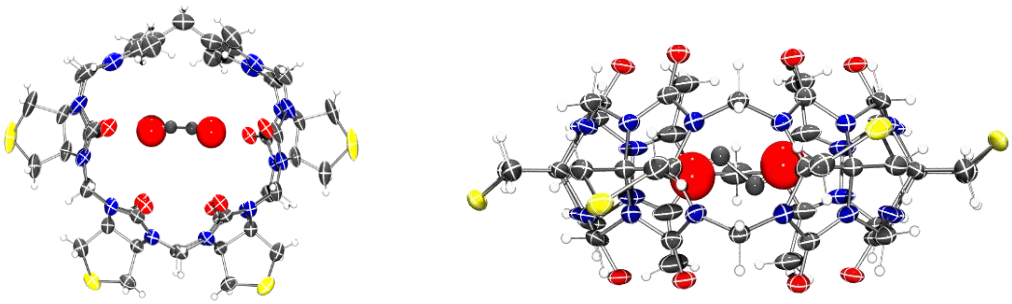

Figure 2.8 The X-ray crystal structure of $THT_4Tu[4]$, top view (left) and side view (right) Colour coding C, black; H, white; O, red; N, blue; and S, yellow.

Furthermore, the structural elucidation was substantiated by single crystal X-ray diffraction where a guest was encapsulated within the cavity. In this case, the guest is either formate ion or formic acid, but the data was insufficient to give affirmation with respect to the bound guest (Figure 2.8).

2.4.3 Thermal stability

Following assessment of the structural elements of $THT_nTu[n]$ homologues, their thermal stabilities were determined using thermogravimetric analysis. TGA thermogram under N_2 displayed gradual weight loss by 5.18 and 9.43% for $THT_3Tu[3]Cl_2$ and $THT_4Tu[4]Cl_2$, respectively in the temperature range of 50 °C to 180 °C, and corresponds to the release of bound water of crystallization. In addition, the thermogram revealed the decomposition temperature at 393 and 417.6 °C for $THT_3Tu[3]Cl_2$ and $THT_4Tu[4]Cl_2$ respectively, suggesting high thermal stability of these new Tu[*n*]'s (Appendices A7, A8).

In summary, all of the above evidence confirmed the formation of two homologues of THT substituted Tu[*n*] (*n* = 3, 4) which are featured with a positively charged cavity in two different sizes. These characteristics endow them with the possibility of acting as molecular containers for anionic guests with H-bond donors wherein the guest could associate through ion-ion interactions with positive centres and/or hydrogen bond to the carbonyl portals.

2.5 The template effect on $THT_nTu[n]$ homologue distribution

In the literature, various examples exist that utilizes the concept of template-controlled synthesis of macrocyclic compounds.[29-31] Macrocyclization reactions often result in the formation of a diverse range of reaction products resulting in a low yield of the desired

product with respect to the other unwanted products. Similar to Q[*n*] and a variety of other macrocyclic hosts, Tu[*n*] is also not an exception to this rule. In order to achieve good yields of the particular ring size, optimization of the reaction conditions is necessary wherein it was anticipated that the template could play a pivotal role in controlling the product ratio in a selective manner. Usually, the templates used in these reactions are the ones that are also guests for the target macrocycle, and this has been demonstrated successfully in various literature reports. Day and coworkers observed the templating effect of various metal cationic guests on the distribution of Q[*n*] homologues wherein Li^+ favoured higher homologues Q[6-8], and K^+ exhibited preference for Q[5]. It was proposed that the cation association influenced the reaction through the formation of ribbon-like oligomers because of a cation-dipole interaction between the carbonyl portals and the metal cations.[29] Another example of the template effect is illustrated by the use of p-xylylenediammonium ion that acts as a template in the Q[*n*] forming reaction and influences the reaction toward the formation of methylene bridged glycoluril hexamer and bis-nor-seco-Q[10].[30] Besides cationic templates for Q[*n*] reactions, anionic species have also been explored as templates for the synthesis of other macrocycles such as hemiQ[*n*] and bambus[*n*]uril (BU[*n*]). It was demonstrated that cyclohexylHmQ[8] could be formed from cyclohexylHmQ[6] in the presence of stronger acids such as H_2SO_4, HCOOH, and CF_3COOH where the macrocyclization process is controlled by the anion, acting as template.[31] All these examples are suggestive of the fact that the overall reaction outcome could be altered in a selective manner using suitable templates.

In the case of THT substituted Tu[*n*], the proportion of THT_4Tu[4] formed compared to THT_3Tu[3] was less with the use of 37% HCl. As these functionalized Tu[*n*]'s are endowed with the positively charged cavity, attempts were made to increase the proportion of the higher homologue using different acids. Apart from acting as a catalyst

for these reactions, their conjugate anions could serve as the anionic templates that could perhaps influence the distribution ratios of the formed homologues. The plausible reason for this anticipation might be the possible correlation between the anion radii and stabilizing association in the formation of particular intermediate oligomers having a condensed pyrazole moiety at one end. Based on the size of conjugate anions, H_2SO_4 and CH_3SO_3H were chosen as the substitutes to HCl. The reactions were carried out following the general procedure outlined in the experimental section. In short, the reaction between THT glycoluril diether and tetramethylpyrazole methane salt (**5b** and **5c**) was catalyzed using H_2SO_4 and CH_3SO_3H, at 12 M respectively. The acid concentration used was 12 M in both the cases so as to match the acid strength of 37% HCl employed in the actual procedure. These reactions were repeated four times. In the case of 37% HCl, following the isolation and identification of the two homologues (THT_3Tu[3] and THT_4Tu[4]), it became possible to clearly identify the two in the crude NMR spectrum by the different chemical shifts for the CH_3 resonances. Therefore, the average of the THT_3Tu[3] : THT_4Tu[4] product ratio for H_2SO_4 and CH_3SO_3H catalyzed reactions were calculated from the integral of the CH_3 resonances in the ^1H NMR spectra of the crude reaction mixtures (Figure 2.5, Appendices A9, A10). Table 2.2 represents the $THT_nTu[n]$ product ratios for three different acids used for the reaction.

Table 2.2 The product ratios of $THT_nTU[n]$ under the influence of anionic templates.

Acid	Templating anions	THT_3Tu[3] : THT_4Tu[4]
HCl	Cl^-	70:30
CH_3SO_3H	$CH_3SO_3^-$	64:36
H_2SO_4	HSO_4^-	57:43

A trend was observed wherein the use of CH_3SO_3H and HCl were less efficient in increasing the proportion of $THT_4Tu[4]$ compared to H_2SO_4. Also, the utilization of 12M concentration of these acids resulted in cleaner spectra of the crude reaction mixtures, indicating a decrease in the formation of undesired products that affects the overall yields of the $THT_nTu[n]$'s. A conceivable explanation for this variation apart from anion size could be that the HSO_4^- ion might facilitate the formation and stabilization of the longer oligomers terminated with a pyrazolium, due partly to its hydrogen bonding ability with the carbonyl oxygen of the glycolurils. Whereas, in the case of $CH_3\ SO_3^-$, it cannot hydrogen bond, but its slight lipophilic nature may favour association with the concave faces of the glycoluril moieties. This type of behaviour was also observed in the hyperchem-modelled structures. The insertion of HSO_4^- and $CH_3SO_3^-$ within the cavity lead to the relocation of HSO_4^- towards the portal, indicating bonding through H-atom at the portals while $CH_3SO_3^-$ remains encapsulated within the cavity, following geometry optimization.[32] This could further be explained based on the ESP map of $THT_4Tu[4]$ (described in the next section) where the interior of the cavity is less positive compared to the outside thereby making the pyrazolium ions less effective compared to the hydrogen bonding aspects of the carbonyl groups. Based on the above findings, the templates appear to be beneficial in driving the reaction towards higher homologues, and it could be envisioned that by utilizing suitable templates useful Tu[*n*] hosts with larger cavities could become accessible for other derivatives also.

2.6 Electron surface potential map (ESP) - $THT_4Tu[4]$

The charge distribution of the molecules is important in predicting the behaviour of complex molecules, and this information could be obtained from their respective ESP map. Figure 2.9 illustrates the top and side view of the ESP map of $THT_4Tu[4]$ that

demonstrates the distribution of the electrostatic potential (EP) along the molecular region of high (+0.24) and low molecular (+0.014) electrostatic potential. The different colours observed in the images determine the regions of different EP. The red area indicates the EP to be more negative, suggesting the electron-dense region and denotes to the carbonyl portals of the $THT_4Tu[4]$. The blue area specifies positive EP wherein the intense blue colour is confined predominately to the outside of the cavity while the light blue coats the inside of the cavity around the pyrazolium moieties, suggesting a more positive environment outside compared to the cavity interior. The highest potential observed within the cavity is on the side of the cavity, i.e. around the diffuse positive pyrazolium groups, at +0.19, whereas the lowest potential in the cavity is determined to be at +0.12.

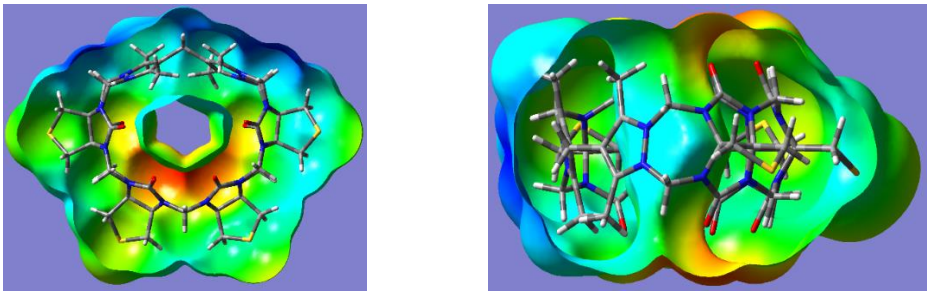

Figure 2.9 The electron surface potential map of $THT_4Tu[4]$, top view (left) and side view (right).*

Overall, this information is important in the qualitative assessment of the behavioural aspects of the macrocycle and the exhibited usefulness for investigating the interaction toward an assortment of guest molecules that could be anionic or electronegative.

*ESP modelling was performed by Dr. Terry Frankcombe, School of Science, UNSW, Canberra.

2.7 Conclusion

As an extension to the success of the methyl substituted Tu[*n*] (Me_{10}Tu[3]), cyclopentano substituted Tu[*n*] (CyP_3Tu[3]) was investigated by a past member of our group in an effort to obtain Tu[*n*] with larger cavities. However, the cavity sizes beyond Tu[3] were not observed in the reaction mixture. Intrigued by this outcome, a synthetic procedure was explored and demonstrated to synthesize new Tu[*n*] derivatives. The main objective was aimed at achieving homologues higher than Tu[3] that could potentially facilitate the encapsulation of larger guest molecules owing to their larger cavities. This objective was fulfilled by employing the substituted glycoluril diether, with a larger dihedral angle, i.e. THT substituted glycoluril diether as the starting precursor. Besides THT_3Tu[3], it resulted in the formation of the first higher homologue of Tu[*n*] family (THT_4Tu[4]). Further to this, these homologues were isolated, purified, and characterized by the standard methods that uncovered the structural details and completely supported the depicted structures of these compounds.

This chapter also explored the templating effect of HSO_4^- and $CH_3SO_3^-$ ions on the reaction outcome when catalyzed with H_2SO_4 and CH_3SO_3H acids. The outcome revealed a trend that demonstrated the effectiveness of H_2SO_4 in increasing the proportional ratio of the THT_4Tu[4] relative to THT_3Tu[3] when compared to HCl and CH_3SO_3H.

Having access to these new Tu[*n*]'s with different functionality and two cavity sizes, it is assumed that the properties of these new Tu[*n*] would be different than the basic Tu[3] (Me_{10}Tu[3]) due to different substitutions. Thus, further studies are required to gain a comprehensive understanding of their properties in order to exploit their full potential for relevant applications. The studies concerning the exploration of their properties are discussed in Chapter 3 of this thesis.

2.8 References

1. Rheineck, H., Ueber das Verhalten des Allantoïns zu Natrium. *Justus Liebigs Annalen der Chemie* **1865,** *134* (2), 219-228.
2. Schiff, H., Ueber Acetylenharnstoff. *Justus Liebigs Annalen der Chemie* **1877,** *189* (1-2), 157-161.
3. Li, J.-T.; Liu, X.-R.; Sun, M.-X., Synthesis of Glycoluril Catalyzed by Potassium Hydroxide Under Ultrasound Irradiation. *Ultrasonics Sonochemistry* **2010,** *17* (1), 55-57.
4. Rezaei-Seresht, E.; Tayebee, R., Synthesis of Glycoluril Derivatives Catalyzed by Some Heteropolyoxometalates. *Journal of Chemical and Pharmaceutical Research* **2011,** *3*, 103-107.
5. Micheletti, G.; Delpivo, C.; Baccolini, G., A Green Synthesis of Glycoluril Derivatives in Aqueous Solution with Recycle of the Waste. *Green Chemistry Letters and Reviews* **2013,** *6* (2), 135-139.
6. Assaf, K. I.; Nau, W. M., Cucurbiturils: From Synthesis to High-affinity Binding and Catalysis. *Chemical Society Reviews* **2015,** *44* (2), 394-418.
7. Kim, K.; Selvapalam, N.; Ko, Y. H.; Park, K. M.; Kim, D.; Kim, J., Functionalized Cucurbiturils and Their Applications. *Chemical Society Reviews* **2007,** *36* (2), 267-279.
8. Ma, D.; Hettiarachchi, G.; Nguyen, D.; Zhang, B.; Wittenberg, J. B.; Zavalij, P. Y.; Briken, V.; Isaacs, L., Acyclic Cucurbit[*n*]uril Molecular Containers Enhance the Solubility and Bioactivity of Poorly Soluble Pharmaceuticals. *Nature Chemistry* **2012,** *4* (6), 503.

9. Wu, A.; Mukhopadhyay, P.; Chakraborty, A.; Fettinger, J. C.; Isaacs, L., Molecular Clips Form Isostructural Dimeric Aggregates from Benzene to Water. *Journal of the American Chemical Society* **2004,** *126* (32), 10035-10043.

10. Sijbesma, R.; Nolte, R., Synthesis of Concave Receptors Derived from Diphenylglycoluril. *Recueil des Travaux Chimiques des Pays-Bas* **1993,** *112* (12), 643-647.

11. Kostyanovsky, R. G.; Lyssenko, K. A.; Kravchenko, A. N.; Lebedev, O. V.; Gul'nara, K. K.; Kostyanovsky, V. R., Crystal Properties of N-alkyl-substituted Glycolurils as the Precursors of Chiral Drugs. *Mendeleev Communications* **2001,** *11* (4), 134-136.

12. Cow, C.; Valentini, D.; Harrison, P., Synthesis of the Fatty Acid of Pramanicin. *Canadian Journal of Chemistry* **1997,** *75* (6), 884-889.

13. Boileau, J.; Carail, M.; Wimmer, E.; Gallo, R.; Pierrot, M., Derives Nitres Acetyles du Glycolurile. *Propellants, Explosives, Pyrotechnics* **1985,** *10* (4), 118-120.

14. Wu, W.-J.; Wu, F.; Day, A. I., Molecular Snuggle and Stretch of a Tetraammonium Chain in the Construction of a Hetero-[4] pseudorotaxane with CyclopentanoQ[6] and Classical Q[7]. *The Journal of Organic Chemistry* **2017,** *82* (11), 5507-5515.

15. Chandrakumar, P. K.; Dhiman, R.; Woodward, C. E.; Iranmanesh, H.; Beves, J. E.; Day, A. I., Tiara[*n*]uril: A Glycoluril-Based Macrocyclic Host with Cationic Walls. *The Journal of Organic Chemistry* **2019,** *84* (7), 3826-3831.

16. Wu, F.; Wu, L.-H.; Xiao, X.; Zhang, Y.-Q.; Xue, S.-F.; Tao, Z.; Day, A. I., Locating the Cyclopentano Cousins of the Cucurbit[*n*]uril Family. *The Journal of Organic Chemistry* **2011,** *77* (1), 606-611.

17. Zhao, Y.; Mandadapu, V.; Iranmanesh, H.; Beves, J. E.; Day, A. I., The Inheritance Angle: A Determinant for the Number of Members in the Substituted Cucurbit[*n*]uril Family. *Organic Letters* **2017,** *19* (15), 4034-4037.

18. Sasmal, S.; Sinha, M. K.; Keinan, E., Facile Purification of Rare Cucurbiturils by Affinity Chromatography. *Organic Letters* **2004,** *6* (8), 1225-1228.

19. Zhao, J.; Kim, H. J.; Oh, J.; Kim, S. Y.; Lee, J. W.; Sakamoto, S.; Yamaguchi, K.; Kim, K., Cucurbit[*n*]uril Derivatives Soluble in Water and Organic Solvents. *Angewandte Chemie International Edition* **2001,** *40* (22), 4233-4235.

20. Chandrakumar, P. K. Exploration of New Cucurbit[*n*]uril and a Novel Glycoluril Based Macrocycle-tiara[*n*]uril. PhD Thesis, University of New South Wales, Canberra, 2016.

21. Atthar, A. Novel Equatorially Attached Cucurbit[*n*]uril Forming Gold Nanoparticle Conjugates as Drug Delivery Vehicles. PhD Thesis, University of New South Wales, Canberra, 2018.

22. Cong, H.; Ni, X. L.; Xiao, X.; Huang, Y.; Zhu, Q.-J.; Xue, S.-F.; Tao, Z.; Lindoy, L. F.; Wei, G., Synthesis and Separation of Cucurbit[*n*]urils and Their Derivatives. *Organic & Biomolecular Chemistry* **2016,** *14* (19), 4335-4364.

23. Mandadapu, V. Combined Delivery Methodologies that Can Increase the Effectiveness of Existing Drugs. PhD Thesis, University of New South Wales, Canberra, 2014.

24. Cuadro, A.; Elguero, J.; Navarro, P., Binuclear Pyrazoles. I. Synthesis and Cytotoxic Activity of 1, 1'-Dibenzyl and 1, 1'-Dihydroxymethyl 4, 4'-Bispyrazoles. *Chemical and Pharmaceutical Bulletin* **1985,** *33* (6), 2535-2540.

25. Tabacaru, A.; Pettinari, C.; Masciocchi, N.; Galli, S.; Marchetti, F.; Angjellari, M., Pro-porous Coordination Polymers of the 1, 4-Bis ((3, 5-dimethyl-1 H-pyrazol-4-yl)-methyl) benzene Ligand with Late Transition Metals. *Inorganic Chemistry* **2011,** *50* (22), 11506-11513.

26. Wheate, N. J.; Broomhead, J. A.; Collins, J. G.; Day, A. I., Thermal Rearrangement of N-Substituted Pyrazoles to 4, 4'-Dipyrazolylmethane and 1, 1, 2-(4, 4', 4''-Tripyrazolyl)ethane. *Australian Journal of Chemistry* **2001,** *54* (2), 141-144.

27. Huang, W.-H.; Zavalij, P. Y.; Isaacs, L., Cucurbit[*n*]uril Formation Proceeds by Step-growth Cyclo-oligomerization. *Journal of the American Chemical Society* **2008,** *130* (26), 8446-8454.

28. Häkkinen, H., The Gold-sulfur Interface at the Nanoscale. *Nature Chemistry* **2012,** *4* (6), 443.

29. Day, A. I.; Blanch, R. J.; Coe, A.; Arnold, A. P., The Effects of Alkali Metal Cations on Product Distributions in Cucurbit[*n*]uril Synthesis. *Journal of Inclusion Phenomena and Macrocyclic Chemistry* **2002,** *43* (3-4), 247-250.

30. Lucas, D.; Minami, T.; Iannuzzi, G.; Cao, L.; Wittenberg, J. B.; Anzenbacher Jr, P.; Isaacs, L., Templated Synthesis of Glycoluril Hexamer and Monofunctionalized Cucurbit[6]uril Derivatives. *Journal of the American Chemical Society* **2011,** *133* (44), 17966-17976.

31. Prigorchenko, E.; Öeren, M.; Kaabel, S.; Fomitšenko, M.; Reile, I.; Järving, I.; Tamm, T.; Topić, F.; Rissanen, K.; Aav, R., Template-controlled Synthesis of Chiral Cyclohexylhemicucurbit[8]uril. *Chemical Communications* **2015,** *51* (54), 10921-10924.

32. HyperChem professional 8.0.7 for Windows Molecular Modelling System, Hyperchem Inc., Ontario, Canada, 2009.

33. Sheldrick, G. SADABS, University of Göttingen, Germany, 1996.

34. Bruker APEX3, Bruker AXS Inc.: Madison, Wisconsin, USA, 2016.

35. Sheldrick, G., SHELXT - Integrated Space-group and Crystal-structure Determination. *Acta Crystallographica Section A* **2015,** 71 (1), 3-8.

36. Dolomanov, O. V.; Bourhis, L. J.; Gildea, R. J.; Howard, J. A. K.; Puschmann, H., OLEX2: A Complete Structure Solution, Refinement and Analysis Program. *Journal of Applied Crystallography* **2009,** 42 (2), 339-341.

CHAPTER 3
EXPLORATION TOWARDS THE PROPERTIES OF TIARA[*n*]URIL (TU[*n*]) FAMILY

3.1 Introduction

In Chapter 2, the new functionalized THT substituted Tu[*n*]'s were synthesized, purified, and characterized. The defining structural features of the Tu[*n*] homologues are their positively charged cavities and two portals rimmed partly by the ureidyl carbonyls and the remainder with methyl groups present at the pyrazolium moieties. In addition, the equatorial region of these macrocycles is electron deficient due to the ureido-π system strongly polarized towards the C=O's and the presence of the substitution at the glycoluril units. It was expected that these features would impart to them the ability to bind anionic species with H-bond donor groups through a combination of H-bond interactions at the portals and ion-dipole and hydrophobic effects, primarily in the cavity. In our group, the use of pyrazole as formaldehyde scavenger in the synthesis of fully substituted $THT_nQ[n]$ and $Me_nQ[n]$ lead to the unexpected formation of the positively charged acyclic congeners.[1-2] These findings were then extended further as an area of research for the development of a new class of acyclic congeners named as "pincers" (Chapter 1, Section 1.4.2). Except for their acyclic nature, these pincers resemble Tu[*n*]'s in having central glycoluril units and positively charged pyrazolium side-walls. Due to their dicationic nature, preliminary investigations of the host-guest properties revealed that there was an interaction with carboxylate groups. The binding constants were determined for three anionic guests that included potassium hydrogen tartrate, sodium ascorbate, and sodium D-glucuronate.[3]

Some of the work discussed in this chapter has been published in citation 1.

Based on some structural similarity between the Tu[*n*]'s and pincers in terms of the moieties present, it was assumed that Tu[*n*]'s might facilitate a function as an anionic receptor due to the positively charged cavity, supported by the H-bonding acceptor potential of the C=O arcs. To test this hypothesis and to develop an understanding of the binding capability of Tu[*n*]'s as a molecular container, attempts were made to obtain outcomes with respect to their structural features. This chapter discusses the host-guest chemistry of the methyl and THT substituted Tu[*n*]'s as model compounds to serve as a preliminary study towards the practical applications of this new family of molecular hosts.

3.2 Aims of the study

The aims of this chapter are as follows,

1. To determine the pK_a value of $Me_{10}Tu[3]^{2+}$, $THT_3Tu[3]^{2+}$ and $THT_4Tu[4]^{2+}$ and to establish the effect of substitution upon this property.
2. To explore the host-guest complexation properties of the methyl and THT substituted Tu[*n*]'s with the purpose to understand the binding potential in relation to their structural features.
3. To explore the potential of $Me_{10}Tu[3]^{2+}$ as a solubilizing agent for the poorly soluble oral anionic drugs.

3.3 Experimental

3.3.1 Materials

Sodium 6-(p-toluidino)-2-naphthalenesulfonate (TNS) and drugs for the solubility studies were purchased from commercial sources and were used without any further purification. $THT_3Tu[3]^{2+}$ and $THT_4Tu[4]^{2+}$ were obtained as described in Chapter 2, $Me_{10}Tu[3]^{2+}$ was

synthesized following the procedure mentioned in the literature[1], and $Me_4Q[6]$ was provided by Dr Anthony Day.

3.3.2 Instrumental methods

^1H NMR and ^2H NMR spectra were recorded using a Varian at 400 MHz for ^1H nuclei and 100 MHz for ^{13}C nuclei. All the NMR experiments were performed at 25 °C unless otherwise specified. Mass spectral analysis were carried out at the Australian National University. pH meter was used for measuring the pH of the solution for carrying out the pK_a measurements. Jasco J-815 CD spectrometer was used for the collection of circular dichroism data with the wavelength ranging from 205 to 300 nm at 20 °C with a rectangular quartz cell of 1 mm path length. Fluorescence spectroscopy was measured on a Fluoromax spectrometer at a constant temperature of 25 °C. The excitation wavelength was at 360 nm, and the fluorescence response was recorded from 380 to 700 nm. UV/Vis studies were performed on a Varian Cary 500 Bio UV-Vis spectrophotometer from 220 to 500 nm wavelength range. Hyperchem modelling was carried out on HyperChem professional 8.0.7 for Windows Molecular Modelling System.

3.3.3 Methodology

3.3.3.1 pK_a titration of $Me_{10}Tu[3]^{2+}$, $THT_3Tu[3]^{2+}$ and $THT_4Tu[4]^{2+}$

Samples of 1mM Tu[*n*] were standardized in D_2O by a tert-butanol standard solution. The concentration of tert-butanol was determined using benzoic acid solution prepared from known weight and volume dissolved in D_2O/Na_2CO_3.

For the pH measurements, the solution of each Tu[*n*] of concentration 1mM was made by dissolving a known weight in water and titrating it with the aqueous solution of standard

NaOH of concentration 1mM, 2mM, 10mM and 20mM, based on the experimental requirement for each Tu[*n*].

Deuterium exchange experiments for each Tu[*n*] were conducted at concentrations of 20 mM dissolved in NaOD/D_2O (0.54 M) and run overnight on NMR with programmed runs every hr. The 7 hr samples were then neutralized, freeze-dried and dissolved in H_2O and ^2H NMR recorded.

3.3.3.2 Circular Dichroism (CD) measurement of L-glutamine (L-Gln)

The stock solution of L-Gln of concentration 0.5 mM was prepared using phosphate buffer solution (PBS buffer) of pH 6.6. The CD spectra of 400 µL of guest solution at 0.5 mM was first collected. Subsequently, solid $Me_{10}Tu[3]Cl_2$, $THT_3Tu[3]Cl_2$ and $THT_4Tu[4]Cl_2$ were added in increasing equivalents of 2, 2.25 and 2.5 mol equiv. to separate solutions of 0.5 mM L-Gln and CD spectra recorded.

3.3.3.3 Fluorescence spectroscopy (Competitive binding of L-Gln with methyl and THT substituted Tu[*n*]'s)

Three different hosts ($Me_{10}Tu[3]^{2+}$, $THT_3Tu[3]^{2+}$ and $THT_4Tu[4]^{2+}$) were employed individually to study their interaction with the fluorescent dye (TNS) in order to establish the fluorescence response for further studies. The dye was dissolved in PBS buffer (10 mM, pH 6.6) to a concentration of 46.7µM. Solid samples of the hosts were added to the 3mL of dye solution as 25 separate additions up to a mole ratio of 42.3. After each addition, the solutions were degassed with nitrogen and the increase in fluorescence intensity recorded.

For competitive binding studies, the stock solution of the guest (L-Gln) of concentration 15.4mM was prepared by weight using PBS buffer. The TNS solution of concentration 46.7 μM was used and its fluorescence spectrum collected. Approximately 20 times higher concentration of $Me_{10}Tu[3]^{2+}$ was then added and the fluorescence spectrum recorded to be used as a reference. The competitive guest was then subsequently titrated at intervals into TNS@$Me_{10}Tu[3]^{2+}$ solution to obtain the fluorescence emission spectra.

3.3.3.4 ^{1}H NMR binding experiments

To measure the binding affinity, binding studies were carried out using ^{1}H NMR at constant temperature of 25 °C. The relaxation delay for the binding studies was 10s to maximise integral accuracy. Experiments were performed in either D_2O, PBS (pD 6.6) or ($K^+C_8H_5O_4^-$)/DCl buffer (pD 4.0) based on the requirements of different studies. Accordingly, the concentrations of host and the guest samples were determined using standard tert-butanol solution and ($K^+C_8H_5O_4^-$)/DCl buffer solution.

3.3.3.4.1 Determination of stoichiometry of dioxane@$THT_4Tu[4]^{2+}$ complex

For determining the stoichiometry of dioxane@$THT_4Tu[4]^{2+}$ complex, a series of samples containing $THT_4Tu[4]^{2+}$ and dioxane in 500 μL of 10 mM ($K^+C_8H_5O_4^-$)/DCl buffer system of pD 4.0 were prepared and allowed to reach equilibrium. The molar ratio of dioxane and $THT_4Tu[4]^{2+}$ was varied while keeping the total molar concentration of the solutions constant at 0.8 mM. The concentrations of the dioxane@$THT_4Tu[4]^{2+}$ complexes were determined through integration of the resonances corresponding to bound dioxane in the ^{1}H NMR spectra. The binding stoichiometry was then obtained from the x-coordinate at the maximum point of the Job's curve.

3.3.3.4.2 Comparative binding studies of dioxane with $THT_4Tu[4]^{2+}$ and $Me_4Q[6]$

The comparative binding of $THT_4Tu[4]^{2+}$ and $Me_4Q[6]$ was performed by adding dioxane to 500 μL solution of $THT_4Tu[4]^{2+}$ (8.3×10^{-4} M) and $Me_4Q[6]$ (8.8×10^{-4} M), to achieve an approximate ratio 1:1. The solutions were prepared in ($K^+C_8H_5O_4^-$)/DCl buffer of 10 mM concentration. The experiment was repeated 4 times and ^1H NMR recorded after the binding competition had reached equilibrium.

3.3.3.4.3 Comparative binding studies of dioxane and d_8-dioxane with $THT_4Tu[4]^{2+}$

The stock solution of the competitive guests was prepared by adding 3μL and 2.5μL of dry d_8-dioxane and 1,4-dioxane, respectively in 950 μL of 10 mM ($K^+C_8H_5O_4^-$)/DCl buffer solution using a micro syringe. The two guests were added to the $THT_4Tu[4]^{2+}$ solution of known concentration (6.8×10^{-4} M) to achieve an approximate relative ratio of 1:1:1. The experiment was repeated 3 times and ^1H NMR recorded after reaching the binding equilibrium.

3.3.3.5 Solubility experiments

For carrying out the solubility studies, an excess of the drugs alone and in combination with three different concentrations (13.9, 27.7 and 41.5 μM) of $Me_{10}Tu[3]Cl_2$ were added to citric acid buffer (pH - 3.5). Similarly, the solubility studies were also performed with three different concentrations (0.07, 0.14 and 0.21 μM) of $Me_{10}Tu[3]Cl_2$ in PBS (pH - 7.4) buffer. The suspensions were sonicated for 90 min and then stirred for a total of 16 hr at 20 °C. After 16 hr, the suspensions were filtered through a 0.5 μm PETE syringe filter and the absorbance for each sample was determined using UV/Vis spectroscopy.

3.4 Results and Discussion

As a new family of potential molecular hosts, the binding properties of the Tu[*n*] family were unknown. Therefore, it was of interest to determine if the positively charged pyrazolium walls of the cavity in combination with the arc of C=O's had any binding potential. This section examines the host-guest chemistry of the methyl and THT substituted Tu[*n*]'s.

3.4.1 pK_a measurement of $Me_{10}Tu[3]^{2+}$, $THT_3Tu[3]^{2+}$ and $THT_4Tu[4]^{2+}$

One of the methods for assessing the binding capability of macrocyclic compounds is the effect it has on the pK_a value of the guest. The change in the pK_a value compared to the absolute value for the guest symbolize its association with the host molecule. Numerous examples that demonstrates the pK_a shift (Δ pK_a) because of host-guest complexation are available in literature. Q[7] has been shown to exhibit Δ pK_a of approximately 2-3 units for the included guests.[4-5] Also, the shift in pK_a values has been exploited for therapeutic applications wherein the addition of Q[7] to the proton pump inhibitors lead to their activation and stabilization in aqueous solution.[6] Similar to these studies, attempts were made to measure and compare the pK_a values of the new class of macrocyclic hosts, Tu[*n*]. This study was conducted with an intention to determine the pK_a of the host molecules along with their ability to influence the guest pK_a's. In addition, this might also provide insight into the variation of properties due to the presence of different substitutions in Tu[*n*]'s.

Initially, this study was performed on $Me_{10}Tu[3]^{2+}$ in the form of chloride salt to establish its pK_a as a host. For carrying out the pK_a studies, the aqueous solution of $Me_{10}Tu[3]Cl_2$

was titrated with aliquots of aqueous NaOH to obtain a titration curve that displayed two buffer regions, consequently revealing two pK_a values. The obtained pK_a value at 3.4 correspond to the release of bound HCl, indicating the first of two host-dependent pK_a's (pK_a of HCl alone = -5.9).[7] The released HCl is the acid of crystallization bound to $Me_{10}Tu[3]^{2+}$. A second example was for $Me_{10}Tu[3](HSO_4)_2$, which was reported to have the first pK_a at 3 for the HSO_4^- ion.[1] This variance in pK_a values indicate the difference in behavior of $Me_{10}Tu[3]^{2+}$ toward two different guests, HCl and the HSO_4^- anion. In addition, $Me_{10}Tu[3]^{2+}$ irrespective of the guest (HCl/HSO_4^-) has a second pK_{a2} of 11.1, which relates to the acidity of the methyl groups on the pyrazolium moieties[1] (Appendices A11, A12). After having established these pK_a's a similar investigation was performed for the new substituted derivatives - $THT_3Tu[3]Cl_2$ and $THT_4Tu[4]Cl_2$ with the first pK_a value determined at 2.58 and 2.52, respectively (Appendices A13, A15). Although there was little distinction of the first pK_a's between the two THT substituted Tu[n]'s; however, there was a difference for the $Me_{10}Tu[3]^{2+}$ (~1 pK_a unit higher). This suggests that HCl might be bound more tightly to $Me_{10}Tu[3]^{2+}$ compared to $THT_nTu[n]^{2+}$. The results pertaining to the pK_{a2} value, however, were similar to $Me_{10}Tu[3]^{2+}$ (Appendices A14, A16).

In order to support the relationship between the second pK_a and the acidity of methyl groups, deuterium exchange experiments were performed. The procedure involved the preparation of Tu[n] solutions to a concentration of 20 mM in NaOD 0.54 M and recording the ^{1}H NMR at 1 hr intervals. It was observed that the resonance corresponding to the pyrazolium methyl groups displayed a decrease in the intensity for all 3 Tu[n]'s. This decrease was attributed to the conversion of methyl groups to methyl-d_3 for each Tu[n] under basic conditions (Scheme 3.1).

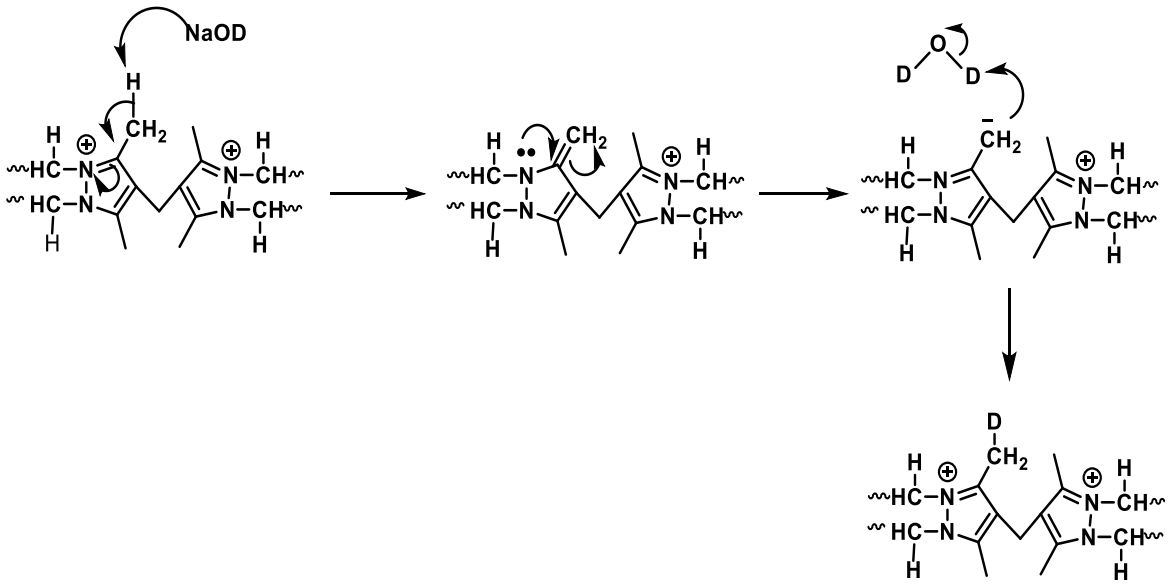

Scheme 3.1 Representation of the stepwise mechanism of deuterium exchange at the pyrazolium moiety of Tu[n]

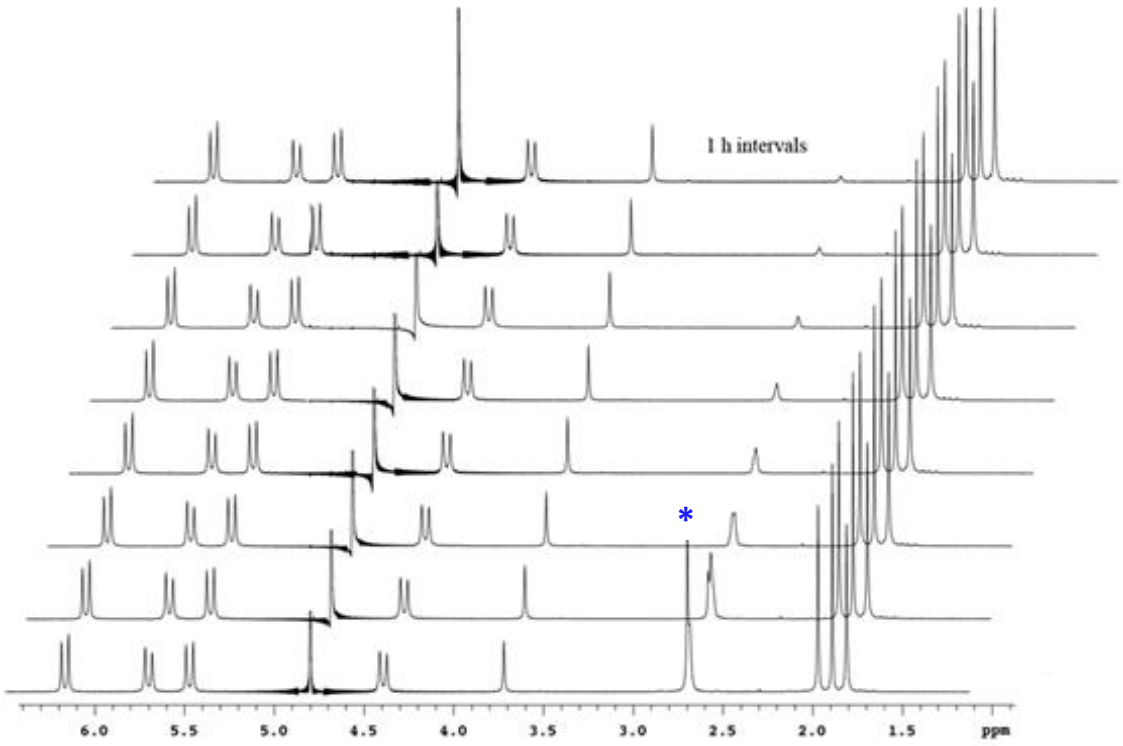

Figure 3.1 ^{1}H NMR time course of $Me_{10}Tu[3]Cl_2$ (20 mM) in D_2O after the addition of NaOD/D_2O (0.54 M). The mark (*) indicates the pyrazole methyl resonance.[1]

(This figure has been taken from my own published work)

However, a noticeable difference was observed in the rate of exchange, with 60% and 73% occurring within the first hr for $THT_3Tu[3]^{2+}$ and $THT_4Tu[4]^{2+}$, respectively, compared to only 20% in the case of $Me_{10}Tu[3]^{2+}$ (Figure 3.1). Also, $THT_nTu[n]$'s conjointly illustrated the change in the peak intensities for the methylene protons, predominately in the chemical shift range of 5.90 - 6.40 ppm for $THT_3Tu[3]^{2+}$ and 5.67 - 6.40 ppm for $THT_4Tu[4]^{2+}$, possibly indicating deuteration of the methylene protons present adjacent to the pyrazolium moieties. Another important aspect was the difference in deuterium exchange rate for the two methylene protons. It was observed that the methylene proton orthogonal to the pyrazolium ion (labelled at **b**) is exchanged faster compared to the proton aligned in plane with the pyrazolium units (labelled at **a**) (Chapter 2 - Figure 2.6, 2.7, Figure 3.2, Appendices A17). This was not observed in the case of $Me_{10}Tu[3]^{2+}$.

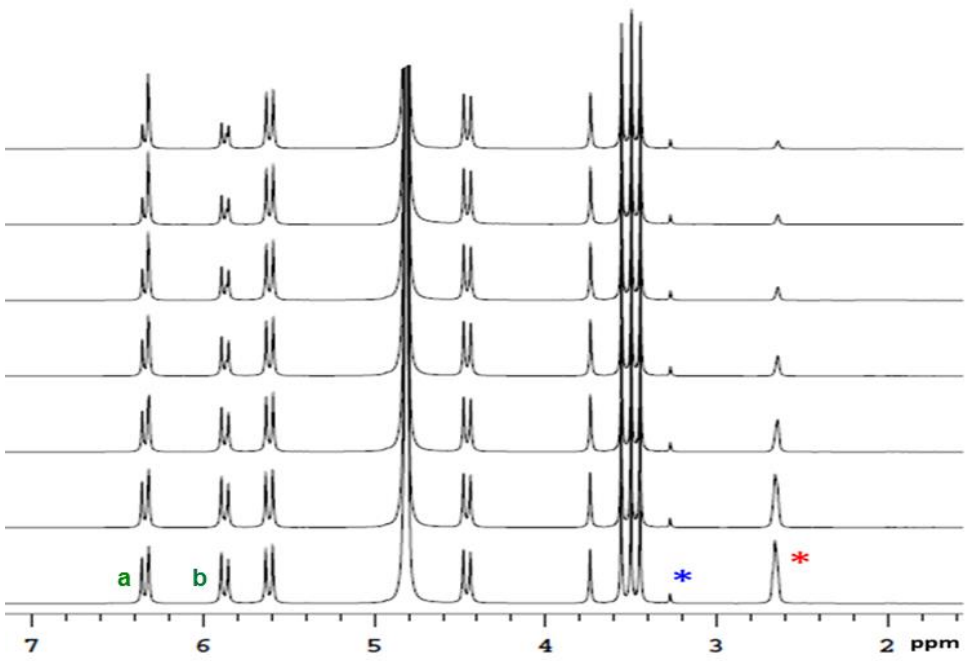

Figure 3.2 ^{1}H NMR time course of $THT_3Tu[3]Cl_2$ (20 mM) in D_2O after the addition of NaOD/D_2O 0.54 M. The mark (*) indicates the pyrazole CH_3 resonance (red) and methanol (blue).

Further confirmation regarding the deuterium exchange was furnished through ^{2}H NMR experiment of 7 hr old samples, which were neutralized and then freeze-dried. ^{2}H NMR spectrum provided CD_3 resonances occurring slightly isotopically shifted to 2.66, 2.60 and 2.54 ppm for $Me_{10}Tu[3]^{2+}$ (Figure 3.3), $THT_3Tu[3]^{2+}$ and $THT_4Tu[4]^{2+}$, respectively (Appendices A18, A19). Noteworthy is the ^{2}H NMR outcome for $THT_nTu[n]^{2+}$'s, which apart from CD_3 resonances displayed broad lump around the methylene proton resonances, giving insufficient information in relation to deuteration of these protons.

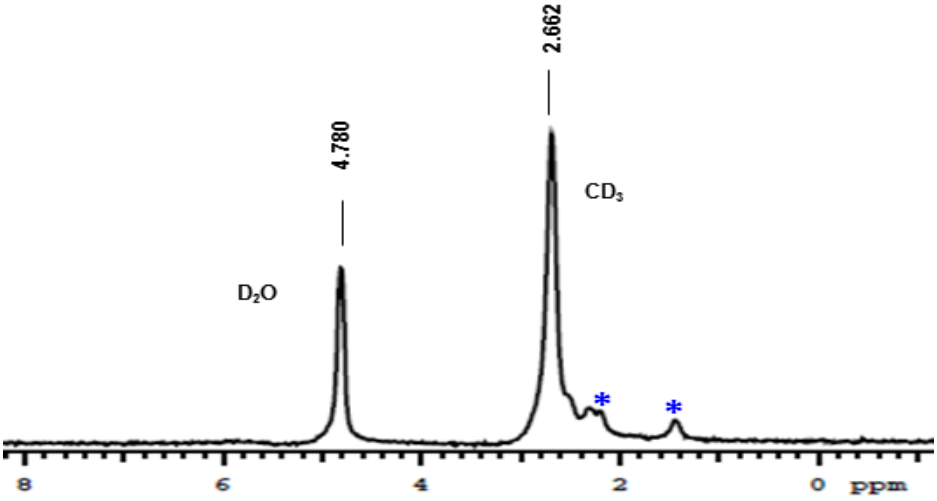

Figure 3.3 ^{2}H NMR spectrum of crude deuterium exchange product d_{12} - $Me_{10}Tu[3]Cl_2$ in H_2O, the mark (*) indicates unknown impurities.

The mass spectroscopic results for a 7 hr exchange process, further substantiated the above findings with the maximum intensity for $(M^{2+}/2)$ appearing at 460.187 consistent with 16 deuterium exchange for $THT_3Tu[3]^{2+}$ and 570.71 consistent with 14 deuterium exchange for $THT_4Tu[4]^{2+}$. The mass spectra also displayed additional peaks corresponding to lower as well as higher mass ions depending on the number of deuterium's exchanged (Appendices A20, A21).

These outcomes indicate that the deuteration of pyrazolium methyl groups are first replaced followed by some of the methylene protons present adjacent to the pyrazolium rings. In the case of $Me_{10}Tu[3]^{2+}$, the methylene proton exchange was not observed, however, the possibility for it to occur at a rate slower than $THT_nTu[n]^{2+}$ cannot be ruled out. A possible consideration for the differences in the deuterium exchange may be explained on steric grounds. The out of plane methylene proton is most readily exchanged except when sterically hindered from equatorial substitution at the glycoluril units. This steric hindrance varies with the distance between orthogonal methylene proton and equatorially present methyl and THT methylene protons. The calculated distances obtained from the crystal structures (Figure 3.4) suggests that these protons are in close proximity in the case of $Me_{10}Tu[3]^{2+}$ (~ 2.3 Å) compared to $THT_4Tu[4]^{2+}$ (~ 2.77 Å), leading to steric hindrance which in turn influences the rate of deuterium exchange, making it slower for $Me_{10}Tu[3]^{2+}$. While the distance between the in plane methylene proton and pyrazolium CH_3 group remains the same at ~ 2 Å.

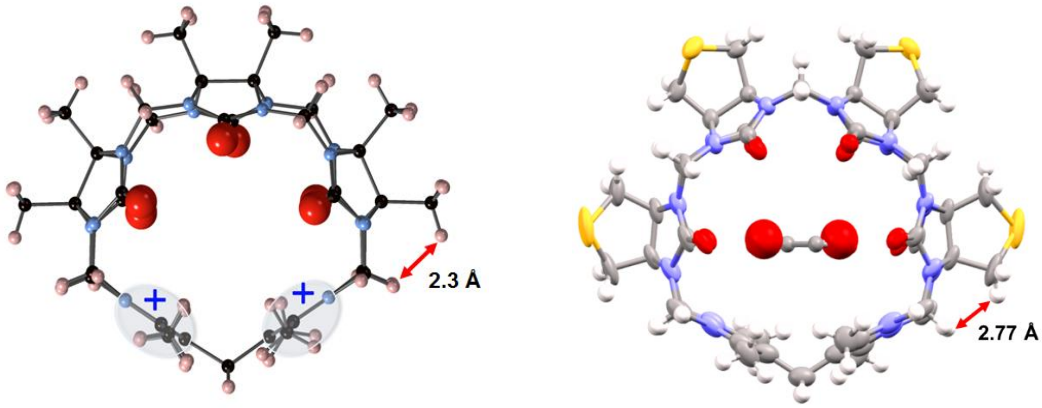

Figure 3.4 Representation of the distance between the orthogonal methylene proton and CH_3 proton at glycoluril in $Me_{10}Tu[3]^{2+}$ (left) and THT axial methylene proton at glycoluril in $THT_4Tu[4]^{2+}$ (right).

Overall, the pK_a studies provided an indication of the binding of the guest and this binding can vary with the substitution present at the equatorial position. Even though an effect is observed, it cannot however be concluded that this pK_a effect is specifically due to cavity encapsulation. The results obtained regarding the acidity of the pyrazolium methyl protons open up a new route to derivatization at the portals, through a base catalyzed substitution reaction.

3.4.2 Binding of L-glutamine (L-Gln) with Tu[*n*]'s

Following the pK_a studies that involved the study with an inorganic guest, preliminary exploration of the association of an organic molecule through ion-ion and H-bond interaction was conducted. In this case, the selected molecule was an amino acid, L-Gln. L-Gln is a chiral amino acid and in the zwitterionic form it simultaneously possesses both an ammonium cation and the carboxylate anion that allows interaction either at the portal and/or inside the cavity. However, the presence of an extra amino group offers an additional possibility of H-bond interaction at the portals, anticipated to enhance binding association with Tu[*n*]'s. All these structural features of L-Gln precisely fit the binding criteria according to our hypothesis and so was the reason for choosing it as a candidate for this study (Figure 3.5).

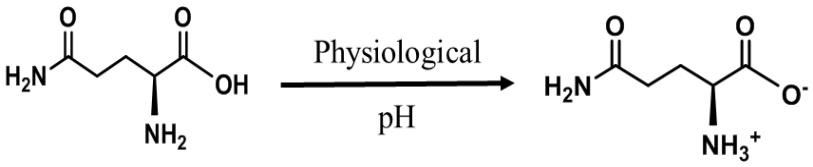

Figure 3.5 Representation of the zwitterionic form of L-glutamine (L-Gln).

A binding interaction was tested by three different approaches - CD, competitive binding with a fluorescent dye and ^{1}H NMR. Preliminary measurements were first tested with $Me_{10}Tu[3]^{2+}$ to develop a method to be applied to $THT_nTu[n]^{2+}$. The measurements were carried out as described in the experimental section with the solutions prepared in phosphate buffer (pH 6.6) to facilitate zwitterion formation.

3.4.2.1 Circular Dichroism measurements

Being highly sensitive and the ability to detect a change in molar ellipticity of the chiral complexes, the CD technique was used as an approach to the observation of interactions between Tu[*n*]'s and L-Gln. Tu[*n*] itself is an achiral molecule (Appendices 22b-d); however, its association with chiral guests could lead to induced chirality because of host-guest complexation, forming chiral supramolecular constructs.[8-9] These constructs could then be easily detected through CD spectroscopy. In the case of $Me_{10}Tu[3]^{2+}$, the CD spectra displayed a significant maxima which was red shifted by 4 nm to 210 nm and a positive increase in molar ellipticity [θ] to 1.2 and 2.9 after the addition of 2 and 2.25 mole equiv. of $Me_{10}Tu[3]^{2+}$, respectively (Figure 3.6, Appendices A22a - UV/Vis spectrum of 2.25 mole equiv. of $Me_{10}Tu[3]^{2+}$). The response was relatively weak but there was a small change suggesting an association.

Similarly, the CD spectra of $THT_3Tu[3]^{2+}$ also displayed a small increase in molar ellipticity [θ] to 0.8 after the addition of 2 mole equiv. (Figure 3.7). Of considerable importance were the peaks observed at 225 and 227 nm ([θ] = 13 and 11.1 deg M^{-1} cm^{-1}) that were similar in shape to the peaks at 228 and 232 nm ([θ] = 7.1 and 5.5 deg M^{-1} cm^{-1}) for $Me_{10}Tu[3]^{2+}$ (Note - a small difference of 0.25 mole equiv. exist for 2.25 and 2.5 mole equiv. readings in the two cases). The comparison of the CD spectra of two

Tu[*n*]'s illustrated hypsochromic shift and increased molar ellipticity for the two peaks in $THT_3Tu[3]^{2+}$ compared to $Me_{10}Tu[3]^{2+}$.

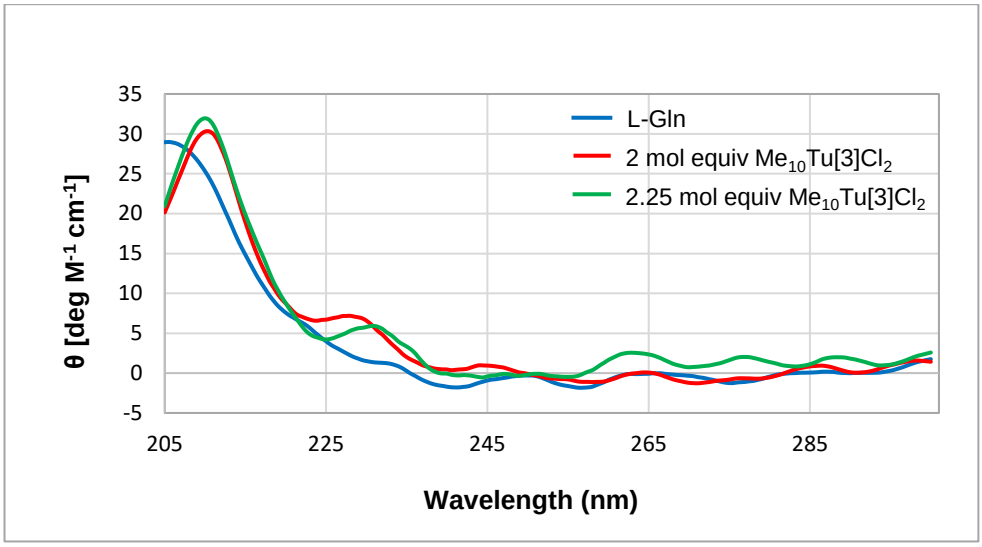

Figure 3.6 The CD spectra of L-Gln 0.5 mM (blue), after the addition of 2 mole equiv of $Me_{10}Tu[3]Cl_2$ (red), 2.25 mole equiv (green) all dissolved in buffer 10 mM (pH 6.6).

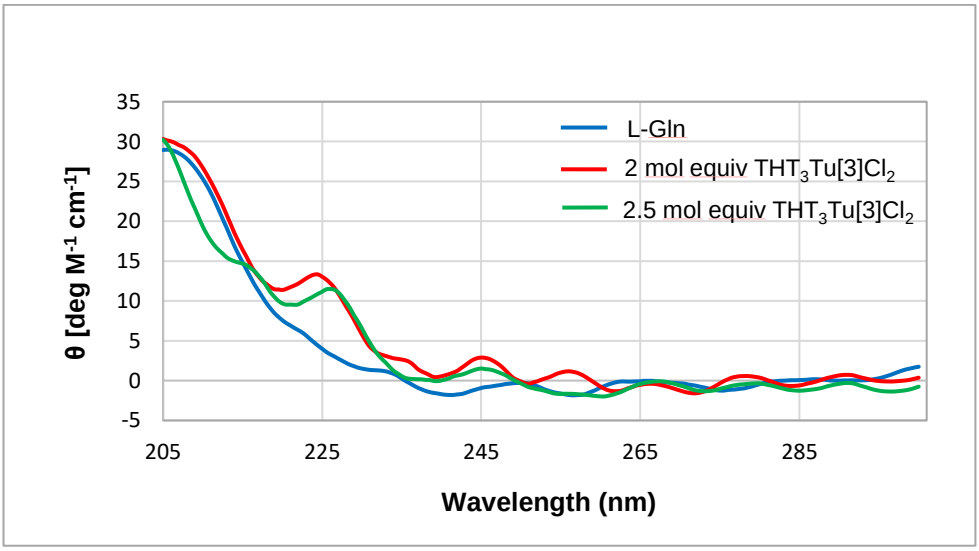

Figure 3.7 The CD spectra of L-Gln 0.5 mM (blue), after the addition of 2 mole equiv of $THT_3Tu[3]Cl_2$ (red), 2.5 mole equiv (green) all dissolved in buffer 10 mM (pH 6.6).

Analogous to $Me_{10}Tu[3]^{2+}$ and $THT_3Tu[3]^{2+}$, changes were observed in CD spectra of L-Gln upon addition of $THT_4Tu[4]^{2+}$. The 2 mole equiv. of $THT_4Tu[4]^{2+}$ illustrated a change with an inversion of ellipticity at 211 nm. In addition, the CD spectra also displayed the appearance of two new peaks at 217 and 239 nm for 2 mole equiv. and at 223 and 238 nm for 2.5 mole equiv. A positive increase in molar ellipticity was observed for both the peaks, being higher for 2.5 mole equiv. compared to 2.0 mole equiv. of $THT_4Tu[4]^{2+}$ (Figure 3.8).

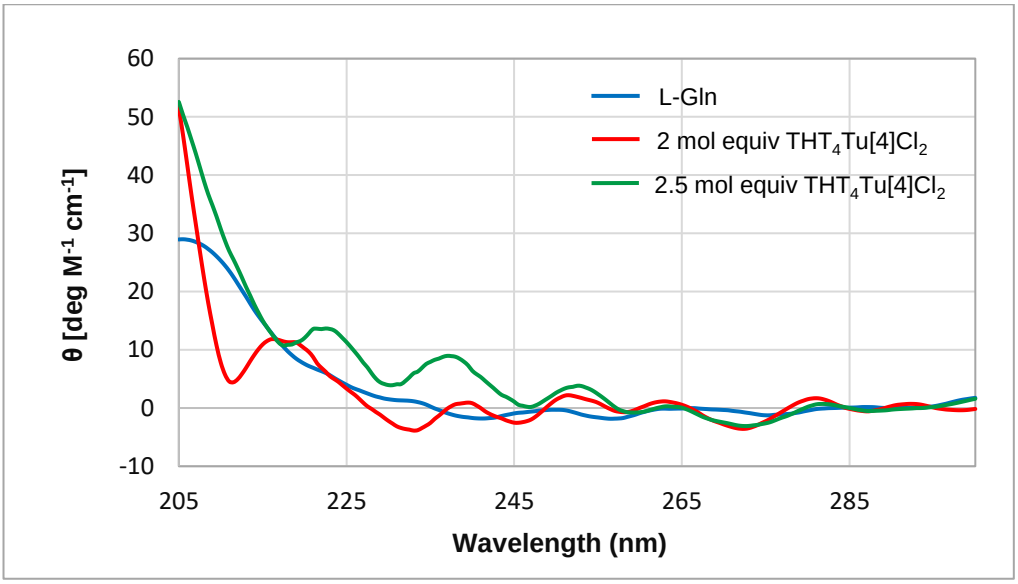

Figure 3.8 The CD spectra of L-Gln 0.5 mM (blue), after the addition of 2 mole equiv of $THT_4Tu[4]Cl_2$ (red), 2.5 mole equiv (green) all dissolved in buffer 10 mM (pH 6.6).

Note: The oscillatory signals observed in the CD spectra of all the Tu[*n*]'s in the higher wavelength region is noise.

These were interesting results and suggested a possible interaction of L-Gln with $Me_{10}Tu[3]^{2+}$, $THT_3Tu[3]^{2+}$ and $THT_4Tu[4]^{2+}$ forming new chiral supramolecular species. However, it was difficult to quantify the observed changes and hence required an alternative method for calculating the binding constants. As an alternative, a competitive fluorescent dye displacement experiment was considered and tested.

3.4.2.2 Competitive binding using fluorescence spectroscopy

The positive results from the CD analysis prompted us to carry out the binding investigations quantitatively, using fluorescence spectroscopy. There have been several examples in the study of Q[*n*] and related compounds that had applied this method for investigating host-guest chemistry.[10-14] In a study of a Q[6] analogue, it has been demonstrated that the host-guest association can be directly measured employing fluorescence due to chromophoric nature of the host.[14-15] However, in the case of UV/Vis inactive host, an alternative approach is to use a fluorescent dye, and the binding of different guests can be determined by competitive binding studies. The procedure involves finding the binding constant of the dye@host complex, as the complex formation with the host is monitored which should be sufficiently weak to allow its displacement and the change in fluorescent intensity to be quantified. The reversible association of a dye therefore is used to monitor the binding of other guests through changes in fluorescence emission as the guest competitively displaces the dye. The binding constant of the guest can then be obtained based on the K_a value of dye@host complex and the concentrations employed, by the application of competitive binding equations. This approach was used in our study to obtain the binding constant of L-Gln upon interaction with the Tu[*n*]'s.

Sodium 6-(p-toluidino)-2-naphthalenesulfonate (TNS) (Figure 3.9) is a fluorescent dye, reported to display minimal fluorescence emission in water and is sensitive to the polarity of the local environment wherein its fluorescence emission is greatly enhanced in less polar or non-polar medium.[16] This property has been exploited for observing its interaction with other molecules. TNS contains a negatively charged group that could interact with the positively charged pyrazolium moieties and amino group could engage in the H-bond interactions with the C=O arcs of Tu[*n*]'s. These structural characteristics

are aligned with the binding requirements of the Tu[*n*]'s. Hence, TNS was selected as a fluorescent anionic probe for this study.

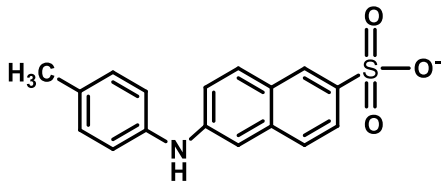

Figure 3.9 Representation of the structure of TNS.

The study was carried out following the procedure outlined in the experimental section. The use of PBS buffer (pH 6.6) facilitated the formation of anion and excluded any pH effects throughout the titration. Figure 3.10 shows the fluorescent spectra obtained during the titration of $Me_{10}Tu[3]^{2+}$ into TNS. An increase in fluorescence intensity was observed with the addition of $Me_{10}Tu[3]^{2+}$, accompanied by the blue shift from 513 to 495 nm at the end of titration. The fluorescence enhancement data was fitted to the binding model assuming a binding ratio of 1:1, to determine the association constant (K_a) for TNS@$Me_{10}Tu[3]^{2+}$ complex. A moderate K_a of value ~ 2.4×10^2 M^{-1} was obtained. Having determined the K_a for TNS@$Me_{10}Tu[3]^{2+}$, the binding constant for L-Gln@$Me_{10}Tu[3]^{2+}$ was then obtained through the competitive release of TNS that lead to a decrease in the fluorescence emission (Figure 3.11). The association constant for L-Gln@$Me_{10}Tu[3]^{2+}$ was calculated to be ~ 2.2×10^2 M^{-1} (Appendices A23).

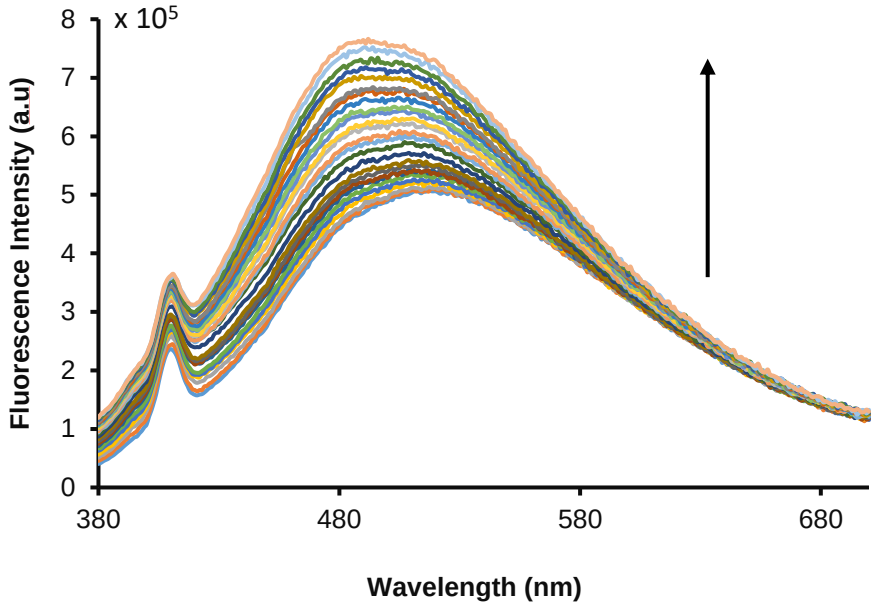

Figure 3.10 Fluorescence spectrum of $Me_{10}Tu[3]Cl_2$ titration into the fixed concentration of TNS (46.7μM). The peak around 400 nm represents Raman emission from the solvent and the arrow indicates the direction of fluorescence change.

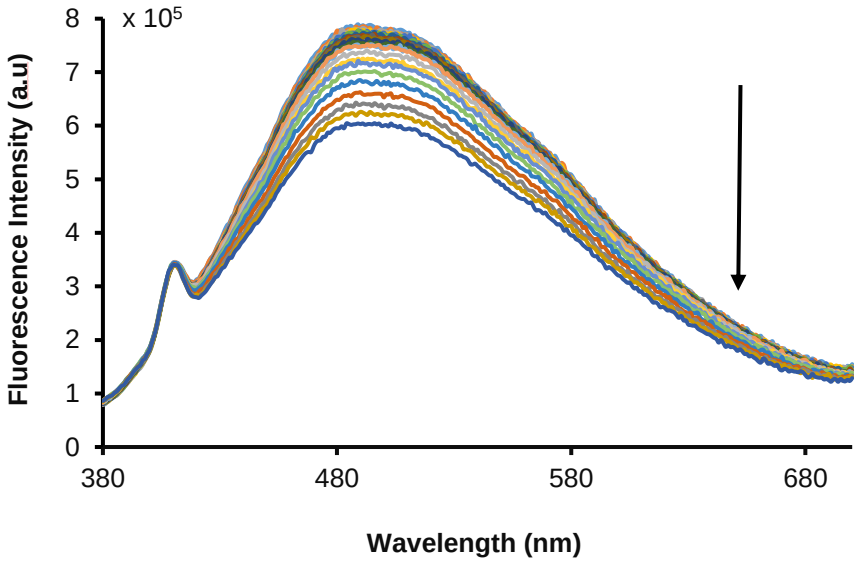

Figure 3.11 Fluorescence spectrum of L-Gln titration into the $Me_{10}Tu[3]Cl_2$@TNS solution. The peak around 400 nm represents Raman emission from the solvent and the arrow indicates the direction of fluorescence change.

A similar experiment was conducted for the determination of TNS association with $THT_3Tu[3]^{2+}$ and $THT_4Tu[4]^{2+}$, respectively. However, in both the cases, the titration did not reach a point where the fluorescence enhancement begins to level off. This could be due to the loose binding of TNS with these $THT_nTu[n]^{2+}$'s. Therefore, this technique proved unsuccessful in obtaining the binding constants for $TNS@THT_nTu[n]^{2+}$ complexes.

The analysis of this competitive process provided a measure of the host-guest binding ability of $Me_{10}Tu[3]^{2+}$. TNS is known to form inclusion complex with cyclodextrin with great enhancement in its fluorescence emission.[16] 2,6-ANS dye which is similar to TNS except for the presence of phenyl group rather than toluyl group has been utilized in binding investigations of different guests with Q[6], Q[7] and cyclodextrins.[4, 13, 17] Analogous to TNS, inclusion of 2,6-ANS in cyclodextrin has also been shown to enhance fluorescence with a significantly large blue shift (28 - 40 nm) due to encapsulation of naphthalene fluorophore in its cavity.[17] However, the blue shifts and fluorescence enhancement were small for 2,6-ANS@Q[6] and 2,6-ANS@Q[7] complexes and was attributed to the encapsulation of anilino group rather than the naphthalene moiety. It was proposed that due to complexation, the intramolecular rotation freedom of the phenyl ring relative to the naphthalene ring was constrained that reduces the rate of charge transfer of 2,6-ANS in the excited state, which was the major pathway for non-radiative decay. Therefore, only moderate enhancement in the fluorescence intensity was observed for Q[*n*] compared to cyclodextrins.[13, 15] In the case of $Me_{10}Tu[3]^{2+}$, a relatively large (17 nm) blue shift observed for the $TNS@Me_{10}Tu[3]^{2+}$ could be an indication of the naphthalene fluorophore binding, which also suggested that $Me_{10}Tu[3]^{2+}$cavity could be less polar than the bulky water, but is more polar than the inside of the cyclodextrin cavities. However, the enhancement in fluorescence due to the association with

$Me_{10}Tu[3]^{2+}$ was smaller than those with Q[*n*], which could be due to the increased rate of non-radiative decay and the lack of cavity encapsulation as the cavity was expected to be too small. The toludino group should be perpendicular to the plane of the naphthalene ring for the charge transfer process to occur.[18] It is possible that the ion-dipole interactions between the NH and the carbonyl groups of $Me_{10}Tu[3]^{2+}$ may favour this conformation of TNS by a portal association. The binding constant obtained for L-Gln which is of the same order as TNS thus suggested that L-Gln could be portal bound to $Me_{10}Tu[3]^{2+}$ similar to TNS.

3.4.2.3 ^{1}H NMR experiments

Beside the use of the above mentioned techniques, ^{1}H NMR spectra of $Me_{10}Tu[3]^{2+}$, $THT_3Tu[3]^{2+}$ and $THT_4Tu[4]^{2+}$ in buffered D_2O (pD 6.6) with the addition of L-Gln also displayed no significant change in proton resonances for either of the hosts or the guest. Given that the binding affinity of $Me_{10}Tu[3]^{2+}$ was on the order of 10^2 M^{-1} and the anticipated that association would be at the portal, a resonance shift was not expected. If cavity encapsulation was to occur it would most likely be the carboxylate ($-CO_2^-$), and H-bonding from the ammonium group ($-NH_3^+$) to the C=O portals. Under this situation, the peaks corresponding to the protons exterior and near the portals would result in very small or insignificant chemical shifts consistent with the finding.

Also, the expected outcome is supported by the ESP map for the $THT_4Tu[4]^{2+}$ (Chapter 2, Section 2.6), indicating that the carbonyl portals should be effective for H-bond association and that anionic or electronegative groups should reside inside the diffuse positively charged cavity. In addition, as discussed in the section for binding of dioxane with $THT_4Tu[4]^{2+}$ (Section 3.4.3, Table 3.1), the cavity has sufficient capacity to accommodate L-Gln. However, further studies employing different amino acids and

different techniques for quantitative assessment of the binding towards methyl and THT substituted Tu[*n*]'s are required to obtain a clear understanding of the features required to promote binding.

3.4.3 Binding of dioxane with $THT_4Tu[4]^{2+}$

The contribution of THT substituted glycoluril towards the formation of $THT_4Tu[4]^{2+}$, indicates that higher homologues are possible. Having achieved the larger cavity size and the outcomes revealing the portal binding of L-Gln, the next goal was to explore preferable guests for cavity encapsulation. From the crystal structure, the dimensions calculated for $THT_4Tu[4]^{2+}$ can be related to Q[6] and Q[7], wherein the cavity of $THT_4Tu[4]^{2+}$ is nearly the same as Q[7] and the portals are in alignment with the Q[6] values (Table 3.1). This also suggests that larger guests can be accommodated within the cavity of $THT_4Tu[4]^{2+}$.

Table 3.1 Dimensions of $THT_3Tu[3]^{2+}$, $THT_4Tu[4]^{2+}$, Q[6] and Q[7]. [19-20]
(The values in the table includes the van der Waals radii)

Parameters	**$THT_3Tu[3]^{2+}$**	**$THT_4Tu[4]^{2+}$**	**Q[6]**	**Q[7]**
Cavity diameter (Å)	5.09	7.18	5.8	7.3
Portal diameter (Å)	2.15	3.8	3.9	5.4

In pioneering work by Day et al., the crystal structure of $Me_{10}Tu[3]^{2+}$ was found to have MeOH encapsulated within the cavity with its oxygen atom in close proximity to the pyrazolium ions (~3Å), indicating a possible ion-dipole interaction.[1] This example may suggest that an electronegative moiety favours binding to Tu[3] within its cavity.

Therefore, it was predicted that the guest molecule containing electronegative atoms could be an appropriate choice for cavity occupancy. It has been reported that differently substituted Q[6] exhibit different binding affinities toward dioxane.[21] Given that the cavity size of $THT_4Tu[4]^{2+}$ is in between Q[6] and Q[7], dioxane appeared to be a guest of choice for investigating the host-guest association based upon size and the presence of electronegative O. In addition, hyperchem modelling[20] indicated that dioxane can be accommodated within the cavity of $THT_4Tu[4]^{2+}$. To test this proposition, binding studies were performed with both $THT_3Tu[3]^{2+}$ and $THT_4Tu[4]^{2+}$.

Being a symmetrical molecule, 1,4-dioxane has the advantage of having a clearly defined resonance as a singlet of 8 protons. It was expected that the resonance corresponding to dioxane would shift upfield in case of inclusion within $THT_nTu[n]^{2+}$. No binding was observed towards $THT_3Tu[3]^{2+}$ due to its smaller size, as expected. Contrary to $THT_3Tu[3]^{2+}$ result, an upfield shift from 3.77 to 2.51 ppm in ^{1}H NMR indicated cavity encapsulation of dioxane in $THT_4Tu[4]^{2+}$ (Figure 3.12).

However, it was difficult to differentiate and assign the chemical shift value to the bound dioxane signal due to the presence of an additional peak at 2.76 ppm. This peak corresponded to the bound methyl of $THT_4Tu[4]^{2+}$ and the confirmation to this was accomplished by using d_8-dioxane, which lead to the disappearance of 2.51 ppm resonance in ^{1}H NMR, while the shifted methyl resonance remained, affirming the signal for bound dioxane (Figure 3.13).

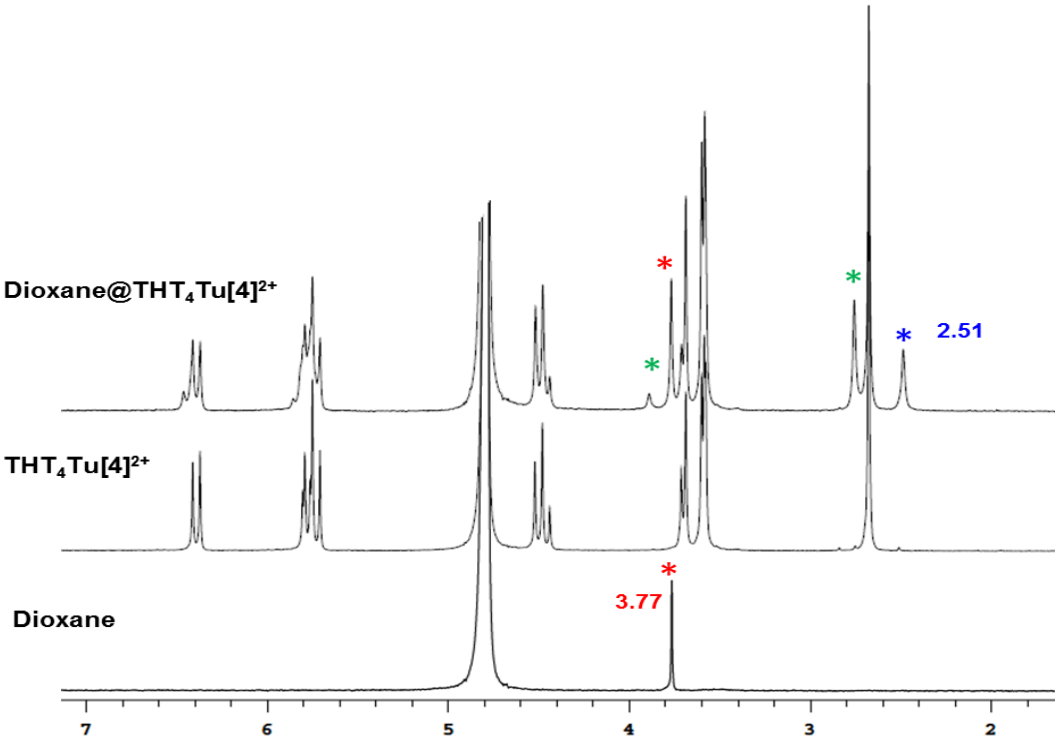

Figure 3.12 The ^{1}H NMR comparison between dioxane, $THT_4Tu[4]^{2+}$ and dioxane@$THT_4Tu[4]^{2+}$. The mark (*) indicates free dioxane (red), bound dioxane (blue) and the methyl of $THT_4Tu[4]^{2+}$ when associated with dioxane (green).

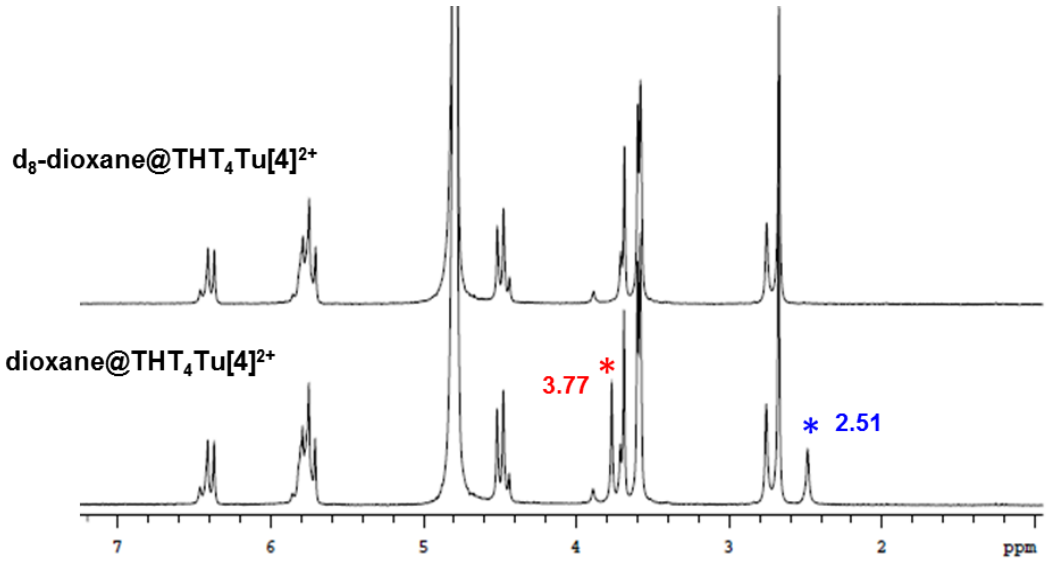

Figure 3.13 The comparison of ^{1}H NMR of dioxane@$THT_4Tu[4]^{2+}$ and d_8-dioxane@$THT_4Tu[4]^{2+}$.

In order to understand the host-guest complexation between dioxane and $THT_4Tu[4]^{2+}$, the first step required measuring the binding stoichiometry by employing a Job's plot for continuous variation. The experiment was performed following the procedure outlined in the experimental section 3.3.3.4.1. Figure 3.14 represents the Job's plot with the maximum of complex product appearing at 0.36, indicating a 2:1 complexation predominant at the equilibrium. Having calculated the binding stoichiometry, we resorted to the competitive binding experiments to obtain the corresponding binding constant.

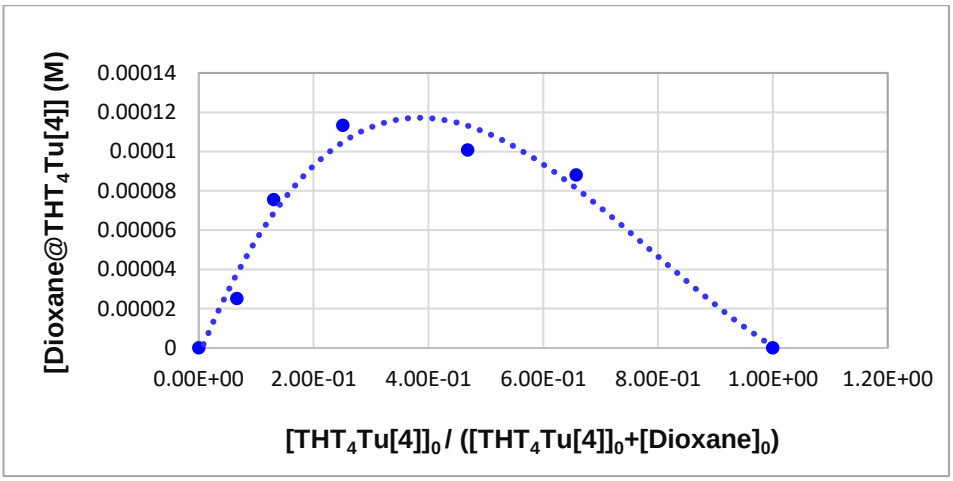

Figure 3.14 Representation of Job's plot for dioxane binding with $THT_4Tu[4]^{2+}$.

3.4.3.1 Comparative binding studies of dioxane with $THT_4Tu[4]^{2+}$ and $Me_4Q[6]$

In case of the Q[*n*] family, the binding studies of a new Q[*n*] are carried out by comparing with the known substituted or unsubstituted Q[*n*]. Mock et al. in their pioneering work introduced a method for competitive binding studies that involved using an excess of two competitive guests that compete for a limited quantity of host leading to host-guest complexes, which exhibit slow exchange kinetics between free and bound guests on the ^{1}H NMR timescale.[22] The concentrations of host and the guest molecules were then

determined by integrating corresponding free and bound resonances. In this experiment, a slightly modified procedure to the method proposed by Mock was followed to study the relative binding studies. This method involved employing two hosts competing for a limited amount of the guest.[21]

For the implementation of this method, a tight binding of host-guest that exhibits slow exchange on the ^{1}H NMR chemical shift timescale was necessary, therefore $Me_4Q[6]$ reported to encapsulate 1,4-dioxane was chosen as the competitive host.[21] $Me_4Q[6]$ illustrates 1:1 binding with dioxane compared to 2:1 in case of $THT_4Tu[4]^{2+}$, therefore, this comparative method measures the relative binding affinity by comparing 2:1 binding ratio of $dioxane_2@THT_4Tu[4]^{2+}$ with 1:1 binding ratio of $dioxane@Me_4Q[6]$.

$$Me_4Q[6] + G \rightleftharpoons G@Me_4Q[6] \quad (1)$$

$$THT_4Tu[4]^{2+} + 2\,G \rightleftharpoons G_2@THT_4Tu[4]^{2+} \quad (2)$$

$$G_2@THT_4Tu[4]^{2+} + Me_4Q[6] + G \rightleftharpoons G@Me_4Q[6] + THT_4Tu[4]^{2+} + 2\,G \quad (3)$$

$$K_{rel} = ([G@Me_4Q[6]]\,[THT_4Tu[4]^{2+}]\,[G]^2) / ([G_2@THT_4Tu[4]^{2+}]\,[Me_4Q[6]\,[G]) \quad (4)$$

$$(K_{THT_4Tu[4]}{}^{2+}) = (K_{Me_4Q[6]}) / (K_{rel}) \quad (5)$$

Where G = 1,4-dioxane

Experiment was performed in $(K^+C_8H_5O_4^-)$/DCl buffer (pD 4.0) to maintain constant pH and measurements were taken using ^{1}H NMR after the binding competition had reached equilibrium and the approximate mole ratios of hosts and the guest were 1:1:1. The observed upfield shifts of 1,4-dioxane confirmed its inclusion inside of the $THT_4Tu[4]^{2+}$ cavity.

The thermodynamics of the host-guest system and the competition experiments are defined by equations 1-3. Integration of resonances for the free and bound hosts and guest peaks enabled the calculation of relative binding constant (K_{rel}) employing equation 4. K_{rel} was calculated to have a value of 4.17×10^{-4} M. The binding constant of dioxane encapsulated in $Me_4Q[6]$ is 834 M^{-1}. Using the known K_a for dioxane@$Me_4Q[6]$[21], the relative binding constant for dioxane$_2$@$THT_4Tu[4]^{2+}$ was calculated as (2.03 ± 0.30) x 10^6 M^{-2}.

3.4.3.2 Comparative binding studies of dioxane and d_8-dioxane with $THT_4Tu[4]^{2+}$

This competitive study was carried out with an aim to determine the effect of isotope on the binding affinity of the guest. The method proposed by Mock was employed using an excess of dioxane and d_8-dioxane as the competing guests for limited quantity of $THT_4Tu[4]^{2+}$. The ^{1}H NMR experiment was performed after thermodynamic equilibrium had reached and the mole ratio of the host and guests were approximately 1:1:1. As no signal was observed for the free and bound d_8-dioxane in ^{1}H NMR, indirect method for calculating bound d_8-dioxane was used. The method involved subtracting the moles for bound dioxane from total moles for bound $THT_4Tu[4]^{2+}$ to obtain bound d_8-dioxane moles. The competitive binding study yielded $K_{rel} = 1.0 \times 10^{-1}$ following equations 6-9, which when referenced to the equation 10 gave binding constant $K_{(d_8\text{-dioxane}_2@THT_4Tu[4]^{2+})}$ = (2.03 ± 0.64) x 10^7 M^{-2}.

$$2\ \text{Dioxane} + \text{H} \rightleftharpoons \text{H@dioxane}_2 \qquad (6)$$

$$2\ d_8\text{-Dioxane} + \text{H} \rightleftharpoons \text{H@}d_8\text{-dioxane}_2 \qquad (7)$$

$$\text{H@}d_8\text{-dioxane}_2 + 2\ \text{Dioxane} \rightleftharpoons \text{H@dioxane}_2 + 2\ d_8\text{-Dioxane} \qquad (8)$$

$$K_{rel} = ([H@dioxane_2]\ [d_8\text{-Dioxane}]^2) / ([H@d_8\text{-dioxane}_2]\ [Dioxane]^2) \quad (9)$$

$$(K_{d8\text{-Dioxane}}) = (K_{Dioxane}) / (K_{rel}) \quad (10)$$

Where H = $THT_4Tu[4]^{2+}$

It is important to note that the increased binding of d_8-dioxane towards $THT_4Tu[4]^{2+}$ could perhaps be related to size and mass of the deuterium atom. Deuterium has a smaller packing radius than hydrogen with C-D bond shorter than an equivalent C-H bond by approximately 0.005Å.[23-24] Based on its size, the binding constant is expected to be lower than the corresponding dioxane.[24] However, the higher binding affinity observed in our case could be explained based on the kinetic factors that are influenced by the mass of deuterium atoms. These kinetic factors may include conformational changes, packing of guest molecules inside the host and the rate of exchange between the free and bound state of the guest. The larger mass of deuterium atoms could render the dissociation of $THT_4Tu[4]^{2+}@d_8\text{-dioxane}_2$ complex to be slow when competing with dioxane, thereby displaying higher binding affinity.

In conclusion, the binding of dioxane demonstrates the importance of ion-dipole interactions in driving the guest occupancy within the cavity of $THT_4Tu[4]^{2+}$. This indicates that $THT_4Tu[4]^{2+}$ may have the potential to bind guests endowed with electronegative groups. However, further studies with an assortment of guests is required to shed light on the host-guest complexation capacity of $THT_4Tu[4]^{2+}$ in relation to its unique structural features and probable ion-dipole interactions. However, it was beyond the scope of this thesis due to time constraints.

While there was insufficient time to explore the binding features of $THT_4Tu[4]^{2+}$ or $THT_3Tu[3]^{2+}$ in greater depth, $Me_{10}Tu[3]^{2+}$ was investigated further to determine it's

possible effectiveness as an excipient for the improvement of aqueous solubility of poorly soluble oral drugs.

3.4.4 Drug solubility studies

Approximately 40-70% of the therapeutic agents belong to Class II of the Biopharmaceutics Classification System (BCS), which encompasses compounds with high intestinal permeability and low solubility.[25] Due to their poor solubilities, the rate and the extent of dissolution is significantly reduced, affecting the drug's oral bioavailability. To address the drug solubility issue, numerous approaches such as the formation of salt[26], high solubility prodrugs[27], nanocrystal solid forms of the drug[28], solid dispersions[29], etc. have been developed. Other than these, the complexation of these drugs with the molecular containers has been of high relevance to the supramolecular chemists. Among these containers, cyclodextrin derivatives have shown enhanced solubility through encapsulation of the drugs within their cavity, in spite of their low K_a and selectivity.[30-31] Moreover, Q[*n*]'s have also been employed for this class of application. The solubility of albendazole, an insoluble drug is enhanced by 2000-fold through inclusion within Q[6] and Q[7], reported by Day et al.[32] More recently, Isaacs's group has been involved in the synthesis of acyclic Q[*n*] congeners that were employed for improving the solubility of the poorly soluble drugs.[25, 33-34] The acyclic Q[*n*] congeners with sulphonate side arms were demonstrated to be particularly well suited for elevating the drug solubility due to their high water solubility.[34]

In our case, the purpose of conducting the solubility studies was to establish the preliminary investigations regarding the ability of $Me_{10}Tu[3]^{2+}$ to act as a solubilizing agent for poorly soluble oral anionic drugs. The inherent solubility of the molecular container is an important feature to serve as a solubilizing excipient for the insoluble

drugs. The solubility of $Me_{10}Tu[3]Cl_2$ in pure water is relatively high (73g/L).[1] Due to its good inherent solubility, it was assumed that the solubilities of anionic drugs might be influenced through association with the positively charged pyrazolium walls and/or two C=O portals of $Me_{10}Tu[3]^{2+}$.

The drugs for this study were chosen based on their structural attributes and limited inherent solubilities under aqueous conditions. Figure 3.15 shows the structures of the drugs used in this study. These drugs fall into different pharmaceutical classes, which includes non-steroidal anti-inflammatory (Indomethacin, Mefenamic acid), uricosuric (Probenecid), anti-fungal (Griseofulvin) and diuretic (Furosemide). Of these, four drugs have a carboxylic acid group and a nitrogen atom in an amino or amido form. The carboxyl group is converted into protonated or deprotonated form depending upon the experimental conditions applied. The experiment was performed in two buffer systems (citric acid buffer - pH 3.5 and PBS buffer - pH 7.4) in order to evaluate the behaviour of $Me_{10}Tu[3]^{2+}$ towards the solubility parameter at two different pH conditions. In addition, these two pH levels mimic gastric and intestinal physiological environments, which are crucial for practical applications in the biological system. UV/Vis spectroscopic technique was applied as an alternate method of observation for the experiment, as the efforts for measuring the solubilities using ^1H NMR did not furnish any detectable signals for the drugs alone or in combination with $Me_{10}Tu[3]Cl_2$.

Experimentally, the solutions of excess drugs were stirred individually and with three different known concentrations of $Me_{10}Tu[3]Cl_2$ in order to find out their intrinsic and combined solubilities in citric acid and PBS buffer. The change in the solubility for each sample was observed through the difference in the absorbance value relative to the absorbance of the drug alone. The change in the absorbance indirectly reflects the change in the corresponding solubility of the drug.

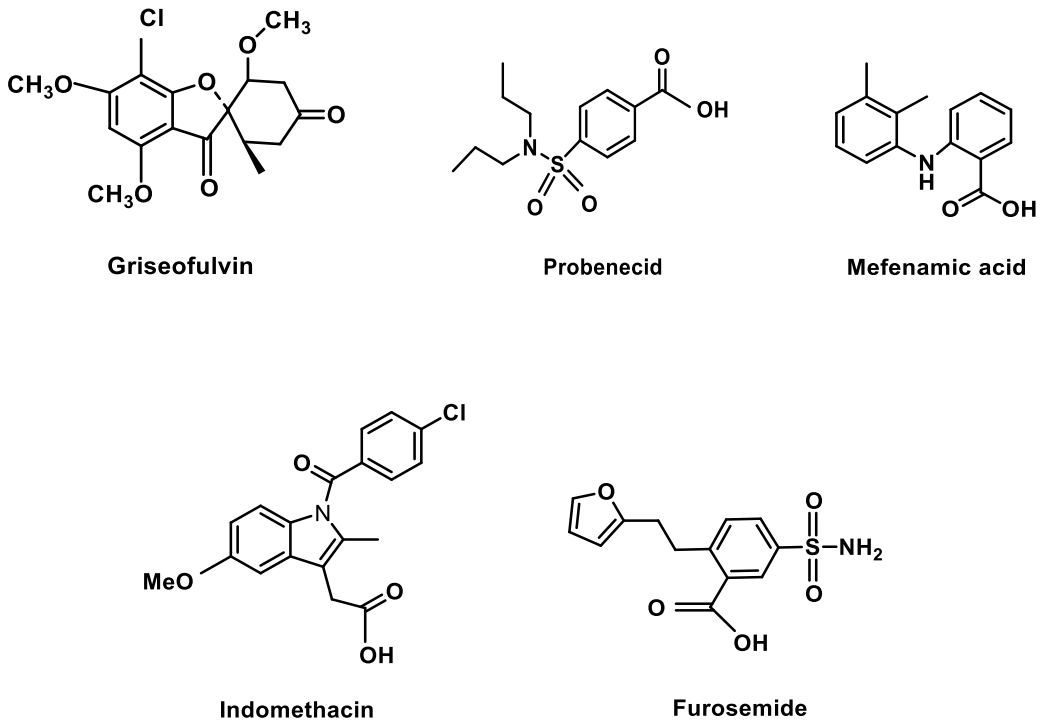

Figure 3.15 The structures of poorly soluble oral drugs used in the study.

3.4.4.1 Solubility studies in Citric acid buffer

Indomethacin and mefenamic acid belong to the same class of anti-inflammatory drugs with pK_a values of 4.5 and 4.2 and aqueous solubilities of 8.8 and 0.5 µg/mL, respectively.[35-37] With indomethacin, the greatest increase in the absorbance (13-fold) was observed with the addition of 13.9 µM $Me_{10}Tu[3]Cl_2$ and reflected the point of maximum effect that could be achieved with $Me_{10}Tu[3]Cl_2$. In the case of mefenamic acid substantial enhancement in absorbance by 13.5-fold was noticed at 41.5 µM concentration of $Me_{10}Tu[3]Cl_2$, indicating a propensity to increase further with more amount of $Me_{10}Tu[3]Cl_2$ (Figure 3.16, Appendices A24 (a-b)).

Similar to these drugs, probenecid (pK_a[38] = 3.4, aqueous solubility[39] = 3.98 µg/mL) and furosemide (pK_a[40] = 3.8, aqueous solubility[39] = 19.68 µg/mL) relate structurally in having

a carboxylic acid and N as an amido group. Probenecid exhibited a consistent increase of more than 3-fold at each employed concentration of $Me_{10}Tu[3]Cl_2$ (Figure 3.16, Appendices A24 (c)). Likewise, furosemide, a diuretic drug displayed an absorbance increase by 4.2 and 3.1-fold when mixed with 27.7 µM and 41.5 µM of $Me_{10}Tu[3]Cl_2$, respectively (Figure 3.16, Appendices A24(d), A25).

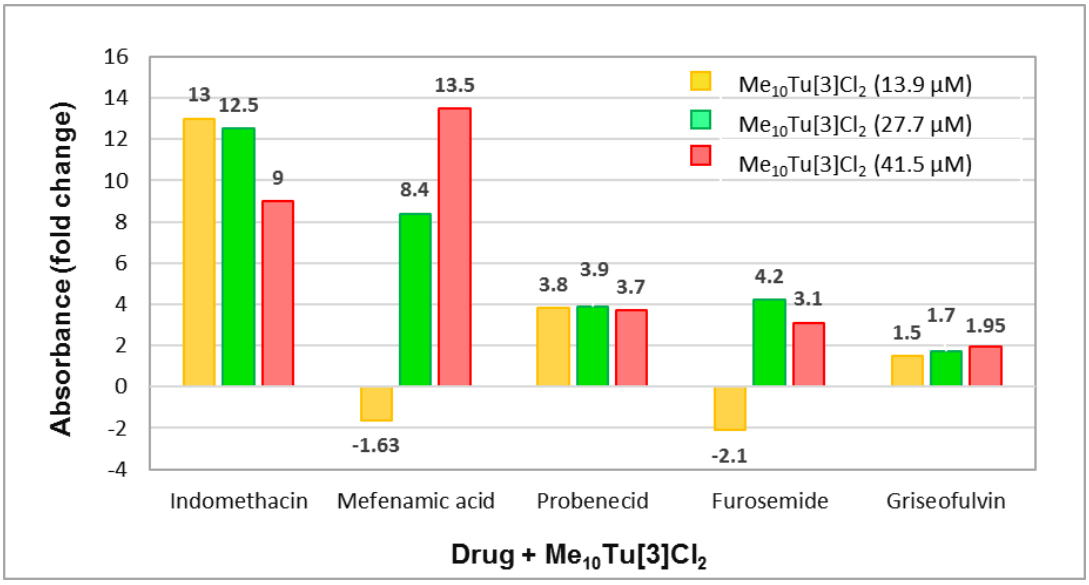

Figure 3.16 Shows the results for the fold change in the absorbance of drugs as a result of the addition of three concentrations of $Me_{10}Tu[3]Cl_2$, all dissolved in 20 mM citric acid buffer (pH 3.5). The values were calculated at λ = 237 nm, except for griseofulvin (λ = 293 nm)

The values shown in Figure 3.16 were calculated at λ = 237 nm (except for griseofulvin) which required the subtraction of the contribution of the absorbance from $Me_{10}Tu[3]Cl_2$ to arrive at the amount of absorption due only to the solubilised drug (Appendices 22). In all these cases, a plausible explanation for this behaviour might be the existence of protonated form of carboxyl group at pH 3.5, possibly allowing H-bond interaction at the C=O portals of $Me_{10}Tu[3]Cl_2$.

Interestingly, griseofulvin, an antifungal agent that has been recently reported to exert anti-proliferative activity in mammalian cancer cells is different in structural aspects compared to the above mentioned anionic drugs.[41] In contrast, it does not feature a carboxylic acid nor N as amino or amido group yet displayed an increase in the absorbance by > 1.5 to 1.95 over 3 addition of $Me_{10}Tu[3]Cl_2$. This is best attributed to the presence of three electron donating methoxy groups, making the rings more electronegative thereby enabling interaction with the positively charged pyrazolium moieties. In addition, a contribution from a hydrophobic interaction with the more lipophilic parts of the $Me_{10}Tu[3]Cl_2$ may also provide part of the explanation (Figure 3.16, Appendices A24 (e)).

3.4.4.2 Solubility studies in PBS buffer

Figure 3.17 show the fold change in the absorbance with the addition of $Me_{10}Tu[3]Cl_2$ in PBS buffer. The corresponding absorption wavelength used for the calculations was different for each drug and is shown in Appendices A27. In PBS buffer, the formation of sodium salt of the drugs lead to an increase in their corresponding intrinsic solubilities, reflected by the significant increase in the UV/Vis absorbance for each drug. In order to obtain the correct absorbance data, the solutions were diluted and this accounted for the lower values of $Me_{10}Tu[3]Cl_2$ concentrations in the figure specified. The trend observed for the solubilities of the drugs in PBS buffer was different, and the outcome is most likely related to the use of different pH condition of 7.4, where the carboxylic acid group would be deprotonated. Indomethacin and furosemide illustrated a decrease in the absorbance while mefenamic acid and probenecid demonstrated an increase on subsequent addition of different concentrations of $Me_{10}Tu[3]Cl_2$ (Figure 3.17, Appendices A26 (a – d)). The change in solubility whether slightly decreased or slightly increased for indomethacin and

mefenamic acid respectively, these differences are too small to be of value. However, significant changes were observed for furosemide with up to a 2 fold decrease and probenecid with a 1.8 fold increase. Both are likely to reflect a complex formation as a consequence of ion-ion interactions with the cationic centres of $Me_{10}Tu[3]^{2+}$ but in one case the complex is less soluble whereas in other it is more soluble compared to the drugs alone.

Similarly, griseofulvin demonstrated the absorbance increase of 1.08 to 1.22-fold with the largest increase after the 3rd addition but this was still small. As in the citrate buffer, the solubility could be related to the overall electronegative character of the molecule allowing interaction with the positive centres of the pyrazolium moieties. (Figure 3.17, Appendices A26 (e)).

Comparison of the results at two different pH conditions indicate the influence of anionic and protonated form of the anion on the intrinsic solubilities of the drugs through association with $Me_{10}Tu[3]^{2+}$. Both the forms revealed interaction with $Me_{10}Tu[3]^{2+}$ but to different extent, with protonated form of the carboxyl group being more efficient in enhancing the solubilities through H-bond interactions at the portals than electrostatic interactions between the carboxylate or electronegative groups and the positively charged pyrazolium units.

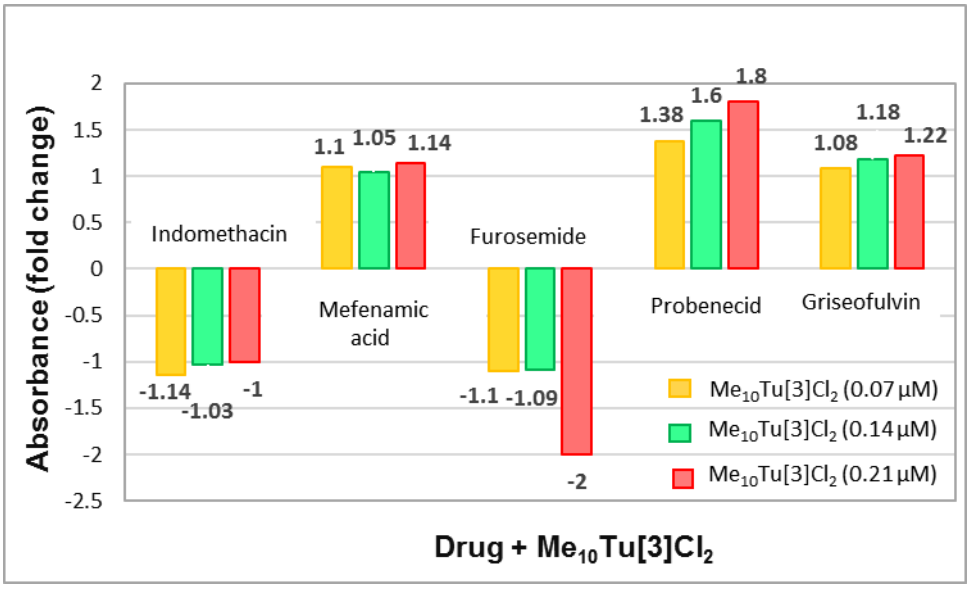

Figure 3.17 Shows the results for the fold change in the absorbance of drugs as a result of addition of three concentrations of $Me_{10}Tu[3]Cl_2$, all dissolved in 20 mM PBS buffer (pH 7.4).

The above-mentioned preliminary results suggest that in the presence of $Me_{10}Tu[3]^{2+}$, the gastric acidic conditions would favour the solubilisation of the drug in the carboxylic acid form and as the drug transit along the small intestine the solubility would be influenced due to the transformation of carboxylic acid to carboxylate form, consequently affecting drug's absorption through the gastric and intestinal mucosa. Therefore, $Me_{10}Tu[3]^{2+}$ holds a potential to act as a solubilizing agent, which could be used as an alternative to other molecular containers for practical applications. A more conclusive assessment of the variation in the solubility of the drug can be obtained through quantitative assessment of the binding constant of the complex formed between the drug and $Me_{10}Tu[3]Cl_2$. However, due to the limitation of time, this study could not be extended further and will be the subject for future work.

3.5 Conclusion

Every new class of macrocyclic hosts requires an understanding of their physical and chemical properties before they can be applied in functional applications. In order to come to an understanding of the unknown host-guest chemistry of the new Tu[*n*]'s with methyl and THT substitutions, a number of preliminary studies were performed following a hypothesis of possible interactions as demonstrated in this chapter.

The pK_a's of $Me_{10}Tu[3]^{2+}$, $THT_3Tu[3]^{2+}$ and $THT_4Tu[4]^{2+}$ were determined and these hosts were found to have two pK_a values. The first pK_a indicated the effect of host molecule on the pK_a value of bound guests such as HCl or HSO_4^- relative to their free forms. In addition, the second pK_a value observed for the three Tu[*n*]'s was of the host and related to the acidity of the methyl groups present on their pyrazolium moieties. The evidence that supported the acidity of the methyl groups was obtained through the deuterium exchange experiments verified by ^{1}H, ^{2}H NMR and mass spectroscopy that elucidated the primary exchange occurred at the methyl groups on the pyrazolium moieties. It was found that slower exchange also occurred on the methylene groups between the pyrazolium moieties and the immediately attached glycoluril moiety. The propensity for exchange on these group was greater for THT substituted Tu[*n*]'s than for $Me_{10}Tu[3]^{2+}$.

Further, the binding property of the methyl and THT substituted Tu[*n*]'s were explored for an organic guest (L-Gln) using different spectroscopic techniques (CD, Fluorescence and ^{1}H NMR). Indication of the association of L-Gln through CD spectral analysis led to the quantitative assessment of binding constants of Tu[*n*]'s employing competitive binding assay using a fluorescence dye (TNS). A binding constant of the order ~ 2.4 × 10^2 M^{-1} was obtained for TNS@$Me_{10}Tu[3]^{2+}$ which was further used for determining the

binding constant of L-Gln@$Me_{10}Tu[3]^{2+}$ (~ 2.2×10^2 M^{-1}). The fluorescence technique, however, was not successful in providing the association constant for TNS@$THT_nTu[n]^{2+}$ complexes, possibly due to weaker binding of TNS to $THT_nTu[n]^{2+}$. Additionally, the ^1H NMR technique was also utilized in an attempt to calculate the binding constants for the complex of L-Gln with methyl and THT substituted Tu[*n*]'s but displayed an insignificant change in the chemical shift values for all the hosts and the guest. All the aforementioned results indicated the portal binding of L-Gln rather than inclusion within the cavity, which is consistent with the binding constant of order 10^2 M^{-1} for L-Gln@$Me_{10}Tu[3]^{2+}$.

This chapter also described the relative binding constant studies for dioxane with the larger Tu[*n*] homologue ($THT_4Tu[4]^{2+}$). The results obtained demonstrated 2:1 binding ratio of dioxane$_2$@$THT_4Tu[4]^{2+}$ with a binding constant value of 2.03×10^6 M^{-2}. Further, the binding behaviour towards an isotopic guest (d_8-dioxane) was also observed that displayed higher binding affinity compared to dioxane.

Finally, the potential of $Me_{10}Tu[3]Cl_2$ to serve as a solubilizing agent for five poorly soluble anionic drugs was explored. These preliminary investigations revealed that at acidic pH of 3.5, the absorbance of these drugs increased upon addition of three different concentrations of $Me_{10}Tu[3]Cl_2$ relative to the drugs alone. However, at pH 7.4 three of the drugs (mefenamic acid, probenecid and griseofulvin) exhibited modest increase whereas the furosemide and indomethacin presented a modest decrease in the absorbance.

Overall, the results suggested the relevance of both H-bonding and electrostatic/ion-dipole interactions in driving the association between the guests and Tu[*n*]'s, indicating that the anionic or electronegative molecules that also carry H-bond donor groups could be ideal guest for this new class of macrocyclic hosts. Clearly, the results that have been

discussed in this chapter are only the beginning to an understanding of the chemical and physical properties of these new macrocyclic hosts.

3.6 References

1. Chandrakumar, P. K.; Dhiman, R.; Woodward, C. E.; Iranmanesh, H.; Beves, J. E.; Day, A. I., Tiara[*n*]uril: A Glycoluril-Based Macrocyclic Host with Cationic Walls. *The Journal of Organic Chemistry* **2019,** *84* (7), 3826-3831.
2. Chandrakumar, P. K. Exploration of New Cucurbit[*n*]uril and A Novel Glycoluril Based Macrocycle-tiara[*n*]uril. PhD Thesis, University of New South Wales, Canberra, 2016.
3. Lu, W. Exploration of Cucurbit[*n*]uril (Q[*n*]) and Their Derivatives as Potential Linkers in Hydrogels and Metal-organic Frameworks (MOF). PhD Thesis, University of New South Wales, Canberra, 2018.
4. Wagner, B. D.; Stojanovic, N.; Day, A. I.; Blanch, R. J., Host Properties of Cucurbit[7]uril: Fluorescence Enhancement of Anilinonaphthalene Sulfonates. *The Journal of Physical Chemistry B* **2003,** *107* (39), 10741-10746.
5. Koner, A. L.; Nau, W. M., Cucurbituril Encapsulation of Fluorescent Dyes. *Supramolecular Chemistry* **2007,** *19* (1-2), 55-66.
6. Saleh, N. i.; Koner, A. L.; Nau, W. M., Activation and Stabilization of Drugs by Supramolecular pK_a Shifts: Drug-Delivery Applications Tailored for Cucurbiturils. *Angewandte Chemie* **2008,** *120* (29), 5478-5481.
7. Trummal, A.; Lipping, L.; Kaljurand, I.; Koppel, I. A.; Leito, I., Acidity of Strong Acids in Water and Dimethyl Sulfoxide. *The Journal of Physical Chemistry A* **2016,** *120* (20), 3663-3669.
8. Kikuchi, Y.; Kobayashi, K.; Aoyama, Y., Molecular Recognition. 18 Complexation of Chiral Glycols, Steroidal Polyols, and Sugars with a Multibenzenoid, Achiral Host as Studied by Induced Circular Dichroism Spectroscopy: Exciton Chirality Induction in Resorcinol-aldehyde Cyclotetramer and Its Use as a Supramolecular

Probe for the Assignments of Stereochemistry of Chiral Guests. *Journal of the American Chemical Society* **1992,** *114* (4), 1351-1358.

9. Wu, W.; Cronin, M. P.; Wallace, L.; Day, A. I., An Exploration of Induced Supramolecular Chirality Through Association of Chiral Ammonium Ions and Tartrates with the Achiral Host Cucurbit[7]uril. *Israel Journal of Chemistry* **2018,** *58* (3-4), 479-486.
10. Apurba, K. L.; Nau, W., Cucurbituril Encapsulation of Fluorescent Dyes. *Supramolecular Chemistry* **2007**; Vol. 19, p 55-66.
11. Nau, W. M.; Mohanty, J., Taming Fluorescent Dyes with Cucurbituril. *International Journal of Photoenergy* **2005,** *7* (3), 133-141.
12. Mohanty, J.; Bhasikuttan, A. C.; Nau, W. M.; Pal, H., Host-Guest Complexation of Neutral Red with Macrocyclic Host Molecules: Contrasting pK_a Shifts and Binding Affinities for Cucurbit[7]uril and β-Cyclodextrin. *The Journal of Physical Chemistry B* **2006,** *110* (10), 5132-5138.
13. Wagner, B. D.; Fitzpatrick, S. J.; Gill, M. A.; MacRae, A. I.; Stojanovic, N., A Fluorescent Host-guest Complex of Cucurbituril in Solution: a Molecular Jack O'Lantern. *Canadian Journal of Chemistry* **2001,** *79* (7), 1101-1104.
14. Wagner, B. D.; Boland, P. G.; Lagona, J.; Isaacs, L., A Cucurbit[6]uril Analogue: Host Properties Monitored by Fluorescence Spectroscopy. *The Journal of Physical Chemistry B* **2005,** *109* (16), 7686-7691.
15. Lagona, J.; Wagner, B. D.; Isaacs, L., Molecular-Recognition Properties of a Water-Soluble Cucurbit[6]uril Analogue. *The Journal of Organic Chemistry* **2006,** *71* (3), 1181-1190.
16. Gravett, D. M.; Guillet, J. E., Synthesis and Photophysics of a Water-soluble, Naphthalene-containing Beta-cyclodextrin. *Journal of the American Chemical Society* **1993,** *115* (14), 5970-5974.

17. Wagner, B. D.; Fitzpatrick, S. J., A Comparison of the Host-guest Inclusion Complexes of 1,8-ANS and 2,6-ANS in Parent and Modified Cyclodextrins. *Journal of Inclusion Phenomena and Macrocyclic Chemistry* **2000,** *38* (1-4), 467-478.

18. Kosower, E. M.; Dodiuk, H.; Kanety, H., Intramolecular Donor-acceptor System. 4. Solvent Effects on Radiative and Nonradiative Processes for the Charge-transfer States of N-arylaminonaphthalenesulfonates. *Journal of the American Chemical Society* **1978,** *100* (13), 4179-4188.

19. Kim, K.; Selvapalam, N.; Ko, Y. H.; Park, K. M.; Kim, D.; Kim, J., Functionalized Cucurbiturils and Their Applications. *Chemical Society Reviews* **2007,** *36* (2), 267-279.

20. HyperChem professional 8.0.7 for Windows Molecular Modelling System, Hyperchem Inc., Ontario, Canada, 2009.

21. Wu, W.-J.; Wu, F.; Day, A. I., Molecular Snuggle and Stretch of a Tetraammonium Chain in the Construction of a Hetero-[4] pseudorotaxane with CyclopentanoQ [6] and Classical Q[7]. *The Journal of Organic Chemistry* **2017,** *82* (11), 5507-5515.

22. Mock, W. L.; Shih, N. Y., Structure and Selectivity in Host-guest Complexes of Cucurbituril. *The Journal of Organic Chemistry* **1986,** *51* (23), 4440-4446.

23. Dunitz, J. D.; Ibberson, R. M., Is Deuterium Always Smaller than Protium? *Angewandte Chemie International Edition* **2008,** *47* (22), 4208-4210.

24. Mugridge, J. S.; Bergman, R. G.; Raymond, K. N., Does Size Really Matter? The Steric Isotope Effect in a Supramolecular Host-Guest Exchange Reaction. *Angewandte Chemie International Edition* **2010,** *49* (21), 3635-3637.

25. Ma, D.; Hettiarachchi, G.; Nguyen, D.; Zhang, B.; Wittenberg, J.; Zavalij, P.; Briken, V.; Isaacs, L., Acyclic Cucurbit[*n*]uril Molecular Containers Enhance the

Solubility and Bioactivity of Poorly Soluble Pharmaceuticals. *Nature Chemistry* **2012,** *4*, 503-10.

26. Serajuddin, A. T., Salt Formation to Improve Drug Solubility. *Advanced Drug Delivery Reviews* **2007,** *59* (7), 603-616.
27. Stella, V. J.; Nti-Addae, K. W., Prodrug Strategies to Overcome Poor Water Solubility. *Advanced Drug Delivery Reviews* **2007,** *59* (7), 677-694.
28. Muller, R. H.; Keck, C. M., Challenges and Solutions for the Delivery of Biotech drugs-A Review of Drug Nanocrystal Technology and Lipid Nanoparticles. *Journal of Biotechnology* **2004,** *113* (1-3), 151-170.
29. Leuner, C.; Dressman, J., Improving Drug Solubility for Oral Delivery using Solid Dispersions. *European Journal of Pharmaceutics and Biopharmaceutics* **2000,** *50* (1), 47-60.
30. Okimoto, K.; Rajewski, R. A.; Uekama, K.; Jona, J. A.; Stella, V. J., The Interaction of Charged and Uncharged Drugs with Neutral (HP-β-CD) and Anionically Charged (SBE7-β-CD) β-Cyclodextrins. *Pharmaceutical Research* **1996,** *13* (2), 256-264.
31. Rajewski, R. A.; Stella, V. J., Pharmaceutical Applications of Cyclodextrins. 2. In vivo Drug Delivery. *Journal of Pharmaceutical Sciences* **1996,** *85* (11), 1142-1169.
32. Zhao, Y.; Buck, D.; Morris, D.; Pourgholami, M.; Day, A.; Grant Collins, J., Solubilisation and Cytotoxicity of Albendazole Encapsulated in Cucurbit[*n*]uril. *Organic & Biomolecular Chemistry* **2009,** *6*, 4509-15.
33. Zhang, B.; Isaacs, L., Acyclic Cucurbit[*n*]uril-type Molecular Containers: Influence of Aromatic Walls on their Function as Solubilizing Excipients for Insoluble Drugs. *Journal of Medicinal Chemistry* **2014,** *57* (22), 9554-9563.

34. Zhang, B.; Zavalij, P.; Isaacs, L., Acyclic CB[*n*]-Type Molecular Containers: Effect of Solubilizing Group on their Function as Solubilizing Excipients. *Organic & Biomolecular Chemistry* **2014,** *12*.

35. Guo, J.; Elzinga, P. A.; Hageman, M. J.; Herron, J. N., Rapid Throughput Solubility Screening Method for BCS Class II Drugs in Animal GI Fluids and Simulated Human GI Fluids Using a 96-well Format. *Journal of Pharmaceutical Sciences* **2008,** *97* (4), 1427-1442.

36. Comer, J.; Judge, S.; Matthews, D.; Towes, L.; Falcone, B.; Goodman, J.; Dearden, J., The Intrinsic Aqueous Solubility of Indomethacin. *ADMET and DMPK* **2014,** *2* (1), 18-32.

37. O'Brien, M.; McCauley, J.; Cohen, E., Indomethacin. In *Analytical Profiles of Drug Substances*, Florey, K., Ed. Academic Press: 1984; Vol. 13, pp 211-238.

38. Cunningham, R.; Israili, Z.; Dayton, P., Clinical Pharmacokinetics of Probenecid. *Clinical Pharmacokinetics* **1981,** *6* (2), 135-151.

39. Hopfinger, A. J.; Esposito, E. X.; Llinas, A.; Glen, R. C.; Goodman, J. M., Findings of the Challenge to Predict Aqueous Solubility. *Journal of Chemical Information and Modeling* **2008,** *49* (1), 1-5.

40. Granero, G.; Longhi, M.; Mora, M.; Junginger, H. E.; Midha, K. K.; Shah, V. P.; Stavchansky, S.; Dressman, J. B.; Barends, D. M., Biowaiver Monographs for Immediate Release Solid Oral Dosage Forms: Furosemide. *Journal of Pharmaceutical Sciences* **2010,** *99*, 2544-56.

41. Hamdy, A. K.; Sheha, M. M.; Abdel-Hafez, A. A.; Shouman, S. A., Design, Synthesis, and Cytotoxicity Evaluation of Novel Griseofulvin Analogues with Improved Water Solubility. *International Journal of Medicinal Chemistry* **2017,** *2017*, 12.

CHAPTER 4
CONCLUSIONS

The recent discovery of Tu[*n*] family has provided a new direction toward cucurbit[*n*]uril like macrocycles with cationic centres.[1] As has been the case for many macrocyclic molecules, higher homologues have always been fascinating challenges sparked by a research interest driven by a quest for larger cavity sizes, with a view to broaden their applicability for the binding of a large variety of guests. The known Tu[*n*] derivatives having methyl and cyclopentano substitutions on their glycoluril moieties - Me_{10}Tu[3] and CyP_3Tu[3] have been successfully demonstrated in previous work by Day and co-workers.[1] However, the intriguing synthetic result observed in both cases was the absence of homologues larger than Tu[3] and this has served as a motivation for the work presented in this thesis. The prime objective of this research work was to establish a reaction sequence for the synthesis of Tu[*n*]'s favourable to higher homologues through an alternative functionality placed equatorially in the glycoluril moieties. In addition, it was anticipated that the properties of the substituted Tu[*n*]'s in relation to their modified electronic structure and functionality could also facilitate a potential for future applications.

4.1 Synthesis of Tetrahydrothiophenetiara[*n*]uril

The work demonstrated in Chapter 2 of this thesis focused on the possibility of higher homologue formation through the introduction of a different functional group i.e., THT at the equatorial position of the glycoluril units. It was anticipated that THT had the potential to provide two main features - possible higher homologues and a functional group that could be modified in the future. During this expedition, the first higher

homologue of the Tu[*n*] family - $THT_4Tu[4]$ was successfully achieved along with $THT_3Tu[3]$. The potential factor responsible for higher homologue accessibility in this case, was the β angle observed at concave faces of fused imidazole rings of the employed THT glycoluril diether. The increase in the β angle by 0.33° and 1.53° for THT functionality compared to cyclopentano and methyl substituents enabled the formation of homologue higher than Tu[3]. This was achieved possibly through the formation of the precursor glycoluril oligomers with larger curvature during the acid catalyzed synthesis of Tu[*n*].[2-3] In addition, synthetic access to an improved higher homologue distribution was achieved through reaction method modification using HCl with a higher strength (37% HCl) and also utilization of the salt form of tetramethylpyrazolyl methane instead of a free base. Furthermore, studies were performed to investigate the effect of anionic templates toward preferential formation of the larger homologue, employing H_2SO_4 and CH_3SO_3H acid, both with the same concentration as the 37% HCl. The results revealed an increased proportion of $THT_4Tu[4]$ for the reaction catalyzed by H_2SO_4, suggesting beneficial influence of anionic templates in driving the reaction towards the attainment of larger cavities. It was also further observed that with these modifications, overall reactions were higher yielding.

4.1.1 Synthetic recommendation for future studies

In reflection the previously reported synthetic outcome for Tu[*n*] with the cyclopentano substituent is surprising in that the anticipated homologues higher than Tu[3] were not attained in spite of their ability to form higher Q[*n*] homologues.[1-2] In our case, the work with THT functionality demonstrated the usefulness of varying acidic conditions such as acids of different types and strength, which led to positive synthetic outcomes toward the synthesis of a homologue > 3. Given that the β angle for the cyclopentano glycoluril (β =

110.08°) is not significantly different to THT (β = 110.41°), it would be worthwhile to consider re-synthesizing $CyP_nTu[n]$ employing more concentrated acidic conditions. It is expected that this may lead to $CyP_nTu[n]$ where n = 3 and 4. Further to this, the anion templating effect would likely provide an adjunct assisting the formation of Tu[4]'s.

In the pursuit of higher homologues for fully substituted $Me_nQ[n]$, the reaction of pyrazole with dimethyl glycoluril diether afforded two dicationic acyclic congeners characterized by central glycoluril units and pyrazolium side-walls (Chapter 1, Scheme 1.12).[1] The product distribution in this case was confined majorly to congener having one glycoluril unit. Further extension of this study as a new class of hosts, "pincers" illustrated that the replacement of unsubstituted pyrazole with dimethylpyrazole shifted the product distribution towards predominate formation of dipincer (with two glycoluril units). However, of relevance was the formation of the extend oligomer - tripincer in addition to dipincer and monopincer.[4] This trend reflected the influence of substituent present on pyrazole upon oligomer chain length. Replacing the methyl group with an ethyl functionality could be a possible way to achieve oligomers longer than 3 glycoluril units. Thus, this approach has implications in relation to the synthesis of Tu[n] as an alternative method to achieving higher Tu[n] homologue through the use of different pyrazole derivative such as tetraethylpyrazolyl methane. A possible future direction in the quest for higher Tu[n] homologues.

4.2 Exploration towards the properties of Tiara[*n*]uril family

The host-guest properties of three different Tu[n] derivatives ($Me_{10}Tu[3]^{2+}$, $THT_3Tu[3]^{2+}$ and $THT_4Tu[4]^{2+}$) were explored by evaluating their potential to bind a selection of guest molecules. Three different spectroscopic techniques were used to investigate their binding interactions as highlighted in Chapter 3 of this thesis.

The pK_a investigation of these Tu[*n*]'s demonstrated host dependent pK_a shift for bound HCl, providing evidence for a binding association between Tu[*n*]'s and the guest. The second pK_a value was found to relate to the acidic nature of methyl groups present at the pyrazolium moieties and corresponded to the pK_a value of the host itself. This was substantiated through deuterium exchange experiments and mass spectroscopic analysis.

In another binding study with an organic guest (L-glutamine), the interaction with 3 different Tu[*n*]'s ($Me_{10}Tu[3]^{2+}$, $THT_3Tu[3]^{2+}$ and $THT_4Tu[4]^{2+}$) was initially monitored by CD spectroscopy and the change in molar ellipticity signalled the formation of a binding complex. No significant changes were observable by ^{1}H NMR spectroscopy with the addition of L-Gln to each of the mentioned Tu[*n*]'s. However, the fluorescence spectroscopy using TNS dye as a competitive guest proved to be a useful technique in acquiring binding association data, specifically for $Me_{10}Tu[3]Cl_2$. A relatively weak association of the fluorescent dye, TNS was found with $Me_{10}Tu[3]Cl_2$, which was illustrated by enhancement in fluorescence intensity along with a blue shift of 17 nm. The binding constant of TNS@$Me_{10}Tu[3]Cl_2$ was determined to be ~ 2.4×10^2 M^{-1}. Using this dye, the binding constant of L-Gln was then determined by competitive binding and was found to be moderate at ~ 2.2×10^2 M^{-1}. The same approach was applied to $THT_3Tu[3]^{2+}$ and $THT_4Tu[4]^{2+}$. However, their interaction with TNS was found to be too weak rendering it unsuitable for binding in the case of these two Tu[*n*]'s.

Given the lack of changes in ^{1}H NMR spectra with the addition of L-Gln to $Me_{10}Tu[3]Cl_2$ or $THT_3Tu[3]^{2+}$/ $THT_4Tu[4]^{2+}$ and the weak binding of the former measured by changes in fluorescence with titrations, it is assumed that the association is through H-bonding to the C=O's at the portals for L-Gln.

Owing to distinctive structural features that create cationic cavity furnished partly with C=O arcs at the portals and good water solubility, a different binding aspect of $Me_{10}Tu[3]Cl_2$ was explored by assessing its ability to act as a solubilizing agent for poorly soluble oral anionic drugs. The preliminary investigations provided a measurable interaction between $Me_{10}Tu[3]Cl_2$ and the drugs through changes in the solubilities for the drugs at two different pH conditions. The carboxyl group that had the ability to exist in protonated or deprotonated form (carboxylate anion) and the overall electronegative character specifically for griseofulvin, were the structural elements of the drugs that made them relevant for this study. In general, two pH conditions were employed 3.5 and 7.4. The drugs evaluated were found to show enhancement in solubilities except for indomethacin and furosemide that displayed reduced solubilities at pH 7.4. However, the magnitude of solubility increase was distinctly improved at 3.5 with much small changes at 7.4. These preliminary findings suggested that the protonated form of the carboxyl group enhanced the drug's solubility more efficiently through H-bond interactions at the portals than electrostatic interactions between the carboxylate and the positively charged pyrazolium units. Another finding of considerable interest was related to the drug griseofulvin. The absence of carboxyl group and the overall electronegativity of the molecule because of electron donating methoxy groups structurally differentiated it from the rest of the employed drugs. An increase in solubility at both pH conditions suggested that the electronegative molecules could also serve as appropriate guests for association at the pyrazolium positive centres.

$THT_4Tu[4]^{2+}$ represented the first Tu[*n*] with cavity where its dimensions are in between those Q[6] and Q[7]. With a cavity of this size it was expected to be capable of encapsulating larger guests within the cavity. The investigation of the binding behaviour of $THT_4Tu[4]^{2+}$ was demonstrated with the guest dioxane that provided evidence for

encapsulation within the cavity, reflected by the upfield shift of the bound dioxane resonance in ^{1}H NMR spectra with slow exchange kinetics. In addition, $THT_4Tu[4]^{2+}$ was also exploited for its interaction with deuterated dioxane (d_8-dioxane) to determine if there was any deviation in binding efficiency owing to the presence of the deuteron. These guests were determined for their binding affinities employing competitive binding assays and due to slow exchange rate at NMR timescale; it became feasible to determine the binding constants using NMR technique. The binding constants for dioxane and d_8-dioxane were found to be ~ 10^6 and 10^7 M^{-2}, respectively with 2:1 stoichiometry. The d_8-dioxane displayed higher binding affinity compared to dioxane and was ascribed to the higher mass of deuterium. The dioxane binding represented the first example for cavity occupancy within $THT_4Tu[4]^{2+}$ through ion-dipole interactions at the positively charged pyrazolium centres. This indicated a potential capability of $THT_4Tu[4]^{2+}$ to encapsulate similar types of guests bestowed with electronegative atoms or groups.

4.2.1 Recommendation for future studies

The relationship between the binding properties and structural features of Tu[*n*]'s observed from the studies presented in Chapter 3, indicated potential binding capability of methyl and THT substituted Tu[*n*]'s towards anionic/electronegative guests supported by H-bond donor groups.

As an extension to the binding studies with L-Gln, it would be valuable to explore the binding association of methyl and THT substituted Tu[*n*]'s with a range of amino acids and perhaps related compounds depending upon the findings.

In the case of dioxane binding, the electronegative O of dioxane served as one of the driving factor for cavity occupancy within $THT_4Tu[4]^{2+}$ and indicates the potential of

electronegative molecules for interaction with the positive centres through ion-dipole, facilitating their binding within the cavity. Therefore, it would be worthwhile to explore the cavity binding capability of $THT_4Tu[4]^{2+}$ with an assortment of similar guests such as THF, pyran and acyclic polyethers as electronegative guests. Another future study involving $THT_4Tu[4]^{2+}$ could be the modifications at the equatorial sulphur moiety. The propensity of sulphur atom to oxidize to sulphoxide or sulfone could lead to $THT_4Tu[4]^{2+}$ derivatives with altered electronic properties, which in turn could influence the cavity binding of electronegative guests. Further studies of this type would provide a better understanding of the influential factors that affect the binding process and binding behaviour related to equatorial substitution. In addition to the established fluorescence technique for $Me_{10}Tu[3]^{2+}$, isothermal calorimetry[5], ORD[6], and DOSY[7] could be exploited as alternative methods to elucidate the binding affinities quantitatively for the above mentioned guests.

In the area of solubility studies with $Me_{10}Tu[3]^{2+}$, the initial findings were confined only to a limited number of drugs. This provides a future opportunity to broaden the solubility studies to a series of poorly soluble oral drugs. This could include selecting drugs with the structural features similar to griseofulvin, as well as additional drugs with carboxylic acid functionality. These investigations could further be extended to study the effectiveness of $THT_3Tu[3]^{2+}$ and $THT_4Tu[4]^{2+}$ as solubilizing excipients, in comparison to $Me_{10}Tu[3]^{2+}$. This could shed light on the possible effect of two different substitutions as well as the larger cavity size of $THT_4Tu[4]^{2+}$ on the solubilities of the selected oral drugs.

Overall, a comprehensive knowledge of the binding properties of the newly developed class of macrocylic hosts (Tu[*n*]'s) could mark its establishment into future applications.

4.3 References

1. Chandrakumar, P. K.; Dhiman, R.; Woodward, C. E.; Iranmanesh, H.; Beves, J. E.; Day, A. I., Tiara[*n*]uril: A Glycoluril-Based Macrocyclic Host with Cationic Walls. *The Journal of Organic Chemistry* **2019,** *84* (7), 3826-3831.
2. Wu, F.; Wu, L.-H.; Xiao, X.; Zhang, Y.-Q.; Xue, S.-F.; Tao, Z.; Day, A. I., Locating the Cyclopentano Cousins of the Cucurbit[*n*]uril Family. *The Journal of Organic Chemistry* **2011,** *77* (1), 606-611.
3. Atthar, A. Novel Equatorially Attached Cucurbit[*n*]uril Forming Gold Nanoparticle Conjugates as Drug Delivery Vehicles. PhD Thesis, University of New South Wales, Canberra, 2018.
4. Lu, W. Exploration of Cucurbit[*n*]uril (Q[*n*]) and Their Derivatives as Potential Linkers in Hydrogels and Metal-organic Frameworks (MOF). PhD Thesis, University of New South Wales, Canberra, 2018.
5. Pierce, M. M.; Raman, C. S.; Nall, B. T., Isothermal Titration Calorimetry of Protein-Protein Interactions. *Methods* **1999,** *19* (2), 213-221.
6. Wu, W.; Cronin, M. P.; Wallace, L.; Day, A. I., An Exploration of Induced Supramolecular Chirality Through Association of Chiral Ammonium Ions and Tartrates with the Achiral Host Cucurbit[7]uril. *Israel Journal of Chemistry* **2018,** *58* (3-4), 479-486.
7. Fielding, L., Determination of Association Constants (K_a) from Solution NMR Data. *Tetrahedron* **2000,** *56*, 6151-6170.

APPENDIX

A1. DCOSY NMR spectrum of $THT_3Tu[3]Cl_2$ (6) in D_2O.

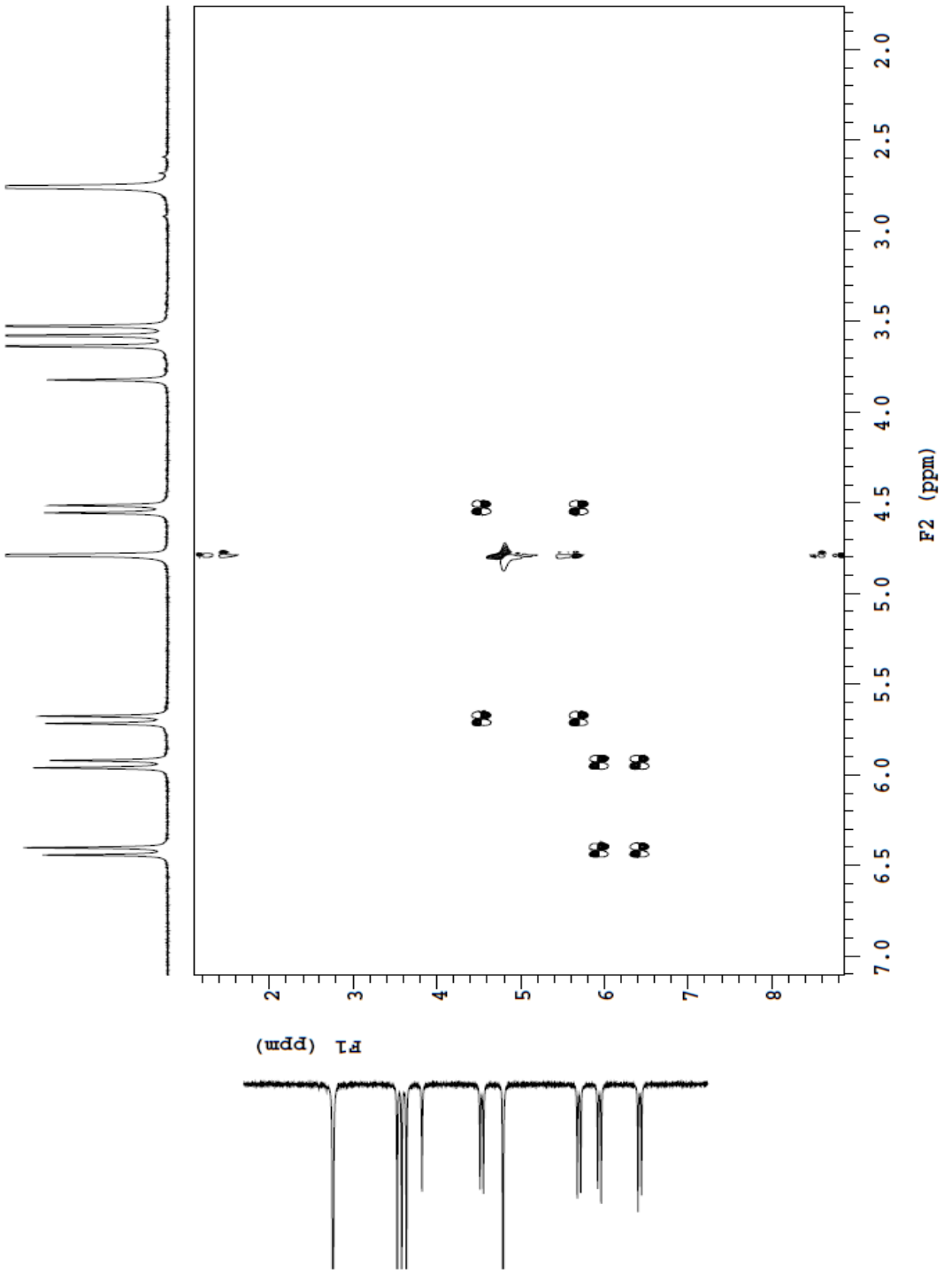

A2. NOESY NMR spectrum of $THT_3Tu[3]Cl_2$ (6) in D_2O.

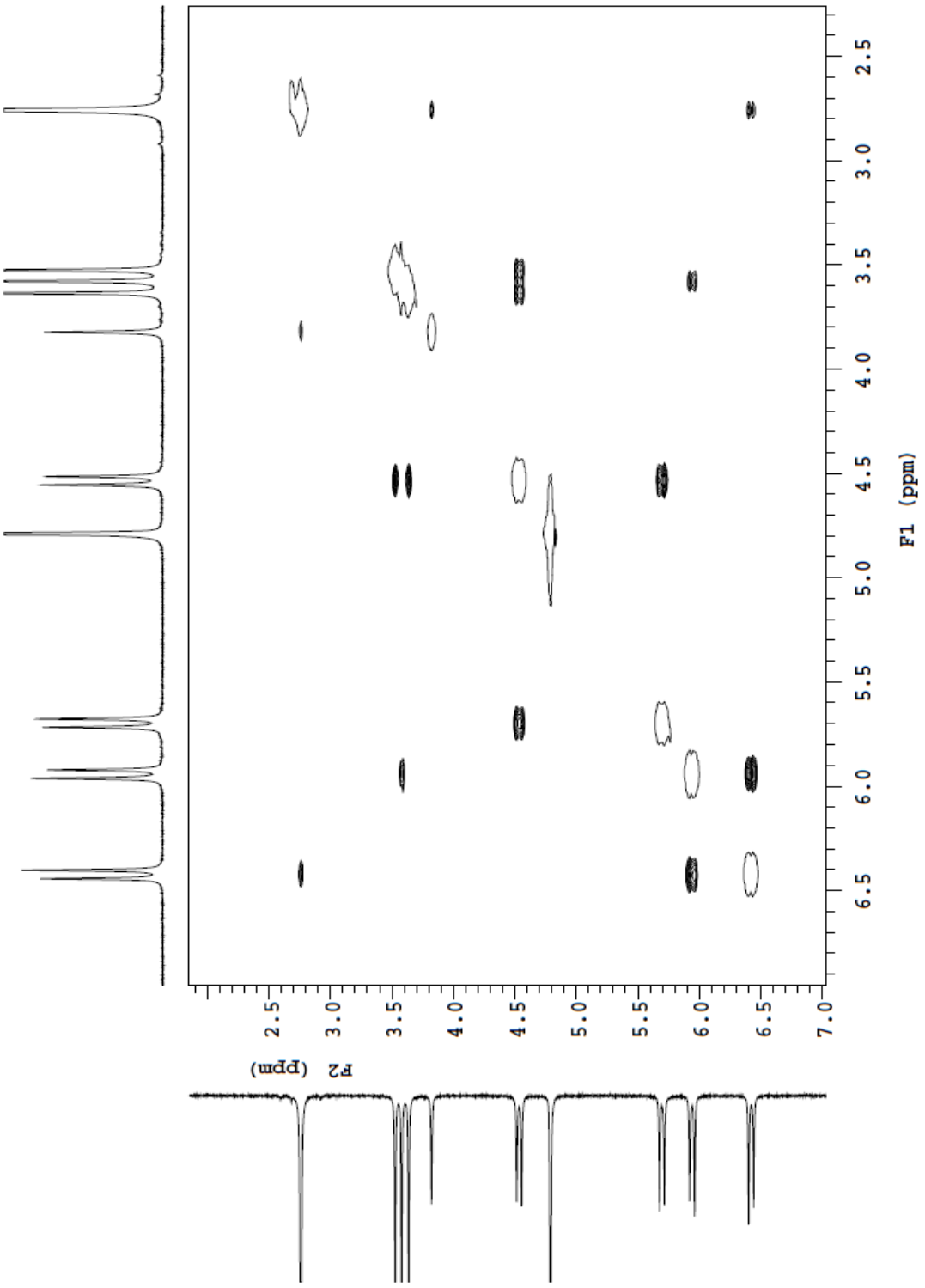

A3. ^{13}C NMR spectra of $THT_3Tu[3]Cl_2$ (6) in D_2O.

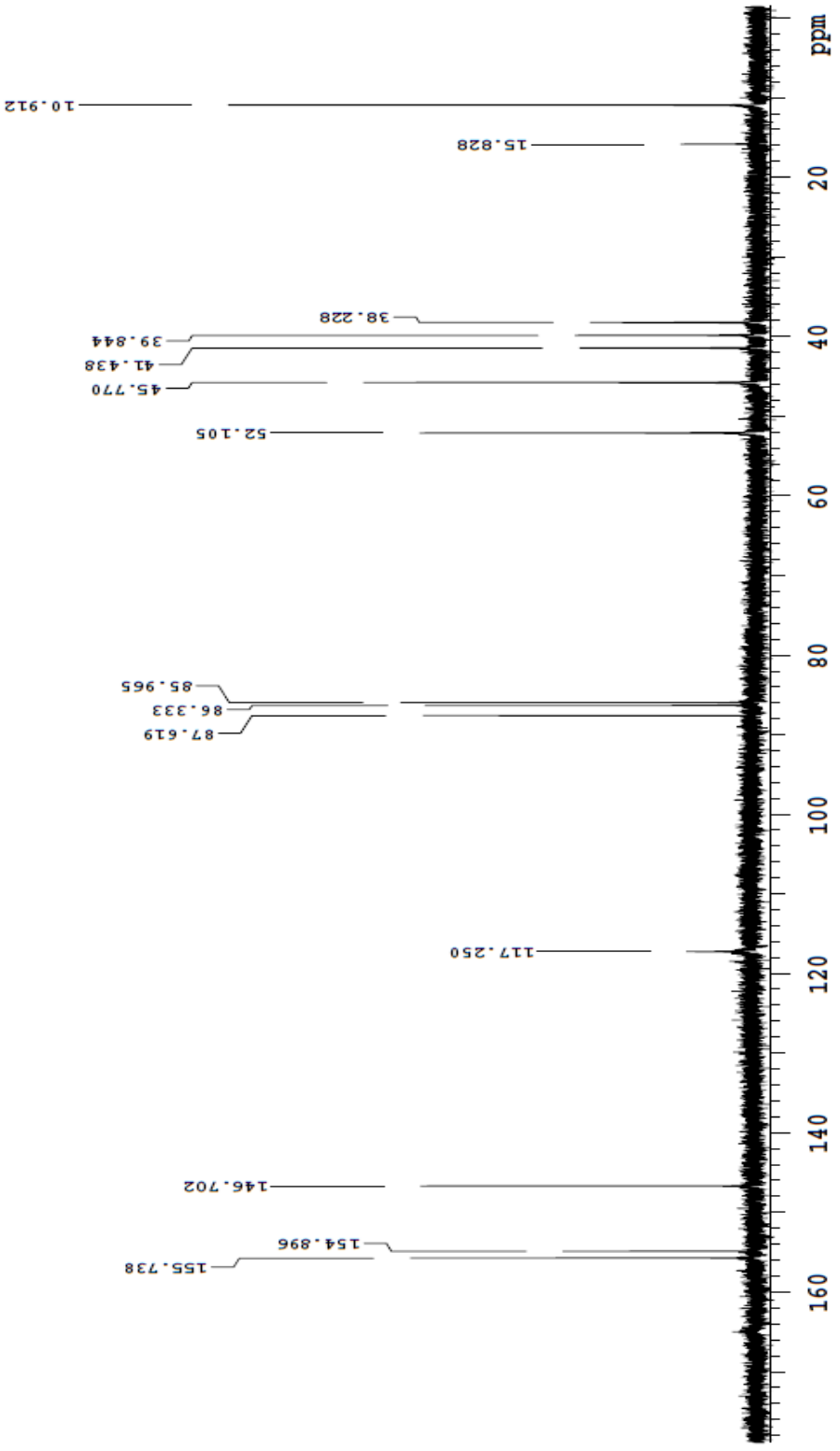

A4. DCOSY NMR spectrum of $THT_4Tu[4]Cl_2$ (7) in D_2O.

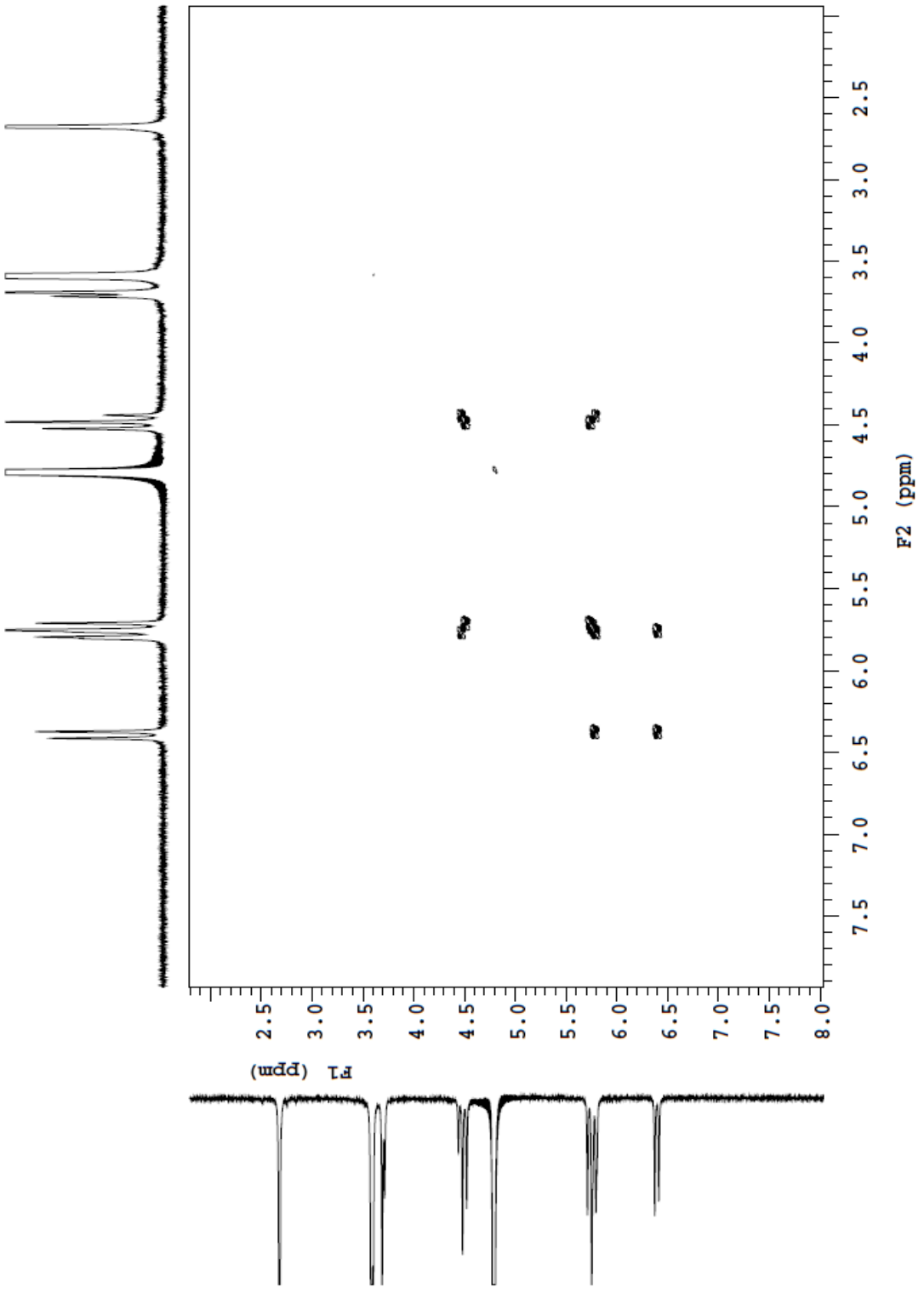

A5. NOESY NMR spectrum of $THT_4Tu[4]Cl_2$ (7) in D_2O.

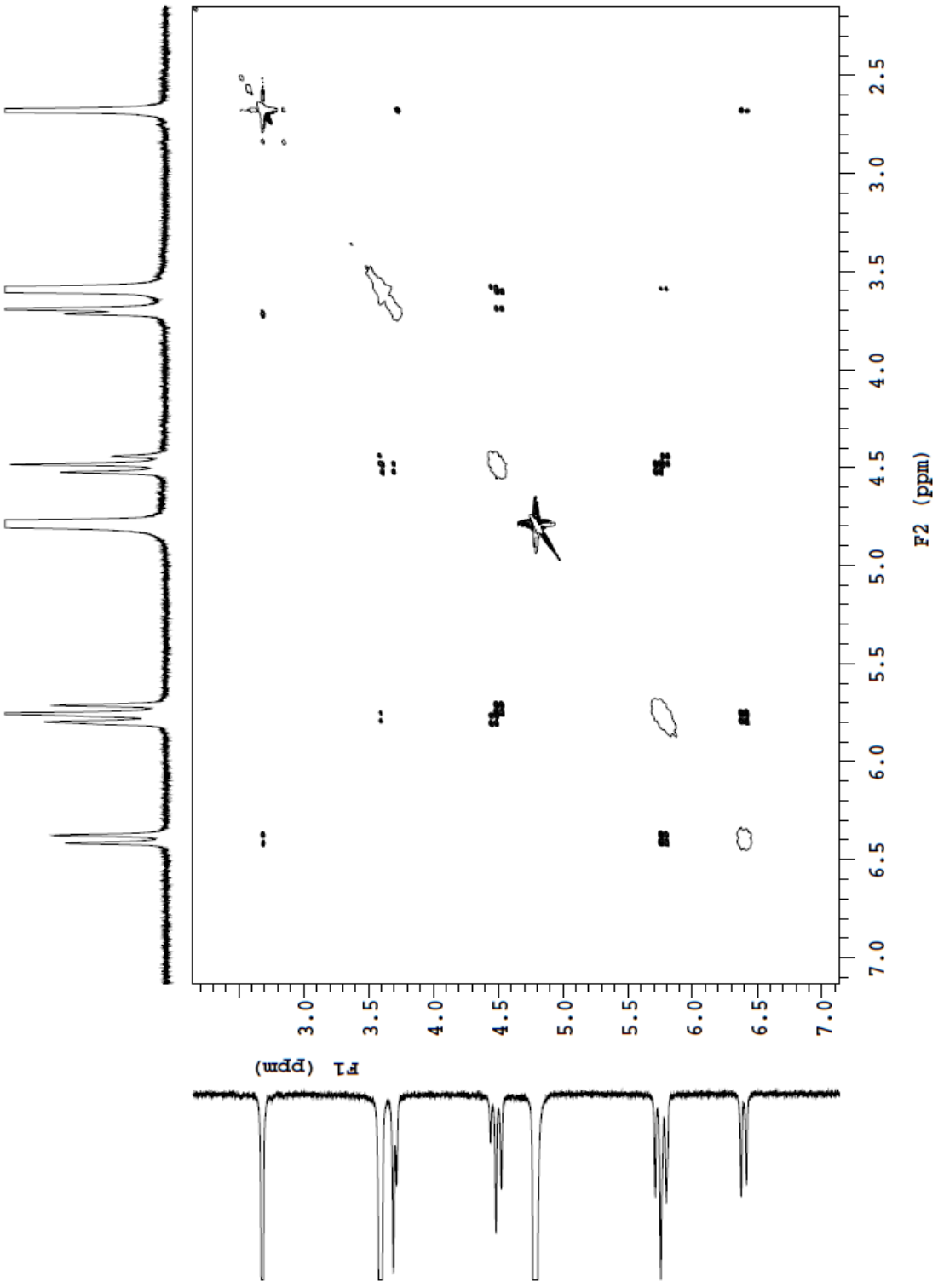

A6. ^{13}C NMR spectra of $THT_4Tu[4]Cl_2$ (7) in D_2O.

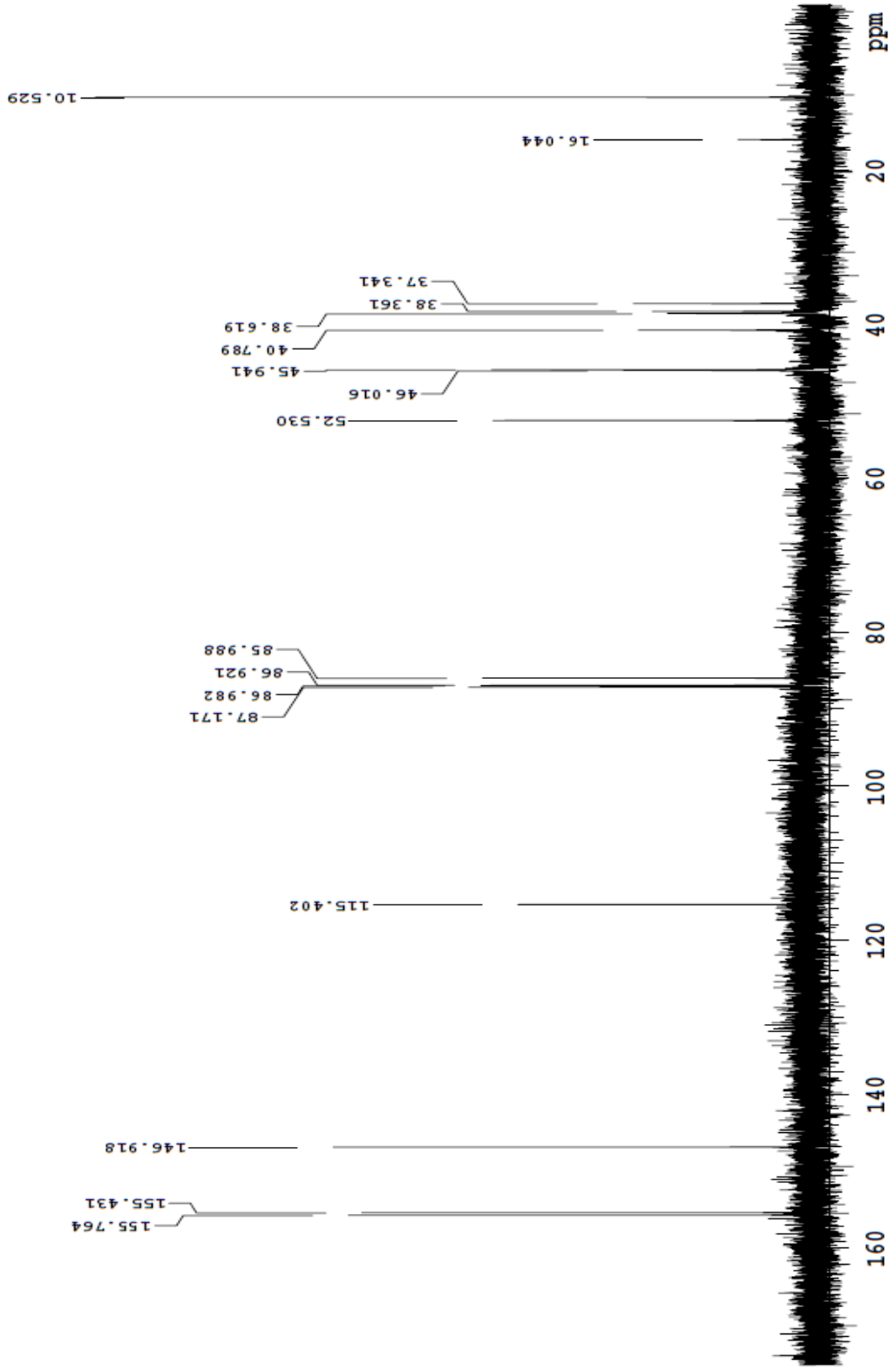

A7. Thermogravimetric analysis of $THT_3Tu[3]Cl_2$ with representation of the mass change and decomposition temperature.

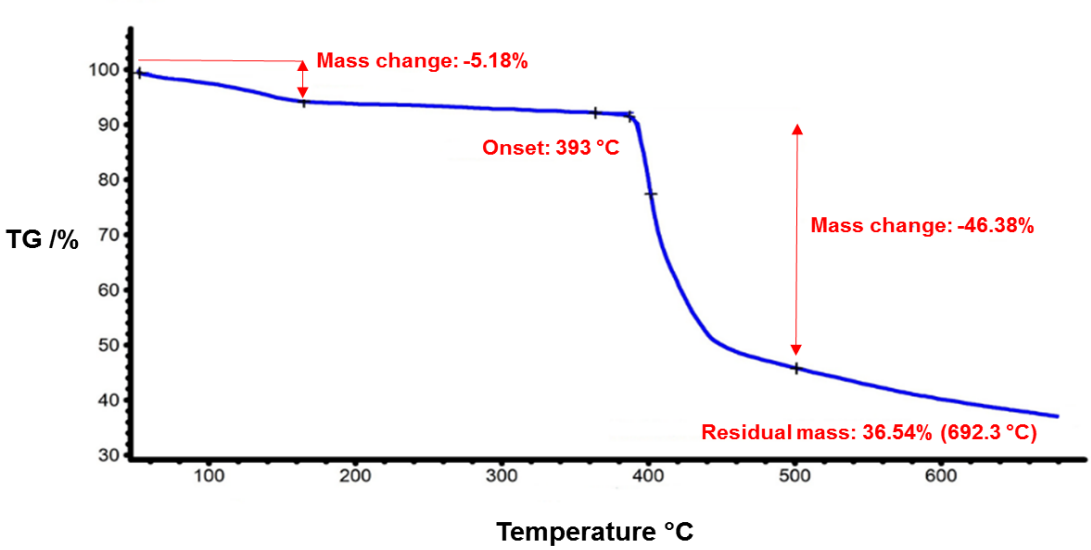

A8. Thermogravimetric analysis of $THT_4Tu[4]Cl_2$ with representation of the mass change and decomposition temperature.

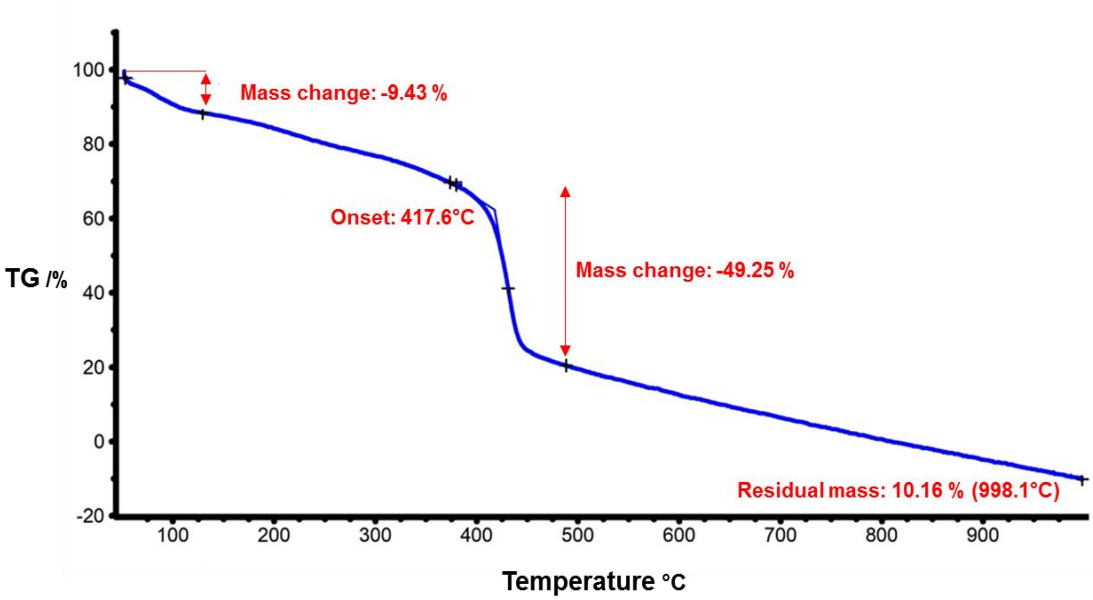

A9. ^{1}H NMR spectrum of crude reaction mixture of THT$_n$Tu[n]$^{2+}$ catalyzed with 12M H_2SO_4.

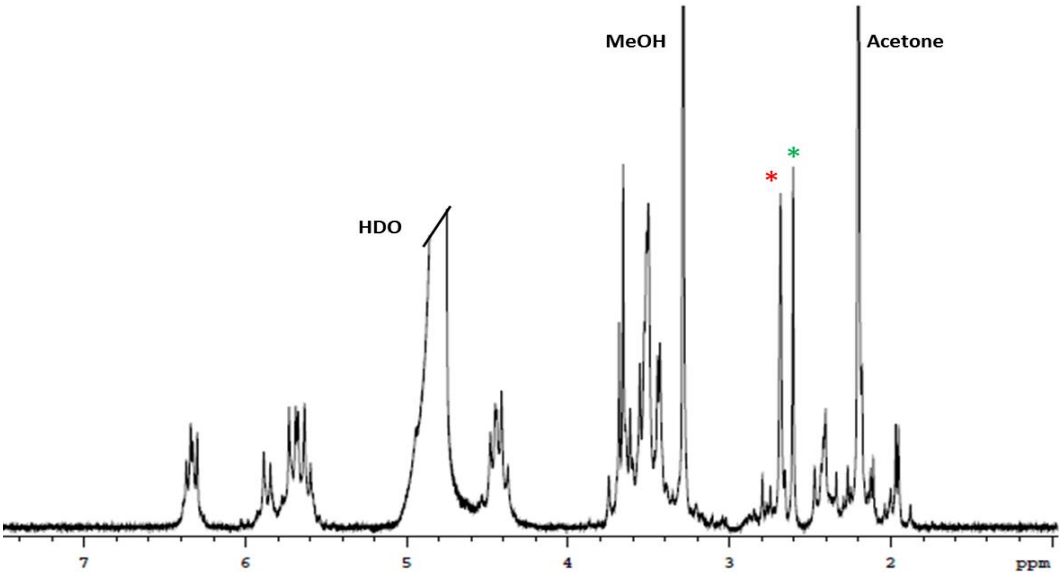

A10. ^{1}H NMR spectrum of crude reaction mixture of THT$_n$Tu[n]$^{2+}$ catalyzed with 12M CH_3SO_3H.

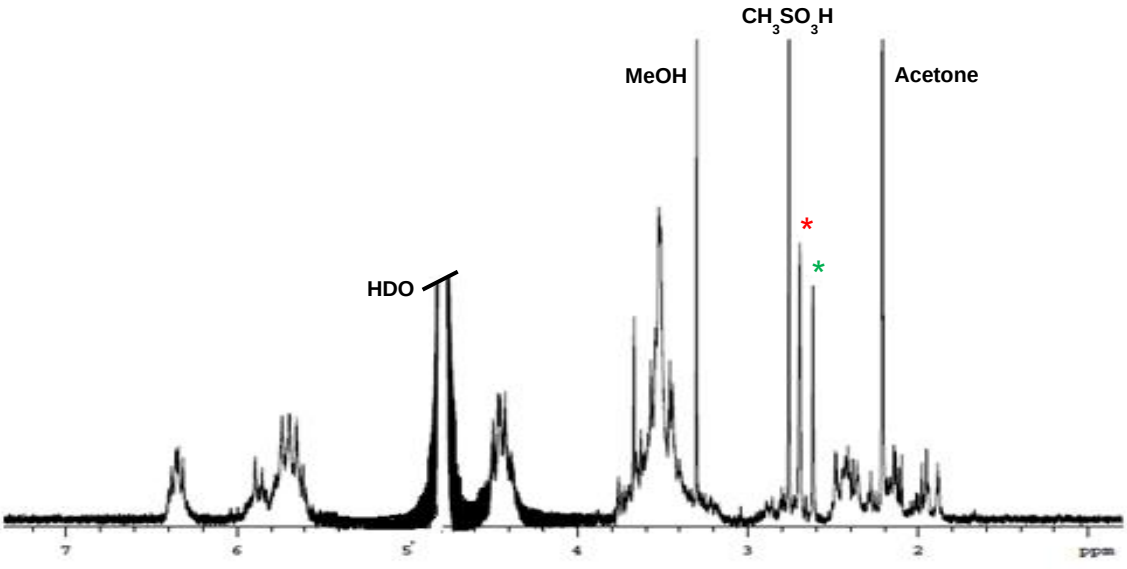

** Represents pyrazolium methyl groups of THT$_3$Tu[3] and THT$_4$Tu[4], respectively.

A11. The change in pH relative to additions of aliquots of aqueous NaOH (1 mM stock solution) titrated into an aqueous solution of $Me_{10}Tu[3]Cl_2$ (0.857 mM).

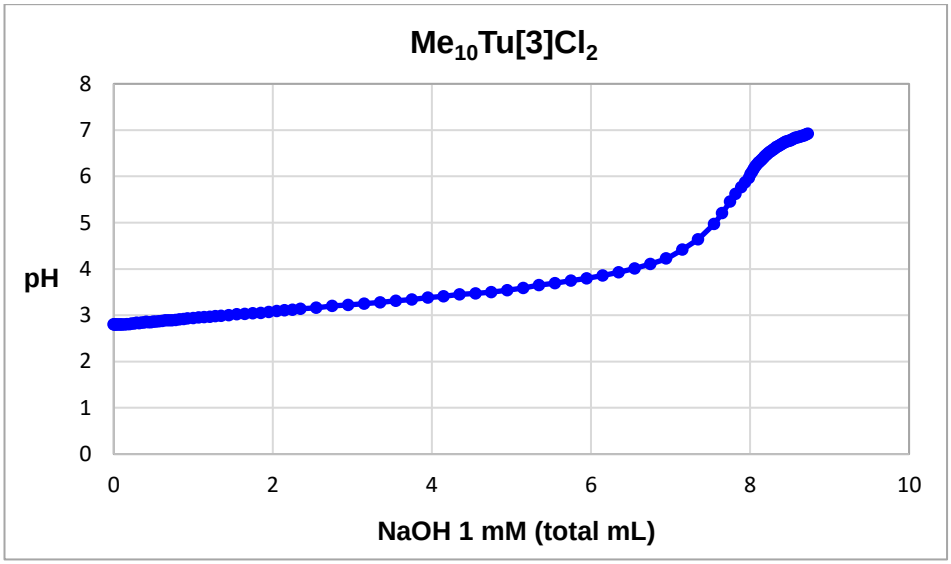

A12. The change in pH relative to additions of aliquots of aqueous NaOH (20 mM stock solution) titrated into an aqueous solution of $Me_{10}Tu[3]Cl_2$ (1mM).

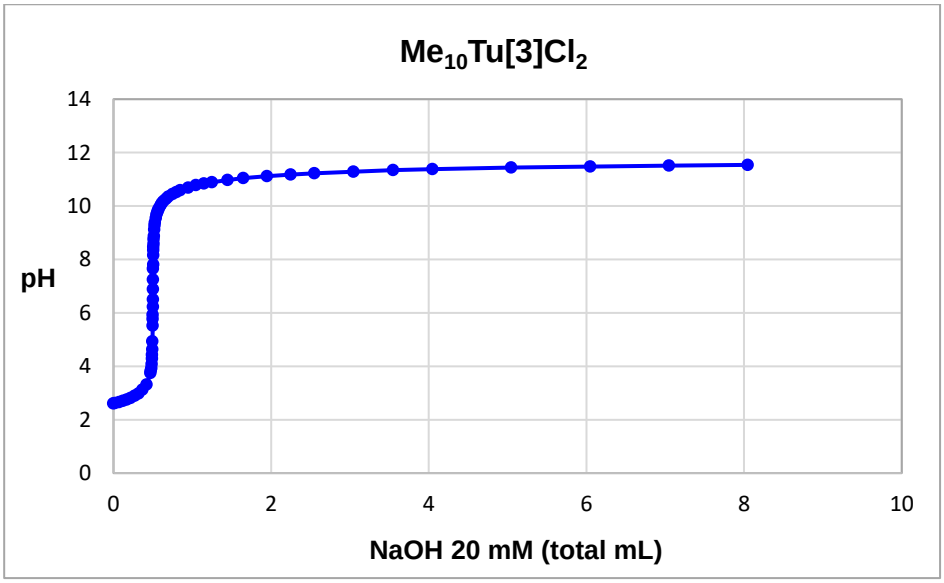

A13. The change in pH relative to additions of aliquots of aqueous NaOH (2 mM stock solution) titrated into an aqueous solution of $THT_3Tu[3]Cl_2$ (1mM).

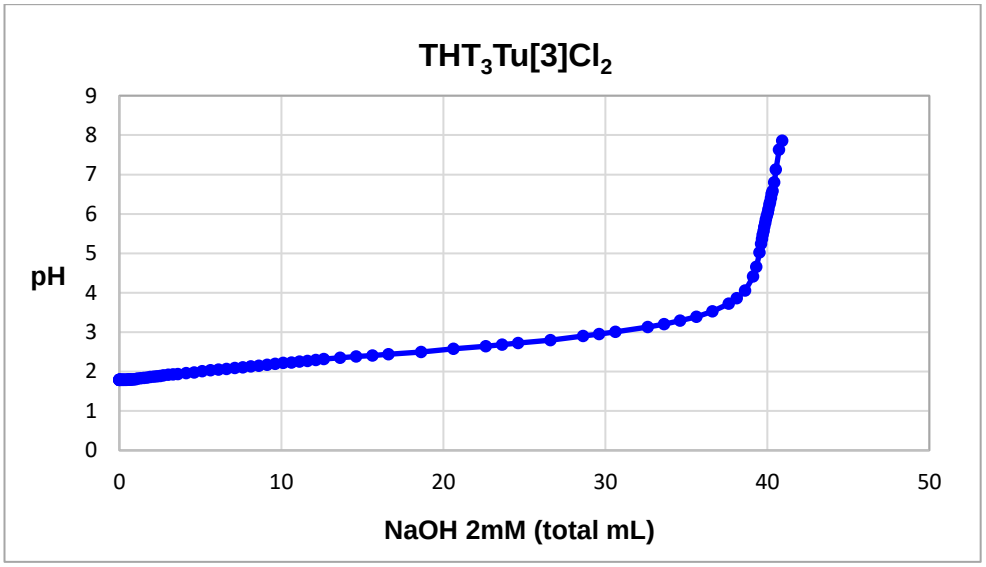

A14. The change in pH relative to additions of aliquots of aqueous NaOH (10 mM stock solution) titrated into an aqueous solution of $THT_3Tu[3]Cl_2$ (1 mM).

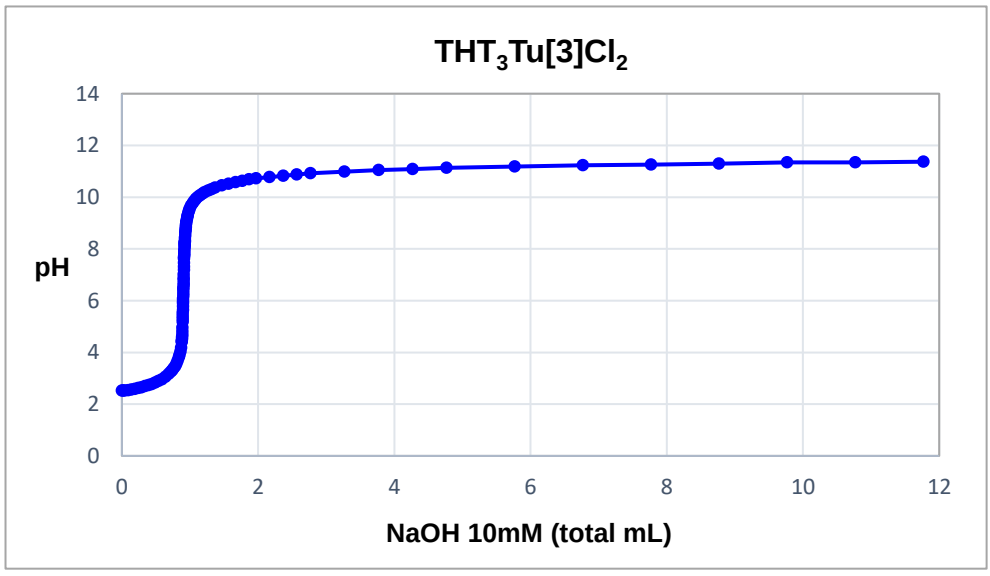

A15. The change in pH relative to additions of aliquots of aqueous NaOH (2 mM stock solution) titrated into an aqueous solution of $THT_4Tu[4]Cl_2$ (1mM).

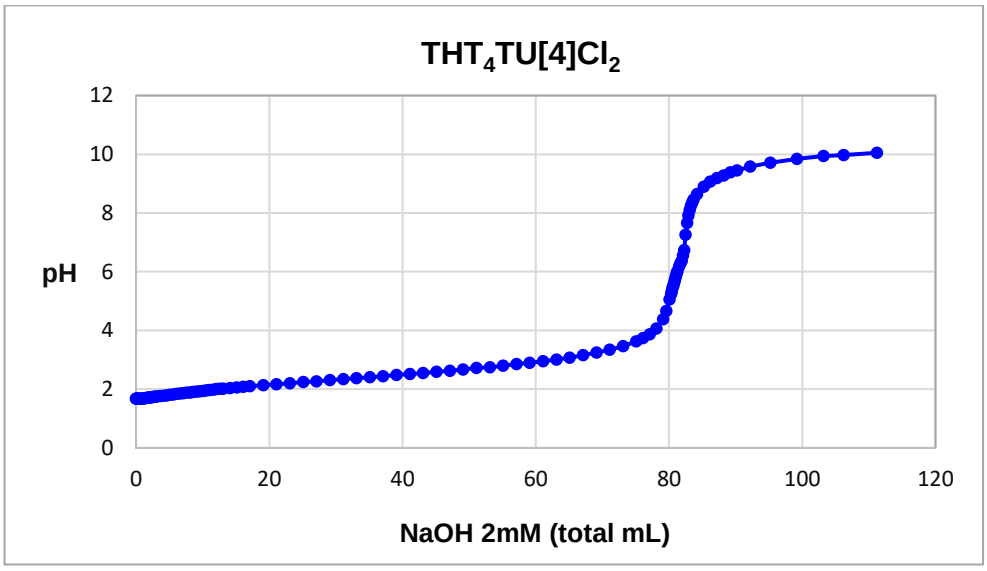

A16. The change in pH relative to additions of aliquots of aqueous NaOH (10 mM stock solution) titrated into an aqueous solution of $THT_4Tu[4]Cl_2$ (1mM).

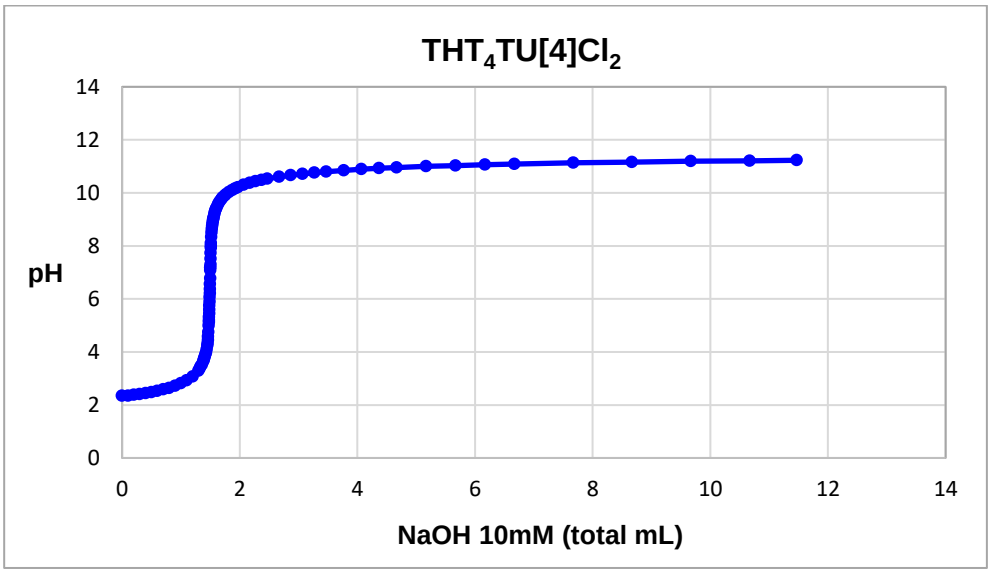

A17. ^{1}H NMR time course of $THT_4Tu[4]Cl_2$ (20 mM) in D_2O after the addition of NaOD/D_2O 0.54 M. The mark (*) indicates the pyrazole methyl resonance.

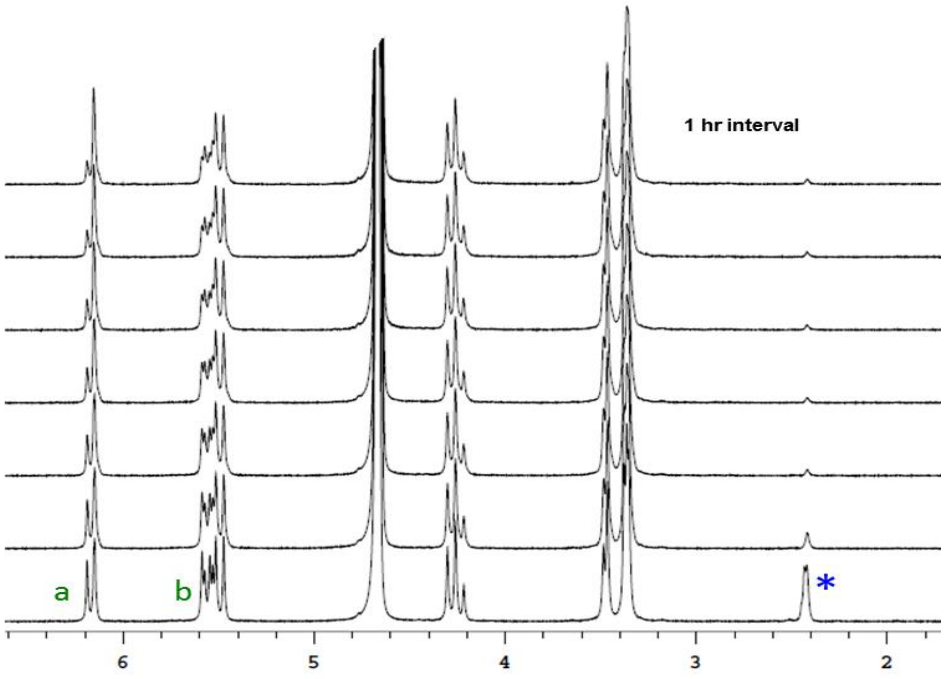

A18. ^{2}H NMR spectrum of crude deuterium exchange product of $THT_3Tu[3]Cl_2$ in H_2O. The mark (*) indicates unknown impurities.

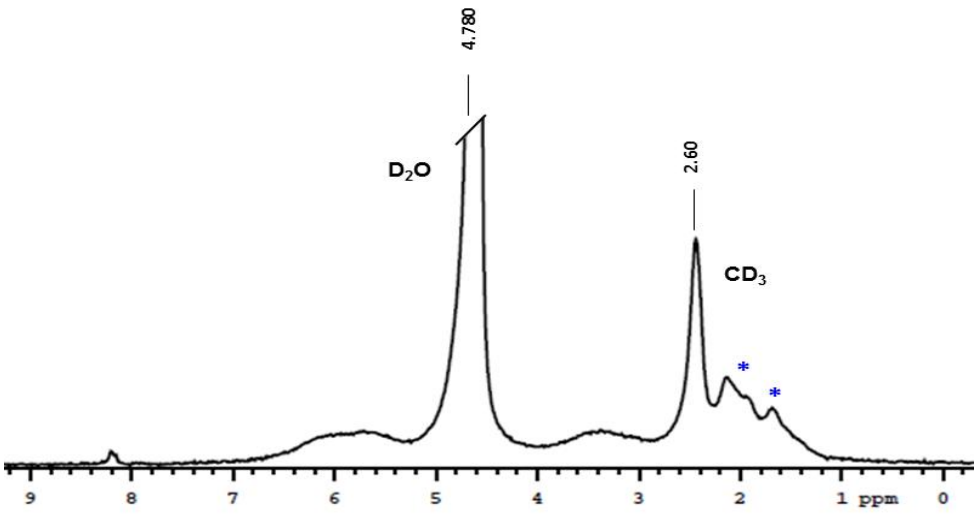

A19. ^{2}H NMR spectrum of crude deuterium exchange product of $THT_4Tu[4]Cl_2$ in H_2O. The mark (*) indicates unknown impurities.

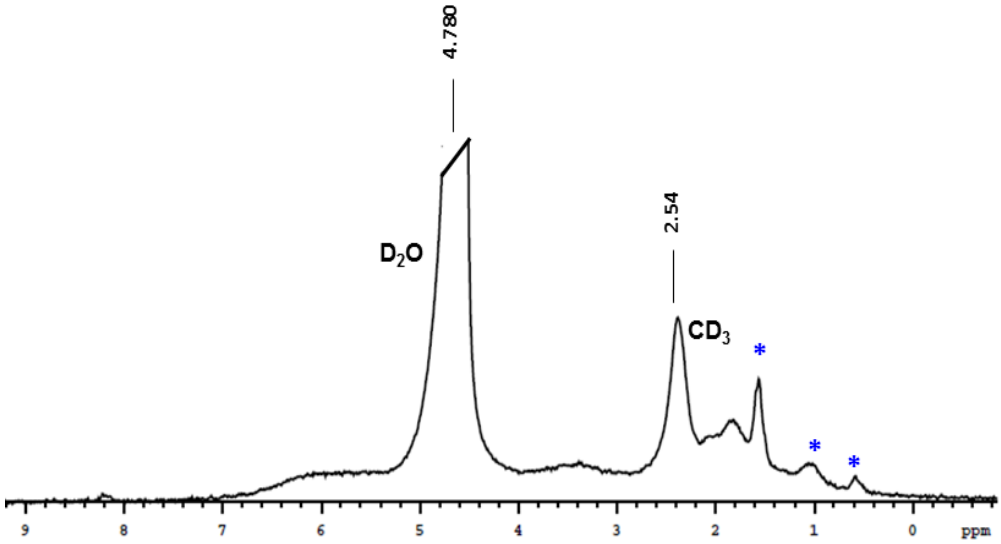

A20. Mass spectrum of $THT_3Tu[3]Cl_2$ showing ($M^{2+}/2$) peaks corresponding to the number of deuterium's exchanged.

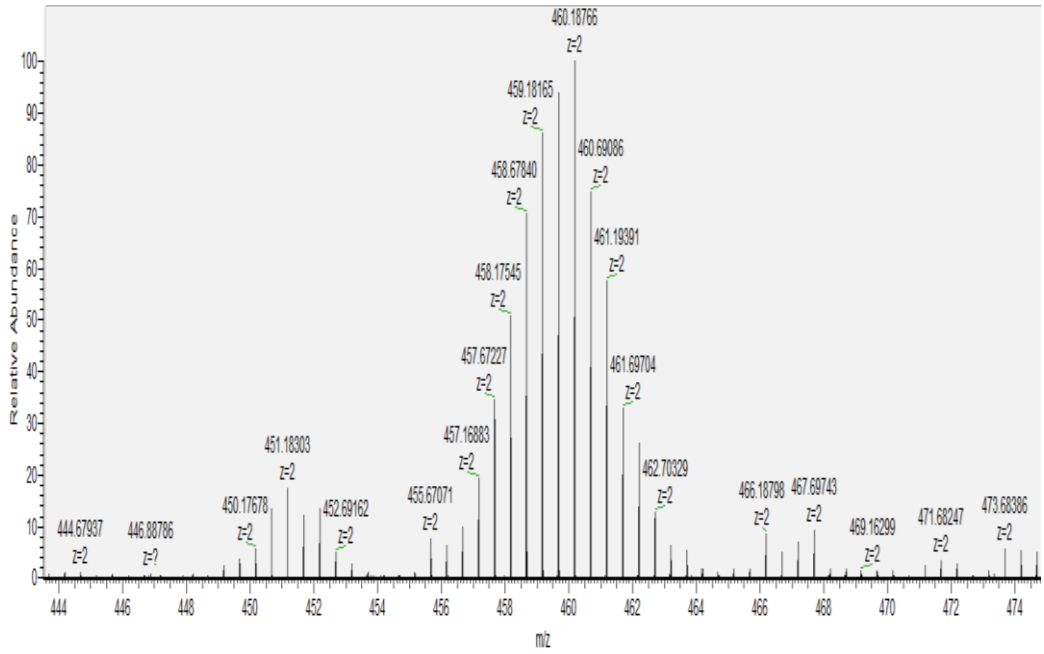

A21. Mass spectrum of $THT_4Tu[4]Cl_2$ showing ($M^{2+/}2$) peaks corresponding to the number of deuterium's exchanged.

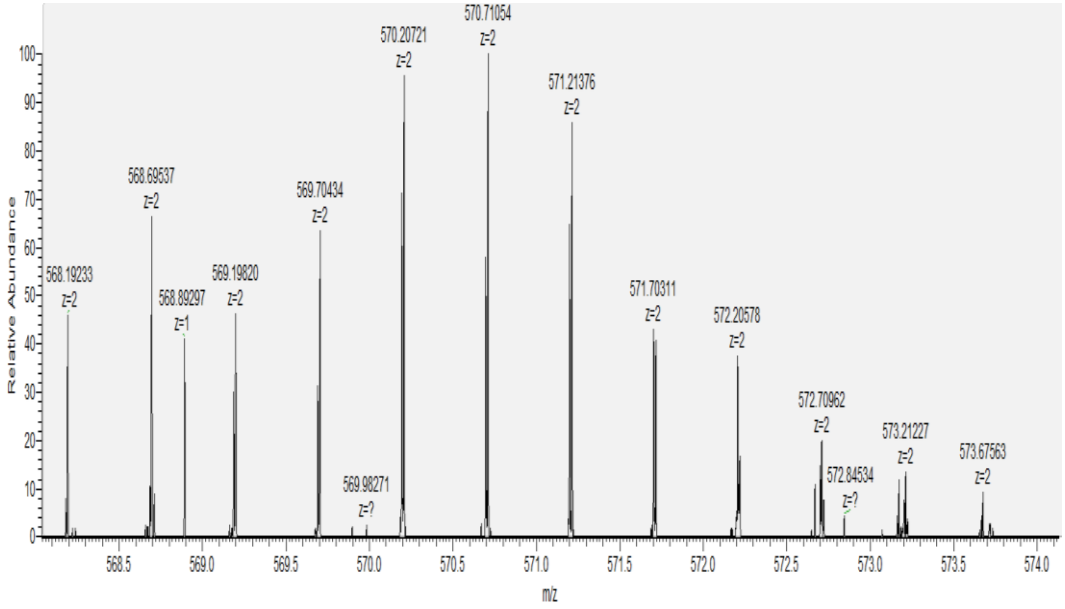

A22a. UV/Vis spectrum of $Me_{10}Tu[3]Cl_{2.}$

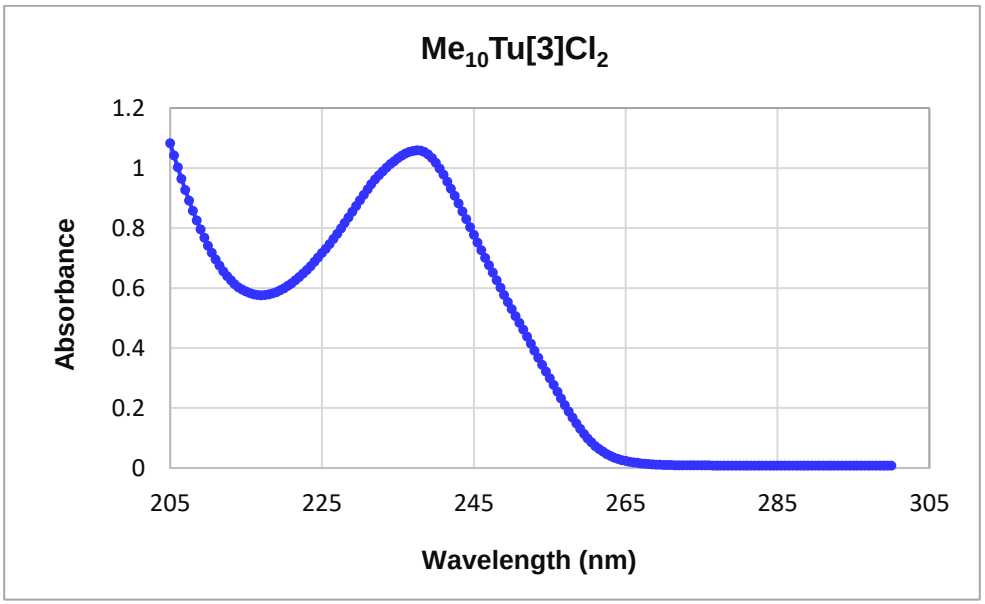

A22b. CD spectrum of 0.5mM of $Me_{10}Tu[3]Cl_2$ with its superimposed uv spectrum.

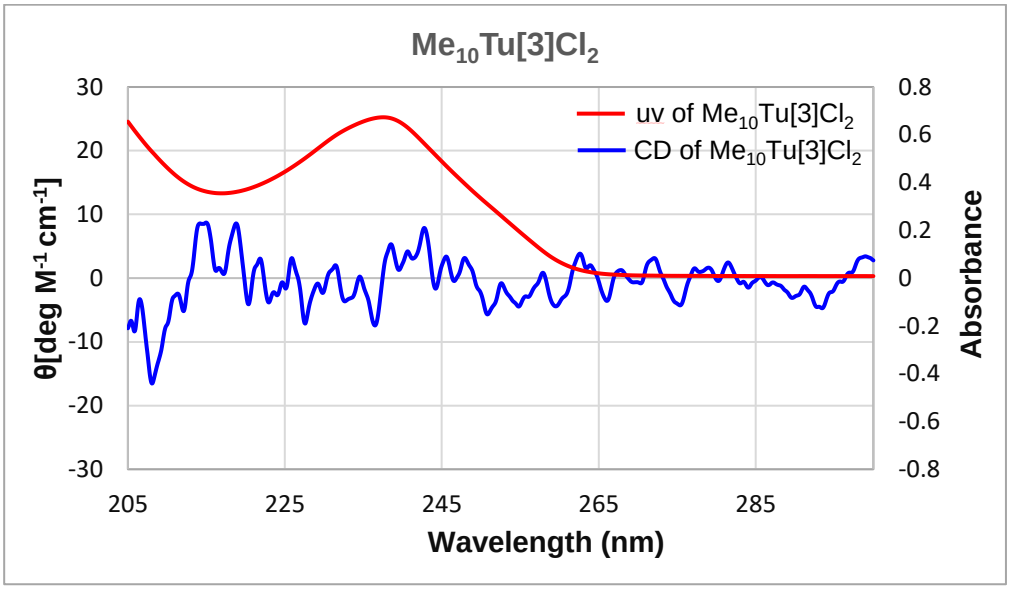

A22c. CD spectrum of 0.5mM of $THT_3Tu[3]Cl_2$ with its superimposed uv spectrum.

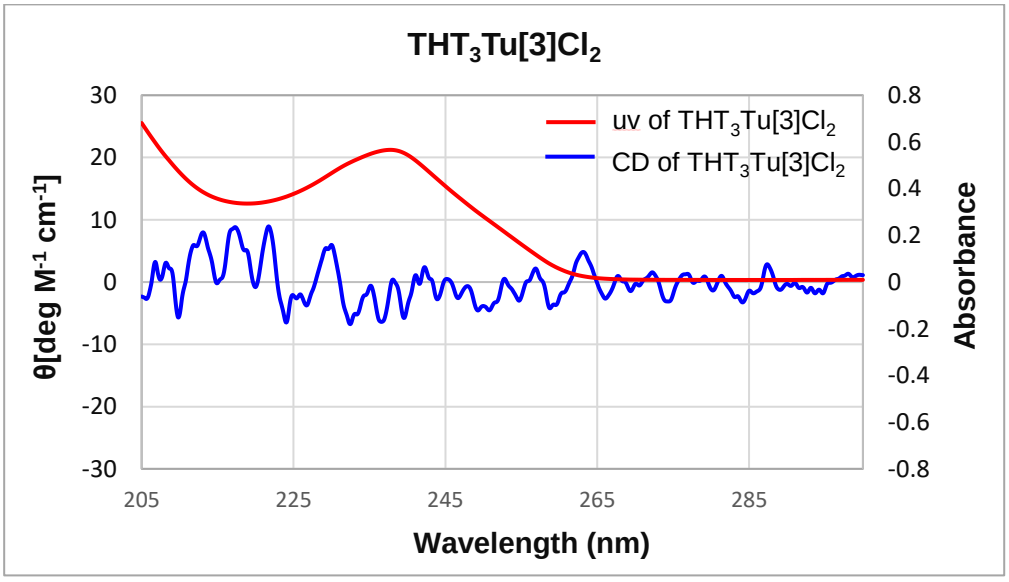

A22d. CD spectrum of 0.5mM of $THT_4Tu[4]Cl_2$ with its superimposed uv spectrum.

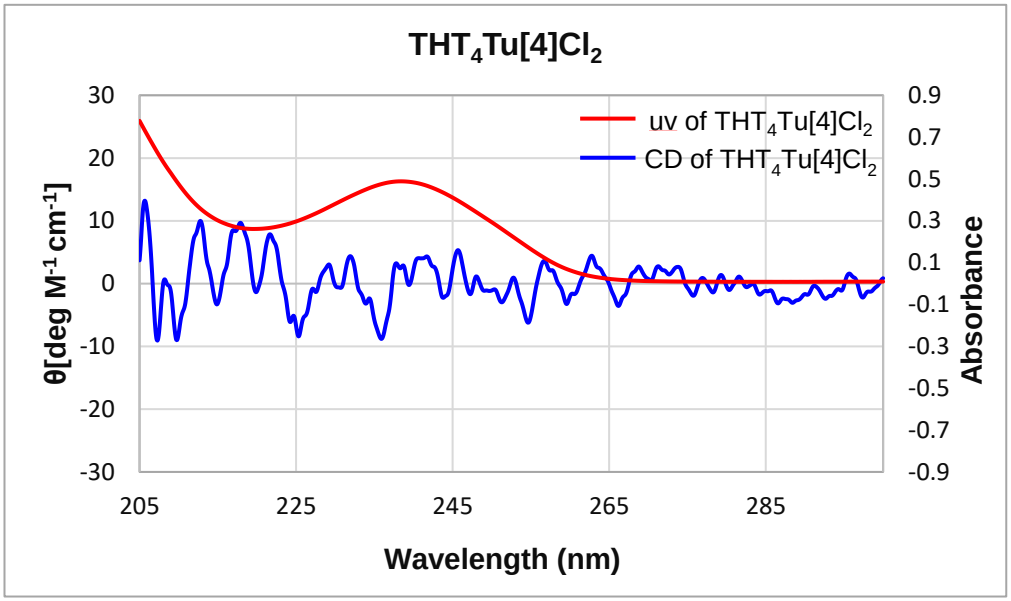

Note: Being achiral in nature, Tu[*n*]'s do not display any CD signals. However, the oscillations observed in the above spectrum are due to noise.

A23. Binding constant measurement for L-glutamine@Me_{10}Tu[3]Cl_2.

Competitive binding model

The binding to the tiara-uril (Tu) with the dye (D) and amino acid (A) is assumed 1:1.

Tu + D = TuD

Tu + A = TuA

We follow the binding of D with the slight enhancement of fluorescence seen upon binding.

Titration of Tu into D

The binding equilibrium for addition of Tu to an initial amount of dye $[D]_0$ (= 4.7×10^{-5}M) can be expressed as

$$\frac{[TuD]}{[Tu][D]} = K_D \quad (1)$$

where [X] = concentration of species X. Normalizing all concentrations with $[D]_0$ the titration experiment consisted of adding aliquots of Tu. At addition (labeled *i*), we denote the initial total normalized Tu concentration to be $R_i = [Tu]_i/[D]_0$. At equilibrium we have

$$\frac{x_i}{(R_i - x_i)(1 - x_i)} = K_D' \quad (2)$$

where we have defined $x_i = [TuD]/[D]_0$ is the normalized equilibrium concentration of the Tu complex after addition at step *i* and $K_D' = K_D[D]_0$. The observed fluorescence intensity at step *i* is assumed linear in concentrations of the fluorescing species and can be written as,

$$F_i = F_0 f_b x_i + F_0(1 - x_i) \quad (3)$$

where F_0 is the fluorescence of the initial dye concentration (before Tu addition). This can be re-expressed as,

$$F_i/F_0 = 1 + \delta f_b x_i \quad (4)$$

with $\delta f_b = f_b - 1$. Eq. (2) is a simple quadratic which can be solved for x_i, once a particular value for K_d' is chosen. The resulting best prediction for the fluorescence, using Eq. (4) was then obtained, by fitting δf_b using least squares. This is easily obtained as,

$$\delta f_b{}^{best}(K_D') = \sum_{i=1}^{Nt} \left(\frac{F_i}{F_0} - 1\right)_{obs} x_i(K_D') \,/\, \sum_{i=1}^{Nt} x_i(K_D')^2 \quad (5)$$

where $(X)_{obs}$ is the experimentally observed quantity X, N_t is the number of titration points and we have explicitly denoted the dependence of the relevant quantities on the chosen value for K_D. The best fit for was then obtained by minimizing the residual Ώ (K_D '),

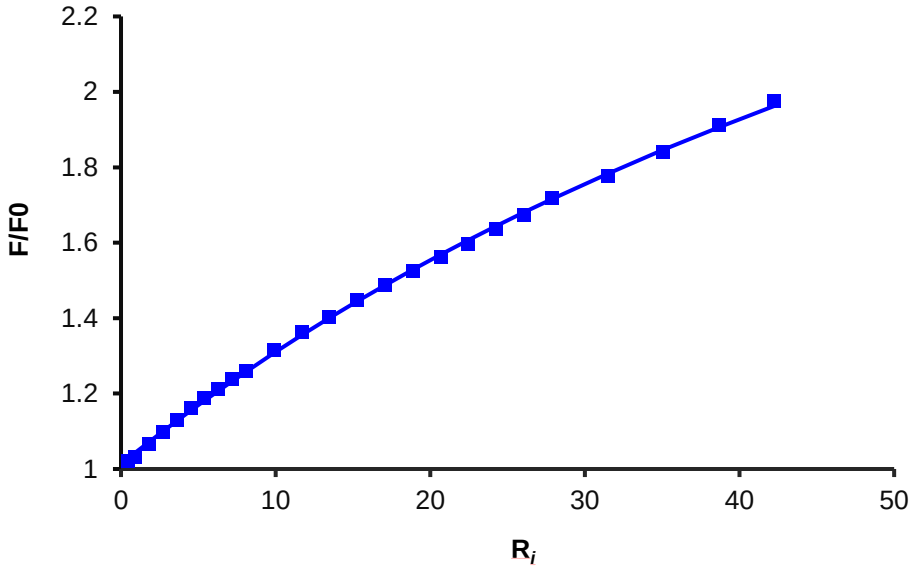

Figure A 20a. Plot of F/F_0 vs R. Points are experiments and the line is the best fit to the data using the model.

$\Omega(K_D') = \sum_{i=1}^{Nt}\left[\left(\frac{F_i}{F_0}-1\right)_{obs} - \delta f_b^{\ best}(K_D')x_i(K_D')\right]^2$ with respect to K_D'.

In Figure A 20a we show the resulting fit to F/F_0 *vs* R_i. The fitted parameters were: K_D' = 1.13 x 10^{-2} (K_D = 2.4 x 10^2) and $\delta f_b^{\ best}$ = 3.91.

Competitive Binding titrations

At the point $R = R_c$, a sample of the above Tu/D mixture was then titrated with the amino acid (A). The species A competed with D in binding to the Tu. The new equilibrium equations in this system were expressed as

$$\frac{x}{(R_c-x-y)(1-x)} = K_D' \quad (7)$$

and

$$\frac{y}{(R_c-x-y)(A-y)} = K_A \quad (8)$$

where we have introduced the new quantities $y = [TuA]/[D]_0$, $A = [A]_{add}/[D]_0$ and $K_A' = K_A[D]_0$. Observation of the change in fluorescence ΔF as a function of A shows a linear variation, i.e,

$$\Delta F/F_0 = \lambda A \quad (9)$$

where $\Delta F = F - F_c$, with F the measured fluorescence intensity and F_c the fluorescence intensity with no added A. The quantity F_0 was defined earlier. The slope λ is a function of the binding constant K_A'. Assuming a linear dependence for the equilibrium concentrations of the present species, we adopt the following functional forms for the equilibrium quantities,

$$x = x_c + \alpha A \quad (10a)$$

$$y = \beta A \tag{10b}$$

where x_c is the equilibrium concentration of TuA before addition of A. That is,

$$\frac{x_c}{(R_c - x_c)(1 - x_c)} = K_D' \tag{11}$$

Substituting Eq. (10b) into Eq. (8) and keeping only linear terms in A, we obtain,

$$\beta = \frac{K_A'}{(R_c - x_c)^{-1} + K_A'} \tag{12}$$

Similarly substituting Eq. (10a) into Eq. (7) and using Eq.s (11) and (12) finally gives the result,

$$\alpha = -\frac{K_A'}{(1 + K_A'(R_c - x_c)k} \tag{13}$$

with

$$k = \left(\frac{1}{x_c} + \frac{1}{1 - x_c} + \frac{1}{R_c - x_c}\right) \tag{14}$$

Using Eq. (4) for the fluorescence intensity, we obtain,

$$\Delta F / F_0 = 1 + \alpha \delta {f_b}^{best} A \tag{15}$$

In terms of the slope λ in Eq. (9) we obtain,

$$K_A' = -\frac{k\lambda}{\delta {f_b}^{best} + k\lambda(R_c - x_c)} \tag{16}$$

We chose the value $R_c = 20.7$, with $x_c = 0.19$. The graph of $\Delta F/F_0$ vs A in Figure A 20b, gave a slope of $\lambda = -3.1 \times 10^{-3}$. Using Eq. (16), we obtain $K_A' \approx 4.6 \times 10^{-3}$ ($K_a \sim 2.2 \times 10^2$ M^{-1})

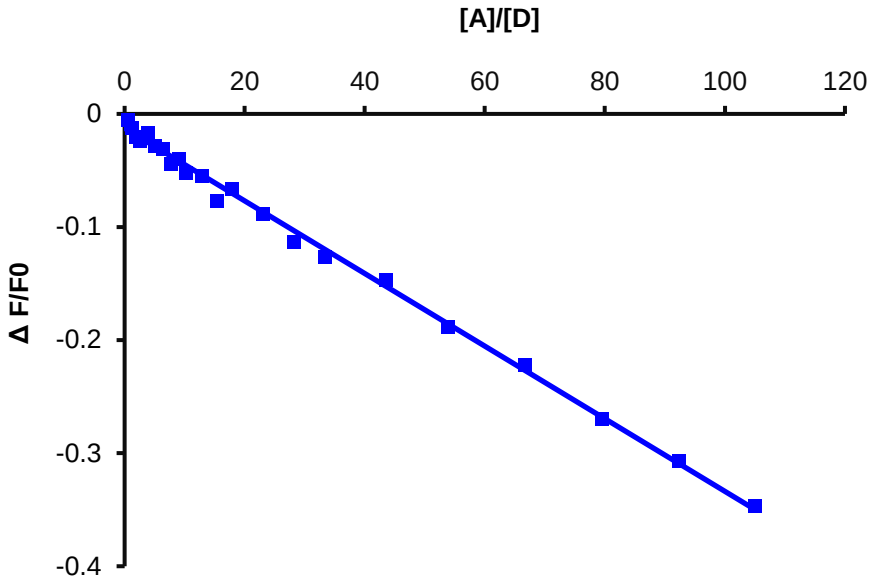

Figure A 20b. Plot of $\Delta F/F_0$ vs A. Points are experiments and the line is the best fit to the data using a linear model.

The binding model was constructed and performed by Woodward C. E., School of Science. UNSW Canberra.

A24. UV/Vis absorption spectra of (a) Indomethacin (b) Mefenamic acid (c) Probenecid (d) Furosemide and (e) Griseofulvin on addition of three different concentrations of $Me_{10}Tu[3]Cl_2$, all dissolved in citric acid buffer (20 mM, pH 3.5).

(a)

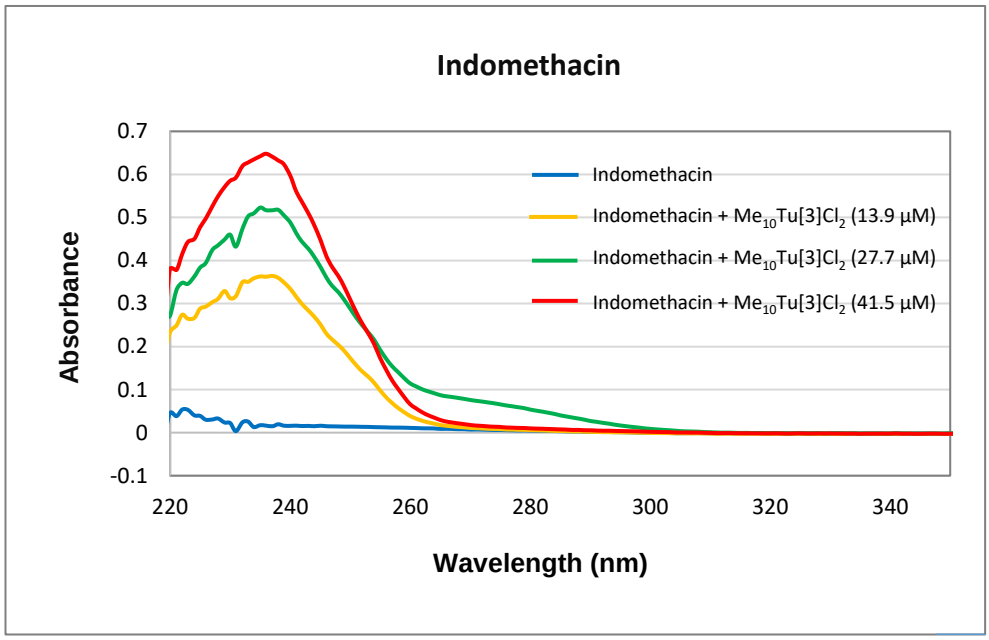

(b)

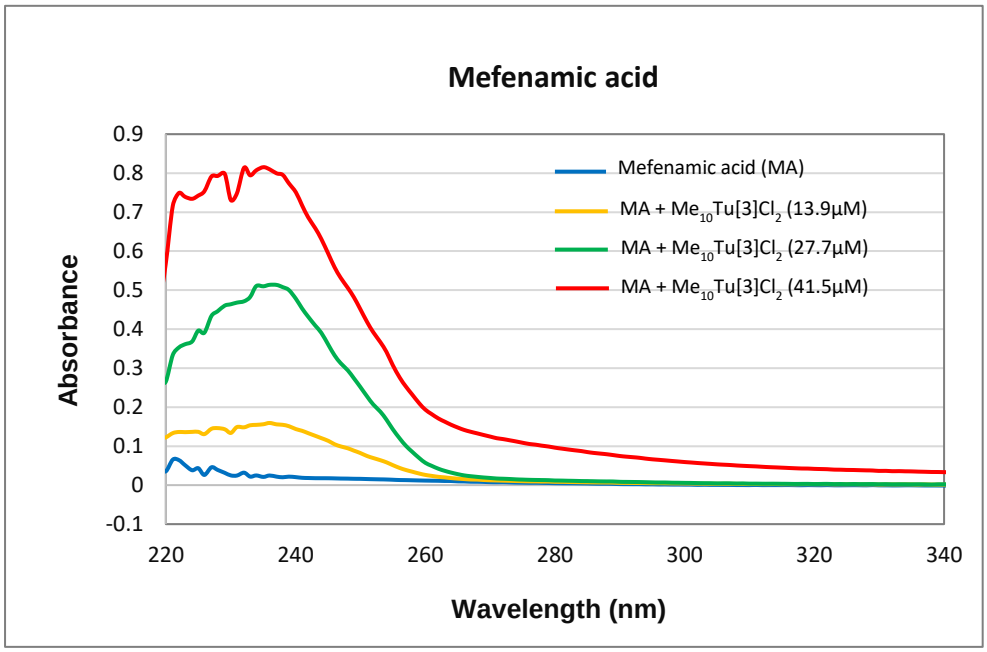

(c)

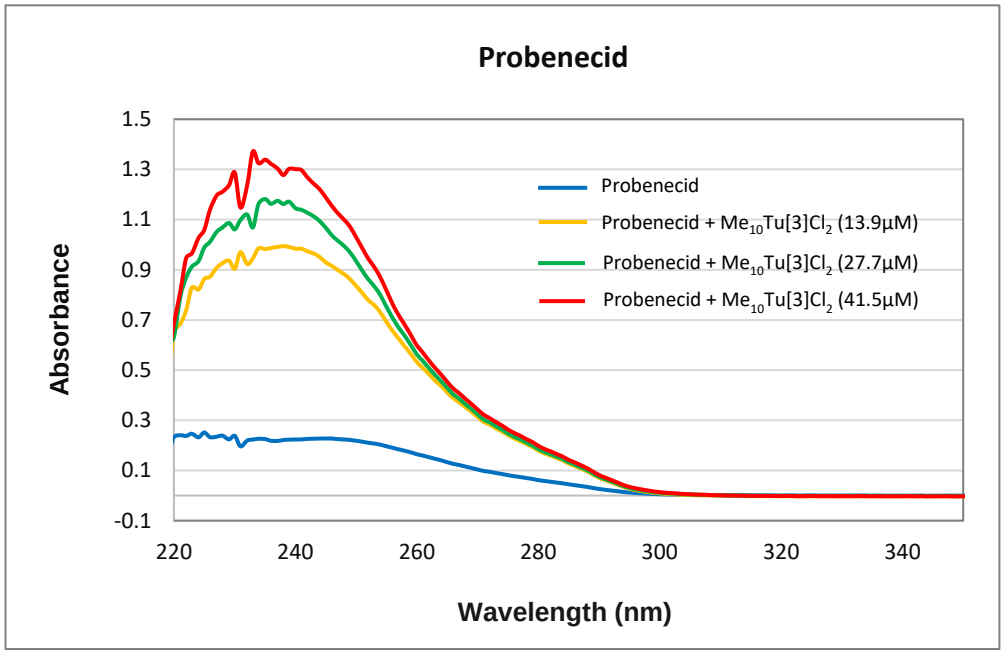
Probenecid
Absorbance
1.5
1.3
1.1
0.9
0.7
0.5
0.3
0.1
-0.1
220
240
260
280
300
320
340
Wavelength (nm)
Probenecid
Probenecid + Me10Tu[3]Cl2 (13.9µM)
Probenecid + Me10Tu[3]Cl2 (27.7µM)
Probenecid + Me10Tu[3]Cl2 (41.5µM)

(d)

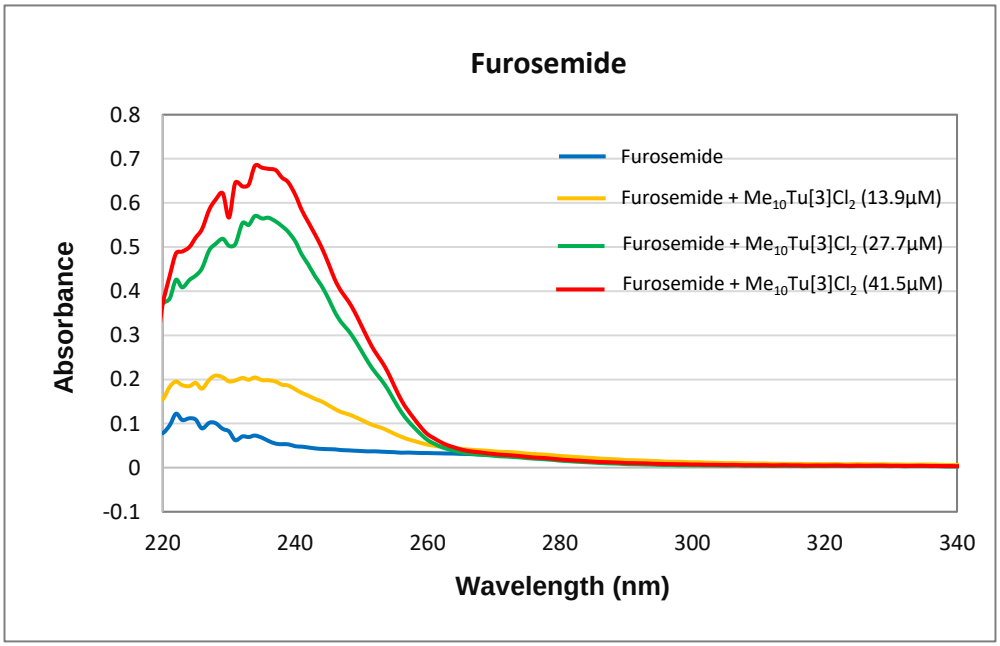
Furosemide
Absorbance
0.8
0.7
0.6
0.5
0.4
0.3
0.2
0.1
0
-0.1
220
240
260
280
300
320
340
Wavelength (nm)
Furosemide
Furosemide + Me10Tu[3]Cl2 (13.9µM)
Furosemide + Me10Tu[3]Cl2 (27.7µM)
Furosemide + Me10Tu[3]Cl2 (41.5µM)

(e)

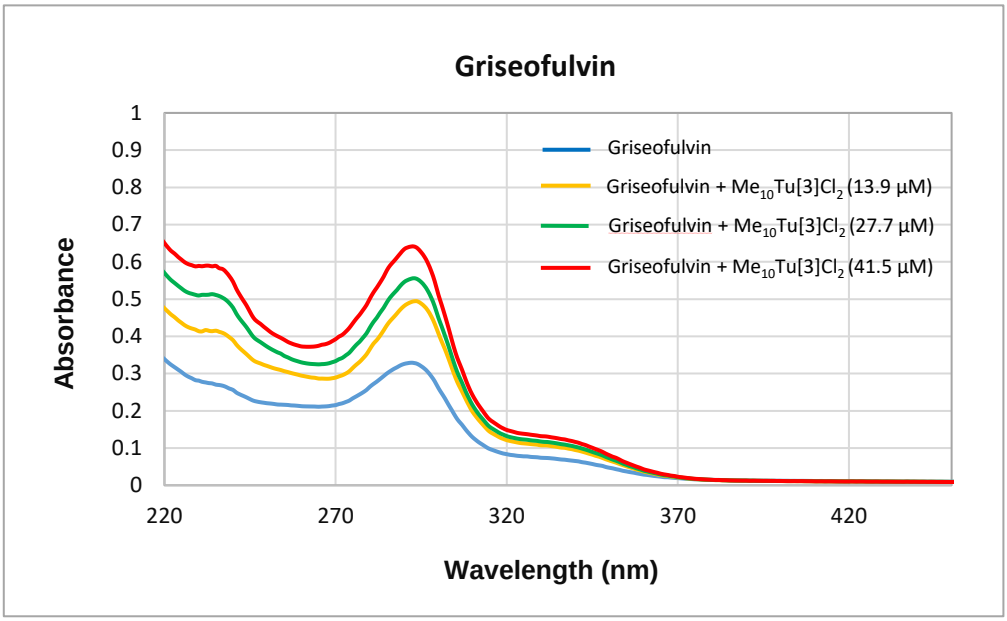

A25. The fold change in the absorbance of drugs with three different concentrations of $Me_{10}Tu[3]Cl_2$, all dissolved in citric acid buffer (20 mM, pH 3.5). The values were calculated at λ = 237 nm, except for griseofulvin (λ = 293 nm).

Drugs	**$Me_{10}Tu[3]Cl_2$** (13.9 µM)	**$Me_{10}Tu[3]Cl_2$** (27.7 µM)	**$Me_{10}Tu[3]Cl_2$** (41.5µM)
Indomethacin	13.0 ↑	12.5 ↑	9.0 ↑
Mefenamic acid	1.63 ↓	8.4 ↑	13.5 ↑
Probenecid	3.8 ↑	3.9 ↑	3.7 ↑
Furosemide	2.1 ↓	4.2 ↑	3.1 ↑
Griseofulvin	1.5 ↑	1.7 ↑	1.95 ↑

The up and down arrows represent the increase and decrease in the absorbance, respectively

A26. UV/Vis absorption spectra of (a) Indomethacin (b) Probenecid (c) Furosemide (d) Mefenamic acid and (e) Griseofulvin on addition of three different concentrations of $Me_{10}Tu[3]Cl_2$, all dissolved in PBS buffer (20 mM, pH 7.4).

(a)

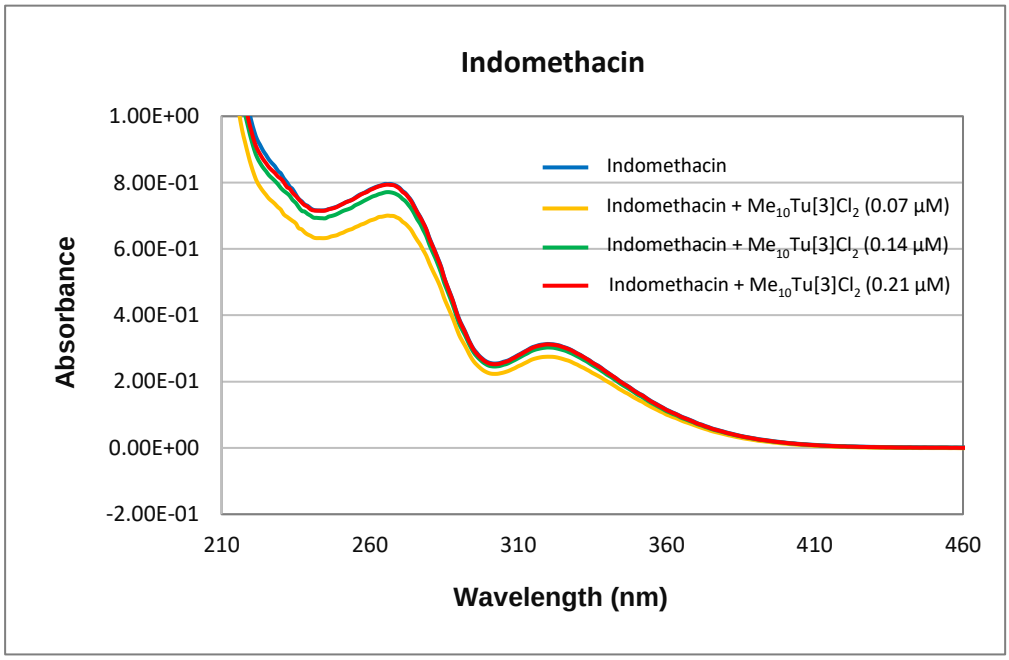

(b)

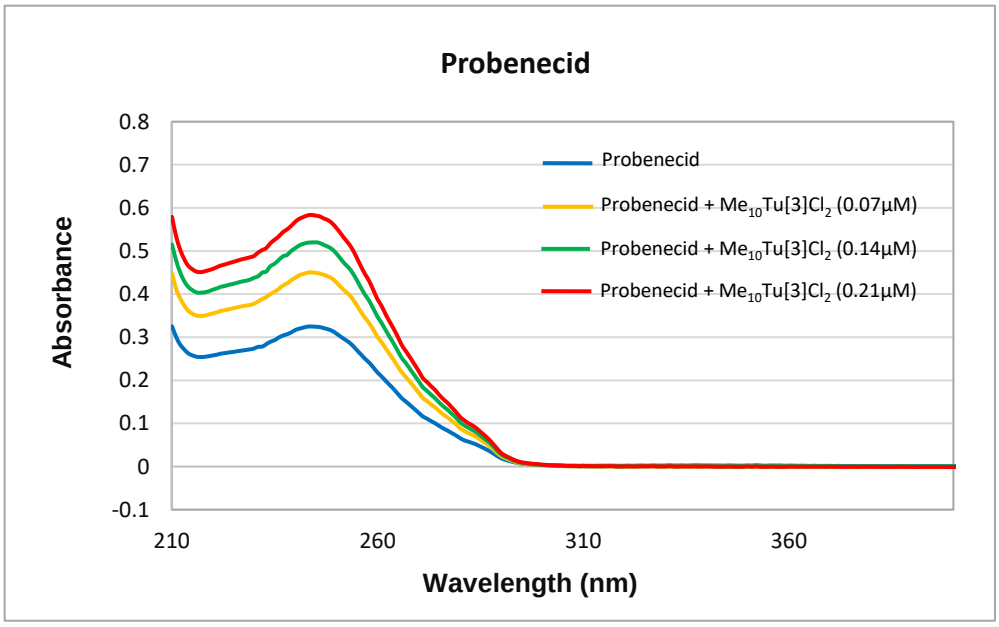

(c)

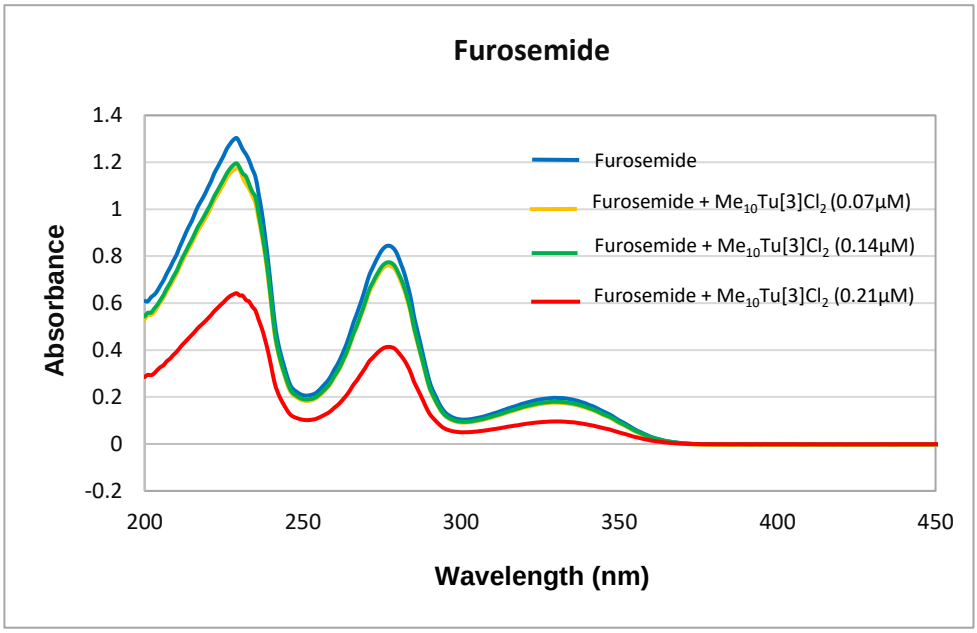
Furosemide
Absorbance
Wavelength (nm)
Furosemide
Furosemide + Me10Tu[3]Cl2 (0.07µM)
Furosemide + Me10Tu[3]Cl2 (0.14µM)
Furosemide + Me10Tu[3]Cl2 (0.21µM)
1.4
1.2
1
0.8
0.6
0.4
0.2
0
-0.2
200
250
300
350
400
450

(d)

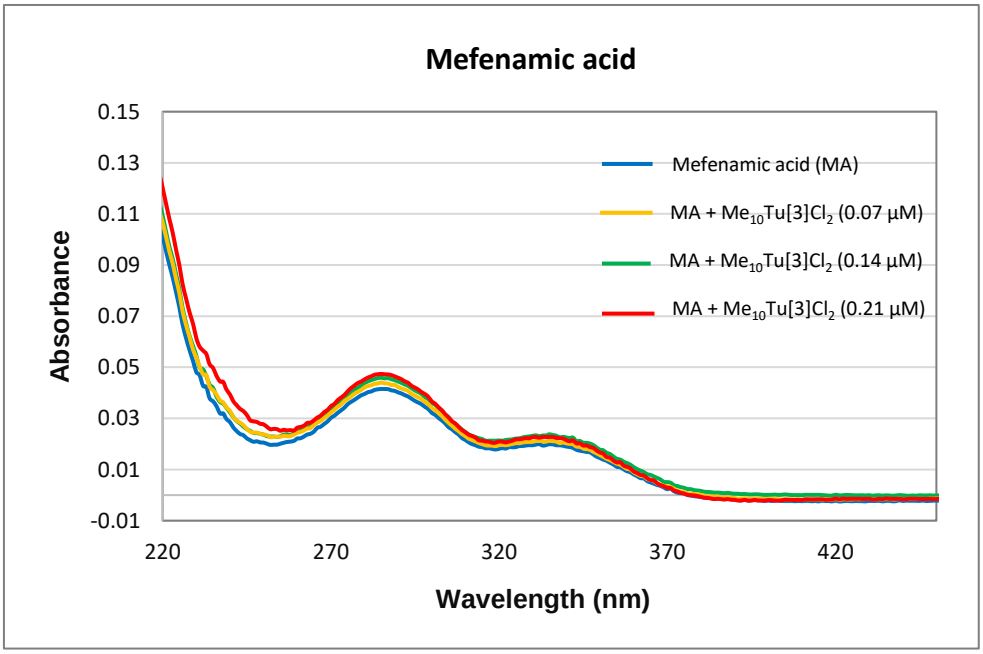
Mefenamic acid
Absorbance
Wavelength (nm)
Mefenamic acid (MA)
MA + Me10Tu[3]Cl2 (0.07 µM)
MA + Me10Tu[3]Cl2 (0.14 µM)
MA + Me10Tu[3]Cl2 (0.21 µM)
0.15
0.13
0.11
0.09
0.07
0.05
0.03
0.01
-0.01
220
270
320
370
420

(e)

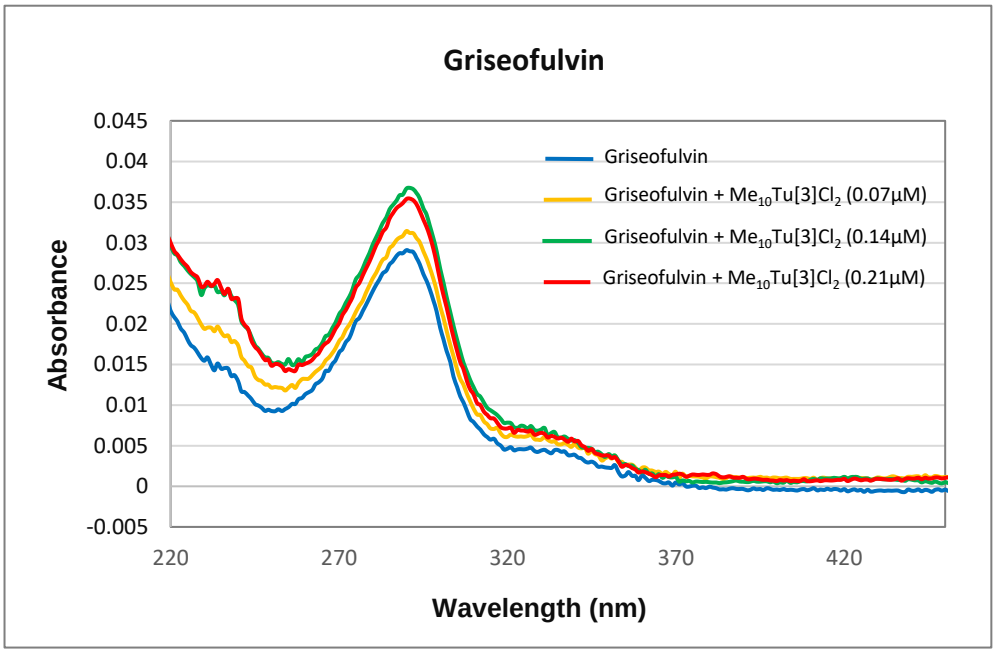

A27. The fold change in the absorbance of drugs with three different concentrations of $Me_{10}Tu[3]Cl_2$, all dissolved in PBS buffer (20 mM, pH 7.4).

Drugs	**$Me_{10}Tu[3]Cl_2$** (0.07 µM)	**$Me_{10}Tu[3]Cl_2$** (0.14 µM)	**$Me_{10}Tu[3]Cl_2$** (0.21 µM)
Indomethacin (λ = 270 nm)	1.14 ↓	1.03 ↓	1.0 ↓
Mefenamic acid (λ = 285 nm)	1.1 ↑	1.05 ↑	1.14 ↑
Furosemide (λ = 279 nm)	1.1 ↓	1.09 ↓	2.0 ↓
Probenecid (λ = 246 nm)	1.38 ↑	1.60 ↑	1.8 ↑
Griseofulvin (λ = 291 nm)	1.08 ↑	1.18 ↑	1.22 ↑

The up and down arrows represent the increase and decrease in the absorbance, respectively.